

From the Institute of Plant Nutrition and Soil Science at Kiel University

**Tracing Plant- and Microbial Carbon and Nutrients Pathways  
in Soil with Isotope and Imaging Techniques**

Dissertation

in fulfilment of the requirements for the doctoral degree  
of the Faculty of Agricultural and Nutritional Sciences  
at Christian-Albrechts-Universität zu Kiel

submitted by

**M.Sc Yijie Shi**

born in Hebei, China

Kiel, 2024

---

Dean: Prof. Dr. Tim Diekötter

First examiner: Prof. Dr. Sandra Spielvogel

Second examiner: Jun-Prof. Bahar S. Razavi

Date of the oral examination: 06.11.2024



Published with the approval of the Faculty of Agricultural and Nutritional Sciences



## Summary

Understanding soil microbial control over carbon (C), nitrogen (N), and phosphorus (P) pathways in plant-soil systems is crucial for advancing our knowledge of biogeochemical feedback mechanisms and ecosystem responses to global change. Belowground plant-soil interactions form vital links between abiotic and biotic soil components and provide hotspots for microbial processes. Isotope labeling techniques and soil enzyme kinetics are effective in studying C and nutrient dynamics to unravel the complex and diverse interactions between roots, soil particles and biota. This study aims to further elucidate C and N turnover in the rhizosphere in maize production systems and P mobilization in the detritosphere of beech forests, guide sustainable soil management, and develop new visualization technologies for soil microorganisms and enzymes.

To investigate the potential for resource reuse in existing root channels by cash crops, I conducted a field experiment using  $^{13}\text{C}$  and  $^{15}\text{N}$  to trace resource uptake by maize from root channels of cover crop mixtures (legume/grass, legume/brassica, brassica/grass). Results reveal that the legume/grass mixture allocated the most C and N to subsoil root channels, with maize taking up to 6.5% of N from these root channels. Legume/grass and brassica/grass mixtures enhanced C-cycling enzyme activities in maize rhizosphere under drought, demonstrating significant potential for enhancing C stabilization and N supply during maize growth, as well as maintaining microbial activity in maize rhizosphere under drought.

P is an essential nutrient for microorganisms and plants. Thus, understanding the microbial P use strategies is of great value. I conducted an experiment using  $^{33}\text{P}$  as tracer to investigate whether microorganisms maintain high P mobilization when microbial diversity decreases. The results show higher acid phosphatase activity in P-poor soil compared to P-rich soil, indicating strong microbial P mobilization under P-deficient conditions. Additionally, higher incorporation of litter- $^{33}\text{P}$  in soil microbial biomass in P-poor soil with the decrease of microbial diversity suggests functional redundancy and rapid litter-P acquisition by microorganisms in P-poor soil.

Based on these experiments, I identified limitations in existing visualization technologies for microorganisms and enzymes and developed new approaches to address them. These include using micro-zymography with fluorescent substrates to visualize peroxidase activity on root tissue and Fluorescence Lifetime Imaging Microscopy with phasor plot separation to differentiate stained microorganisms from soil particles, enhancing microorganism localization in complex soil matrices. The outcome of my research contributes to a better understanding of C and nutrient pathways in the soil, provides sustainable strategies for agricultural and forest soil management, and offers powerful tools for future soil biochemistry research.



## **Zusammenfassung**

Um unser Wissen über biogeochemische Rückkopplungsmechanismen und die Reaktionen von Ökosystemen auf den globalen Wandel voranzubringen ist das Verständnis der mikrobiellen Einflüsse auf Kohlenstoff- (C-), Stickstoff- (N-) und Phosphor- (P-) Flüsse in Pflanze-Boden-Systemen entscheidend. Unterirdische Pflanze-Boden-Interaktionen, insbesondere in der Rhizosphäre und Detritussphäre, stellen wesentliche Verbindungen zwischen abiotischen und biotischen Bodenkomponenten her und sind Hotspots für mikrobielle Prozesse. Isotopenmarkierungstechniken und die Kinetik von Bodenenzymen eignen sich zur Untersuchung der C- und Nährstoffdynamik, um die komplexen und vielfältigen Wechselwirkungen zwischen Wurzeln, Bodenpartikeln und Biota zu entschlüsseln. Diese Studie zielt darauf ab, den C- und N-Umsatz in der Rhizosphäre eines Maisproduktionssystems, sowie die P-Mobilisierung in der Detritussphäre eines Buchenwaldes zu entschlüsseln, Leitlinien für nachhaltiges Bodenmanagement zu definieren, und neue Visualisierungstechnologien für Bodenmikroorganismen und Enzyme zu entwickeln.

Um das Potenzial der Wiederverwendung von Ressourcen in bestehenden Wurzelkanälen durch Hauptkulturen zu untersuchen, habe ich ein Feldexperiment mit  $^{13}\text{C}$ - und  $^{15}\text{N}$ -Markierungen durchgeführt, um die Nutzung von Ressourcen aus Wurzelkanälen von Zwischenfruchtmischungen (Leguminosen/Gras, Leguminosen/Brassica, Brassica/Gras) durch Mais nachzuverfolgen. Die Ergebnisse zeigen, dass die Leguminosen/Gras-Mischung am meisten C und N in die Unterboden-Wurzelkanäle verlagerte wobei Mais bis zu 6,5 % des N aus diesen Wurzelkanälen aufnahm. Die Leguminosen/Gras- und Brassica/Gras-Mischungen förderten die Aktivität der C-Kreislauf-Enzyme in der Mais-Rhizosphäre unter Trockenstress, und zeigten signifikantes Potenzial zur Verbesserung der C-Stabilisierung und N-Versorgung während des Maiswachstums sowie zur Aufrechterhaltung der mikrobiellen Aktivität in der Mais-Rhizosphäre unter Trockenheit.

P ist ein essentieller Nährstoff für Mikroorganismen und Pflanzen. Daher ist das Verständnis der mikrobielle P-Nutzungsstrategien von großer Bedeutung. Ich führte ein Experiment mit  $^{33}\text{P}$  als Tracer durch, um zu untersuchen, ob Mikroorganismen bei abnehmender mikrobieller Diversität eine hohe P-Mobilisierung aufrechterhalten. Die Ergebnisse zeigen eine höhere Aktivität der sauren Phosphatase in P-armen Böden im Vergleich zu P-reichen Böden, was auf eine starke mikrobielle P-Mobilisierung unter P-Mangelbedingungen hinweist. Zusätzlich deutet die höhere Überführung von Streu- $^{33}\text{P}$  in die mikrobielle Biomasse in P-armen Böden bei abnehmender mikrobieller Vielfalt auf funktionale Redundanz und eine schnelle P-Akquisition durch Mikroorganismen in P-armen Böden hin.

Auf Grundlage dieser Experimente habe ich Einschränkungen bestehender Visualisierungstechnologien für Mikroorganismen und Enzyme identifiziert und neue Ansätze

entwickelt, um diese zu überwinden. Dazu gehören die Anwendung der Mikro-Zymographie mit fluoreszierenden Substraten zur Visualisierung der Peroxidaseaktivität in Wurzelgewebe und die Fluoreszenz-Lebensdauer-Imaging-Mikroskopie mit Phasendiagrammtrennung, um angefärbte Mikroorganismen von Bodenpartikeln zu unterscheiden und so die Lokalisierung von Mikroorganismen in komplexen Bodenmatrizen zu verbessern.

Die Ergebnisse meiner Forschung tragen zu einem besseren Verständnis der C- und N-Wege im Boden bei, bieten nachhaltige Strategien für das landwirtschaftliche und forstliche Bodenmanagement und stellen leistungsstarke Werkzeuge für die zukünftige Forschung zur Bodenbiochemie zur Verfügung.

## **Acknowledgement**

I would like to express my sincere gratitude to all who helped and supported me on my way to the doctoral degree, and to those who showed their selfless love and assistance, which allowed me to come this far.

First and foremost, I sincerely thank Prof. Dr. Sandra Spielvogel for trusting me and offering me the opportunity to be a doctoral student and work on such an interesting project, as well as for her invaluable guidance and feedback throughout my research. Her extensive knowledge and experience were instrumental in the completion of my study. I am also extremely thankful to Prof. Dr. Michaela A. Dippold for her guidance in my work, for providing me with opportunities to study in her laboratory, and for offering me strong support and care during my time there. I deeply thank Jun-Prof. Dr. Bahar S. Razavi for teaching me experimental skills and providing me with laboratory space to complete my research on enzyme activity. I would also like to thank Prof. Dr. Georg Guggenberger and Dr. Evgenia Blagodatskaya for providing me with samples and experimental equipment for my studies, and for carefully guiding my research.

I acknowledge BMBF for the financial support of the “RootWayS” project entitled “Deep-rooting cover crop mixtures: Creating highways to subsoil water and nutrient resources” within the Project Network of Rhizo4Bio, which supported me in completing my PhD.

A special thanks to Dr. Iris Zimmermann for her careful organization of the project I was involved in, for always being there when I needed her support, for constantly reviewing my progress, and for guiding me through my PhD studies. I would also like to extend my thanks to Dr. Sebastian Loepmann for his patient guidance during the early stages of my PhD, and for always answering my questions and encouraging me to be creative in my scientific work. In addition, I would like to deeply thank Dr. Callum Banfield for providing various technical support for my research related to isotopes. It was also my great pleasure to collaborate with the groups from Uni Kiel (Prof. Dr. Henning Kage and Katja Holzhauser), Uni Göttingen (Tobias Stürzebecher and Henrik Füllgrabe), and UFZ Leipzig (Dr. Jochen A. Müller, Dr. Nico Jehmlich, and Debjyoti Ghosh). Thanks for all of your valuable contributions to my study.

My appreciation also goes out to all the colleagues in our group, including PhD students, postdocs, and technicians. I would also like to thank all the farmers working on the experimental farms, thanks to their care of the plants and soil, I was able to complete the experiment.

Finally, I would like to thank all the friends from around the world whom I met in Kiel for their love and care after work. I would also like to thank my family in China for their selfless support of my studies abroad.



## Table of Contents

Summary.....	1
Zusammenfassung.....	3
Acknowledgement.....	5
Table of Contents.....	7
List of Figures.....	9
List of Tables.....	12
Abbreviations.....	13
<b>1 Extended summary.....</b>	<b>15</b>
<b>1.1 Introduction.....</b>	<b>15</b>
1.1.1 Using isotopes in tracing soil carbon and nutrient cycles.....	15
1.1.2 Imaging techniques in soil enzyme visualization.....	17
1.1.3 Microscopy-based localization of microorganisms in soil.....	19
<b>1.2 Objectives.....</b>	<b>19</b>
<b>1.3 Materials and Methods.....</b>	<b>20</b>
1.3.1 Experimental setup.....	20
1.3.2 Soil and plant sampling.....	21
1.3.3 Isotope labeling methods.....	21
1.3.3.1 <sup>13</sup> C pulse labeling.....	21
1.3.3.2 <sup>15</sup> N leaf labeling.....	22
1.3.3.3 <sup>33</sup> P labeling.....	22
1.3.4 Enzyme kinetics and zymography methods.....	22
1.3.4.1 Enzyme kinetics.....	22
1.3.4.2 In-situ zymography.....	23
1.3.4.3 Resorufin-based Micro-zymography.....	23
1.3.5 Florescent imaging of soils and microorganisms.....	23
<b>1.4 Main results and discussion.....</b>	<b>23</b>
1.4.1 Synthesis of highlights and main results of the studies.....	23
1.4.2 Stable isotope tracing reveals reuse of cover crop root channels by the following cash crops.....	29
1.4.3 Radio isotope tracing reveals functional redundancy of microbial P mobilization.....	29
1.4.4 Novel imaging techniques to visualize and localize soil microorganisms and enzymes.....	30
<b>1.5 Conclusions.....</b>	<b>31</b>
<b>1.6 References.....</b>	<b>32</b>
<b>1.7 Contribution to the included manuscripts.....</b>	<b>38</b>
<b>1.8 Declaration of coauthor form.....</b>	<b>39</b>
<b>2. Manuscript.....</b>	<b>45</b>

<b>2.1 Study 1. Deep- and Shallow-rooting Legume/Grass Mixture Optimize Carbon and Nitrogen Allocation to the Subsoil through Root Channels during Maize (<i>Zea mays</i> L.) Cultivation.....</b>	<b>45</b>
<b>2.2 Study 2. Site-specific Legacy Effect of Cover Crop Mixtures on C-cycling Enzyme Activities in the Subsequently Growing Maize (<i>Zea mays</i> L.) Rhizosphere under Drought...</b>	<b>67</b>
<b>2.3 Study 3. Redundancy of Microbial P Mobilization in Beech Forest Soils with Contrasting P Stock: A Microbial Dilution Experiment.....</b>	<b>85</b>
<b>2.4 Study 4. Peroxidase Activity of Fresh Apple Root: A Novel Approach of Resorufin-based Micro-zymography.....</b>	<b>105</b>
<b>2.5 Study 5. Using Fluorescence Lifetime Imaging to Disentangle Microbes from the Heterogeneous Soil Matrix .....</b>	<b>117</b>

## List of Figures

### Extended summary

<b>Figure 1</b> The main <sup>13</sup> C fluxes between the C pools within the plant-soil-microorganism system.....	16
<b>Figure 2</b> Historical timeline of the soil zymography method. Only those papers with the most important methodological steps are presented.....	18
<b>Figure 3</b> Experimental sites in Germany. The numbers on the figure represent the study numbers in this thesis.....	20
<b>Figure 4</b> <sup>13</sup> C pulse labeling of cover crops.....	22
<b>Figure 5</b> <sup>15</sup> N labeling for (a) red clover, (b) tall fescue, and (c) oil radish.....	22
<b>Figure 6</b> Graphical abstract summarizing the main results of Study 1.....	24
<b>Figure 7</b> Graphical abstract summarizing the main results of Study 2.....	25
<b>Figure 8</b> Graphical abstract summarizing the main results of Study 3.....	26
<b>Figure 9</b> Graphical abstract summarizing the main results of Study 4.....	27
<b>Figure 10</b> Graphical abstract summarizing the main results of Study 5.....	28

### Study 1

<b>Figure 1-1</b> Cover crop-derived C incorporated in (a) total C pool of empty cover crop root channels, (b) C <sub>mic</sub> , and (c) labile C pool in empty cover crop root channels in the topsoil and the (d-e) subsoil at two time points (T1: maize germination; T2: maize growth stage BBCH 33).....	51
<b>Figure 1-2</b> Cover crop-derived N incorporated in (a) total N pool of empty cover crop root channels, (b) N <sub>mic</sub> , and (c) labile N pool in empty cover crop root channels in the topsoil and the (d-e) subsoil at two time points (T1: maize germination; T2: maize growth stage BBCH 33).....	51
<b>Figure 1-3</b> Cover crop-derived C incorporated in (a) total C pool of maize rhizosphere reusing cover crop root channels, (b) C <sub>mic</sub> , and (c) labile C pool in maize rhizosphere reusing cover crop root channels in the topsoil and the (d-e) subsoil at T2 (maize growth stage BBCH 33).....	53
<b>Figure 1-4</b> Cover crop-derived N incorporated in (a) total N pool of maize rhizosphere reusing cover crop root channels, (b) N <sub>mic</sub> , and (c) labile N pool in maize rhizosphere reusing cover crop root channels in the topsoil and the (d-e) subsoil at T2 (maize growth stage BBCH 33).....	53
<b>Figure 1-5</b> β-glucosidase activity in the (a) topsoil and (c) subsoil, and leucine aminopeptidase activity in the (b) topsoil and (d) subsoil activities in maize rhizosphere reusing cover crop root channels in the topsoil and the subsoil at T2 (maize growth stage BBCH 33).....	54
<b>Figure 1-6</b> Percentage of (a) maize uptake of cover crop-derived N (%) and (b) cover crop-derived N in maize N (%). .....	54

### Study 1 Supplementary

<b>Figure S1-1</b> Contents of soil organic C and N in (a, b) soil, in (c, d) microbial biomass, and in (e, f) extractable pool in the rhizosphere of cover crops in the topsoil and the subsoil at two time points..	63
<b>Figure S1-2</b> C:N ratios in (a) soil, (b) microbial biomass, and (c) extractable pool in the rhizosphere of cover crops in the topsoil and the subsoil at two time points.....	64
<b>Figure S1-3</b> Contents of soil organic C and N in (a, b) soil, in (c, d) microbial biomass, and in (e, f) extractable pool in the rhizosphere of maize in cover crop root channels in the topsoil and the subsoil at T2 (maize growth stage BBCH 33).....	65
<b>Figure S1-4</b> C:N ratios in (a) soil, (b) microbial biomass, and (c) extractable pool in maize rhizosphere in cover crop root channels in the topsoil and the subsoil at T2 (maize growth stage BBCH 33). .....	66

## Study 2

- Figure 2-1** Zymograms of  $\beta$ -glucosidase activity and hotspots distribution of maize rhizosphere in the subsoil (30-60 cm) under drought and rainfall condition at three sites. Maize was growing after cover crop mixtures or control..... 73
- Figure 2-2** Effects of using cover crop mixtures on C-cycling enzyme activities in maize rhizosphere under drought and rainfall conditions. (a)  $\beta$ -glucosidase activity at HS; (b) cellobiohydrolase activity at HS; (c) xylanase activity at HS; (d)  $\beta$ -glucosidase activity at KD; (e) cellobiohydrolase activity at KD; (f) xylanase activity at KD; (g)  $\beta$ -glucosidase activity at RH; (h) cellobiohydrolase activity at RH; (i) xylanase activity at RH..... 74
- Figure 2-3** Geometric mean enzyme activity (GMea) in the rhizosphere of maize in control and after cover cropping at three sites. .... 75
- Figure 2-4** Shannon's diversity index based on enzyme activities at (a) HS, (b) KD and (c) RH.. ... 75
- Figure 2-5** Linear relationship of soil water content (%) with (a) Shannon's diversity index with (b) geometric mean of enzyme activity, (c) hotspots area (d)  $\beta$ -glucosidase activity in the rhizosphere of maize in control plots..... 76
- Figure 2-6** Linear relationship of Shannon's diversity index with (a) geometric mean of enzyme activity and effect size of cover crop mixtures on (b)  $\beta$ -glucosidase activity, (c) cellobiohydrolase activity and (d) xylosidase activity. .... 76

## Study 3

- Figure 3-1** (a) Potential extracellular activity ( $V_{max}$ ) and (b) catalytic efficiency of acid phosphatase across dilutions of microbial inoculum after mixed litter addition in P-rich (BBR) and P-poor (LUE) soil..... 92
- Figure 3-2** Content of (a) dithionite-citrate extractable P and (b) oxalate-extractable P in P-rich (BBR) and P-poor (LUE) soils. .... 92
- Figure 3-3** (a) Specific  $^{33}\text{P}$  activity of total soil P pool, (b) Recovery of applied litter-derived  $^{33}\text{P}$  in total soil P pool, (c) specific  $^{33}\text{P}$  activity of SMB, (d) Recovery of applied litter-derived  $^{33}\text{P}$  in SMB, (e) specific  $^{33}\text{P}$  activity of  $P_{resin}$ , and (f) Recovery of applied litter-derived  $^{33}\text{P}$  in  $P_{resin}$ . .... 93
- Figure 3-4** P immobilization of P-rich and P-poor soil..... 94
- Figure 3-5** The C: N: P ratios of microbial biomass (MBC, MBN, and MBP) and the correspondent extractable C, N, and P pools (EOC, EN, and EP) in P-rich (BBR) and P-poor (LUE) soil..... 95

## Study 3 Supplementary

- Figure S3-1** Microbial biomass C, N, and P and the correspondent extractable C, N, and P pools (EOC, EN, and EP) in P-rich (BBR) and P-poor (LUE) soil. .... 104

## Study 4

- Figure 4-1** Calibration of micro-zymography images based on (a) resorufin concentration ( $\text{mM pixel}^{-1}$ ) and the mean gray value across each image..... 109
- Figure 4-2** (a) An example of 2.5D surface topography of fluorescent intensity at the root surface after adding Amplex Red; (b) root tissue imaged in bright field; (c) autofluorescence of root tissue in C1 red channel wavelength; (d) the fluorescence on the root tissue 500s after adding Amplex Red. .... 110
- Figure 4-3** Overlay of bright field image and fluorescent images of root tissue with soil particles at every minute after application of Amplex Red. 0 min: before application of Amplex Red (autofluorescence)..... 110
- Figure 4-4** Overlay of bright field image and fluorescent image of root with (a) organic soil particles and (b) quartz 5 minutes after adding Amplex Red. (c) The mean gray value of organic soil particles, quartz, and root.. .... 110

**Figure 4- 5** Spatial and temporal distribution of peroxidase activity at the root tips. (a) Variation of gray value over time from the root cap to the region of cell division..... 111

**Figure 4- 6** Spatial distribution of peroxidase activity on roots with dense root hair (a-b, two pieces of root tissues with dense root hair), and roots with sparse root hair (c-d, two pieces of root tissues with sparse root hair) at the same reaction time of 5 minutes after application of Amplex Red..... 111

**Study 5**

**Figure 5-1** Fluorescence lifetime adds information which is not available in steady-state imaging. .... 122

**Figure 5-2** CLSM image of soil collected from the Ah horizon at BBR site showed strong autofluorescence.. .... 122

**Figure 5-3** Visualization by steady-state intensity imaging of treatment (iv) mineral particles (sized < 63 μm) from LUE site spiked with BacLight™ Green stained *Rhodotorula mucilaginosa*.. .... 123

**Figure 5-4** Visualization by steady-state intensity of *Rhodotorula mucilaginosa*. **a** Reflection signal of the surfaces of soil mineral particles < 63 μm spiked with *Rhodotorula mucilaginosa*, **b** Confocal fluorescence signal of BacLight™ Green stained *Rhodotorula mucilaginosa*, and **c** transmitted light image; **d** an overlay of a, b, and c; blue area identified oversaturation of the signal. .... 123

**Figure 5-5** Visualization of *B. subtilis*. **a** Steady-state intensity image of cultured *B. subtilis* imaged in PBS via CLSM. **b** Overview steady-state intensity image of *B. subtilis* imaged in PBS (CLSM image). **c** Fluorescence lifetime image of *B. subtilis*. **d** Fluorescence lifetime distribution of *B. subtilis* in the phasor plot. **d** Phasor plot of *B. subtilis* in PBS imaged via CLSM (red).. .... 125

**Figure 5-6 a** Phasor distribution of purely stained *Rhodotorula mucilaginosa* and **b** in combination with glucose-activated forest soil (BBR, Ah horizon)... .... 125

**Figure 5-7 a** Zoomed view to the steady-state intensity image of natural soil (LUE). Both channels have been combined for FLIM analysis. **b** In the phasor plot, five different populations can be discriminated. All separated channels are shown in a maximum intensity projection of the stack in all five channels; additionally, all 5 channels represented in an overlay **c** 5 separated phasor population channels of the natural soil (LUE) directly stained with BacLight™ Green, based on specific phasor plot analysis. Average fluorescence lifetime after phasor plot separation in nanoseconds: mineral surface light-blue 0.18, different mineral surface (attached with microbes in red color in the upper middle part of the image) yellow 0.36, mineral material in green 0.67, microorganisms in red 0.99, possibly mineral coatings violet 3.61. **d** FLIM image of this sample is presented as a 3D movie in the Supplementary and as a screenshot in d (red color depicts the fluorescence lifetime of the microorganisms..... 126

## List of Tables

### Study 1

**Table 1-1** Variations of cover crop mixtures with deep- and shallow-rooting species and control. The variations are named according to the functional plant species groups they represent. ....47

**Table 1-2** Description of cover crops and following maize cultivation, sowing dates/density, fertilization levels.....48

### Study 2

**Table 2-1** Soil properties in the subsoil of three experimental sites. Soil water content was measured at rainfall side and simulated drought side at sampling time.....69

### Study 3

**Table 3-1** Soil properties of the study sites. ....87

**Table 3-2** Analysis of variance for the recovery of  $^{33}\text{P}$  and specific  $^{33}\text{P}$  activity in soil P pools. ....94

## Abbreviations

C	Carbon
N	Nitrogen
P	Phosphorus
SOM	Soil organic matter
OC	Organic carbon
SOC	Soil organic carbon
SMB	Soil microbial biomass
MBC	Microbial biomass C
MBN	Microbial biomass N
MBP	Microbial biomass P
EN	Extractable N
EOC	Extractable organic C
EP	Extractable P
TN	Total nitrogen
$V_{\max}$	Enzyme activity
$K_m$	Substrate affinity
S	Substrate concentration
$C_{\text{mic}}$	Microbial biomass C
$N_{\text{mic}}$	Microbial biomass N
GLU	$\beta$ -glucosidase activity
MUF	4-methylumbelliferone
AMC	7-amino-4-methylcoumarin
LAP	Leucine-amino-peptidase
$P_{\text{oxal}}$	Oxalate-extractable P
$P_{\text{dith}}$	Dithionite-/citrate-extractable P
GMea	Geometric mean of the assayed enzyme activities
BG	$\beta$ -glucosidase
CE	Cellobiohydrolase
BX	Xylanase
BBR	Bad Brückenau
LUE	Lüss
CLSM	Confocal laser scanning fluorescence microscopy

FLIM	Fluorescence lifetime imaging
FISH	Fluorescence in situ hybridization
STED	Stimulated Emission Depletion Microscopy
PBS	Phosphate-buffered saline
HS	Hohenschulen
KD	Karkendamm
RH	Reinshof

# 1 Extended summary

## 1.1 Introduction

In terrestrial ecosystems, plants provide energy and nutrients for microbial metabolism through root exudation and litter decomposition (Zhao et al., 2021; Hobbie et al., 2015; Finzi et al., 2015). They significantly influence biogeochemical cycles and are crucial in regulating ecosystem biogeochemistry (Bardgett and Wardle, 2010; Bastida et al., 2021). Plant-derived carbon (C) and nutrients follow different pathways based on their properties, localization, and availability to soil microorganisms (Feng et al., 2022; Ladygina and Hedlund, 2010; Lange et al., 2019). Soil microbial activity plays a vital role in C stabilization and nutrient retention, underlining the importance of understanding key microbial processes in soil (Lange et al., 2015; Trivedi et al., 2013). However, quantifying plant- and microbial-driven reactions remains challenging due to the heterogenous distribution of microorganisms in soil and the high dynamic of these reactions (Smercina et al., 2021). In recent years, isotope technologies have been widely applied to trace organic matter transformations driven by plant and soil microorganisms (Dorodnikov et al., 2011; Chen et al., 2019; Kuzyakov and Schneckenberger, 2004). Moreover, it is well-known that exoenzymes, released by plants and microorganisms in order to generate soluble oligomers and monomers that can be readily transported into cells, play a central role in the depolymerization of macromolecular organic compounds in soils (Sinsabaugh et al., 2002). Accordingly, the combination of enzyme quantification and tracing techniques has proven effective in analyzing microbially controlled transformation processes in soils (Ai et al., 2023; Dippold and Kuzyakov, 2013; Sun et al., 2024). Integrating isotope tracing technologies with soil enzyme analyses allows the determination of direct and indirect contributions of various factors to soil organic matter (SOM) transformation. This approach helps identifying key driving factors in SOM transformation. Understanding soil microbial control over C, nitrogen (N), and phosphorus (P) pathways is crucial for advancing our knowledge of biogeochemical feedback mechanisms and long-term ecosystem responses to global change.

### 1.1.1 Using isotopes in tracing soil carbon and nutrient cycles

In recent decades, radioactive isotopes, e.g.,  $^{14}\text{C}$ ,  $^{33}\text{P}$ , and  $^{35}\text{S}$  and stable isotopes, e.g.,  $^{13}\text{C}$ ,  $^{15}\text{N}$  and  $^{18}\text{O}$  have been widely used to trace element pathways and understand the mechanisms of SOM dynamics (Ai et al., 2023; Lehmann et al., 2018; Ma et al., 2021; Müller and Bünemann, 2014; Kuzyakov et al., 2000; Sauer et al., 2006; Wang et al., 2023; Werth and Kuzyakov, 2008), especially in the rhizosphere (Mayer, et al., 2003; Pausch and Kuzyakov, 2011; Spohn and Kuzyakov, 2013; Stevenel et al., 2019; Teixeira et al., 2024; Wang et al., 2021), a hotspot for microbial activity, cycling of nutrients, and turnover of organic matter (Kuzyakov and Blagodatskaya, 2015).

The application of the stable isotope  $^{13}\text{C}$  for tracing soil C turnover in soils was introduced by Kuzyakov et al. (2000). Later, applications of the radioisotope  $^{14}\text{C}$  in soil-plant systems were introduced (Sauer et al., 2006), and used to study the spatial distribution of root exudates. Based on tracer studies using  $^{14}\text{C}$  enrichment of wheat and barley, it has been shown that, after 1–4 months, 30% of the total assimilates were transferred into the soil: 2–4% of the C from rhizodeposition remains in SOM, while 0.8–3.2% is incorporated into microbial biomass (Kuzyakov and Domanski, 2000; van Ginkel et al., 2000), the remaining C was either used for root growth or root respiration. However, the use of  $^{14}\text{C}$  poses safety and environmental concerns, which makes the application of these methods rather difficult despite their high sensitivity. The use of the stable isotope  $^{13}\text{C}$  as tracer allows for safer, long-term ecological studies (Kuzyakov et al., 2002), and the method has been successfully applied, e.g., to (1) quantify rhizosphere C deposition in soil aggregates and pore structures (Qiao et al., 2014), and (2) track the pathways of plant C inputs (Bore et al., 2017; Ladygina and Hedlund, 2010; Pang et al., 2021; Werth and Kuzyakov, 2008).

$^{13}\text{C}$  labeling has been successfully used to determine the heterogeneous distribution of rhizodeposit-C from the root surface to the surrounding soil, and to detect and quantify the root-derived C in soil aggregates and soil pores (Qiao et al., 2014; Teixeira et al., 2023; Quigley and Kravchenko, 2022). For instance, Teixeira et al. (2023) reported that the majority (57 %) of recently deposited root-derived C was stored in macroaggregates ( $> 250 \mu\text{m}$ ). Moreover, most of the root-derived C was found in the soil pores that were  $> 2 \mu\text{m}$  in diameter (Qiao et al., 2014). These results underline the heterogeneous accessibility of root-derived C for soil microorganisms.

Notably, growing plant roots can deeply penetrate the soil and leave continuous biopores coated in root-derived C after their decay (Petzoldt et al., 2020). These biopores are preferentially reused by the following plants. This is supported by the observation of Stewart et al. (1999) that 80 % of the living roots in soil are distributed within 1 mm distance from soil macropores. The exudates in the rhizosphere of the plants that reuse biopores will enhance the microbial activity and, thus, affect the dynamics of C cycling within these pores. A study using  $^{13}\text{C}$  successfully traced the distribution of rye root-derived C in a soil with intact pore architecture, and found that the root-derived  $^{13}\text{C}$  was positively associated with  $> 90 \mu\text{m}$  pores, providing evidence for preferential rye root growth into legacy root channels (Quigley and Kravchenko, 2022). However, the utilization of root-derived C accumulated in biopores by microorganisms in the rhizosphere of living roots needs further research.

The pathways of plant-derived C in the rhizosphere (Figure 1) are (1) mineralization to  $\text{CO}_2$ ; (2) assimilation in microbial biomass; (3) storage as soil OC; and (4) release as microbial exudates/extracellular polymeric substances into the soil (Ge et al., 2015; Pang et al., 2021; Paterson et al., 2007). It has been demonstrated that the total release of assimilated photosynthetic C to the soil by exudation varied in different ecosystems: approximately 1–10 % is released in forests, which is notably lower than agricultural systems (20–30 %) and grasslands (30–50 %) (Qiao et al., 2014, Pausch and Kuzyakov, 2018, Zang et al., 2019). In a tree-crop-grass agroforestry system, grassland transferred 7.0 % of total assimilated C into the soil, which is more than the transfer generated by rape (9.2 %) and willow (1.6 %) (Zhou et al., 2022). About half of the assimilated C that cereal crops allocate to belowground is found in roots, another third is associated with rhizodeposition and root-derived  $\text{CO}_2$ , and the remaining C is transferred to SOC and soil microbial biomass (Kuzyakov and Domanski, 2000). Another study using  $^{13}\text{C}$  pulse labeling to trace C loss through soil respiration in grassland demonstrated that rhizodeposit decomposition accounted for 7–31 % of total below-ground respiration (Wang et al., 2020). Previous results have shown that  $^{13}\text{C}$  labeling is a successful method for tracking the OC cycle in soil and continues to be an effective approach to fill the existing knowledge gaps.

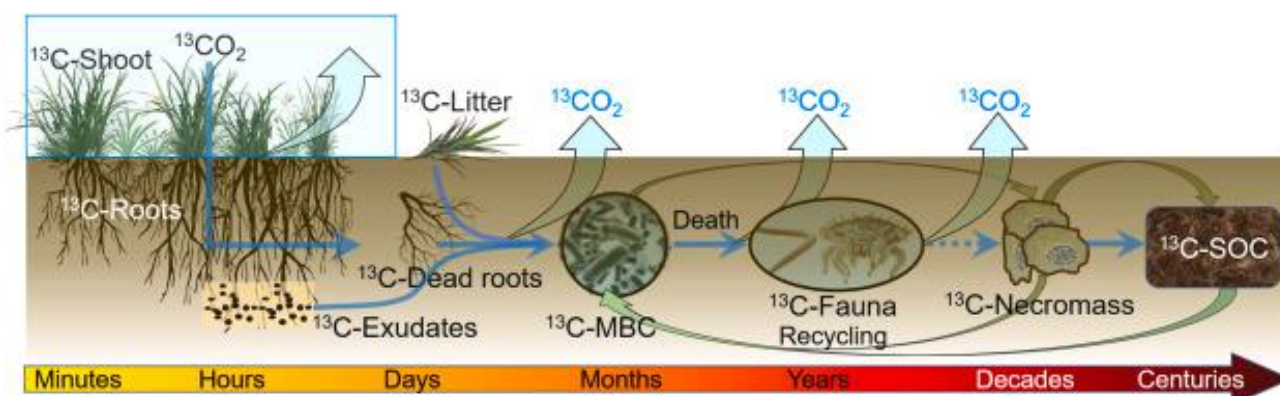


**Figure 1** The main  $^{13}\text{C}$  fluxes between the C pools within the plant-soil-microorganism system (Pang et al., 2021).

Labeling techniques with the stable N isotope  $^{15}\text{N}$  are widely used to investigate N transformations in soil ecosystems, offering detailed insights into N dynamics and management practices referring to three aspects: (1) inorganic N as plant nutrient, and (2) organic N transformation, and (3) the coupled

mobilization of C and N (and/or P) in OM. In detail, a study using  $^{15}\text{N}$  techniques reported that 40–50 % of N applied as fertilizer was utilized by maize (Guo et al., 2021), providing insights into N uptake efficiency for high-yield crops.  $^{15}\text{N}$  labeling through the stem was successfully applied to *Brassica napus*, *Centaurea jacea* and *Lolium perenne*, and 4–6 % of the total applied  $^{15}\text{N}$  was retraced as root exudates in the soil (Hertenberger and Wanek, 2004). Interestingly, the oxidation of labile organic N to  $\text{NO}_3^-$  accounted for between 63 and 83% of total  $\text{NO}_3^-$  production especially in a low-P soil, suggesting a novel nitrification pathway (O'Neill et al., 2021). The efficiency of  $^{13}\text{C}$  allocation and  $^{15}\text{N}$  uptake showed similar patterns between daytime and nighttime in maize and wheat, suggesting a close coupling between C allocation and N utilization (Liu et al., 2021). The combined use of  $^{15}\text{N}$  and  $^{13}\text{C}$  allowed quantification of the C: N ratio of SOM mineralization processes, e.g., C: N ratio of the basal (non-primed) mineralized flux from SOM was reported to be 20 for rhizosphere soil (Murphy et al., 2015). Combining  $^{13}\text{C}$  and  $^{15}\text{N}$  stable isotope labeling effectively clarifies the coupling patterns of C and N allocation, and the competition between plants and soil microorganisms for N uptake (Kušlienė et al., 2014; Fu et al., 2021).

The P radioisotope ( $^{32}\text{P}$  and  $^{33}\text{P}$ ) technique qualitatively determines P uptake, transformation, and movement in soils (Di et al., 1997; Meyer et al., 2017; Müller and Bünemann, 2014; Siegenthaler et al., 2020; Wang et al., 2024; Zhang et al., 2021).  $^{33}\text{P}$  has lower radioactivity and longer half-life time than  $^{32}\text{P}$ , making it more suitable for experiments that focus on tracing P in the plant-soil system (Robinson et al., 1969). Many studies using  $^{33}\text{P}$  tracing follow the approaches of Oehl et al. (2001) and Bünemann et al. (2004). Recent studies have applied  $^{33}\text{P}$  labeling to prove that subsoil communities are well capable of mobilizing and using complex organic P sources (Ai et al., 2023), and that P can be taken up by perennial crop species from soil depths down to 4.2 m, especially under P-limited conditions in the topsoil (Han et al., 2021). It is worth noting that key studies have focused on discussing P turnover in low-P soils and on proposing sustainable suggestions to alleviate P deficiency. Previous researches have provided substantial insights into plant and microbial strategies for P acquisition. However, with the increasing trend of microbial diversity loss due to human activities, it remains unclear whether soil microbial communities will be able to maintain their high P-mobilization capacities.

### 1.1.2 Imaging techniques in soil enzyme visualization

Enzymes play a crucial role in breaking down large organic molecules that originate from plants and microorganisms. These processes are fundamental to the cycling of C, N, P, and other essential nutrients in soil (Sinsabaugh, 2010). The possibilities for the study of soil enzymes have evolved significantly, particularly through developing enzyme kinetics and zymography (Bilyera et al., 2021; Ma et al., 2018; Tian et al., 2020). Enzyme kinetics, based on the Michaelis-Menten model (Michaelis and Menten, 1913), has been pivotal for understanding enzyme activities by quantifying the rates of substrate conversion. Early research in this area, e.g., by Sinsabaugh (2010) and Nannipieri et al. (2012), established foundational principles for soil enzyme functions. Razavi et al. (2015, 2016) explored nonlinear temperature sensitivities in enzyme kinetics to improve the understanding of soil enzyme dynamics under different climate conditions. Alvarez et al. (2018) further expanded this work by showing that increasing temperature decreases enzyme catalytic power in soil C cycling. Moreover, the method of zymography emerged as a technique for visualizing enzyme activity distribution in the rhizosphere, providing a more comprehensive view of enzyme functions (Razavi et al., 2019; Spohn et al., 2013). Zymography addresses the limitations of enzyme kinetics by allowing for the spatial and temporal mapping of enzyme activities in the natural soil matrix.

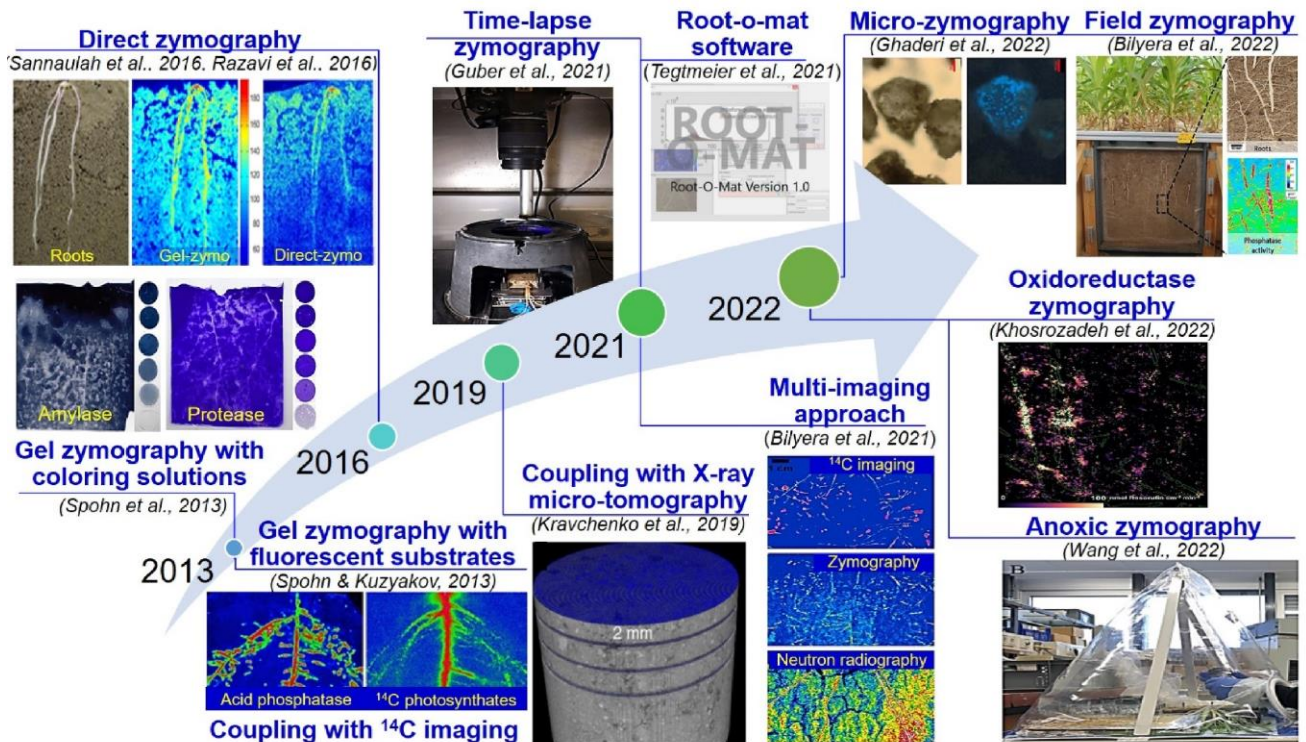


**Figure 2** Historical timeline of the soil zymography method. Only those papers with the most important methodological steps are presented (Bilyera and Kuzyakov, 2024).

Zymography techniques have evolved considerably since their introduction, from initial visual methods to advanced quantitative approaches (Figure 2) (Bilyera and Kuzyakov, 2024). The development of soil zymography was based on a colorimetric gel to analyze amylase and protease activity on the rooted soil surface (Spohn et al., 2013). Later, Spohn and Kuzyakov (2014) advanced fluorescent substrate-based zymography by recording the signal by camera under ultraviolet (UV) light. Guber et al. (2018) made a major advancement by developing quantitative soil zymography, which improved measurement accuracy through detailed examinations of substrate and enzyme diffusion processes. Guber and Kravchenko (2021) introduced time-lapse soil zymography, addressing previous limitations in temporal resolution.

Recent applications of zymography techniques have demonstrated their effectiveness in exploring soil enzyme functions and their implications for soil health and management. Bilyera et al. (2020) used advanced imaging techniques to identify hotspots in bulk soil and rhizosphere, revealing significant spatial variability of enzyme activities. Hoang et al. (2016) used zymography to study enzyme kinetics and distribution in earthworm burrows, finding that the hotspot areas were 2.4–14 times larger in the burrows versus soil without earthworms. Kravchenko et al. (2019) combined X-ray micro-tomography with 2D zymography to investigate extracellular enzyme spatial patterns, showing that extracellular enzymes were positively associated with 60–90  $\mu\text{m}$  pores. Wang et al. (2022) applied in-situ zymography techniques to reveal anoxic enzyme activities in paddy soils, and documented how short-term aeration can overestimate enzymatic hotspot area in anoxic ecosystems.

The above-mentioned zymography technology is based on camera imaging, which can have insufficient magnification accuracy for studying tiny hotspots. Recently, Ghaderi et al. (2022) innovated a micro-zymography method to detect hydrolase activity under the microscope, allowing for high-resolution visualization of enzyme activities in soil aggregates and the rhizosphere. These advancements have significantly enhanced the sensitivity, resolution, and temporal observation capabilities of zymography, though challenges, such as sensitivity for fast-reacting oxidase, remain. In fact, soil oxidoreductase zymography was successfully developed by Khosrozadeh et al. (2022), who

first introduced Amplex Red as a reagent to visualize and quantify distributions of phenol oxidase and peroxidase activities in the rhizosphere of *Zea mays* L. However, this is also a membrane-based imaging technology and it cannot fully reflect the enzyme dynamics in plants and soil.

### 1.1.3 Microscopy-based localization of microorganisms in soil

Soil biochemical processes are mediated by microbial communities whose composition and activity are influenced by their habitat (Eickhorst and Tippkötter, 2008; Loepmann et al., 2018; Wang et al., 2020). Although various methods have been developed and refined to study the localization of microorganisms in soil, a large knowledge gap remains in understanding the dynamics and metabolic landscapes of soil microbial communities at relevant spatial scales. Early advancements in microscopic techniques for soil microorganisms involved traditional light and electron microscopy (Beveridge and Moyles, 2014). Currently, direct microscopy techniques such as confocal laser scanning fluorescence microscopy (CLSM) are invaluable for determining the spatial distribution of soil microorganisms in their microhabitats (Eickhorst and Tippkötter, 2008; Li et al., 2004; Tippkötter et al., 1986).

CLSM has proven effective for visualizing a diverse range of soil microorganisms, including protists, fungi, bacteria, and rhizosphere microorganisms (Jaafar et al., 2014; Li et al., 2004; Lo Piccolo et al., 2010). However, this technique faces various challenges for soil microorganism localization, including interference from the primary fluorescence of soil particles, intrinsic fluorescent proteins, and autofluorescent compounds, such as aromatic amino acids, siderophores, and cytochromes (Alimova et al., 2003), in bacteria. These challenges can obscure the accurate interpretation of microbial spatial distributions and interactions.

To enhance the visualization of soil microorganisms, improved fluorescent staining methods have been developed. Techniques such as fluorescence in situ hybridization (FISH) are now commonly used, often applied with CLSM to improve resolution and specificity (Tippkötter et al., 1986; Fernández-Suárez and Ting, 2008; Pett-Ridge and Firestone, 2018; Bokota et al., 2021). However, the technical limitations of the targeted detection of fluorescence in a soil matrix persist, including issues with autofluorescence, resolution, and photobleaching artifacts from soil minerals and organic matter that complicate digital image processing and analysis (Li et al., 2004; Watt et al., 2006).

In recent years, molecular fluorescence lifetime imaging (FLIM) has emerged as a technique that provides both complementary and unique information about target biomarkers in cells (Balke et al., 2018; Digman et al., 2008; Hayek et al., 2007). FLIM offers significant advantages by distinguishing between different fluorophores and the intrinsic fluorescence of samples. For example, Lee et al. (2022) reported obviously different signals of unstained fungal hypha and soil organic matter. However, the application of FLIM is constrained by limitations such as slow image acquisition and processing, complex implementation, and high instrument costs (Mannam et al., 2021). Thus, a better approach to simplify the analysis of FLIM images is required to provide detailed insights into the spatial distribution and interactions of soil microorganisms.

## 1.2 Objectives

The main purpose of this work is to utilize modern isotope and imaging technologies to quantify and visualize key processes in the C, N and P cycles of agricultural and forest soils, and to derive sustainable soil use strategies that are applicable to production practices. Additionally, it introduces new methods, based on existing technologies, to accurately localize and quantify key processes driven by plants and microorganisms in the soil. The presented studies include the following approaches to obtain these objectives:

- 1) Using stable isotope ( $^{13}\text{C}$  and  $^{15}\text{N}$ ) labeling methods combined with soil zymography to assess the allocation of plant-derived C and N in root channels, and assess microbial C and N mobilization during the reuse of these root channels by following plants (Study 1 and 2).
- 2) Using radioisotope ( $^{33}\text{P}$ ) labeling combined with soil enzyme kinetics to identify the functional redundancy of microbial P mobilization (Study 3).

- 3) Developing novel methods, based on microscopy techniques, to localize soil microorganisms and visualize the spatial distribution of fast-reacting oxidase enzyme activity, in order to contribute to a comprehensive understanding of soil C and nutrient cycling processes (Study 4 and 5).

### 1.3 Materials and Methods

#### 1.3.1 Experimental setup



**Figure 3** Experimental sites in Germany. The numbers on the figure represent the study numbers in this thesis. [[https://de.wikipedia.org/wiki/Datei:Germany\\_general\\_map.png](https://de.wikipedia.org/wiki/Datei:Germany_general_map.png)]

The studies presented in this work include seven sampling sites in central and northern Germany (Figure 3). To achieve the first objective, field experiments with maize as the main crop after different winter cover crops were established. The experiment in **Study 1** was conducted only at the site Hohenschulen (54°18'44"N, 9°59'46"E), an experimental farm of Kiel University, Germany. The soil is a Luvisol with sandy loam texture. The experimental plots, including three cover crop mixtures and control (black fallow in winter), were set up in the autumn of 2020. Maize was sown in May 2021 after the cover crops had been killed by herbicide, and the topsoil had been shallowly tilled to prepare the seedbed.

To compare the maize reuse of cover crop root channels under different soil types, the experiments for **Study 2** were expanded to three sites in the second year. Rain exclusion experiments were set up at the three experimental sites to explore whether the C and N in the root channels of cover crops help maintaining microbial activity in maize rhizosphere under drought stress. The three sites included two experimental farms of Kiel University: (1) Hohenschulen; (2) Karkendamm (KD, 53°55'38.8"N

9°55'51.0"E), with a gleyic Podzol and sandy texture; and one experimental farm of Göttingen University: (3) Reinshof (RH, 51°29'08.5"N 9°53'34.9"E), with a Phaeozem soil and silty loam texture. With the objective of identifying the functional redundancy of microbial P mobilization, two beech forest sites with contrasting soil P storage were selected for **Study 3**. The Bad Brückenau (BBR) site with a P-rich soil with 904 g m<sup>-2</sup> of P stock (Brödlin et al., 2019) located in Northern Bavaria, Germany (50°21'7.26" N, 9°55'44.53" E) was chosen to take P-rich soil samples. The soil is a Dystric skeletal Cambisol (WRB 2015) and has developed from Basalt (Lang et al., 2017). The Lüss (LUE) site with 164 g m<sup>-2</sup> of P stock (Brödlin et al., 2019) located in Lower Saxony, Germany (52°50'21.77" N, 10°16'2.37" E) was chosen to take P-poor soil samples. The soil is a Hyperdystric Folic Cambisol and has developed on sandy till (WRB 2015; Lang et al., 2017).

With the objective of developing novel methods to visualize the spatial distribution of fast-reacting oxidase enzyme activity that occurs intensively in living root rhizosphere, a rhizotron experiment with apple seedlings growing in two different soils from Heidgraben (53°41'57.5"N 9°40'59.6"E) and Ruthe (52°14'39.8"N 9°49'08.2"E) were set up for **Study 4**. The soil in Heidgraben is an Luvisol with sandy texture. The soil in Ruthe is a Luvisol with silty texture (Rohr et al., 2020).

To develop a novel microscopy method to localize soil microorganisms, the successfully verified living microbial communities extracted from BBR and LUE sites in study 3 were chosen for **Study 5**.

### 1.3.2 Soil and plant sampling

Both plant and soil samples were collected for **Study 1**: Aboveground biomass of the cover crops (labeled with <sup>13</sup>C and <sup>15</sup>N, details in 1.3.3.1 and 1.3.3.2) was sampled before sowing maize in May 2021 to determine the assimilated <sup>13</sup>C and <sup>15</sup>N. Soil samples from cover crop root channels (initially empty at the first sampling time, with and without maize rhizosphere at the second sampling time) were collected from 0–30 cm and 30–60 cm depth increments from soil profiles by carefully scraping out the inside of the channels with a micro spatula, and bulk soil samples were collected from both the cover crop variations and the control (only bulk soil). Additionally, two maize plants growing within the sampling area were collected to determine the transfer of <sup>15</sup>N from the cover crop root channels to the maize crop.

For **Study 2**, soil samples from maize rhizosphere in the subsoil layer (30–60 cm) were collected.

Soil samples for **Study 3 and 5** were taken from the Ah horizon of the respective site at six randomly chosen positions. European beech seedlings (*Fagus sylvatica* L.) were also collected from the randomly chosen positions at the two sampling sites.

The rhizotrons in **Study 4** were filled with soil from the sites Heidgraben and Ruthe. After dried and sieved, the soil was filled into the rhizotron with a bulk density of 1.1 g cm<sup>-3</sup>, and the water content was adjusted to 60 % of water holding capacity.

### 1.3.3 Isotope labeling methods

#### 1.3.3.1 <sup>13</sup>C pulse labeling

The <sup>13</sup>CO<sub>2</sub> pulse labeling was performed in **Study 1** according to Bromand et al. (2001) and Zhou et al. (2022) in November 2020 and April 2021 on a subplot of each plot with cover crop mixture (Figure 4). The labeling area was covered with a cuboid chamber to allow for unhindered photosynthesis during the label. Every chamber had two beakers with NaH<sup>13</sup>CO<sub>3</sub> (98 atom % <sup>13</sup>C, Sigma-Aldrich, Germany). The <sup>13</sup>CO<sub>2</sub> was released by injecting an excess amount of H<sub>3</sub>PO<sub>4</sub> (85 % w/w) into the beakers by using a syringe from outside the chamber.



**Figure 4**  $^{13}\text{C}$  pulse labeling of cover crops. (a) Preparation of the labeling area; (b) Placement of  $\text{NaH}^{13}\text{CO}_3$  in the chamber; (c) Sealed chamber with temperature monitoring.

### 1.3.3.2 $^{15}\text{N}$ leaf labeling

In **Study 1**,  $^{15}\text{N}$  leaf labeling was used to trace the allocation of cover crop-derived N in their root channels and the reuse of this N by maize. The  $^{15}\text{N}$  was prepared in a solution containing  $(^{15}\text{NH}_4)_2\text{SO}_4$  and  $\text{Na}^{15}\text{NO}_3$ . For labeling, three leaves from three adjacent cover crop plants were cut off from both sides of the midrib, leaving only the midvein. These three midveins were immersed together in a plastic vial containing  $^{15}\text{N}$  solution and sealed with parafilm (Figure 6). The midveins remained fixed in the vials for one week to allow for plant uptake.



**Figure 5**  $^{15}\text{N}$  labeling for (a) red clover, (b) tall fescue, and (c) oil radish.

### 1.3.3.3 $^{33}\text{P}$ labeling

In **Study 3**, beech trees collected from two experimental sites were cultivated in climate chambers under artificial light at  $20^\circ\text{C}$  for four weeks, until the buds opened and leaves emerged. Each plant was fed with  $^{33}\text{P}$  as a 1 ml  $\text{H}_3^{33}\text{PO}_4$  solution applied to the beech stem using the wick labeling method (Russell and Fillery, 1996; Mayer et al., 2003). A small hole was drilled into the stem, into which a cotton wick was inserted and the hole sealed with plasticine to minimize harm to the plant. The other end of the cotton wick was submerged in the  $\text{H}_3^{33}\text{PO}_4$  solution to facilitate the transfer into the plant. After 96 hours, the solution was completely absorbed.

## 1.3.4 Enzyme kinetics and zymography methods

### 1.3.4.1 Enzyme kinetics

The kinetics of enzymes that target C- and N-containing organic compounds were assayed using fluorogenically labeled substrates (Razavi et al., 2015). The 4-methylumbelliferone (MUF)-based fluorogenic substrate 4-methylumbelliferyl- $\beta$ -D-glucoside was used to assess  $\beta$ -glucosidase activity (GLU), and the 7-amino-4-methylcoumarin (AMC)-based fluorogenic substrate L-Leucine-7-amido-4-methylcoumarin hydrochloride was used to assess the activity of leucine-amino-peptidase (LAP) in

**Study 1.** Three types of 4-methylumbelliferone (MUF)-based fluorogenic substrates were used to assess the activity of C-cycling enzymes in **Study 2**: 4-methylumbelliferyl- $\beta$ -D-glucoside for  $\beta$ -glucosidase (BG) activity, 4-methylumbelliferyl- $\beta$ -N-acetyl-D-glucosaminide for cellobiohydrolase (CE) activity, and 4-methylumbelliferyl- $\beta$ -D-xylopyranoside for xylanase (BX) activity. The enzyme activities were determined at a range of substrate concentrations. Fluorescence (caused by the release of MUF from the substrate) was measured with the micro-plate reader CLARIOstar Plus (BMG LABTECH, Ortenberg, Germany). Enzyme activity was calculated according to the Michaelis-Menten equation (Michaelis and Menten, 1913; Nannipieri et al., 2012).

#### 1.3.4.2 *In-situ* zymography

Zymography was conducted in the maize rhizosphere to examine the spatial patterns of C-cycling enzyme activity influenced by cover crop mixtures in **Study 2**, following the protocol established by Razavi et al. (2016). Membranes saturated with 4-Methylumbelliferyl- $\beta$ -D-glucoside (abcr GmbH, Karlsruhe, Germany) were used to detect  $\beta$ -glucosidase activity. The calibration was performed using membranes soaked in MUF solutions with a range of concentrations. Membranes were photographed (EOS 6D, Canon, Tokyo, Japan) under UV light (365 nm wavelength). The membranes were attached to cover rhizosphere soil and maize roots, and photographed as described above. Image analysis was performed using ImageJ (Fiji 1.54f) and MATLAB R2023a (The MathWorks, Inc., USA).

#### 1.3.4.3 Resorufin-based Micro-zymography

In **Study 4**, a novel technique to quantify and visualize the activity of peroxidase on fresh roots, based on the substrate Amplex Red, which forms the fluorescent product resorufin when oxidized, e.g., in the presence of H<sub>2</sub>O<sub>2</sub> (Khosrozadeh et al., 2022), was developed and introduced. A microscope (Zeiss Axio Imager M1, setting: 540–552 nm excitation and 575–640 nm emission length) was used to detect the fluorescence caused by the peroxidase activity of the root tissues. A series of images recorded as a video of approximately 5 to 10 min was used to monitor and quantify the peroxidase activity.

#### 1.3.5 Florescent imaging of soils and microorganisms

In **Study 5**, a novel method for localizing microorganisms in the soil was developed and introduced. To test the designed technique, *Rhodotorula mucilaginosa* and *Bacillus subtilis* were cultured, and stained with BacLight™ Green (absorption/emission ~ 480/516 nm). Imaging was conducted via CLSM and STED using a STELLARIS 8 confocal scanner unit (LEICA Microsystems, Wetzlar, Germany) to assemble a high-resolution image of the cells' sizes and morphology. The integration of fluorescence lifetime imaging microscopy (FLIM) into the STELLARIS confocal platform (LEICA, Wetzlar, Germany) allows for comprehensive FLIM analysis during image acquisition.

### 1.4 Main results and discussion

#### 1.4.1 Synthesis of highlights and main results of the studies

Using stable isotope (<sup>13</sup>C and <sup>15</sup>N) labeling methods combined with *in-situ* zymography successfully confirmed the allocation of cover crop-derived C and N to the subsoil, and the reuse of the N resources in the cover crop root channels in the rhizosphere of the following maize (**Study 1**). Furthermore, the positive effect of cover crop-derived C on the maintenance of enzymatic processes in the rhizosphere of maize under drought was confirmed by the *in-situ* zymography and enzyme kinetics analysis (**Study 2**). In addition, the functional redundancy of microbial P mobilization was confirmed by radioisotope (<sup>33</sup>P) labeling combined with soil enzyme kinetics analysis. Microorganisms maintained a high P mobilization capacity despite reduced microbial community diversity, especially in P-deficient soil (**Study 3**). The novel methods to visualize the spatial distribution of fast-reacting oxidase enzyme activity (**Study 4**) and localize soil microorganisms (**Study 5**) were successfully established, providing more possibilities for a comprehensive understanding of redox processes in the rhizosphere via the combination with already established technologies.

**Study 1:** The results show that the root channels of the legume/grass cover crop mixture in the subsoil contained 5-fold more C at BBCH33 compared to the root channels of the brassica/grass cover crop mixture, whereas the N content in the root channels of all three cover crop mixtures was comparable. The microbial biomass in the subsoil root channels of the legume/grass mixture contained 3 times more cover crop-derived C at maize germination and 5 times more cover crop-derived C at BBCH33 compared to both mixtures with brassica (Figure 6). In the rhizosphere of maize reusing brassica/grass root channels in the subsoil,  $\beta$ -glucosidase and leucine-amino-peptidase activities were considerably higher than in the root channels of the two mixtures containing legumes. Maize used up to 6.5 % of the cover crop derived N from the legume/grass mixture, which covered up to 1.1 % of the N demand of maize at BBCH33, indicating a high potential of legume/grass mixtures to contribute to the N supply of maize through the provision of nutrient-rich root channels (Figure 6).

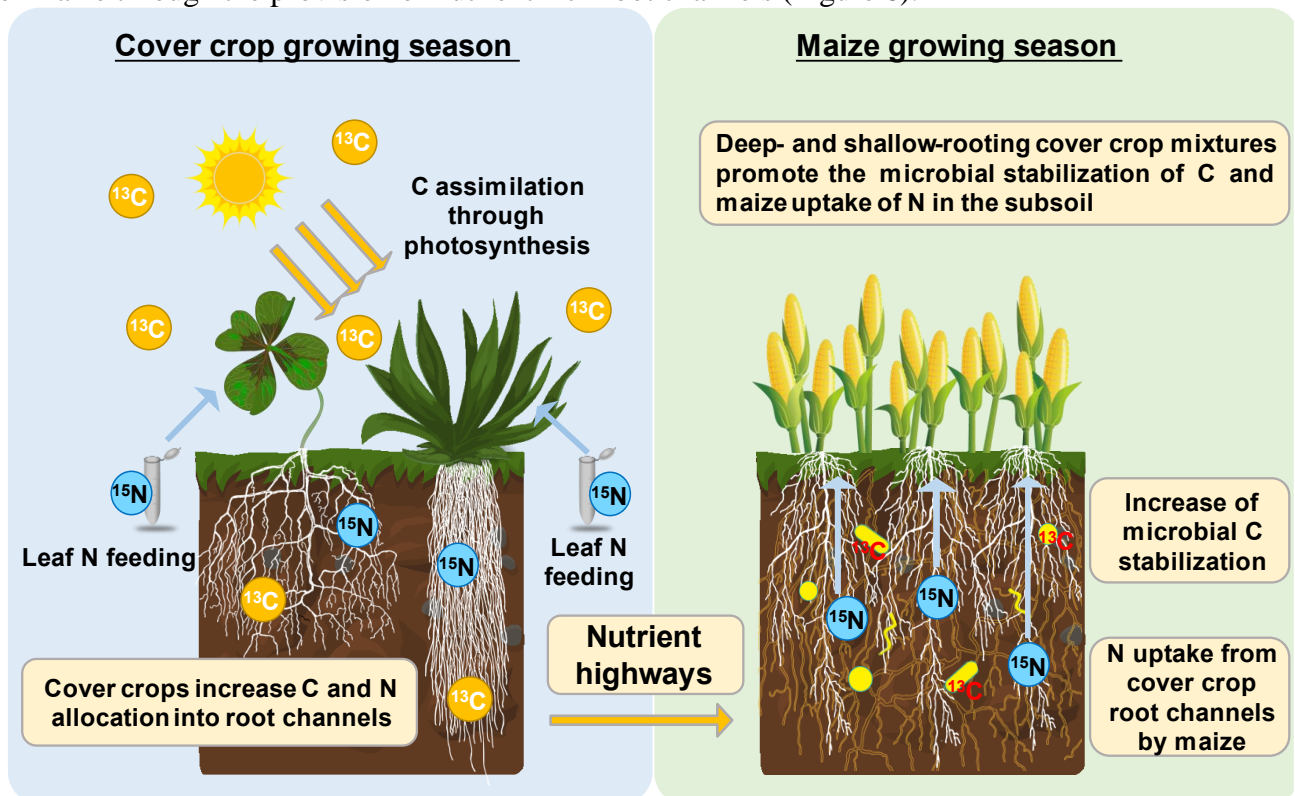


**Figure 6** Graphical abstract summarizing the main results of Study 1. Deep- and shallow-rooting cover crop mixtures optimize C and N allocation in the subsoil and provide C and nutrient resources in their root channels for the following maize root.

**Study 2:** Cover crop residues induce site-specific effects on microbial C mobilization in the rhizosphere of maize reusing the root channels of the cover crops (Figure 7). Pre-cropping with cover crops significantly enhanced the activities of  $\beta$ -glucosidase, cellobiohydrolase, and xylanase in the rhizosphere of maize under drought stress in root channels in soil with a sandy loam texture (HS), suggesting active cellulose and hemicellulose degradation at maize growth stage BBCH50. In contrast,  $\beta$ -glucosidase and cellobiohydrolase activities were lower in the rhizosphere of maize reusing root channels of both cover crop mixtures containing grass in soil with sandy texture (KD), independently of the water supply, indicating lower decomposition rates in these root channels compared to the root channels in the soil with sandy loam texture. In soil with silty loam texture (RH), activities of all three carbon-cycling enzymes in the rhizosphere of maize reusing cover crop root channels was reduced under drought condition compared to the respective activities under non-drought conditions.

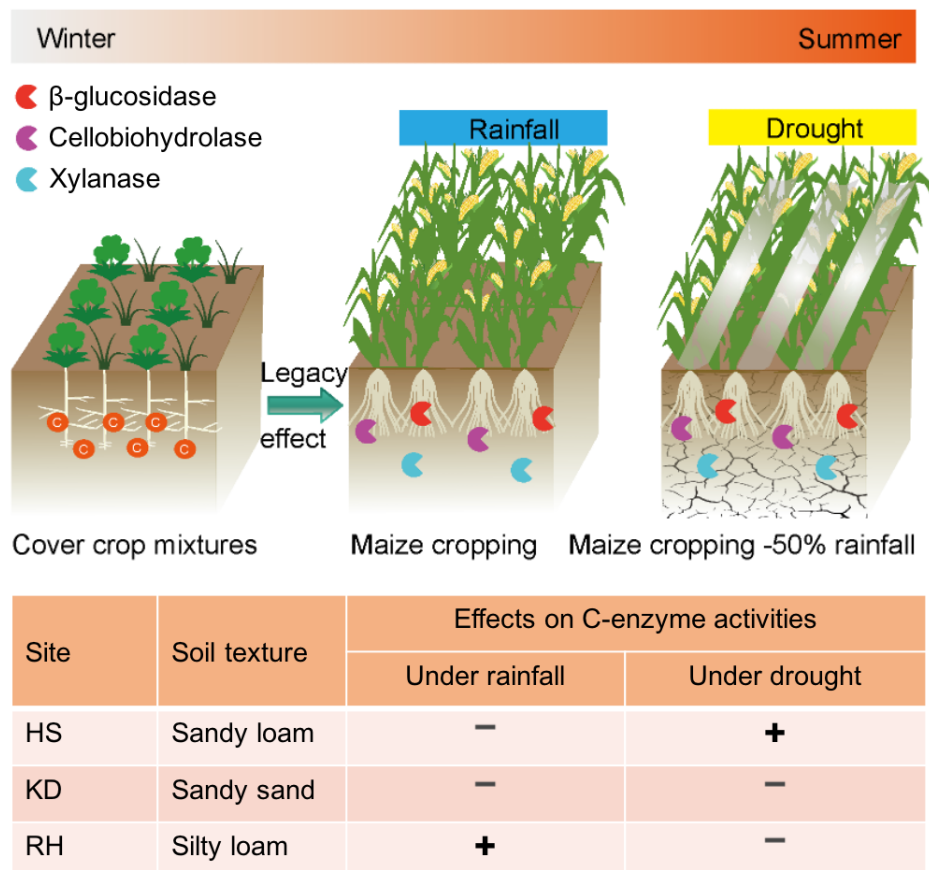


**Figure 7** Graphical abstract summarizing the main results of Study 2. The effect of cover crop mixtures on three C-related enzyme activities in maize rhizosphere under rainfall and drought conditions. (HS: Hohenschulen, KD: Karkendamm, RH: Reinshof. '+' represents increase of enzyme activities by cover crop mixtures. '-' represents reduction of enzyme activities by cover crop mixtures. The two cover crop mixtures (Legume/grass and legume/brassica) used in this experiment performed similarly across sites.)

**Study 3:** The acid phosphatase activity at the P-poor site was overall higher than the acid phosphatase activity at the P-rich site, and it was unaffected by the microbial diversity reduction (Figure 8). This indicates that microbial P mobilization exhibits a high functional redundancy, particularly at the site with low P stock. Higher recovery rates of litter-derived  $^{33}\text{P}$  in the soil microbial biomass and in the soil labile P pool were detected in the P-poor soils, suggesting a tight cycling of litter-derived P in the microbial biomass and the soil solution. The results suggest that the functional redundancy of microbial P acquisition at P-poor forest sites keeps all essential processes ongoing even under loss of biodiversity.

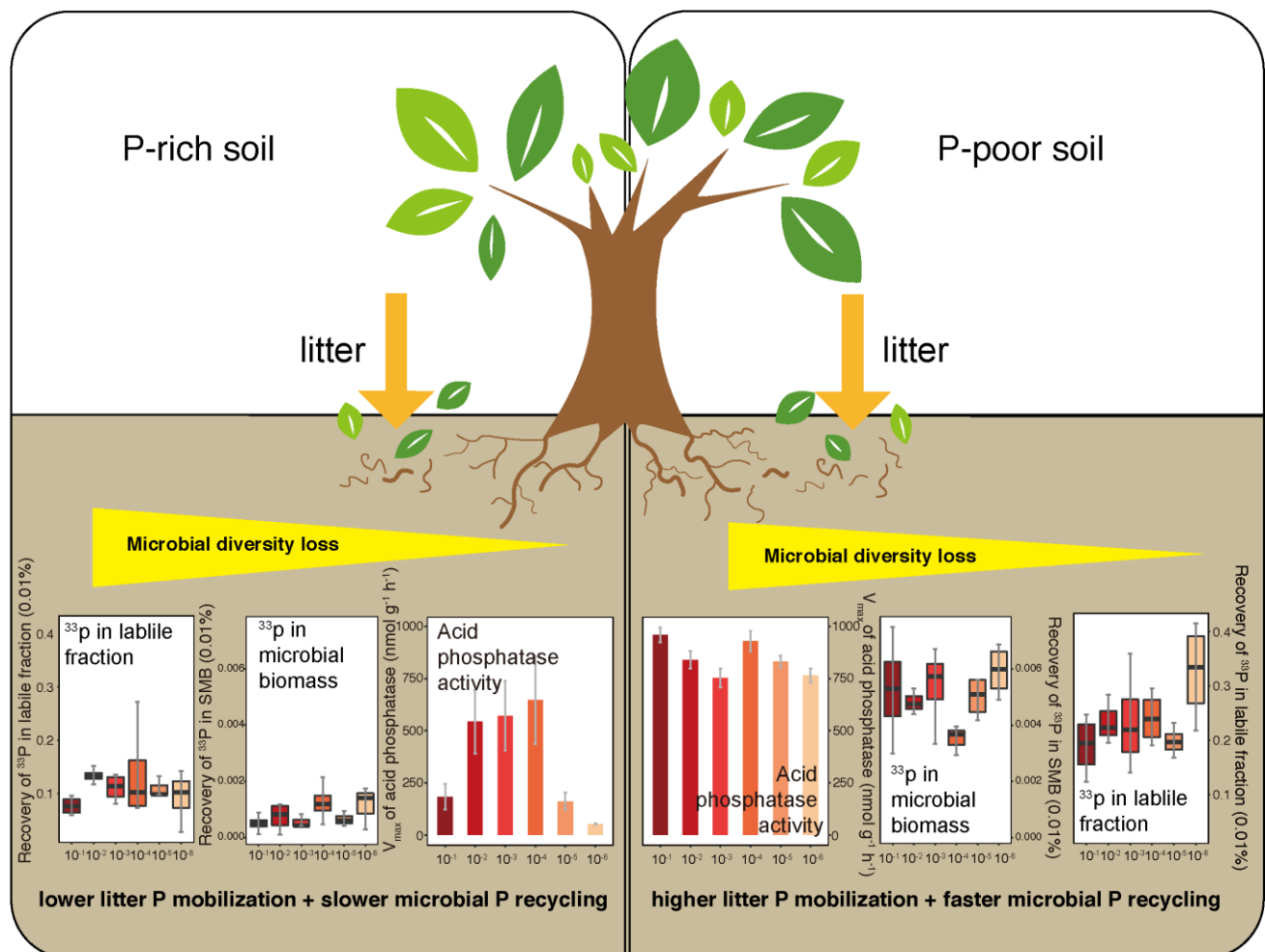


**Figure 8** Graphical abstract summarizing the main results of Study 3. The microbial P mobilization under the stress of microbial diversity reduction in beech forest soils at P-rich and P-poor site. The recovery of  $^{33}\text{P}$  in soil labile fractions and soil microbial biomass, as well as the acid phosphatase activity at each experimental site, are displayed.

**Study 4:** A visualization approach, based on micro-zymography with a fluorometric assay via Amplex Red, with high resolution for spatial and temporal investigation of the oxidative reactions of peroxidases was developed in this study (Figure 9). The linear correlation between the concentrations of resorufin (0–0.01 mmol) and the average gray values proves an accurate reference for quantifying the rate of peroxidase activity in the rhizosphere. The roots covered densely with root hair had 2-fold higher peroxidase activity and 11-fold larger hotspot extend than the roots with sparse root hair coverage. Peroxidase activity was 2-fold higher at the calyptra (root cap) than in the apical meristem (region of cell division). The results showed that Amplex Red-based zymography can accurately quantify the peroxidase activity of roots at the microscale, and visualize the spatial distribution of peroxidase hotspots.

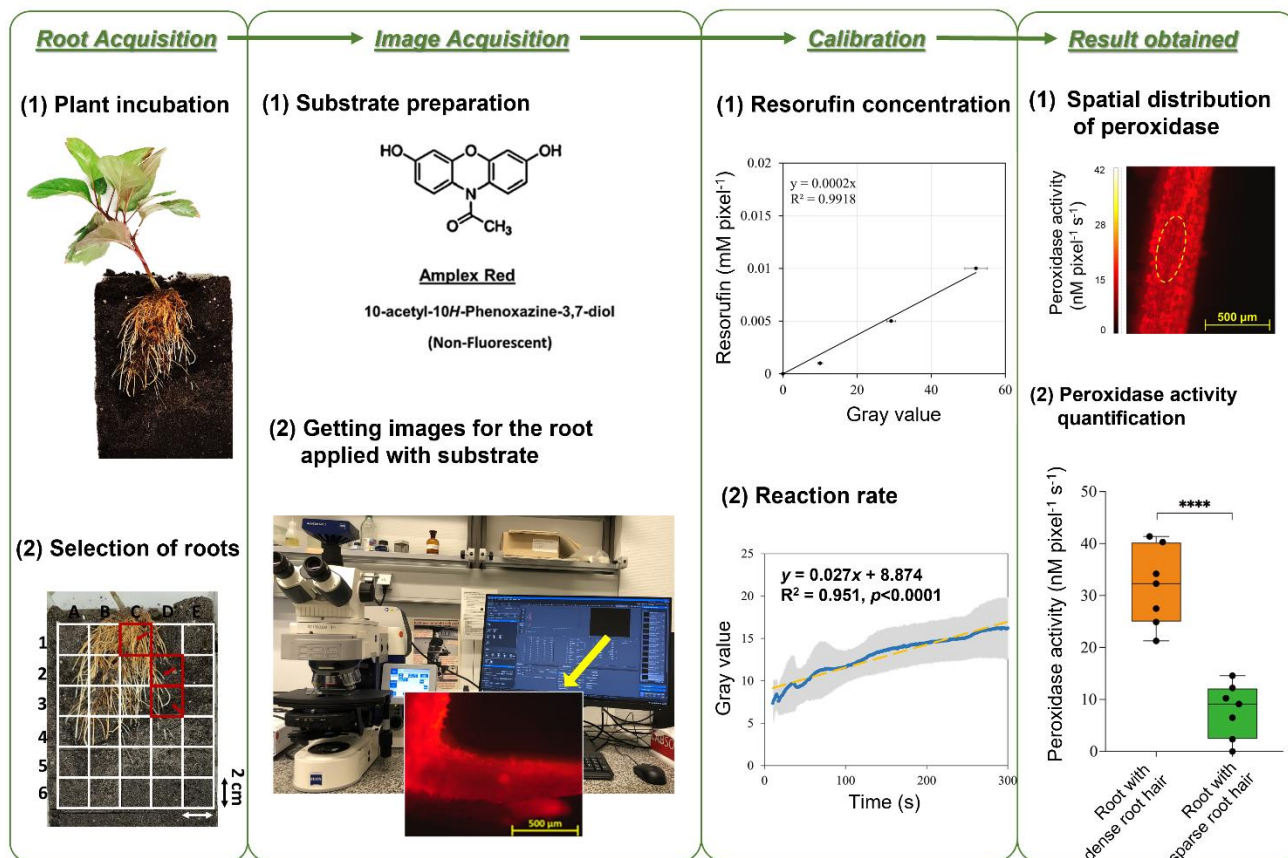


**Figure 9** Graphical abstract summarizing the main results of Study 4. Flow chart of using the Amplex Red-based micro-zymography method to quantify and visualize peroxidase activity in the rhizosphere of Apple seedlings.

**Study 5:** Steady-state fluorescence intensity imaging is a basic microscopic technique in ecological cell biology. However, intensity-based measurements are vulnerable to artifacts, e.g., fluorophores with similar excitation and emission spectra may be impossible to differentiate using steady-state fluorescence intensity imaging. These limitations were overcome by using fluorescence lifetime imaging microscopy (FLIM) in combination with the phasor approach to unravel the spatial distribution of microbial cells in soil and mineral microspheres (Figure 10). The phasor-based FLIM technique revealed that microorganisms had a fluorescence lifetime of 1.2–1.3 ns, whereas minerals and organo-mineral associations generally displayed shorter lifetimes.

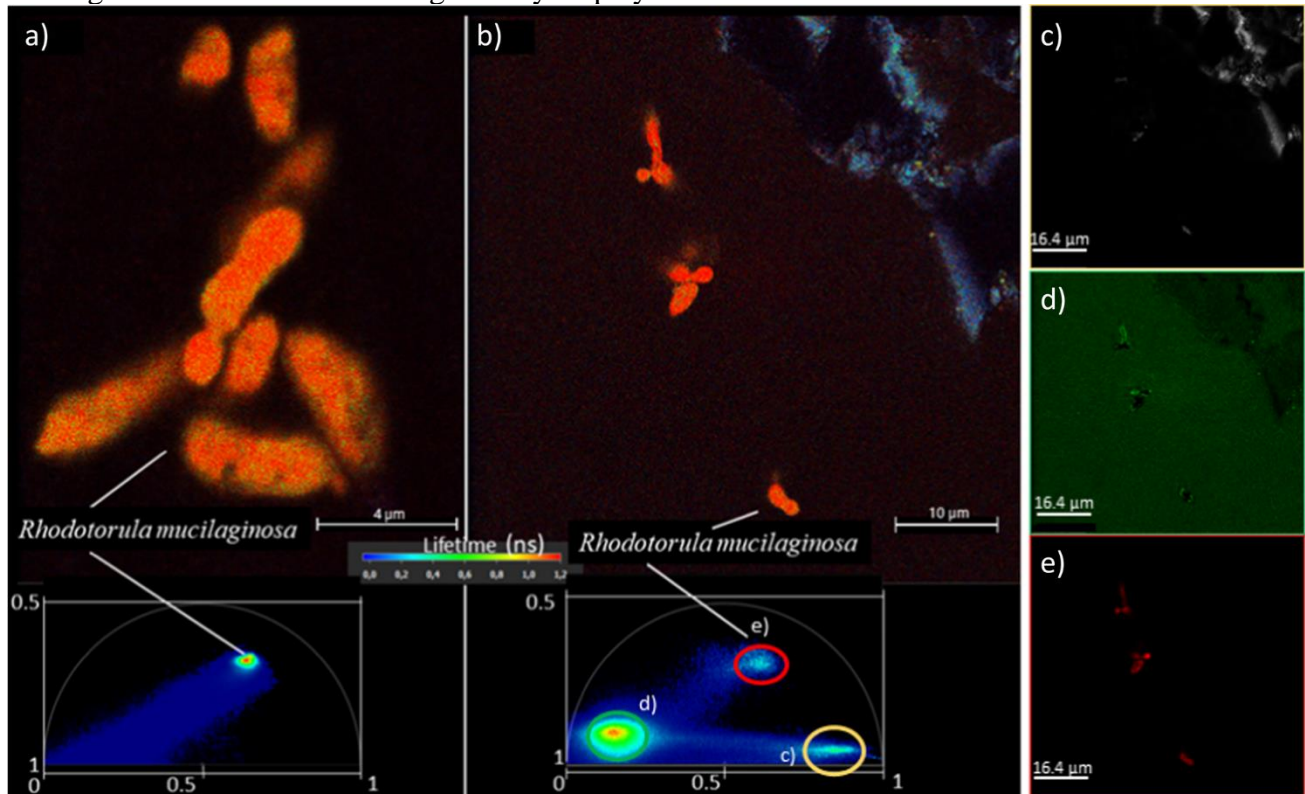


**Figure 10** Graphical abstract summarizing the main results of Study 5. Phasor distributions of purely stained *Rhodotorula mucilaginosa* in combination with glucose-activated forest soil under confocal laser scanning microscope (a and b). c–e: The phasor plot approach allows to distinguish three populations with different fluorescence lifetimes from image b.

### 1.4.2 Stable isotope tracing reveals reuse of cover crop root channels by the following cash crops

Given the importance of the organic material in root channels as resource for soil microorganisms and following plant roots (Banfield, 2022), I first investigated the content and composition of cover crop-derived C and N in the root channels of different cover crop mixtures at different time points after maize germination to determine the potential of cover crop-derived resources to be beneficial for the following cash crops. Total non-particulate cover crop-derived C and N percentage in root channels of the topsoil increased 3- and 305-fold from maize germination to BBCH 33, respectively, indicating the gradual decomposition of root residues thereby releasing C and N from the particulate to the non-particulate pool (*Figure 1-1, 1-2*).

The microbial biomass in the subsoil root channels of the legume/grass mixture contained 3 times more cover crop-derived C at maize germination and 5 times more cover crop-derived C at BBCH33 compared to both mixtures with brassica (*Figure 1-1*). This indicates that the winter-hardy legume/grass mixture enhances intermediate microbial C stabilization. Additionally, the incorporation of cover crop-derived N into microbial biomass ( $N_{mic}$ ) was higher in the root channels of the legume/grass mixtures as well (*Figure 1-2*).

Secondly, I determined the partitioning of C and N from the cover crop root channels to soil organic matter and/or nutrient supply of the maize crop by tracing the  $^{13}C$  and  $^{15}N$  remaining in the root channels of the labeled cover crops when reused by maize root, as well as the proportion of  $^{15}N$  taken up by maize. The root channels of the legume/grass cover crop mixture in the subsoil contained 5-fold more C at BBCH33 compared to the root channels of the brassica/grass cover crop mixture (*Figure 1-1*), whereas the N content in the root channels of all three cover crop mixtures was comparable (*Figure 1-2*). Moreover, 6.5 % of the N in the maize plants at growth stage BBCH33, after cover cropping with the legume/grass mixture, was cover crop-derived, and this covered up to 1.1 % of the N demand of maize at this growth stage (*Figure 1-6*), demonstrating that legume/grass mixture can significantly contribute to the maize N supply.

After proving the reuse of resources in cover crop root channels by maize roots, I investigated the effects of cover crop mixtures on sites with different soil types under drought and non-drought conditions. Cover cropping with legume/grass and brassica/grass mixtures significantly enhanced the activities of  $\beta$ -glucosidase, cellobiohydrolase, and xylanase in the rhizosphere of maize under drought stress in root channels in soil with a sandy loam texture (HS) (*Figure 2-1, 2-2*). This indicates an intensive organic matter degradation in the maize rhizosphere at BBCH 50 (Sinsabaugh and Follstad Shah, 2011). In contrast, enzyme activities were lower in the rhizosphere of maize reusing root channels of these cover crop mixtures in soil with sandy texture (KD), independently of the water supply (*Figure 2-2*), indicating lower decomposition rates in these root channels compared to the root channels in the soil with sandy loam texture, indicating a generally lower microbial activity in sandy soils (*Figure 2-3*). This is in line with the study of Siebielec et al. (2020), which revealed that the microbial community is more sensitive to drought in sandy soils, and the input of additional OC is of great importance to protect microbial activity in sandy soils. In the silty loam soil, although the reduction of the rainfall was the same as the other sites, the soil moisture remained relatively high during the drought experiment due to the high-water holding capacity of this soil. The larger hotspots area in maize rhizosphere in this silty loam soil, compared with the other soils, represented the accelerated  $\beta$ -glucosidase activity in the maize rhizosphere due to the more beneficial soil moisture regime (*Figure 2-1, 2-5*). The observed site-specific effects of cover crop mixtures on maize rhizosphere enzyme activity are in line with Muhammad et al. (2021), who demonstrated that the effect of cover crops on microbial C:N ratio in the soil was higher in medium-textured soils (e.g., sandy loam soil in my study) compared to coarser or finer-textured soils.

### 1.4.3 Radio isotope tracing reveals functional redundancy of microbial P mobilization

The regulation of microbial mobilization of C and nutrients is governed by microbial C:N:P stoichiometry (Mooshammer et al., 2012), therefore, understanding the microbial P use strategies is of

great value. Moreover, P is an essential nutrient for microorganisms and plants, and the amount of plant available P in forest soil decreases with forest succession (Prietz et al., 2020; Zhu et al., 2021). I found a higher activity of acid phosphatase in P-poor soil than in P-rich soil (*Figure 3-1*), this is in line with the high activity of acid phosphatase previously determined in low-P forest soils (Lang et al. 2017; Müller et al. 2020). The P-poor soil showed similar acid phosphatase activity, regardless of the diversity of the microbial community (adjusted by dilution of the microbial inoculum in the experiment), demonstrating the redundancy of microbial functions with respect to P mobilization under P-deficient conditions. As long as C and N availability is not limited, microorganisms remain able to produce acid phosphatases at similar activities as in P-rich soil (Loeppmann et al. 2020). The similar acid phosphatase activity in all dilutions of microbial inoculum demonstrated an overall functional redundancy of microbial P mobilization in the P-poor soil (*Figure 3-1*).

The recovery of litter-derived  $^{33}\text{P}$  in microbial biomass regardless of the dilution degree of the microbial inoculum indicates that the immobilization of litter-derived  $^{33}\text{P}$  was not affected by microbial diversity in the P-poor soil (*Figure 3-3*). The 2-fold higher microbial biomass P in P-poor soil (*Figure 3-3*) is in accordance with the high microbial P immobilization (i.e., the tighter cycle of P among microbial biomass P and soil solution) in P-poor soil as demonstrated by Bünemann et al. (2016), and Pistocchi et al. (2018). Notably, the higher recovery of litter- $^{33}\text{P}$  in soil microbial biomass demonstrates a higher proportion of litter P contribution to the microbial P pool in the P-poor soil (*Figure 3-3*), suggesting the fast acquisition of litter-P by microorganisms under P deficiency. The small variation in microbial C:N:P ratios along the gradient of decreasing microbial diversity showed a clear functional redundancy of microorganisms at the P-poor site (*Figure 3-5*), with the aim to maintain stable microbial element ratios. This reflects a fast recovery and re-growth of the microbial guilds already adapted to a balanced mining of nutrients across all dilutions. Irrespective of the total soil nutrient pools, the microbial elemental demand influences the nutrient concentration in the soil solution through microbial community-specific mobilization mechanisms, which are regulated by the element stoichiometry in the soil solution (Chen et al., 2016). Microbial resilience is connected to specific population traits, such as the ability to grow rapidly and to exhibit physiological plasticity (Allison and Martiny, 2008). Such features allow microbial communities to recover from environmental perturbation (Schimel et al., 2007; Shade et al., 2012).

#### **1.4.4 Novel imaging techniques to visualize and localize soil microorganisms and enzymes**

In previous studies, methods for visualizing enzyme activity have primarily focused on hydrolases. This is partly because studying oxidative enzymes is difficult due to their fast turnover rates e.g., phenol oxidase can turn-over 20-fold faster than the hydrolytic enzyme  $\beta$ -glucosidase (Allison, 2006). To address this limitation, I developed a method using fluorescent substrates to quantify and visualize peroxidase activity and distribution based on the already existing micro-zymography technology (Ghaderi et al., 2022). The calibration showed a strong linear correlation ( $R^2 = 0.99$ ) between gray values in the image and resorufin (fluorescent product of Amplex Red after oxidation) concentrations (*Figure 4-1*), and correlations between time ( $t_0 = 10$  seconds after application) and mean gray values were also proved ( $R^2 = 0.95$ ) (*Figure 4-1*). This technique successfully differentiated peroxidase activity at high spatial resolution, showing 2-fold higher peroxidase activity in the rhizosphere of roots with dense root hair coverage compared to the surface of roots with low density of root hair coverage (*Figure 4-5*). The method also revealed that peroxidase activity is twice as high on the root cap compared to the cell division zone (*Figure 4-6*). This is in line with previous findings that peroxidase activity is predominately localized at the root tip (Hall and Sexton, 1972). Similar observations of low peroxidase activity in the cell division zone were also confirmed by Dunand et al. (2007). Thus, the Amplex Red-based micro-zymography method provides a robust tool for distinguishing specific peroxidase activities at the micro-scale with high spatial resolution.

Fluorescence-based microscopy methods not only provide advantages in enzyme activity imaging but can also contribute to exploring the spatial distribution of microorganisms in the complex soil matrix.

Current soil imaging techniques are challenged by, e.g., the autofluorescence of soil components such as quartz minerals and organo-mineral associations, which complicate post-processing and biases outcomes (Schultz et al., 2011). Combining transmitted light and reflection channels in confocal scanning enhances the distinction between microorganisms and mineral surfaces, supporting the direct visualization of aggregate formation processes at the microscale (Krause et al., 2019). To isolate artifacts, I determined the characteristic fluorescence lifetime profiles for *Bacillus subtilis* ( $1.3 \pm 0.1$  ns) and *Rhodotorula mucilaginosa* ( $1.2 \pm 0.2$  ns) in phosphate-buffered saline (Figure 5-5, 5-6). The fluorescence lifetime imaging microscopy (FLIM) combined with the phasor approach effectively differentiates between soil microorganisms and soil particles by capturing dynamic quenching effects and providing a two-dimensional phasor space visualization (Chen et al., 2013; Becker et al., 2004). This method demonstrated minimal interference from mineral backgrounds and enabled a clear separation of microbial signals from soil components (Datta et al., 2020; Ma et al., 2016). The phasor-based FLIM approach demonstrated that microorganisms exhibited a distinct fluorescence lifetime (1.2–1.3 ns) compared to minerals and organo-mineral associations, which typically showed shorter lifetimes (Figure 5-6, 5-7; Chen et al., 2013). Moreover, the technique is more reliable than intensity-based methods for distinguishing microbial signals from the soil matrix, as it minimizes interference from autofluorescence and provides stable lifetime measurements over time (Datta et al., 2020; Lakowicz et al., 1992). Despite limitations like variability due to cell age or metabolic state, FLIM combined with the phasor approach is a promising tool for future soil microbiology research.

## 1.5 Conclusions

The results in my study underline that:

- 1) Plant root-derived OM in root channels can provide easily available resources for subsequent growing plant roots and their microbiome, as demonstrated by  $^{13}\text{C}$  and  $^{15}\text{N}$  labeling. Specific cover crop mixtures, such as legume/grass combinations, can promote microbial C fixation in the subsoil and their root channels provide readily available N for maize nutrition.
- 2) Functions involved in microbial P mobilization are highly redundant in soils, and this functional redundancy is highly site-specific, depending on the soil P stock of the site. Microbial biomass P plays an important role as intermediate P reservoir for microorganisms to cope with soil P-deficiency.
- 3) Amplex Red-based micro-zymography method provides a robust tool for visualizing peroxidase activity at the micro-scale with high spatial resolution and FLIM with the phasor approach can effectively differentiate soil microorganisms from the organo-mineral background in soil, providing a reliable tool for soil microbiology research by minimizing autofluorescence interference and offering stable lifetime measurements.

Overall, this study enhances the understanding of the interconnected C, N, and P cycles in soils, and reveals the key role of microorganisms in soil C and nutrient cycling, using advanced imaging techniques and isotope labeling. Future research should combine comprehensive isotope labeling methods ( $^{13}\text{C}$ ,  $^{15}\text{N}$ ,  $^{33}\text{P}$ ) with advanced imaging techniques such as FLIM to precisely track and visualize nutrient cycling at the soil-plant-microbial interface.

## 1.6 References

- Ai, J. et al. What controls the availability of organic and inorganic P sources in top-and subsoils? A  $^{33}\text{P}$  isotopic labeling study with root exudate addition. *Soil Biol. Biochem.* 185, 109129 (2023). <https://doi.org/10.1016/j.soilbio.2023.109129>
- Alimova, A. et al. Native fluorescence and excitation spectroscopic changes in *Bacillus subtilis* and *Staphylococcus aureus* bacteria subjected to conditions of starvation. *Appl. Opt.* 42, 4080 (2003). <https://doi.org/10.1364/ao.42.004080>
- Allison, S. D., & Martiny, J. B. Resistance, resilience, and redundancy in microbial communities. *Proceedings of the National Academy of Sciences*, 105, 11512-11519 (2008). <https://doi.org/10.1073/pnas.0801925105>
- Allison, S.D. Soil minerals and humic acids alter enzyme stability: implications for ecosystem processes. *Biogeochemistry* 81, 361–373 (2006). <https://doi.org/10.1007/s10533-006-9046-2>
- Alvarez, G. et al. Catalytic power of enzymes decreases with temperature: New insights for understanding soil C cycling and microbial ecology under warming. *Glob. Change Biol.* 24, 4238-4250 (2018). <https://doi.org/10.1111/gcb.14281>
- Balke, J. et al. Visualizing oxidative cellular stress induced by nanoparticles in the subcytotoxic range using fluorescence lifetime imaging. *Small* 14, 1–11 (2018). <https://doi.org/10.1002/smll.201800310>
- Banfield, C. C. New tools for dead roots: Radioisotope labelling and compound-specific analysis reveal how subsoil hotspots work. *Journal of Plant Nutrition and Soil Science*, 185(6), 707-719 (2022). <https://doi.org/10.1002/jpln.202200272>
- Bardgett, R.D. & Wardle, D.A. Aboveground-belowground linkages: biotic interactions, ecosystem processes, and global change. (Oxford University Press, 2010).
- Bastida, F. et al. Soil microbial diversity–biomass relationships are driven by soil carbon content across global biomes. *ISME J.* 15, 2081-2091 (2021). <https://doi.org/10.1038/s41396-021-00925-0>
- Becker W, Bergmann A, Hink MA, König K, Benndorf K, Biskup C. Fluorescence lifetime imaging by time-correlated single-photon counting. *Microsc Res Tech* 63:58–66 (2004). <https://doi.org/10.1002/jemt.10421>
- Beveridge, T.J., Moyles, D. & Harris, B. Electron Microscopy. in *Methods for General and Molecular Microbiology* (eds. Reddy, C.A. et al.) 54–81 (ASM Press, 2014). <https://doi.org/10.1128/9781555817497.ch4>
- Bilyera, N. et al. How “hot” are hotspots: Statistically localizing the high-activity areas on soil and rhizosphere images. *Rhizosphere* 16, 100259 (2020). <https://doi.org/10.1016/j.rhisph.2020.100259>
- Bilyera, N., Kuzyakov, Y. Soil zymography: A decade of rapid development in microbial hotspot imaging. *Soil Biol. Biochem.* 109264 (2023). <https://doi.org/10.1016/j.soilbio.2017.01.009>
- Bokota, G. et al. PartSeg: a tool for quantitative feature extraction from 3D microscopy images for dummies. *BMC Bioinformatics* 22, 1–16 (2021). <https://doi.org/10.1186/s12859-021-03984-1>
- Bore, E.K. et al. Microbial metabolism in soil at subzero temperatures: Adaptation mechanisms revealed by position-specific  $^{13}\text{C}$  labeling. *Front. Microbiol.* 8, 946 (2017). <https://doi.org/10.3389/fmicb.2017.00946>
- Brödlin, D., Kaiser, K., Kessler, A. & Hagedorn, F. Drying and rewetting foster phosphorus depletion of forest soils. *Soil Biol. Biochem.* 128, 22-34 (2019). <https://doi.org/10.1016/j.soilbio.2018.10.001>
- Bromand, S. et al. A pulse-labelling method to generate  $^{13}\text{C}$ - enriched plant materials.
- Bünemann, E.K. et al. Phosphorus Dynamics in a Highly Weathered Soil as Revealed by Isotopic Labeling Techniques. *Soil Sci. Soc. Am. J.* 68, 1645-1655 (2004). <https://doi.org/10.2136/sssaj2004.1645>
- Bünemann, E.K., Augstburger, S. & Frossard, E. Dominance of either physicochemical or biological phosphorus cycling processes in temperate forest soils of contrasting phosphate availability. *Soil Biol. Biochem.* 101, 85-95 (2016). <https://doi.org/10.1016/j.soilbio.2016.07.005>
- Chen LC, Lloyd III WR, Chang CW, Sud D, Mycek MA. Fluorescence lifetime imaging microscopy for quantitative biological imaging. In: *Methods in cell biology*, vol 114. Academic Press, pp 457–488 ((2013). <https://doi.org/10.1016/B978-0-12-407761-4.00020-8>
- Chen, G., & Weil, R. R. Penetration of cover crop roots through compacted soils. *Plant and Soil*, 331, 31-43 (2010). <https://doi.org/10.1007/s11104-009-0223-7>
- Chen, J. et al. Microbial C:N stoichiometry and turnover depend on nutrients availability in soil: A  $^{14}\text{C}$ ,  $^{15}\text{N}$  and  $^{33}\text{P}$  triple labelling study. *Soil Biol. Biochem.* 131, 206-216 (2019). <https://doi.org/10.1016/j.soilbio.2019.01.017>
- Chen, Yong-Liang, Lei-Yi Chen, Yun-Feng Peng, Jin-Zhi Ding, Fei Li, Gui-Biao Yang, Dan Kou, et al. Linking microbial C:N:P stoichiometry to microbial community and abiotic factors along a 3500-km grassland transect on the Tibetan Plateau. *Global Ecology and Biogeography* 25: 1416–1427 (2016). <https://doi.org/10.1111/geb.12500>
- Cleveland, C. C., & Liptzin, D. C: N: P stoichiometry in soil: is there a “Redfield ratio” for the microbial biomass?. *Biogeochemistry*, 85, 235-252 (2007). <https://doi.org/10.1007/s10533-007-9132-0>
- Datta R, Heaster TM, Sharick JT, Gillette AA, Skala MC. Fluorescence lifetime imaging microscopy: fundamentals and advances in instrumentation, analysis, and applications. *J Biomed Opt* 25:1 (2020). <https://doi.org/10.1117/1.jbo.25.7.071203>
- Di, H.J., Condon, L.M. & Frossard, E. Isotope techniques to study phosphorus cycling in agricultural and forest soils: a review. *Biol. Fertil. Soils* 24, 1-12 (1997). <https://doi.org/10.1007/BF01420213>

- Digman, M. A., Caiolfa, V. R., Zamai, M. & Gratton, E. The phasor approach to fluorescence lifetime imaging analysis. *Biophys. J.* 94, 14–16 (2008). <https://doi.org/10.1529/biophysj.107.120154>
- Dippold, M.A. & Kuzyakov, Y. Biogeochemical transformations of amino acids in soil assessed by position-specific labelling. *Plant Soil* 373, 385–401 (2013). <https://doi.org/10.1007/s11104-013-1764-3>
- Dorodnikov, M., Kuzyakov, Y., Fangmeier, A. & Flessa, H. C and N in soil organic matter density fractions under elevated atmospheric CO<sub>2</sub>: turnover vs. stabilization. *Soil Biol. Biochem.* 43, 579–589 (2011). <https://doi.org/10.1016/j.soilbio.2010.11.026>
- Dufil, G., Parker, D., Gerasimov, J.Y., Nguyen, T.-Q., Berggren, M., Stavriniidou, E. Enzyme-assisted in vivo polymerisation of conjugated oligomer-based conductors. *J. Mater. Chem. B* 8, 4221–4227 (2020). <https://doi.org/10.1039/D0TB00212G>
- Dunand, C., Crèvecoeur, M., Penel, C. Distribution of superoxide and hydrogen peroxide in Arabidopsis root and their influence on root development: possible interaction with peroxidases. *New Phytologist* 174, 332–341 (2007). <https://doi.org/10.1111/j.1469-8137.2007.01995.x>
- Eickhorst, T. & Tippkötter, R. Detection of microorganisms in undisturbed soil by combining fluorescence in situ hybridization (FISH) and micropedological methods. *Soil Biol. Biochem.* 40, 1284–1293 (2008). <https://doi.org/10.1016/j.soilbio.2007.06.019>
- Fahey, T.J., Yavitt, J.B. & Sherman, R.E. Partitioning of belowground C in young sugar maple forest. *Plant Soil* 367, 379–389 (2013). <https://doi.org/10.1007/s11104-012-1459-1>
- Feng, J. et al. Changes in plant inputs alter soil carbon and microbial communities in forest ecosystems. *Glob. Change Biol.* 28, 3426–3440 (2022). <https://doi.org/10.1111/gcb.16107>
- Fernández-Suárez, M. & Ting, A. Y. Fluorescent probes for super-resolution imaging in living cells. *Nat. Rev. Mol. Cell Biol.* 9, 929–943 (2008). <https://doi.org/10.1038/nrm2531>
- Finzi, A.C. et al. Rhizosphere processes are quantitatively important components of terrestrial carbon and nutrient cycles. *Glob. Change Biol.* 21, 2082–2094 (2015). <https://doi.org/10.1111/gcb.12816>
- Fu, Y. et al. Rhizosphere microbiome modulated effects of biochar on ryegrass 15N uptake and rhizodeposited <sup>13</sup>C allocation in soil. *Plant Soil* 463, 359–377 (2021). <https://doi.org/10.1007/s11104-021-04845-9>
- Ghaderi, N., Schmidt, H., Schlüter, S. et al. Development of micro-zymography: Visualization of enzymatic activity at the microscopic scale for aggregates collected from the rhizosphere. *Plant Soil* 478, 253–271 (2022). <https://doi.org/10.1007/s11104-022-05573-4>
- Gleixner, G. Soil organic matter dynamics: a biological perspective derived from the use of compound-specific isotopes studies. *Ecol. Res.* 28, 683–695 (2013). <https://doi.org/10.1007/s11284-012-1022-9>
- Guber, A. & Kravchenko, A. Time-lapse soil zymography (TLZ) protocol and data processing. *Methods Ecol. Evol.* 12, 1105–1119 (2021). <https://doi.org/10.1016/j.soilbio.2021.108225>
- Guber, A. et al. Quantitative soil zymography: Mechanisms, processes of substrate and enzyme diffusion in porous media. *Soil Biol. Biochem.* 127, 156–167 (2018). <https://doi.org/10.1016/j.soilbio.2018.09.030>
- Guo, R. et al. Exploring optimal nitrogen management for high yielding maize in arid areas via <sup>15</sup>N-labeled technique. *Geoderma* 382, 114711 (2021). <https://doi.org/10.1016/j.geoderma.2020.114711>
- Hagedorn, F., & Bundt, M. The age of preferential flow paths. *Geoderma*, 108(1-2), 119–132 (2002). [https://doi.org/10.1016/S0016-7061\(02\)00129-5](https://doi.org/10.1016/S0016-7061(02)00129-5)
- Hall, J.L., Sexton, R. Cytochemical localization of peroxidase activity in root cells. *Planta* 108, 103–120 (1972). <https://doi.org/10.1007/BF00386073>
- Hayek, A. et al. Cell-permeant cytoplasmic blue fluorophores optimized for in vivo two-photon microscopy with low-power excitation. *Microsc. Res. Tech.* 70, 880–885 (2007). <https://doi.org/10.1002/jemt.20493>
- Hellmuth KH, Sammaljärvi J, Siitari-Kauppi M, Robinet JC, Sardini P. STED nanoscopy—A novel way to image the pore space of geological materials. *Journal of Microscopy*, 283(2), 151–165. (2021) <https://doi.org/10.1111/jmi.13016>
- Hertenberger, G. & Wanek, W. Evaluation of methods to measure differential <sup>15</sup>N labeling of soil and root N pools for studies of root exudation. *Rapid Commun. Mass Spectrom.* 18, 2415–2425 (2004). <https://doi.org/10.1002/rcm.1583>
- Hoang, D.T.T., Razavi, B.S., Kuzyakov, Y., Blagodatskaya, E. Earthworm burrows: Kinetics and spatial distribution of enzymes of C-, N- and P- cycles. *Soil Biol. Biochem.* 99, 94–103 (2016). <https://doi.org/10.1016/j.soilbio.2016.04.021>
- Hobbie, S.E. Plant species effects on nutrient cycling: revisiting litter feedbacks. *Trends Ecol. Evol.* 30, 357–363 (2015). <https://doi.org/10.1016/j.tree.2015.03.015>
- Jaafar, N. M., Clode, P. L. & Abbott, L. K. Microscopy observations of habitable space in biochar for colonization by fungal hyphae from soil. *J. Integr. Agric.* 13, 483–490 (2014). [https://doi.org/10.1016/S2095-3119\(13\)60703-0](https://doi.org/10.1016/S2095-3119(13)60703-0)
- Khosrozadeh, S., Guber, A., Kravchenko, A., Ghaderi, N., Blagodatskaya, E. Soil oxidoreductase zymography: Visualizing spatial distributions of peroxidase and phenol oxidase activities at the root-soil interface. *Soil Biol. Biochem.* 167, 108610 (2022). <https://doi.org/10.1016/j.soilbio.2022.108610>

- Krause L, Biesgen D, Treder A, Schweizer SA, Klumpp E, Knief C, Siebers N. Initial microaggregate formation: association of microorganisms to montmorillonite-goethite aggregates under wetting and drying cycles. *Geoderma* 351:250–260 (2019). <https://doi.org/10.1016/j.geoderma.2019.05.001>
- Kravchenko, A.N., Guber, A.K., Razavi, B.S., Koestel, J., Blagodatskaya, E.V., Kuzyakov, Y. Spatial patterns of extracellular enzymes: Combining X-ray computed micro-tomography and 2D zymography. *Soil Biol. Biochem.* 135, 411–419 (2019). <https://doi.org/10.1016/j.soilbio.2019.06.002>
- Kušlienė, G., Rasmussen, J., Kuzyakov, Y., et al. Medium-term response of microbial community to rhizodeposits of white clover and ryegrass and tracing of active processes induced by <sup>13</sup>C and <sup>15</sup>N labelled exudates. *Soil Biol. Biochem.* 76, 22–33 (2014). <https://doi.org/10.1016/j.soilbio.2014.05.003>
- Kuzyakov, Y., Blagodatskaya, E. Microbial hotspots and hot moments in soil: concept & review. *Soil Biol. Biochem.* 83, 184–199 (2015). <https://doi.org/10.1016/j.soilbio.2015.01.025>
- Kuzyakov, Y., Domanski, G. Carbon Input by Plants into the Soil. *J. Plant Nutr. Soil Sci.* 163, 389–408 (2000). [https://doi.org/10.1002/1522-2624\(200008\)163:4<421::AID-JPLN421>3.0.CO;2-R](https://doi.org/10.1002/1522-2624(200008)163:4<421::AID-JPLN421>3.0.CO;2-R)
- Kuzyakov, Y., et al. Carbon Dynamics in the Rhizosphere of Different Plant Species and its Impact on Soil Fertility. *Soil Biol. Biochem.* 34, 1527–1535 (2002). [https://doi.org/10.1016/S0038-0717\(02\)00109-6](https://doi.org/10.1016/S0038-0717(02)00109-6)
- Kuzyakov, Y., Schneckenberger, K. Review of estimation of plant rhizodeposition and their contribution to soil organic matter formation. *Arch. Agron. Soil Sci.* 50, 115–132 (2004). <https://doi.org/10.1080/03650340310001627658>
- Ladygina, N., Hedlund, K. Plant species influence microbial diversity and carbon allocation in the rhizosphere. *Soil Biol. Biochem.* 42, 162–168 (2010). <https://doi.org/10.1016/j.soilbio.2009.10.009>
- Lakowicz JR, Szmanski H, Nowaczyk K, Berndt KW, Johnson M. Fluorescence lifetime imaging. *Anal Biochem* 202:316–330 (1992). [https://doi.org/10.1016/0003-2697\(92\)90112-K](https://doi.org/10.1016/0003-2697(92)90112-K)
- Lang, F., J. Krüger, W. Amelung, S. Willbold, E. Frossard, E. K. Bünemann, J. Bauhus, et al. Soil phosphorus supply controls P nutrition strategies of beech forest ecosystems in Central Europe. *Biogeochemistry* 136: 5–29 (2017). <https://doi.org/10.1007/s10533-017-0375-0>
- Lange, M., Eisenhauer, N., Sierra, C.A., et al. Plant diversity increases soil microbial activity and soil carbon storage. *Nat. Commun.* 6, 6707 (2015). <https://doi.org/10.1038/ncomms7707>
- Lange, M., Koller-France, E., Hildebrandt, A., et al. How plant diversity impacts the coupled water, nutrient and carbon cycles. *Adv. Ecol. Res.* 61, 185–219 (2019). <https://doi.org/10.1016/bs.aecr.2019.06.005>
- Lee, J., Hestrin, R., Nuccio, E. E., Morrison, K. D., Ramon, C. E., Samo, T. J., ... & Weber, P. K.. Label-free multiphoton imaging of microbes in root, mineral, and soil matrices with time-gated coherent Raman and fluorescence lifetime imaging. *Environmental Science & Technology*, 56(3), 1994–2008 (2022). <https://doi.org/10.1021/acs.est.1c05818>
- Lehmann, J., Kleber, M. Better Soil Organic Carbon Management. *Nature* 528, 44–45 (2015). <https://doi.org/10.1038/528044a>
- Lehmann, M.M., Goldsmith, G.R., Schmid, L., et al. The effect of <sup>18</sup>O-labelled water vapour on the oxygen isotope ratio of water and assimilates in plants at high humidity. *New Phytol.* 217, 105–116 (2018). <https://doi.org/10.1111/nph.14788>
- Li, Y., Dick, W. A. & Tuovinen, O. H. Fluorescence microscopy for visualization of soil microorganisms—A review. *Biol. Fertil. Soils* 39, 301–311 (2004). <https://doi.org/10.1007/s00374-004-0722-x>
- Liang, C., Schimel, J. P., & Jastrow, J. D. The importance of anabolism in microbial control over soil carbon storage. *Nature microbiology*, 2(8), 1–6 (2017). <https://doi.org/10.1038/nmicrobiol.2017.105>
- Lo Piccolo, S. et al. Presence of endophytic bacteria in *Vitis vinifera* leaves as detected by fluorescence in situ hybridization. *Ann. Microbiol.* 60, 161–167 (2010). <https://doi.org/10.1007/s13213-010-0023-6>
- Loeppmann, S., Breidenbach, A., Spielvogel, S., Dippold, M. A., & Blagodatskaya, E. Organic nutrients induced coupled C-and P-cycling enzyme activities during microbial growth in forest soils. *Frontiers in Forests and Global Change*, 3, 100 (2020). <https://doi.org/10.3389/ffgc.2020.00100>
- Loeppmann, S., Semenov, M., Kuzyakov, Y. & Blagodatskaya, E. Shift from dormancy to microbial growth revealed by RNA ratio. *Ecol. Indic.* 85, 603–612 (2018). <https://doi.org/10.1016/j.ecolind.2017.11.020>
- Ma N, Digman MA, Malacrida L, Gratton E. Measurements of absolute concentrations of NADH in cells using the phasor FLIM method. *Biomed Opt Express* 7:2441 (2016). <https://doi.org/10.1364/boe.7.002441>
- Ma, Q., Kuzyakov, Y., Pan, W., et al. Substrate control of sulphur utilisation and microbial stoichiometry in soil: Results of <sup>13</sup>C, <sup>15</sup>N, <sup>14</sup>C, and <sup>35</sup>S quad labelling. *ISME J.* 15, 3148–3158 (2021). <https://doi.org/10.1038/s41396-021-00999-7>
- Ma, X., Razavi, B.S., Holz, M., Blagodatskaya, E., Kuzyakov, Y. Warming increases hotspot areas of enzyme activity and shortens the duration of hot moments in the root-detritusphere. *Soil Biol. Biochem.* 107, 226–233 (2017). <https://doi.org/10.1016/j.soilbio.2017.01.009>
- Ma, X., Zarebanadkouki, M., Kuzyakov, Y., et al. Spatial patterns of enzyme activities in the rhizosphere: effects of root hairs and root radius. *Soil Biol. Biochem.* 118, 69–78 (2018). <https://doi.org/10.1016/j.soilbio.2017.12.009>
- Mannam, V. et al. Convolutional neural network denoising in fluorescence lifetime imaging microscopy (FLIM). In *Multiphoton Microscopy in the Biomedical Sciences XXI*, vol. 11648, 101–108 (SPIE, 2021).

- Mayer, J., Buegger, F., Jensen, E.S., et al. Estimating N rhizodeposition of grain legumes using a  $^{15}\text{N}$  in situ stem labelling method. *Soil Biol. Biochem.* 35, 21–28 (2003). [https://doi.org/10.1016/S0038-0717\(02\)00212-2](https://doi.org/10.1016/S0038-0717(02)00212-2)
- Michaelis, L., Menten, M.L. Die kinetik der invertinwirkung. *Biochem. Z.* 49, 352 (1913).
- Mooshammer, Maria, Wolfgang Wanek, Jörg Schneckner, Birgit Wild, Sonja Leitner, Florian Hofhansl, Andreas Blöchl, et al. Stoichiometric controls of nitrogen and phosphorus cycling in decomposing beech leaf litter. *Ecology* 93: 770–782 (2012). <https://doi.org/10.1890/11-0721.1>
- Muhammad, I., Wang, J., Sainju, U.M., Zhang, S., Zhao, F., Khan, A. Cover cropping enhances soil microbial biomass and affects microbial community structure: A meta-analysis. *Geoderma* 381, 114696 (2021). <https://doi.org/10.1016/j.geoderma.2020.114696>
- Müller, C., Bünemann, E.K. A  $^{33}\text{P}$  tracing model for quantifying gross P transformation rates in soil. *Soil Biol. Biochem.* 76, 218–226 (2014). <https://doi.org/10.1016/j.soilbio.2014.05.013>
- Müller, Karolin, Nadine Kubsch, Sven Marhan, Paula Mayer-Gruner, Pascal Nassal, Dominik Schneider, Rolf Daniel, Hans-Peter Piepho, Andrea Polle, and Ellen Kandeler. Saprotrophic and Ectomycorrhizal Fungi Contribute Differentially to Organic P Mobilization in Beech-Dominated Forest Ecosystems. *Frontiers in Forests and Global Change* 3: 47 (2020). <https://doi.org/10.3389/ffgc.2020.00047>
- Murphy, C.J., Baggs, E.M., Morley, N., et al. Rhizosphere priming can promote mobilisation of N-rich compounds from soil organic matter. *Soil Biol. Biochem.* 81, 236–243 (2015). <https://doi.org/10.1016/j.soilbio.2014.11.027>
- Nannipieri, P., Giagnoni, L., Renella, G., et al. Soil enzymology: classical and molecular approaches. *Biol. Fertil. Soils* 48, 743–762 (2012). <https://doi.org/10.1007/s00374-012-0723-0>
- Oehl, F., Oberson, A., Sinaj, S., et al. Organic phosphorus mineralization studies using isotopic dilution techniques. *Soil Sci. Soc. Am. J.* 65, 780–787 (2001). <https://doi.org/10.2136/sssaj2001.653780x>
- O'Neill, R. M., Krol, D. J., Wall, D., Lanigan, G. J., Renou-Wilson, F., Richards, K. G., ... & Müller, C. Assessing the impact of long-term soil phosphorus on N-transformation pathways using  $^{15}\text{N}$  tracing. *Soil Biology and Biochemistry*, 152, 108066 (2021). <https://doi.org/10.1016/j.soilbio.2020.108066>
- Pang, R., Xu, X., Tian, Y., et al. In-situ  $^{13}\text{C}$  labeling to trace carbon fluxes in plant-soil-microorganism systems: Review and methodological guideline. *Rhizosphere* 20, 100441 (2021). <https://doi.org/10.1016/j.rhisph.2021.100441>
- Paterson, E., Gebbing, T., Abel, C., Sim, A., & Telfer, G. Rhizodeposition shapes rhizosphere microbial community structure in organic soil. *New Phytologist*, 173(3), 600–610 (2007). <https://doi.org/10.1111/j.1469-8137.2006.01931.x>
- Pausch, J., & Kuzyakov, Y. Carbon input by roots into the soil: quantification of rhizodeposition from root to ecosystem scale. *Global change biology*, 24(1), 1–12 (2018). <https://doi.org/10.1111/gcb.13850>
- Pausch, J., Kuzyakov, Y. Photoassimilate allocation and dynamics of hotspots in roots visualized by  $^{14}\text{C}$  phosphor imaging. *J. Plant Nutr. Soil Sci.* 174, 12–19 (2011). <https://doi.org/10.1002/JPLN.200900271>
- Pett-Ridge, J. & Firestone, M. K. Using stable isotopes to explore root-microbe-mineral interactions in soil. *Rhizosphere* 3, 244–253 (2018). <https://doi.org/10.1016/j.rhisph.2018.03.001>
- Petzoldt, L., Athmann, M., Buechse, A., & Kautz, T. Root Growth of *Hordeum vulgare* and *Vicia faba* in the Biopore Sheath. *Agriculture*, 10(12), 650 (2020). <https://doi.org/10.3390/agriculture10120650>
- Petzoldt, L., Athmann, M., Buechse, A., et al. Root Growth of *Hordeum vulgare* and *Vicia faba* in the Biopore Sheath. *Agriculture* 10, 650 (2020). <https://doi.org/10.3390/agriculture10120650>
- Pistocchi, Chiara, Éva Mészáros, Federica Tamburini, Emmanuel Frossard, and Else Katrin Bünemann. Biological processes dominate phosphorus dynamics under low phosphorus availability in organic horizons of temperate forest soils. *Soil Biology and Biochemistry* 126: 64–75 (2018). <https://doi.org/10.1016/j.soilbio.2018.08.013>
- Prietzl, J., Falk, W., Reger, B., Uhl, E., Pretzsch, H., & Zimmermann, L. Half a century of Scots pine forest ecosystem monitoring reveals long-term effects of atmospheric deposition and climate change. *Global Change Biology*, 26(10), 5796–5815 (2020). <https://doi.org/10.1111/gcb.15265>
- Qiao, Y., Miao, S., Li, N., et al. Spatial distribution of rhizodeposit carbon of maize (*Zea mays* L.) in soil aggregates assessed by multiple pulse  $^{13}\text{C}$  labeling in the field. *Plant Soil* 375, 317–329 (2014). <https://doi.org/10.1007/s11104-013-1932-5>
- Quigley, M.Y., Kravchenko, A.N. Inputs of root-derived carbon into soil and its losses are associated with pore-size distributions. *Geoderma* 410, 115667 (2022). <https://doi.org/10.1016/j.geoderma.2021.115667>
- Razavi, B.S., Blagodatskaya, E., Kuzyakov, Y. Nonlinear temperature sensitivity of enzyme kinetics explains canceling effect—a case study on loamy haplic Luvisol. *Front. Microbiol.* 6, 336 (2015). <https://doi.org/10.3389/fmicb.2015.00336>
- Razavi, B.S., Blagodatskaya, E., Kuzyakov, Y. Temperature selects for static soil enzyme systems to maintain high catalytic efficiency. *Soil Biol. Biochem.* 97, 15–22 (2016). <https://doi.org/10.1016/j.soilbio.2016.02.018>
- Razavi, B.S., Zhang, X., Bilyera, N., et al. Soil zymography: simple and reliable? Review of current knowledge and optimization of the method. *Rhizosphere* 11, 100161 (2019). <https://doi.org/10.1016/j.rhisph.2019.100161>
- Robinson, J.R.  $^{33}\text{P}$ : a superior radiotracer for phosphorus?. *Int. J. Appl. Radiat. Isot.* 20, 531–540 (1969). [https://doi.org/10.1016/0020-708X\(69\)90007-6](https://doi.org/10.1016/0020-708X(69)90007-6)

- Rohr, A.D., Schimmel, J., Liu, B., et al. Identification and validation of early genetic biomarkers for apple replant disease. *PLoS One* 15, e0238876 (2020). <https://doi.org/10.1371/journal.pone.0238876>
- Russell, C.A., Fillery, I.R.P. In situ <sup>15</sup>N labelling of lupin below-ground biomass. *Aust. J. Agric. Res.* 47, 1035–1046 (1996). <https://doi.org/10.1071/ar9961035>
- Rutan, J., Rosenzweig, N., Steinke, K. Impact of Cover Crops and Nitrogen Management on Soil Bacterial Alpha Diversity. *Commun. Soil Sci. Plant Anal.* 54, 2113–2125 (2023). <https://doi.org/10.1080/00103624.2023.2211605>
- Sauer, D., Kuzyakov, Y., Stahr, K. Spatial distribution of root exudates of five plant species as assessed by <sup>14</sup>C labeling. *J. Plant Nutr. Soil Sci.* 169, 360–362 (2006). <https://doi.org/10.1002/jpln.200621974>
- Schimel, Joshua, Teri C. Balsler, and Matthew Wallenstein. Microbial Stress-Response Physiology and Its Implications for Ecosystem Function. *Ecology* 88: 1386–1394 (2007). <https://doi.org/10.1890/06-0219>
- Schultz L, Pitts B, Mitchell AC, Cunningham AB, Gerlach R. Imaging biologically induced mineralization in fully hydrated flow systems. *Micros Today* 19:12–15 (2011). <https://doi.org/10.1017/s1551929511000848>
- Shade, Ashley, Jordan S. Read, Nicholas D. Youngblut, Noah Fierer, Rob Knight, Timothy K. Kratz, Noah R. Lottig, et al. Lake microbial communities are resilient after a whole-ecosystem disturbance. *The ISME Journal* 6. Nature Publishing Group: 2153–2167 (2012). <https://doi.org/10.1038/ismej.2012.56>
- Siebielec, S., Siebielec, G., Klimkowicz-Pawlas, A., Gałązka, A., Grządziel, J., & Stuczyński, T. Impact of water stress on microbial community and activity in sandy and loamy soils. *Agronomy*, 10(9), 1429 (2020). <https://doi.org/10.3390/agronomy10091429>
- Siegenthaler, M.B., Tamburini, F., Frossard, E., et al. A dual isotopic (<sup>32</sup>P and <sup>18</sup>O) incubation study to disentangle mechanisms controlling phosphorus cycling in soils from a climatic gradient (Kohala, Hawaii). *Soil Biol. Biochem.* 149, 107920 (2020). <https://doi.org/10.1016/j.soilbio.2020.107920>
- Sinsabaugh, R. L., & Follstad Shah, J. J. Ecoenzymatic stoichiometry of recalcitrant organic matter decomposition: the growth rate hypothesis in reverse. *Biogeochemistry*, 102, 31-43 (2011). <https://doi.org/10.1007/s10533-010-9482-x>
- Sinsabaugh, R.L., Carreiro, M.M., Alvarez, S. Enzyme and microbial dynamics of litter decomposition. *Enzymes in the Environment, Activity, Ecology, and Applications* 249–265 (2002). <https://doi.org/10.1201/9780203904039.ch9>
- Smercina, D.N., Bailey, V.L., Hofmockel, K.S. Micro on a macroscale: relating microbial-scale soil processes to global ecosystem function. *FEMS Microbiol. Ecol.* 97, fiab091 (2021). <https://doi.org/10.1093/femsec/fiab091>
- Spohn, M., Carminati, A., Kuzyakov, Y. Soil zymography—a novel in situ method for mapping distribution of enzyme activity in soil. *Soil Biol. Biochem.* 58, 275–280 (2013). <https://doi.org/10.1016/j.soilbio.2012.12.004>
- Spohn, M., Ermak, A., Kuzyakov, Y. Microbial gross organic phosphorus mineralization can be stimulated by root exudates—a <sup>33</sup>P isotopic dilution study. *Soil Biol. Biochem.* 65, 254–263 (2013). <https://doi.org/10.1016/j.soilbio.2013.05.028>
- Spohn, M., Kuzyakov, Y. Spatial and temporal dynamics of enzyme activities in soil: A new approach to measure and map enzyme activities. *Soil Biol. Biochem.* 76, 22–32 (2014). <https://doi.org/10.1016/j.soilbio.2014.04.010>
- Stevenel, P., Frossard, E., Abiven, S., et al. Using a tri-isotope (<sup>13</sup>C, <sup>15</sup>N, <sup>33</sup>P) labelling method to quantify rhizodeposition. *Methods Rhizosphere Biol. Res.* 169–195 (2019). [https://doi.org/10.1007/978-981-13-5767-1\\_10](https://doi.org/10.1007/978-981-13-5767-1_10)
- Stewart, J., Moran, C. & Wood, J. Macropore sheath: quantification of plant root and soil macropore association. *Plant and Soil* 211, 59–67 (1999). <https://doi.org/10.1023/A:1004405422847>
- Sun, L., Qu, L., Moorhead, D.L., et al. Interpreting the differences in microbial carbon and nitrogen use efficiencies estimated by <sup>18</sup>O labeling and ecoenzyme stoichiometry. *Geoderma* 444, 116856 (2024). <https://doi.org/10.1016/j.geoderma.2024.116856>
- Teixeira, P.P.C., Trautmann, S., Buegger, F., et al. Role of root hair elongation in rhizosheath aggregation and in the carbon flow into the soil. *Biol. Fertil. Soils* 59, 351–361 (2023). <https://doi.org/10.1007/s00374-023-01708-6>
- Teixeira, P.P.C., Vidal, A., Teixeira, A.P.M., et al. Decoding the rhizodeposit-derived carbon’s journey into soil organic matter. *Geoderma* 443, 116811 (2024). <https://doi.org/10.1016/j.geoderma.2024.116811>
- Tippkötter, R., Ritz, K. & Darshbury, J. F. The preparation of soil thin sections for biological studies. *J. Soil Sci.* 37, 681–690 (1986). <https://doi.org/10.1111/j.1365-2389.1986.tb00396.x>
- Trivedi, P., Anderson, I. C., & Singh, B. K. Microbial modulators of soil carbon storage: integrating genomic and metabolic knowledge for global prediction. *Trends in microbiology*, 21(12), 641-651(2013). <https://doi.org/10.1016/j.tim.2013.09.005>
- Van Ginkel, J. H., Gorissen, A., & Polci, D. Elevated atmospheric carbon dioxide concentration: effects of increased carbon input in a *Lolium perenne* soil on microorganisms and decomposition. *Soil Biology and Biochemistry*, 32(4), 449-456(2000). [https://doi.org/10.1016/S0038-0717\(99\)00097-8](https://doi.org/10.1016/S0038-0717(99)00097-8)
- Wahlström, E. M., Kristensen, H. L., Thomsen, I. K., Labouriau, R., Pulido-Moncada, M., Nielsen, J. A., & Munkholm, L. J. Subsoil compaction effect on spatio-temporal root growth, reuse of biopores and crop yield of spring barley. *European Journal of Agronomy*, 123, 126225 (2021). <https://doi.org/10.1016/j.eja.2020.126225>

- Wang, C., Dippold, M.A., Kuzyakov, Y., et al. Microbial strategies for phosphorus acquisition in rice paddies under contrasting water regimes: Multiple source tracing by  $^{32}\text{P}$  and  $^{33}\text{P}$ . *Sci. Total Environ.* 918, 170738 (2024). <https://doi.org/10.1016/j.soilbio.2024.109359>
- Wang, C., Thielemann, L., Dippold, M.A., et al. Microbial iron reduction compensates for phosphorus limitation in paddy soils. *Sci. Total Environ.* 837, 155810 (2022). <https://doi.org/10.1016/j.scitotenv.2022.155810>
- Wang, D., Chadwick, D.R., Hill, P.W., et al. Tracing the mineralization rates of C, N and S from cysteine and methionine in a grassland soil: A  $^{14}\text{C}$  and  $^{35}\text{S}$  dual-labelling study. *Soil Biol. Biochem.* 177, 108906 (2023). <https://doi.org/10.1016/j.soilbio.2022.108906>
- Wang, R., Bicharanloo, B., Shirvan, M.B., et al. A novel  $^{13}\text{C}$  pulse-labelling method to quantify the contribution of rhizodeposits to soil respiration in a grassland exposed to drought and nitrogen addition. *New Phytol.* 230, 857–866 (2021). <https://doi.org/10.1111/nph.17118>
- Wang, X. et al. Elevated temperature increases the accumulation of microbial necromass nitrogen in soil via increasing microbial turnover. *Glob. Chang. Biol.* 26, 5277–5289 (2020). <https://doi.org/10.1111/gcb.15206>
- Wang, Y., Liu, X., Sun, L., Wang, X., Zhang, Q., Yang, X. Improved in-situ zymography approach for mapping anoxic enzyme activities in paddy soils. *Soil Biol. Biochem.* 167, 108624 (2022). <https://doi.org/10.1016/j.soilbio.2022.108624>
- Watt, M., Hugenholtz, P., White, R. & Vinall, K. Numbers and locations of native bacteria on field-grown wheat roots quantified by fluorescence in situ hybridization (FISH). *Environ. Microbiol.* 8, 871–884 (2006). <https://doi.org/10.1111/j.1462-2920.2005.00973.x>
- Werth, M., Kuzyakov, Y. Root-derived carbon in soil respiration and microbial biomass determined by  $^{14}\text{C}$  and  $^{13}\text{C}$ . *Soil Biol. Biochem.* 40, 625–637 (2008). <https://doi.org/10.1016/j.soilbio.2007.09.022>
- Xiong, P., Zhang, Z., Peng, X. Root and root-derived biopore interactions in soils: A review. *J. Plant Nutr. Soil Sci.* 185, 643–655 (2022). <https://doi.org/10.1002/jpln.202200003>
- Zang, H., Xiao, M., Wang, Y. et al. Allocation of assimilated carbon in paddies depending on rice age, chase period and N fertilization: Experiment with  $^{13}\text{C}$  labelling and literature synthesis. *Plant Soil* 445, 113–123 (2019). <https://doi.org/10.1007/s11104-019-03995-1>
- Zhang, S., et al. Tracing  $^{33}\text{P}$ -Labelled Organic Phosphorus Compounds in Two Soils. *Plant Soil* 461, 135–149 (2021). <https://doi.org/10.1007/s11104-021-05178-3>
- Zhao, M., Zhao, J., Yuan, J., et al. Root exudates drive soil-microbe-nutrient feedbacks in response to plant growth. *Plant Cell Environ.* 44, 613–628 (2021). <https://doi.org/10.1111/pce.13928>
- Zhou, J., Shao, G., Kumar, A., et al. Carbon fluxes within tree-crop-grass agroforestry system:  $^{13}\text{C}$  field labeling and tracing. *Biol. Fertil. Soils* 58, 733–743 (2022). <https://doi.org/10.1007/s00374-022-01659-4>
- Zhu, X., Fang, X., Wang, L., Xiang, W., Alharbi, H. A., Lei, P., & Kuzyakov, Y. Regulation of soil phosphorus availability and composition during forest succession in subtropics. *Forest ecology and management*, 502, 119706 (2021). <https://doi.org/10.1016/j.foreco.2021.119706>

## 1.7 Contribution to the included manuscripts

The Ph.D. thesis is a cumulative study, which comprises one published, one submitted and three in preparation manuscripts elaborated in cooperation with various co-authors. The extent of the doctoral candidate's contribution to the manuscripts is assessed on the following scale:

- A. Has contributed to the work (0-33%)
- B. Has made a substantial contribution (34-66%)
- C. Did the majority of the work independently (67-100%)

**Study 1. Yijie Shi**, Iris Zimmermann, Tobias Stürzebecher, Debjyoti Ghosh, Michaela A. Dippold, Sandra Spielvogel. Cover Crop Mixtures Enhance Resource Supply to Maize (*Zea mays* L.) Rhizosphere through Their Root Channels. (In preparation)

Conceptual design:	B
Planning:	B
Implementation:	C
Preparation of the manuscript:	C

**Study 2. Yijie Shi**, Iris Zimmermann, Debjyoti Ghosh, Shang Wang, Bahar S. Razavi, Michaela A. Dippold, Sandra Spielvogel. Site-specific Legacy Effect of Cover Crop Mixtures on C-cycling Enzyme Activities in the Subsequently Growing Maize (*Zea mays* L.) Rhizosphere under Drought. (In preparation)

Conceptual design:	B
Planning:	C
Implementation:	C
Preparation of the manuscript:	C

**Study 3. Yijie Shi**, Sasya Samhita, Sebastian Loeppmann, Iris Zimmermann, Michaela A. Dippold, Sandra Spielvogel. Redundancy of microbial P mobilization in beech forest soils with contrasting P stock: A microbial dilution experiment. (Submitted to *Applied Soil Ecology*)

Conceptual design:	A
Planning:	B
Implementation:	B
Preparation of the manuscript:	C

**Study 4. Yijie Shi**, Sebastian Loeppmann, Jiem Krüger, Jens Boy, Sandra Spielvogel, Georg Guggenberger, Evgenia Blagodatskaya. Peroxidase Activity of Fresh Apple Root: A Novel Approach of Resorufin-based Micro-zymography (In preparation)

Conceptual design:	B
Planning:	C
Implementation:	C
Preparation of the manuscript:	C

**Study 5.** Sebastian Loeppmann, Jan Tegtmeier, **Yijie Shi**, Alberto Andrino de la Fuente, Jens Boy, Georg Guggenberger, Andreas Fulterer, Martin Fritsch, Sandra Spielvogel. (2023). Using fluorescence lifetime imaging to disentangle microbes from the heterogeneous soil matrix. *Biology and Fertility of Soils*, 59(2), 249-260.

Conceptual design:	A
Planning:	A
Implementation:	B
Preparation of the manuscript:	A

## 1.8 Declaration of co-authorship forms

### Declaration of co-authorship

If a dissertation is based on co-authored articles, a declaration from each of the authors regarding the part of the work done by the doctoral candidate must be enclosed when submitting the dissertation.

#### 1. Doctoral candidate

Name: Yijie Shi

#### 2. This co-author declaration applies to the following article:

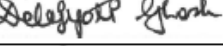
Cover Crop Mixtures Enhance Resource Supply to Maize (*Zea mays* L.) Rhizosphere through Their Root Channels

The extent of the doctoral candidate's contribution to the article is assessed on the following scale:

- A. Has contributed to the work (0-33%)
- B. Has made a substantial contribution (34-66%)
- C. Did the majority of the work independently (67-100%)

3. Declaration on the individual phases of the scientific work (A, B, C)	Extent
<b>Concept:</b> Formulation of the basic scientific problem based on theoretical questions which require clarification, including a summary of the general questions which, it is assumed, will be answerable via analyses or concrete experiments/investigations	B
<b>Planning:</b> Planning of experiments/analyses and formulation of investigative methodology, including choice of method and independent methodological development, in such a way that the scientific questions asked can be expected to be answered	B
<b>Execution:</b> Involvement in the analysis or the concrete experiments/investigation	C
<b>Manuscript preparation:</b> Presentation, interpretation and discussion of the results obtained in article form	C

#### 4. Signature of all co-authors

Date	Name	Signature
12.07.2024	Yijie Shi	
12.07.2024	Iris Zimmermann	
12.07.2024	Tobias Stürzebecher	
12.07.2024	Debjyoti Ghosh	
12.07.2024	Bahar S. Razavi	
12.07.2024	Michaela A. Dippold	
12.07.2024	Sandra Spielvogel	

#### 5. Signature of doctoral candidate

Date	Name	Signature
22.07.2024	Yijie Shi	

### Declaration of co-authorship

If a dissertation is based on co-authored articles, a declaration from each of the authors regarding the part of the work done by the doctoral candidate must be enclosed when submitting the dissertation.

#### 1. Doctoral candidate

Name: Yijie Shi

#### 2. This co-author declaration applies to the following article:

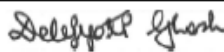
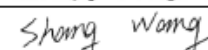
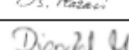
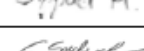
Site-specific Legacy Effect of Cover Crop Mixtures on C-cycling Enzyme Activities in the Subsequently Growing Maize (*Zea mays* L.) Rhizosphere under Drought

The extent of the doctoral candidate's contribution to the article is assessed on the following scale:

- A. Has contributed to the work (0-33%)
- B. Has made a substantial contribution (34-66%)
- C. Did the majority of the work independently (67-100%)

3. Declaration on the individual phases of the scientific work (A, B, C)	Extent
<b>Concept:</b> Formulation of the basic scientific problem based on theoretical questions which require clarification, including a summary of the general questions which, it is assumed, will be answerable via analyses or concrete experiments/investigations	B
<b>Planning:</b> Planning of experiments/analyses and formulation of investigative methodology, including choice of method and independent methodological development, in such a way that the scientific questions asked can be expected to be answered	C
<b>Execution:</b> Involvement in the analysis or the concrete experiments/investigation	C
<b>Manuscript preparation:</b> Presentation, interpretation and discussion of the results obtained in article form	C

#### 4. Signature of all co-authors

Date	Name	Signature
12.07.2024	Yijie Shi	
12.07.2024	Iris Zimmermann	
12.07.2024	Debjyoti Ghosh	
12.07.2024	Shang Wang	
12.07.2024	Bahar S. Razavi	
12.07.2024	Michaela A. Dippold	
12.07.2024	Sandra Spielvogel	

#### 5. Signature of doctoral candidate

Date	Name	Signature
22.07.2024	Yijie Shi	

**Declaration of co-authorship**

If a dissertation is based on co-authored articles, a declaration from each of the authors regarding the part of the work done by the doctoral candidate must be enclosed when submitting the dissertation.

**1. Doctoral candidate**

Name: Yijie Shi

**2. This co-author declaration applies to the following article:**

Redundancy of microbial P mobilization in beech forest soils with contrasting P stock: A microbial dilution experiment

The extent of the doctoral candidate's contribution to the article is assessed on the following scale:

- A. Has contributed to the work (0-33%)
- B. Has made a substantial contribution (34-66%)
- C. Did the majority of the work independently (67-100%)

3. Declaration on the individual phases of the scientific work (A, B, C)	Extent
Concept: Formulation of the basic scientific problem based on theoretical questions which require clarification, including a summary of the general questions which, it is assumed, will be answerable via analyses or concrete experiments/investigations	A
Planning: Planning of experiments/analyses and formulation of investigative methodology, including choice of method and independent methodological development, in such a way that the scientific questions asked can be expected to be answered	B
Execution: Involvement in the analysis or the concrete experiments/investigation	B
Manuscript preparation: Presentation, interpretation and discussion of the results obtained in article form	C

**4. Signature of all co-authors**

Date	Name	Signature
12.07.2024	Yijie Shi	
12.07.2024	Sasya Samhita	
12.07.2024	Sebastian Loepmann	
12.07.2024	Iris Zimmermann	
12.07.2024	Michaela A. Dippold	
12.07.2024	Sandra Spielvogel	

**5. Signature of doctoral candidate**

Date	Name	Signature
22.07.2024	Yijie Shi	

**Declaration of co-authorship**

If a dissertation is based on co-authored articles, a declaration from each of the authors regarding the part of the work done by the doctoral candidate must be enclosed when submitting the dissertation.

**1. Doctoral candidate**

Name: Yijie Shi

**2. This co-author declaration applies to the following article:**

Peroxidase Activity of Fresh Apple Root: A Novel Approach of Resorufin-based Micro-zymography

The extent of the doctoral candidate's contribution to the article is assessed on the following scale:

- A. Has contributed to the work (0-33%)
- B. Has made a substantial contribution (34-66%)
- C. Did the majority of the work independently (67-100%)

3. Declaration on the individual phases of the scientific work (A, B, C)	Extent
<b>Concept:</b> Formulation of the basic scientific problem based on theoretical questions which require clarification, including a summary of the general questions which, it is assumed, will be answerable via analyses or concrete experiments/investigations	B
<b>Planning:</b> Planning of experiments/analyses and formulation of investigative methodology, including choice of method and independent methodological development, in such a way that the scientific questions asked can be expected to be answered	C
<b>Execution:</b> Involvement in the analysis or the concrete experiments/investigation	C
<b>Manuscript preparation:</b> Presentation, interpretation and discussion of the results obtained in article form	C

**4. Signature of all co-authors**

Date	Name	Signature
12.07.2024	Yijie Shi	
12.07.2024	Sebastian Loepmann	
12.07.2024	Jiem Krüger	
12.07.2024	Jens Boy	
12.07.2024	Georg Guggenberger	
12.07.2024	Sandra Spielvogel	
12.07.2024	Evgenia Blagodatskaya	

**5. Signature of doctoral candidate**

Date	Name	Signature
22.07.2024	Yijie Shi	

## Declaration of co-authorship

If a dissertation is based on co-authored articles, a declaration from each of the authors regarding the part of the work done by the doctoral candidate must be enclosed when submitting the dissertation.

### 1. Doctoral candidate

Name: Yijie, Shi

### 2. This co-author declaration applies to the following article:

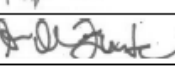
Using fluorescence lifetime imaging to disentangle microbes from the heterogeneous soil matrix

The extent of the doctoral candidate's contribution to the article is assessed on the following scale:

- A. Has contributed to the work (0-33%)
- B. Has made a substantial contribution (34-66%)
- C. Did the majority of the work independently (67-100%)

3. Declaration on the individual phases of the scientific work (A, B, C)	Extent
<b>Concept:</b> Formulation of the basic scientific problem based on theoretical questions which require clarification, including a summary of the general questions which, it is assumed, will be answerable via analyses or concrete experiments/investigations	A
<b>Planning:</b> Planning of experiments/analyses and formulation of investigative methodology, including choice of method and independent methodological development, in such a way that the scientific questions asked can be expected to be answered	A
<b>Execution:</b> Involvement in the analysis or the concrete experiments/investigation	B
<b>Manuscript preparation:</b> Presentation, interpretation and discussion of the results obtained in article form	A

### 4. Signature of all co-authors

Date	Name	Signature
02.07.2024	Sebastian Löppmann	
03.07.2024	Sandra Spielvogel	
25.07.2024	Jan Tegtmeier	
16.07.2024	Alberto Andrino de la Fuente	
11.07.2024	Jens Boy	
11.07.2024	Georg Guggenberger	
09.07.2024	Martin Fritsch	
10.07.2024	Andreas Fulterer	

### 5. Signature of doctoral candidate

Date	Name	Signature
25.07.2024	Yijie Shi	



## 2. Manuscript

### 2.1 Study 1. Cover Crop Mixtures Enhance Resource Supply to the Maize (*Zea mays* L.) Rhizosphere through Their Root Channels

Yijie Shi<sup>1</sup>, Iris Zimmermann<sup>1</sup>, Tobias Stürzebecher<sup>2,3</sup>, Debjyoti Ghosh<sup>4</sup>, Bahar S. Razavi<sup>5</sup>, Michaela A. Dippold<sup>2,3</sup>, Sandra Spielvogel<sup>1</sup>

#### Status: In preparation

<sup>1</sup> Institute of Plant Nutrition and Soil Science, Christian-Albrechts-University Kiel, Germany

<sup>2</sup> Geo-Biosphere Interactions, Department of Geosciences, University of Tuebingen, Germany

<sup>3</sup> Biogeochemistry of Agroecosystems, University of Goettingen, Germany

<sup>4</sup> Molecular Systems Biology, Helmholtz Centre for Environmental Research GmbH, Leipzig, Germany

<sup>5</sup> Department of Soil and Plant Microbiome, Institute of Phytopathology, Christian-Albrecht University of Kiel, Germany

---

#### Abstract

Planting cover crops is well-established as a sustainable farming strategy to improve soil fertility, prevent nutrient leaching and increase soil carbon (C) stocks. Including deep-rooting species in cover crop mixtures increases the proportion of root channels and boosts C and N allocation to the subsoil. However, the turnover of C and nitrogen (N) in cover crop root channels re-used by cash crops remains unclear. To address this gap in current knowledge, we conducted a combined <sup>13</sup>C and <sup>15</sup>N labeling study on three cover crop mixtures (legume/grass, legume/brassica, brassica/grass) with deep- and shallow-rooting species from different functional classes (legume: *Trifolium pratense*, *Trifolium repens*, grass: *Festuca arundinacea*, *Lolium perenne*, brassica: *Raphanus sativus* var. *oleiformis*, *Brassica napus*) at a Luvisol field site in Northern Germany. The kinetics of C- and N-cycling enzymes were determined by fluorometric microplate assays. The results show that the legume/grass mixture allocated 1-, respective 5-fold more C to the empty root channels in the subsoil (30 – 60 cm) compared to the legume/brassica and brassica/grass mixtures, with no significant difference in N allocation among three mixtures. The microbial biomass in the root channels of the legume/grass mixture incorporated 3- to 5- fold more cover crop derived C compared to the microbial biomass in the root channels of the mixtures with brassica, indicating enhanced microbial C stabilization in the subsoil of the legume/grass mixture. The  $\beta$ -glucosidase and leucine-amino-peptidase activity in the subsoil rhizosphere of maize roots reusing brassica/grass root channels was higher compared to the activities in the rhizosphere of maize re-using the root channels of the two cover crop mixtures containing legumes, highlighting the intertwining of root exudate availability, N-demand for enzyme production, and the enzyme requirement to release N from substrate. Maize took up to 6.5 % of the N derived from the legume/grass mixture up, meeting up to 1.1 % of its N demand at BBCH33 stage. We conclude that combining deep- and shallow-rooting species of legumes and grasses in cover crop mixtures promotes the microbial stabilization of C in the subsoil and the N supply of cash crops with cover-crop derived N.

**Keywords:** deep-rooting cover crops, shallow-rooting cover crops, root channels, <sup>13</sup>C pulse labeling, <sup>15</sup>N leaf labeling, enzyme kinetics, C and N mobilization, legume, grass, brassica.

## 1. Introduction

Cover crops are widely used in crop rotations to increase the quantity of organic carbon (OC) returned to the soil (Jian et al., 2020; Kaye and Quemada, 2017; McClelland et al., 2021; O’Dea et al., 2013). Studies have demonstrated links between cover crop diversity and ecosystem services such as soil organic carbon (SOC) sequestration, nutrient acquisition, and weed suppression (Abdalla et al., 2019; Faucon et al., 2017; Finney and Kaye, 2017; Li et al., 2014). However, there is still a lack of information concerning the role of cover crop-derived carbon (C) and nitrogen (N) inputs by different cover crop mixtures and how these mixtures contribute to the growth of subsequent cash crops by providing and retaining root-derived N for crop nutrition and C for enhancing microbial activity in the cover crop root channels.

Cover crop species predominantly belong to three plant families: legumes, grasses, and brassicas. Legumes can provide a good compromise between biomass production, degradability of biomass (Freund et al., 2021) and supply of the succeeding cash crop with N due (Tonitto et al., 2006) to their ability to fix N from the atmosphere. Moreover, the organic N input is beneficial to promote SOC formation (Kirkby et al., 2014, 2011; Zhou et al., 2019). Grasses are characterized by dense, fibrous root systems with high nutrient-scavenging ability. This can prevent N leaching and increase soil organic matter storage in soil (Blanco-Canqui and Jasa, 2019; Moore et al., 2014; Poeplau et al., 2015; Thapa et al., 2018). Brassica can improve the soil structure in deep soil layers through their pivoting roots (Chen and Weil, 2011; Hamza and Anderson, 2005), and suppress weeds due to their allelopathic effects (Asaduzzaman et al., 2014; Gfeller et al., 2018). Cover crop mixtures are becoming increasingly popular, because mixtures of cover crops can combine the beneficial effects of their individual species, such as N fixation and resource capture (Lavergne et al., 2021; Ranells and Wagger, 1997; Smith et al., 2014). For example, the productivity of legumes is not as high as of grasses or brassicas (Holtham et al., 2007; Ramírez-García et al., 2015). However, the high plant biomass production of mixtures of legumes and non-legumes can maximize the provision of ecosystem services, such as reducing nitrate leaching and increasing the pool of organically bound N in soil as slow-supplying N source for the following cash crops. Legumes mixed with brassica reduce nitrate leaching by 24% compared to legume monocultures (Couëdel et al., 2018). Additionally, legumes mixed with grasses are more effective at increasing SOC content due to the higher biomass production and lower decomposition rate of grass residues compared to legumes alone (Sainju et al., 2006; Snapp et al., 2005; St Aime et al., 2023; Vann et al., 2019).

Improving the accessibility of subsoil resources is widely recognized as an effective strategy to promote cash crop productivity (Feng et al., 2018; Kautz et al., 2013; Ning et al., 2022). Deep-rooting cover crops represent a promising and sustainable method to obtain this accessibility (Han et al., 2022; Kell, 2011; Thorup-Kristensen et al., 2020) by creating continuous root channels into the subsoil that can be reused by cash crop roots (Abdollahi et al., 2014; Banfield et al., 2017; Kautz et al., 2013; Rosa et al., 2021). Moreover, the OM residues in the cover crop root channels increase microbial activity (Blagodatskaya et al., 2014; Kuzyakov and Domanski, 2000), thereby accelerating microbial mobilization and incorporation of C and N (Feng et al., 2022; Jilling et al., 2018). Even two years after root death and decomposition, C contents in root channels can still be 2.5 times higher than in bulk soil, leading to up to 5.5 times higher microbial biomass content and concomitantly increased enzyme activities (Banfield et al., 2017; Hoang et al., 2016). Peixoto et al. (2020) have reported a distinct microbial stabilization of legume and grass root-derived C in subsoil layers down to 3.6 m depth by deep-rooting legumes. Combining shallow- and deep-rooting species in a mixture may force the deep-rooting species to grow much deeper to explore resources from deep soil layers due to the competition for water and nutrient resources in the topsoil (Berendse, 1981; Oram et al., 2018). As a consequence, mixtures of deep- and shallow-rooting cover crops are likely advantageous for the succeeding cash crop compared to mixtures of shallow rooting cover crop species, with respect to N and water acquisition from the subsoil. It was also proven that the root length density, the total root biomass and the spatial

expansion of the root system of cover crop mixtures are larger than those of cover crop monocultures (Amsili and Kaye, 2021; Javier Ramirez-Garcia et al., 2015). This enhances the volume of the root channels available to the following cash crops.

The quality of residue predominantly controls the decomposition rate of cover crops (Bradford et al., 2016), e.g., legumes with a low C: N ratio meaning high-quality of residues decompose faster than grass and brassica with high C: N (Barel et al., 2019; da Silva et al., 2022). After the death of cover crops, C and N in the biomass can be incorporated into soil organic matter, or used as energy and nutrient source for soil microorganisms (Liang et al., 2017; Paul, 2016), which allocates part of the C and N to soil microbial biomass (Kuzyakov and Domanski, 2000; Mayer et al., 2003; Walker et al., 2003). Due to the immobility of dead roots, the impact of cover crop residue decomposition on the rhizosphere of cash crops will be amplified in the root channels (Athmann et al., 2017; Banfield et al., 2018; Hoang et al., 2017). The microorganisms in the rhizosphere of cash crops reusing cover crop root channels can directly benefit from nutrient supply from cover crop residues, but its investigation has received little attention.

This study aims to investigate how the root channels of cover crop mixtures with deep- and shallow-rooting species affect the microbial C and N use strategies in the rhizosphere of the following cash crop maize (*Zea mays*). We conducted a field experiment containing three kinds of cover crop mixtures including shallow- and deep-rooting species, followed by maize. <sup>13</sup>C pulse labeling and <sup>15</sup>N leaf labeling (Heinrich et al., 2015; Peixoto et al., 2020; Sommer et al., 2017; Werner et al., 2021) were used to trace the cover crop-derived C and N in different pools, and enzyme activity was determined to compare the C and N mobilization in the maize rhizosphere. We hypothesized that: (i) combinations of deep- and shallow-rooting cover crops differ in their C and N allocation to the soil, and mixtures containing deep-rooting legume species deliver more C and N to root channels in the subsoil; (ii) microbial C and N assimilation in maize rhizosphere is enhanced in cover crop root channels; (iii) N from cover crop root channels can make a notable contribution to the N supply of maize.

## 2. Materials and Methods

### 2.1 Experimental site and design

The field experiment was conducted on the experimental farm “Hohenschulen” (54°18'44"N, 9°59'46"E), of Kiel University, Germany. The main soil type at the experimental field site was classified as Luvisol with sandy loam texture. The average annual precipitation at the site is 769 mm and the mean temperature is 9.4 °C (Merkel, 2022). The pH of the topsoil is 6.5 (0.01 M CaCl<sub>2</sub>), the organic carbon content is 1.2 mg g<sup>-1</sup>, and the total nitrogen content is 0.7 mg g<sup>-1</sup>.

The field experiment in Hohenschulen was set up in autumn 2020. Four replicate blocks (6×12 m) of each of the three cover crop mixtures (Table 1) and four control blocks without cover cropping (black fallow in winter) were established as a randomized block design to account for heterogeneities in terrain and soil. Cover crops were sown in September 2020 and killed by herbicides before shallow tilling and maize sowing in May 2021 (Table 2).

**Table 1-1** Variations of cover crop mixtures with deep- and shallow-rooting species and control. The variations are named according to the functional plant species groups they represent.

Variation	Cover crop species	
	Deep-rooting species	Shallow-rooting species
Control	—	—
Legume/grass	Red clover ( <i>Trifolium pratense</i> L.) Tall fescue ( <i>Festuca arundinaceae</i> )	White clover ( <i>Trifolium repens</i> L.) German ryegrass ( <i>Lolium perenne</i> )
Legume/brassica	Red clover ( <i>Trifolium pratense</i> L.) Oil radish ( <i>Raphanus sativus</i> L. var. <i>oleiformis</i> )	White clover ( <i>Trifolium repens</i> L.) Winter forage rape ( <i>Brassica napus</i> L.)
Brassica/grass	Oil radish ( <i>Raphanus sativus</i> L. var. <i>oleiformis</i> ) Tall fescue ( <i>Festuca arundinaceae</i> )	Winter forage rape ( <i>Brassica napus</i> L.) German ryegrass ( <i>Lolium perenne</i> )

**Table 1-2** Description of cover crops and following maize cultivation, sowing dates/density, fertilization levels.

Variation	Cover crop growing season			Maize growing season				
	Time	Sowing density (kg ha <sup>-1</sup> )		Fertilization (kg N ha <sup>-1</sup> )	Time	Sowing density (plants m <sup>-2</sup> )	Fertilization (kg N ha <sup>-1</sup> )	
		Single	Sum				20.05.2021	23.06.2021
Control	08.2020-05.2021	-	-	-	2021.05-2021.08	10	90	80
Legume/grass	08.2020-05.2021	3.5	14	30	2021.05-2021.08	10	90	80
		3.5						
Legume/brassica	08.2020-05.2021	3.5	14	30	2021.05-2021.08	10	90	80
		3.5						
Brassica/grass	08.2020-05.2021	3.5	14	60	2021.05-2021.08	10	90	80
		3.5						

## 2.2 <sup>13</sup>CO<sub>2</sub> pulse labeling

The <sup>13</sup>CO<sub>2</sub> pulse labeling of the cover crops was performed according to Bromand et al. (2001) and Zhou et al. (2022) in November 2020 and April 2021 on a subplot of each of the four replicated blocks of the randomized block design (see above). The <sup>13</sup>C<sub>2</sub> pulse label was applied in chambers (1.6 × 1.0 m area, 0.5 m height) consisting of four metal bars covered with transparent polyethylene foil with more than 90% transmittance of photosynthetically active radiation. To avoid gas losses, the foil was buried into the soil and sealed with wet soil. Electric fans were used to circulate the <sup>13</sup>CO<sub>2</sub> inside the chambers. Every chamber was equipped with two beakers containing NaH<sup>13</sup>CO<sub>3</sub> (98 atom-% <sup>13</sup>C, Sigma-Aldrich, Germany) to allow two consecutive pulses to be conducted, each of which increased the <sup>13</sup>CO<sub>2</sub> concentration inside the chamber to 2000 ppm. The <sup>13</sup>CO<sub>2</sub> was released by injecting an excess amount of H<sub>3</sub>PO<sub>4</sub> (85 % w/w) into the beakers by using a syringe from outside the chamber. The second pulse was released 3 h after the first, and the chambers remained in place for another 3 h after the second pulse.

## 2.3 <sup>15</sup>N leaf labeling of deep-rooting cover-crop species

To trace the faith of root-derived N in the subsoil, the deep-rooting cover-crop species (red clover, tall fescue and oil radish) were labeled with a solution of (<sup>15</sup>NH<sub>4</sub>)<sub>2</sub>SO<sub>4</sub> and Na<sup>15</sup>NO<sub>3</sub> in distilled water in November 2020 and April 2021. The <sup>15</sup>N solution was prepared in two different concentrations to account for the different biomass of red clover, tall fescue and oil radish. Red clover and tall fescue were leave labeled with 0.98 ml <sup>15</sup>N solution with a concentration of 3.93 mmol <sup>15</sup>N L<sup>-1</sup>. The oil radish was labeled with 27.78 ml <sup>15</sup>N solution with a concentration of 1.48 mmol <sup>15</sup>N L<sup>-1</sup>. Three leaves from three adjacent plants were cut off from both sides of the midrib, leaving only the midvein left. The three midveins were inserted into the vials with the tracer and fixed with elastic film.

## 2.4 Plant biomass and soil sampling

Cover crop aboveground biomass was sampled from all labeling sub-plots shortly before herbicide application to determine the amount of cover crop assimilated <sup>13</sup>C and <sup>15</sup>N.

Soil samples from cover crop root channels in the <sup>13</sup>C and <sup>15</sup>N. labeling sub-plots were taken from the wall of a soil pit (1 m wide, 1.2 m deep) at the time of maize germination (T1, 24.05.2021) and at maize vegetative growth stage BBCH33 (T2, 23.07.2021) when maize roots had reached at least 60 cm soil depth. The soil samples from cover crop root channels (without living roots at the first sampling date, without living roots or re-used by maize roots at the second sampling time) as well as bulk soil

samples (control samples) were separately collected for the topsoil (0–30 cm soil depth) and the subsoil (30–60 cm soil depth). Note: Visible root remains of the cover crops (particulate cover crop root material) were removed from the root channel before sampling of the soil material of the root channel. Each soil sample was separated into two subsamples, of which one was stored at 4 °C to determine soil microbial biomass C within one week after sampling, and the other was stored at -20 °C.

Two maize plants growing within the sampling area were collected at BBCH33 to determine how much of the N in the maize could be traced back to the cover crops.

## 2.5 Enzyme kinetics

The kinetics of  $\beta$ -glucosidase (GLU) and leucine aminopeptidase (LAP) were determined using fluorogenic labeled substrates (4-methylumbelliferyl- $\beta$ -D-glucosidase and L-Leucine-7-amido-4-methylcoumarin hydrochloride, respectively) according to Razavi et al. (2015). Fluorescence was measured with a micro-plate reader CLARIOstar Plus (BMG LABTECH, Ortenberg, Germany).

## 2.6 Microbial biomass carbon and nitrogen

The chloroform-fumigation-extraction method was applied to estimate microbial biomass carbon C ( $C_{mic}$ ) and N ( $N_{mic}$ ) (Brookes et al., 1985; Wu et al., 1990). One set of soil samples were extracted with 0.5 M  $K_2SO_4$  (30 mL), a second set of samples was fumigated with chloroform for 24 h and subsequently extracted with 0.5 M  $K_2SO_4$ . Both fumigated and non-fumigated extracts were filtered and analyzed with a TOC/TIC analyzer (Multi N/C 2100, Analytik Jena, Jena, Germany).  $C_{mic}$  was calculated as the difference between extracted C from fumigated and non-fumigated samples with a conversion factor ( $k_C$ ) of 0.45 (Wu et al., 1990).  $N_{mic}$  was calculated as the difference between extracted N from fumigated and non-fumigated samples with a conversion factor ( $k_N$ ) of 0.54 (Brookes et al., 1985).

## 2.7 $^{13}C$ and $^{15}N$ analysis of plant and soil

Plant aboveground biomass was oven-dried at 60 °C for 72 h for cover crops, and 1 week for maize until constant weight, mechanically shredded, and subsequently milled in a ball mill. Soil samples were oven-dried at 105 °C for 24 h and ground in a ball mill. The samples (5 mg for plant samples, 10 mg soil samples) were sealed in tin capsules to measure total C and N content and  $^{13}C$  and  $^{15}N$  atom-% using an elemental analyzer Costech ECS 4010 (CostechAnalytical Technologies Inc. Valencia, USA) coupled to a Delta C isotope ratio mass spectrometer (Thermo Electron, Bremen Germany).

## 2.8 Calculations

### 2.8.1 Calculations of $^{13}C$ and $^{15}N$ in cover crop biomass and soils

The percentage of cover crop-derived C [ $^{13}C_x$ ] and N [ $^{15}N_x$ ] incorporated into specific C respective N pools (Pausch et al., 2016; Zhou et al., 2022) was determined according to eq. 1 and eq. 2:

$$^{13}C_x (\%) = \frac{[(^{13}C_{atom\%})_{x,L} - (^{13}C_{atom\%})_{x,n.a.}]}{100} \times C_x \quad (eq. 1)$$

$$^{15}N_x (\%) = \frac{[(^{15}N_{atom\%})_{x,L} - (^{15}N_{atom\%})_{x,n.a.}]}{100} \times N_x \quad (eq. 2)$$

where  $(^{13}C_{atom\%})_{x,L}$  and  $(^{13}C_{atom\%})_{x,n.a.}$  represent  $^{13}C_{atom\%}$  in the specific C pool in labeled and unlabeled samples, respectively;  $C_x$  represents the total C content (%) in the specific C pool in the labeled samples.  $(^{15}N_{atom\%})_{x,L}$  and  $(^{15}N_{atom\%})_{x,n.a.}$  represent  $^{15}N_{atom\%}$  in the specific N pool in labeled and unlabeled samples, respectively;  $N_x$  represents the total N content (%) in the specific N pool in the labeled samples. The total C and N content of the soil samples from root channels was considered the total C and N pools of these channels. Note: our definition of the total C and N pool of the cover crop channels does not include visible particulate organic material, as visible root remains of the cover crops (particulate cover crop root material) were removed from the root channel before

sampling of the soil material of the respective root channel (see above). The K<sub>2</sub>SO<sub>4</sub>-extractable C and N represents the labile C and N pool of these channels, and the C<sub>mic</sub> and N<sub>mic</sub> content represents the soil microbial C and N pool in the root channels.

The maize uptake of cover crop-derived N (%) was calculated according to eq. 3:

$$\text{maize uptake of cover crop derived N (\%)} = \frac{[(^{15}\text{N}_{\text{atom}\%})_{\text{maize,L}} - (^{15}\text{N}_{\text{atom}\%})_{\text{maize,n.a.}}]}{[(^{15}\text{N}_{\text{atom}\%})_{\text{CC,L}} - (^{15}\text{N}_{\text{atom}\%})_{\text{CC,n.a.}}]} \times 100 \quad (\text{eq. 3})$$

The cover crop-derived N in maize N (%) was calculated according to eq. 4:

$$\text{Cover crop derived N in maize N (\%)} = \frac{[(^{15}\text{N}_{\text{atom}\%})_{\text{maize,L}} - (^{15}\text{N}_{\text{atom}\%})_{\text{maize,n.a.}}]}{N_{\text{maize}} (\%)} \times 100 \quad (\text{eq. 4})$$

Where  $(^{15}\text{N}_{\text{atom}\%})_{\text{maize,L}}$  represents  $^{15}\text{N}_{\text{atom}\%}$  in the maize from the labeled plots,  $(^{15}\text{N}_{\text{atom}\%})_{\text{maize,n.a.}}$  represents  $^{15}\text{N}_{\text{atom}\%}$  in the maize from the control,  $(^{15}\text{N}_{\text{atom}\%})_{\text{CC,L}}$  represents  $^{15}\text{N}_{\text{atom}\%}$  in the labeled cover crop biomass,  $(^{15}\text{N}_{\text{atom}\%})_{\text{CC,n.a.}}$  represents the nature abundance value of  $^{15}\text{N}_{\text{atom}\%}$  of cover crops,  $N_{\text{maize}} (\%)$  represents the N content (%) in maize biomass.

### 2.8.2 Calculation of enzyme kinetics

Enzyme activities were determined by fitting non-linear saturation curves of the Michaelis-Menten equation (eq. 4) in GraphPad Version 8 (Prism, USA):

$$V = \frac{V_{\text{max}} [S]}{(K_m + [S])} \quad (\text{eq. 4})$$

Where  $V$  is the reaction velocity (nmol g<sup>-1</sup> h<sup>-1</sup>),  $V_{\text{max}}$  is the maximal rate of enzyme activity at saturated substrate concentration,  $K_m$  is the substrate concentration at half of the  $V_{\text{max}}$  and  $S$  is the substrate concentration (Michaelis and Menten, 1913; Nannipieri et al., 2012).

### 2.8.3 Statistical analysis

All statistical analyses were performed using R studio (Version 2023.06.1+524). Prior to the analysis of variance (ANOVA), all data were tested for normal distribution (Shapiro-Wilk test) and homogeneity of variance (Bartlett's test). Two-way ANOVA was performed to test for the main effects of cover crop mixtures and sampling time points on <sup>13</sup>C in the total C pool of the cover crop root channels, <sup>13</sup>C in C<sub>mic</sub> of the cover crop root channels, and <sup>13</sup>C in the labile C pool of the cover crop root channels, <sup>15</sup>N in the total N pool of the cover crop root channels, <sup>15</sup>N in N<sub>mic</sub> of the cover crop root channels, and <sup>15</sup>N in the labile N pool of the cover crop root channels. When the main effects were significant ( $p < 0.05$ ), the means were compared with Tukey's HSD test at the significance level  $p < 0.05$ . Kruskal-Wallis test followed by Dunn's test as post-hoc test was used for testing <sup>13</sup>C and <sup>15</sup>N values in the maize rhizosphere reusing cover crop root channels,  $V_{\text{max}}$  of GLU and LAP, and cover crop-derived <sup>15</sup>N in maize N.

## 3. Results

### 3.1 Allocation of C and N in empty cover crop root channels

The cover crop-derived C incorporated in the total C pool of empty cover crop root channels increased 3-fold from T1 to T2 in the topsoil (0–30 cm) after in the legume/grass and brassica/grass mixtures (Figure 1-1 a), and the cover crop-derived C incorporated in the labile C pool in cover crop root channels increased 4-fold from T1 to T2 (Figure 1-1 c). In contrast, the cover crop derived C in C<sub>mic</sub> did not change from T1 to T2.

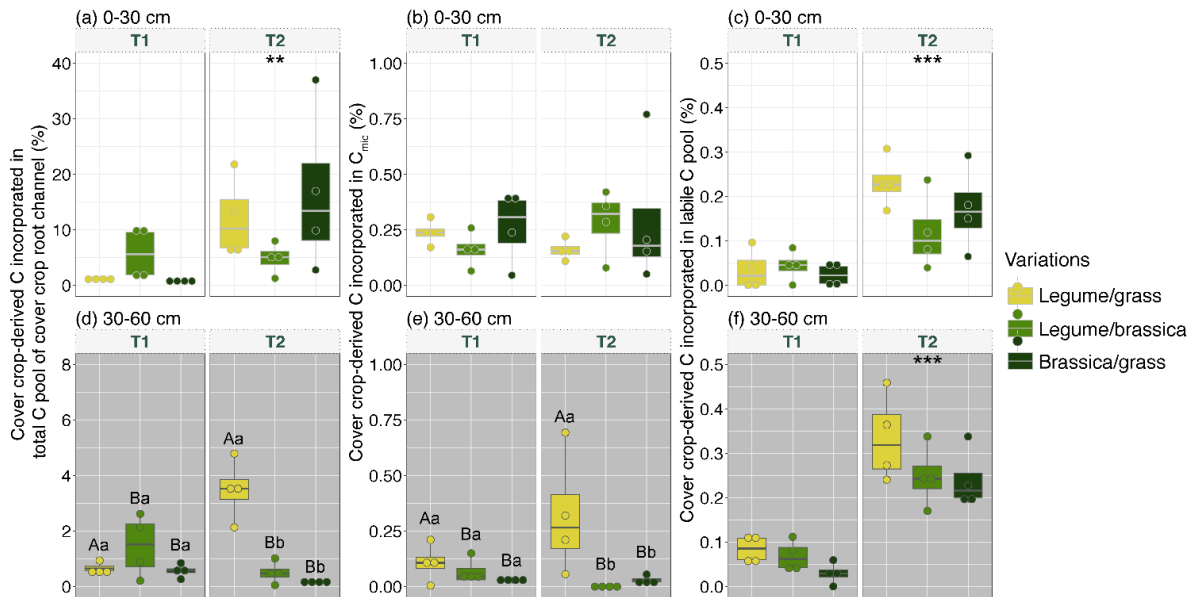


**Figure 1-1** Cover crop-derived C incorporated in (a) total C pool of empty cover crop root channels, (b)  $C_{mic}$ , and (c) labile C pool in empty cover crop root channels in the topsoil and the (d-e) subsoil at two time points (T1: maize germination; T2: maize growth stage BBCH 33). The effects of cover crop mixtures and time points and their interaction were tested using two-way ANOVA. Lowercase letters indicate significant differences between cover crop mixture variations within one time point in each soil layer ( $p < 0.05$ ). Capital letters indicate significant differences between the main factor of cover crop mixtures within a soil layer ( $p < 0.05$ , without interaction effects of time points). Asterisks represent significant differences between the main factor of time points within each soil layers ('\*\*' represents  $p < 0.01$ ; '\*\*\*' represents  $p < 0.001$ ). Asterisks were noted under the time point with a significantly higher result than the other.

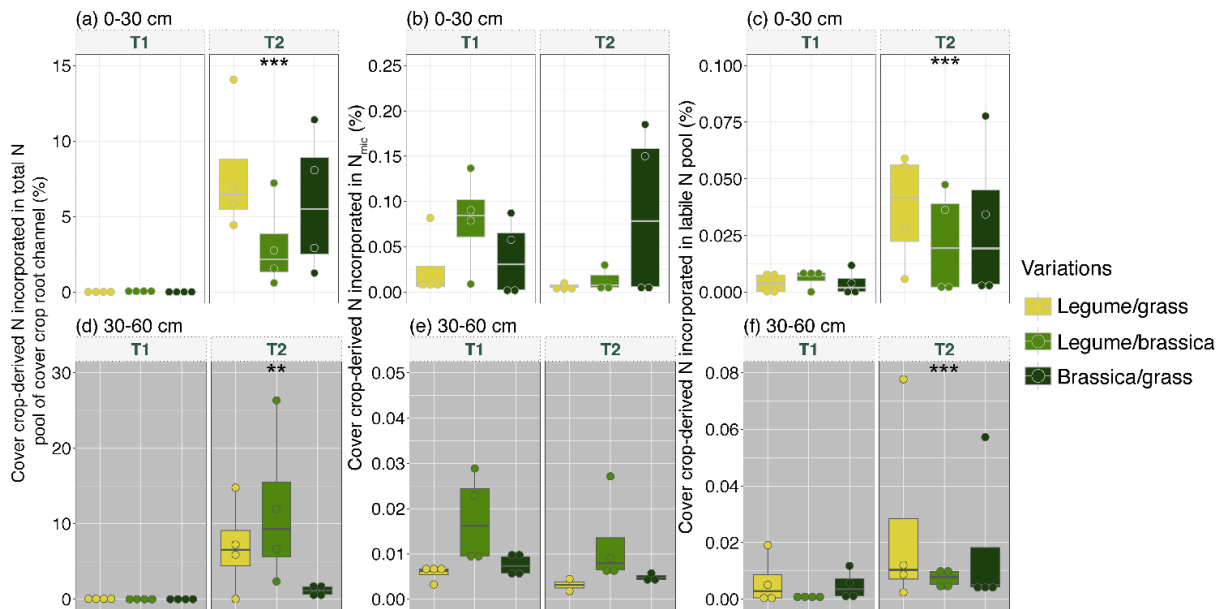


**Figure 1-2** Cover crop-derived N incorporated in (a) total N pool of empty cover crop root channels, (b)  $N_{mic}$ , and (c) labile N pool in empty cover crop root channels in the topsoil and the (d-e) subsoil at two time points (T1: maize germination; T2: maize growth stage BBCH 33). The effects of cover crop mixtures and time points and their interaction were tested using two-way ANOVA. Asterisks represent significant differences between the main factor of time points within each soil layers ('\*\*' represents  $p < 0.01$ ; '\*\*\*' represents  $p < 0.001$ ). Asterisks were noted under the time point with a significantly higher result than the other.

Interestingly, in the subsoil (30–60 cm), the percentage of cover crop-derived C incorporated in the total C pool of the legume/grass root channels was 1- and 5-fold higher compared to the cover crop-derived C incorporated in the total C pool of the legume/brassica and brassica/grass root channels, respectively (Figure 1-1 d). Especially at T2, the percentage of cover crop-derived C incorporated in the total C pool of the legume/grass root channels was 6- and 22-fold higher compared to the cover crop-derived C incorporated in the total C pool of the legume/brassica and brassica/grass root channels. The root channels of the legume/grass mixture showed 3- and 5-fold higher percentage of cover crop-derived C incorporated in  $C_{mic}$  than the root channels of the legume/brassica and the brassica/grass mixtures at both time points (Figure 1-1 e). The highest percentage of cover crop-derived C incorporated in  $C_{mic}$  was found at T2 in legume/grass mixture. The percentage of cover crop-derived C incorporated in the labile C pool of the root channels of all cover crop mixtures in the subsoil increased 4-fold from T1 to T2 (Figure 1-1 f).

In the topsoil, there was only little cover crop-derived N incorporated in the total N pool of the root channels of all three cover crop mixtures at T1 (Figure 1-2 a). However, the cover crop-derived N incorporated into the total N pool of the root channels of all cover crop mixtures increased 305-fold from T1 to T2. Likewise, the percentage of cover crop-derived N incorporated in the labile N pool in the root channels of all cover crop mixture was 5-fold higher at T2 than T1 (Figure 1-2 c). It is worth noting that the microorganisms in the root channels of the legume/brassica had incorporated 0.07 % of cover crop-derived N in  $N_{mic}$  even at T1 when the total percentage of cover crop-derived N was quite low in the root channels (Figure 1-2 b). Despite higher amounts of crop-derived N in the total N pool and the labile N pool of the topsoil root channels of the legume/grass mixture and the legume/brassica mixture at T2 compared to T1, the microorganisms in did not incorporate more cover crop-derived N into their biomass (Figure 1-2 b). A similar trend was also evident in the subsoil, where the cover crop-derived N incorporated in the total N pool and the labile N pool of the root channels of all three cover crop mixtures were significantly higher at T2 than T1 (Figure 1-2 d, f), but the cover crop-derived N incorporated in  $N_{mic}$  showed no difference between T1 and T2 (Figure 1-2 e).

### **3.2 Incorporation of cover crop-derived C and N in cover crop root channels reused by maize roots**

The amount of cover crop-derived C incorporated in the total C pool and in the labile C pool of cover crop root channels reused by maize roots in the topsoil at T2 was similar for all three cover crop mixtures (Figure 1-3 a, c), however, we observed remarkable differences with respect to the incorporation of cover-crop derived C in the microbial biomass. Microorganisms in the topsoil incorporated 15-fold more cover crop-derived C into  $C_{mic}$  in the reused root channels of the legume/grass mixture compared to the reused root channels of the legume/brassica mixture (Figure 1-3 b). In contrast to the topsoil, incorporation of cover-crop derived C in the total C pool differed substantially among the reused root channels of the different cover crop mixtures. The reused root channels of the legume/grass mixture contained 731-fold more cover crop-derived C in their total C pool compared to the reused root channels of the legume/brassica mixture (Figure 1-3 d).

The composition of the cover crop mixtures did not significantly affect the incorporation of cover crop-derived N into the different N pools of the root channels reused by maize in the topsoil (Figure 1-4 a-c). However, the contribution of cover crop-derived N to the total N pool in reused root channels in the subsoil was 20-fold higher at the legume/grass plots compared to the legume/brassica and the brassica/grass plots (Figure 1-4 d). The percentage of cover crop-derived N in the labile N pool of the reused legume/grass root channels in the subsoil was 4-fold higher than the cover crop-derived N in the labile N pool of the reused root channels of the other two cover crop mixtures (Figure 1-4 f).

### **3.3 Enzyme activities in maize rhizosphere and N uptake of maize plant**

In the mixtures containing legumes, both GLU and LAP activities are higher in the topsoil than in the subsoil (Figure 1-5). The brassica/grass mixture shows an opposite trend with overall higher activities

in the subsoil.

In the topsoil,  $V_{max}$  of GLU was 2-fold higher in the legume/grass root channels reused by maize compared to the brassica/grass root channels reused by maize (Figure 1-5 a) and  $V_{max}$  of LAP in the legume/brassica root channels reused by maize was 3- and 4-fold higher compared to  $V_{max}$  of LAP in the legume/grass root channels and the legume/brassica root channels reused by maize, respectively (Figure 1-5 b).

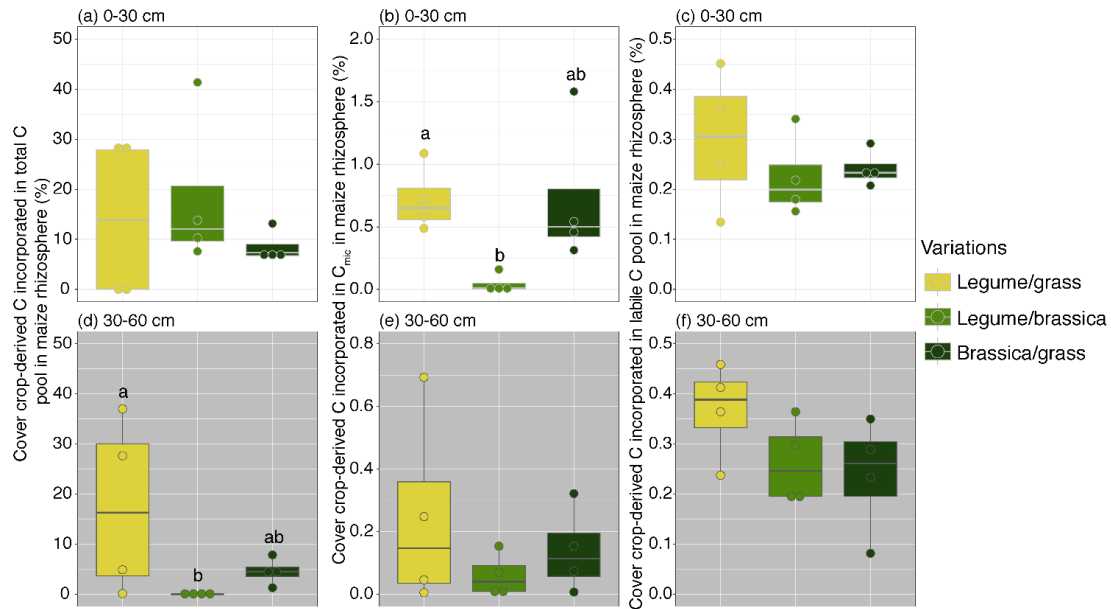


**Figure 1-3** Cover crop-derived C incorporated in (a) total C pool of maize rhizosphere reusing cover crop root channels, (b)  $C_{mic}$ , and (c) labile C pool in maize rhizosphere reusing cover crop root channels in the topsoil and the (d-e) subsoil at T2 (maize growth stage BBCH 33). The effects of cover crop mixtures and soil layers and their interaction were tested using Kruskal-Wallis-Test followed by Dunn's test as post-hoc test. Lowercase letters indicate significant differences between cover crop mixtures in each soil layer ( $p < 0.05$ ).

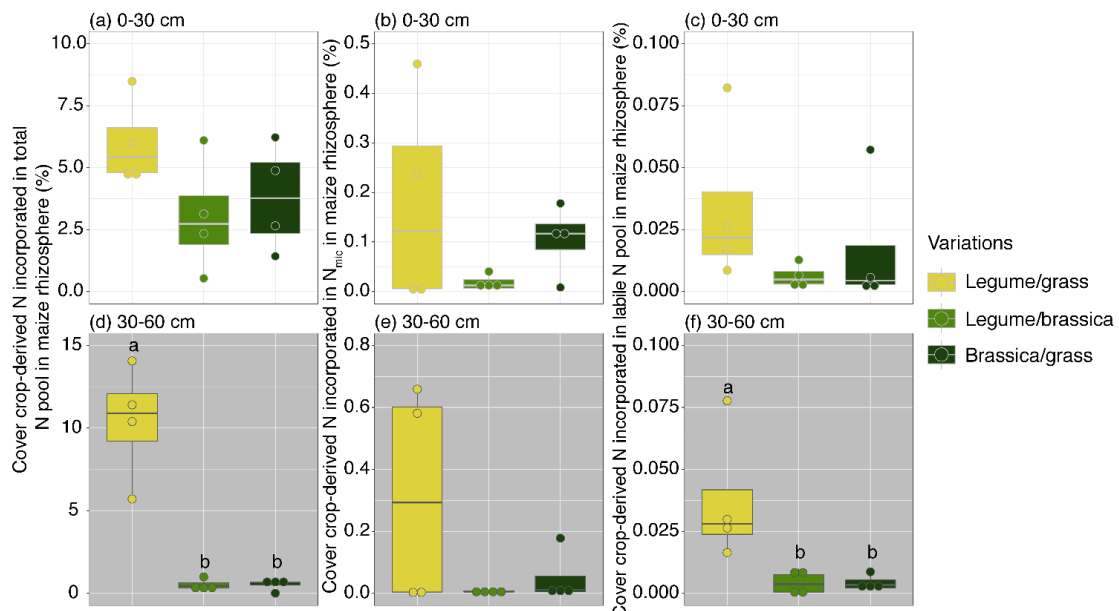


**Figure 1-4** Cover crop-derived N incorporated in (a) total N pool of maize rhizosphere reusing cover crop root channels, (b)  $N_{mic}$ , and (c) labile N pool in maize rhizosphere reusing cover crop root channels in the topsoil and the (d-e) subsoil at T2 (maize growth stage BBCH 33). The effects of cover crop mixtures and soil layers and their interaction were tested using Kruskal-Wallis-Test followed by Dunn's test as post-hoc test. Lowercase letters indicate significant differences between cover crop mixtures in each soil layer ( $p < 0.05$ ).

In the subsoil,  $V_{\max}$  of LAP was 44-fold higher in the brassica/grass root channels reused by maize compared to  $V_{\max}$  of LAP in the legume/grass root channels reused by maize (Figure 1-5 d), and  $V_{\max}$  of GLU showed a similar, although not significant trend (Figure 1-5 c).

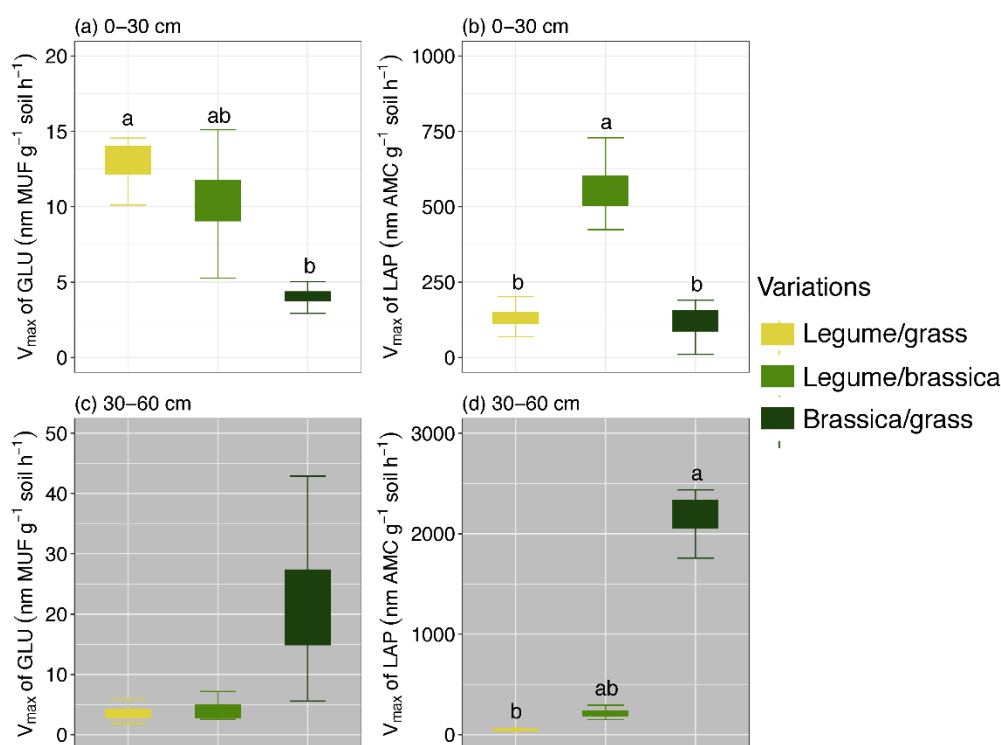


**Figure 1-5**  $\beta$ -glucosidase activity in the (a) topsoil and (c) subsoil, and leucine aminopeptidase activity in the (b) topsoil and (d) subsoil activities in maize rhizosphere reusing cover crop root channels in the topsoil and the subsoil at T2 (maize growth stage BBCH 33). The effects of cover crop mixtures and soil layers and their interaction were tested using Kruskal-Wallis-Test followed by Dunn's test as post-hoc test. Lowercase letters indicate significant differences between cover crop mixtures in each soil layer ( $p < 0.05$ ).

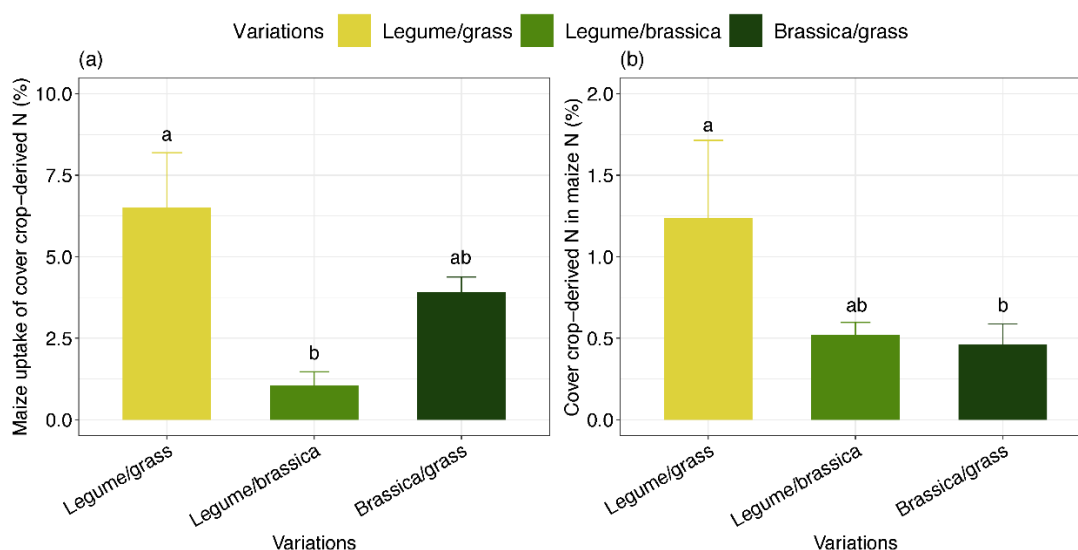


**Figure 1-6** Percentage of (a) maize uptake of cover crop-derived N (%) and (b) cover crop-derived N in maize N (%). The difference of cover crop mixtures was test by Kruskal-Wallis-Test followed by Dunn's test as post-hoc test ( $p < 0.05$ ). Capital letters indicate significant differences between cover crop mixtures.

The composition of the cover crop mixture significantly affected the uptake of cover crop-derived N by maize (Figure 1-6). Maize took up most cover crop-derived N (6.5 %) when reusing the root channels of the legume/grass mixture, followed by brassica/grass (3.9 %) and legume/brassica (1.0 %). Cover crop-derived N contributed most to maize N when the maize was growing after the legume/grass mixture (1.1 %), followed by legume/brassica (0.5 %) and brassica/grass (0.5 %).

## **4. Discussion**

### **4.1 Dynamic of cover crop-derived C and N allocation in cover crop root channels**

In the topsoil, the increase of cover crop-derived C and N in the walls of the root channels from T1 to T2 documents the continuous decomposition of cover crop root residues in all mixtures from maize germination (T1) to maize growth stage BBCH33 (T2). Cover crops have been demonstrated to increase  $C_{mic}$  by 40 % and  $N_{mic}$  by 51 % in a global meta-analysis, especially in medium-textured soils (Muhammad et al., 2021). Comparing cover crop mixtures with different composition in our study, we found that the incorporation of cover crop-derived C and N into microbial biomass was most distinct in the legume/grass and the brassica/grass mixtures in our study. However, with the progressing decomposition of cover crop residues from T1 to T2, the transfer of N from  $N_{mic}$  to the labile pool gradually increased the availability of cover crop-derived N in the topsoil.

In the subsoil, the total amount of cover crop-derived C in the root channels increased during the maize growth period only after the legume/grass mixture, while the root channels of both mixtures containing brassica lost cover crop-derived total C from T1 to T2. This can be explained by the early death of the winter-killed oil radish and consequently already more advanced mineralization of the root residues in these root channels. Accordingly, the results show a greater transfer of cover crop derived C into the labile C pool from T1 to T2 in the root channels of both mixtures containing brassica, suggesting an already more advanced channeling of C through the microbial biomass compared to the completely winter-hardy legume/grass mixture. The primary chemical factors determining the kinetics of cover crop residue decomposition and nutrient release are the C:N ratio, and concentrations of lignin in the plant tissues (Adhikari et al., 2024; Johnson et al., 2007; Parton et al., 2007). Residues of grass with high lignin content and wider C:N ratios generally degrade slower and release nutrients to the soil over longer time periods (Chaves et al., 2021; Kühling et al., 2023; J. Ramirez-Garcia et al., 2015). However, in our study, the higher proportion of cover crop-derived C in subsoil root channels of the legume/grass mixture compared to the legume/brassica mixture at T2 is most likely mainly due to the less advanced decomposition of the winter hardy legumes and grasses compared to the winter-killed brassica. The microorganisms incorporated more cover crop-derived C into their biomass in the subsoil root channels of the legume/grass mixture compared to the other mixtures. This  $C_{mic}$  will subsequently be converted to necromass, one of the primary C-containing constituents contributing to the stable soil organic matter pool (Liang et al., 2017). Different from C, the mineralized N released from the decaying oil radish roots in winter can be used by the winter-hardy partners in the mixtures, which can help to reduce losses via leaching (Hirsh et al., 2021; Sedghi and Weil, 2022).

### **4.2 Partitioning of cover crop-derived C and N in maize rhizosphere**

The total content of cover crop-derived C in cover crop root channels reused by maize was in a similar range as in the empty cover crop root channels at maize growth stage BBCH33 (T2). However, when the root channels were reused by maize, the microorganisms incorporated more cover crop-derived C into their biomass in legume/grass and brassica/grass root channels than in legume/brassica root channels. In the well-fertilized topsoil, microorganisms in maize rhizosphere did not preferentially use cover crop-derived N from the root channels, because the already high N availability rendered microbial N mineralization less crucial (Geisseler et al., 2010; Schimel and Bennett, 2004). However, amongst the mixtures, the assimilation of N by microorganisms showed a similar trend as C, with higher cover crop-derived  $N_{mic}$  in the mixtures with grass than in the legume/brassica mixture.

In agroecosystems, root channel reuse is usually considered to be essential in the subsoil, as it is the

zone where root channels can persist for decades (Hagedorn and Bundt, 2002), and where the penetration resistance is high, making it more difficult for plant roots to grow directly through the soil matrix (Chen and Weil, 2010; Wahlström et al., 2021). Our findings reveal that the subsoil root channels of the legume/grass mixture contained more cover crop-derived C and N than the legume/brassica and brassica/grass root channels at maize growth stage BBCH33 (T2). This is because the root residues in the completely winter hardy legume/grass mixture's root channels are least decomposed. However, they will consequently still hold large amounts of attractive substrates for microbial metabolism, which will be increasingly stimulated by the exudates of the active maize roots that just reached the subsoil at BBCH33 (Kuzyakov and Blagodatskaya, 2015; Liu et al., 2022; Ma et al., 2023). Accordingly, the cover crop-derived C and N were highly partitioned to microbial biomass in the subsoil root channels of the legume/grass mixture that were already reused by maize roots. This high C and N assimilation capacity of microorganisms is linked to an overall high total amount of microbial biomass in these root channels (Fig. S3c).

### **4.3 Nitrogen uptake related to enzyme activity in maize rhizosphere**

The contrasting distribution of enzyme activities in the root channels reused by maize in the topsoil and subsoil suggests that the decomposition processes and stages of the residues in the root channels differ in these two zones, most likely caused by the different temperature, air and water regimes in topsoil and subsoil (Gill and Burke, 2002; Sanaullah et al., 2011). The contrary trend of enzyme activities in topsoil and subsoil between the mixtures containing legumes and the brassica/grass mixture are a result of the intertwining of N-demand for enzyme production, and the enzyme requirement to release N from substrate. In the subsoil, just reached by the maize roots at BBCH33, the proportion of root tips, with intensive release of N-containing root exudates (Baudoin et al., 2003), is high. Thus, the N-supply from root exudates for the formation of microbial exoenzymes (GLU and LAP) is most likely higher in the rhizosphere of maize roots in the subsoil than in the topsoil at BBCH33. However, the actually developing enzyme activity is also a function of the requirements for substrate decomposition for energy and N release, and the decomposition of the residues in the brassica/grass root channels will require more enzyme activity than the more easily degradable residues in the root channels of mixtures containing legumes. In the topsoil, however, the lower abundance of maize root tips reduces the supply with fresh root exudates, so both N-supply for enzyme production and enzyme requirement for substrate decomposition are steered mainly by the substrate provided by the cover crop root residues. This leads to high enzyme activity in the legume/brassica mixture, which provides both easily available N from the legume components and easily available C from the already extensively decomposed remains of the winter-killed brassica.

An important function of cover crops is to catch nutrients that were not used by or are released from the residues of the latest cash crops, and carry them over to the next cash crop (Heuermann et al., 2022; Rouge et al., 2023). We were able to prove that maize assimilates up to 6.5 % of the cover crop derived N already at maize growth stage BBCH33, which is powerful evidence that the legume/grass mixture can significantly contribute to the N supply of the maize. The legume/grass mixture covered up to 1.1 % of the N demand of maize at BBCH33. Our results show that N transfer to maize through the reuse of legume/grass root channels is an effective sustainable farming approach for maize cultivation. The mixture with the lowest capacity of N supply from the root channel to maize was legume/brassica, composed of legumes and a winter-killed brassica. According to the results of Gentsch et al. (2022), cover crops with high N contents, such as clover and the brassica mustard, can cause high leaching losses from litter mineralization over the winter. Additionally, especially winter-killed brassica species have been proven to have no positive effect on maize N uptake and yield (Tadiello et al., 2022). However, winter-killed crops can form a protective mulch layer over winter and spring, and thereby reduce evaporation and preserve water resources for the following maize plants better than black fallow (Gentsch et al., 2022), so when considering the combination of cover crops, winter-killed crops can be included to improve soil moisture, and deep-rooting winter-hardy crops should be used to ensure

maximum N utilization.

## **Conclusion**

This study compared the C and N allocation in root channels formed by mixtures of deep- and shallow-rooting cover crops, and the effect of cover crop-derived C and N on microbial activity in cover crop root channels reused by maize. Our experiment is original in studying the reuse of cover crop root channels by maize roots in the field. Our results prove that mixtures of deep- and shallow-rooting cover crops can not only allocate newly assimilated C and N to the subsoil, but also, to varying degrees, retain this C and N in the root channels during the subsequent cash crop season. Among the different cover crop mixtures, legume/grass showed the highest potential for providing plant-derived C to the microbial community of the soil and thereby enhancing the microbial stabilization of C in subsoil root channels. The legume/grass mixture also showed a high potential of N supply from the root residues in their root channels to the following maize crop. However, the exact role each species plays in the mixture remains unclear. To support the integration of cover crop mixtures into crop rotation in agroecosystems, long-term experiments should be conducted to investigate approaches that will more accurately utilize cover crop-derived nutrients to enhance the growth of cash crops.

## **Acknowledgements**

This work is part of the Rhizo4Bio Project Network (Plant roots and soil ecosystems, significance of the rhizosphere for the bio-economy) RootWayS (Deep-rooting cover crop mixtures: Creating highways to subsoil water and nutrient resources). The authors received the funding from German Federal Ministry of Education and Research (BMBF), project number 031B0911A.

## **Statements and Declarations**

The authors declare no competing interests.

## Reference

- Abdalla, M., Hastings, A., Cheng, K., Yue, Q., Chadwick, D., Espenberg, M., Truu, J., Rees, R.M., Smith, P., 2019. A critical review of the impacts of cover crops on nitrogen leaching, net greenhouse gas balance and crop productivity. *Glob. Change Biol.* 25, 2530–2543. <https://doi.org/10.1111/gcb.14644>
- Abdollahi, L., Munkholm, L.J., Garbout, A., 2014. Tillage System and Cover Crop Effects on Soil Quality: II. Pore Characteristics. *Soil Sci. Soc. Am. J.* 78, 271–279. <https://doi.org/10.2136/sssaj2013.07.0302>
- Adhikari, A.D., Shrestha, P., Ghimire, R., Liu, Z., Pollock, D.A., Acharya, P., Aryal, D.R., 2024. Cover crop residue quality regulates litter decomposition dynamics and soil carbon mineralization kinetics in semi-arid cropping systems. *Appl. Soil Ecol.* 193, 105160. <https://doi.org/10.1016/j.apsoil.2023.105160>
- Amsili, J.P., Kaye, J.P., 2021. Root traits of cover crops and carbon inputs in an organic grain rotation. *Renew. Agric. Food Syst.* 36, 182–191. <https://doi.org/10.1017/S1742170520000216>
- Asaduzzaman, M., An, M., Pratley, J.E., Lockett, D.J., Lemerle, D., 2014. Canola (*Brassica napus*) germplasm shows variable allelopathic effects against annual ryegrass (*Lolium rigidum*). *Plant Soil* 380, 47–56. <https://doi.org/10.1007/s11104-014-2054-4>
- Athmann, M., Kautz, T., Banfield, C., Bauke, S., Hoang, D.T.T., Lüsebrink, M., Pausch, J., Amelung, W., Kuzyakov, Y., Köpke, U., 2017. Six months of *L. terrestris* L. activity in root-formed biopores increases nutrient availability, microbial biomass and enzyme activity. *Appl. Soil Ecol.* 120, 135–142. <https://doi.org/10.1016/j.apsoil.2017.08.015>
- Banfield, C.C., Dippold, M.A., Pausch, J., Hoang, D.T.T., Kuzyakov, Y., 2017. Biopore history determines the microbial community composition in subsoil hotspots. *Biol. Fertil. Soils* 53, 573–588. <https://doi.org/10.1007/s00374-017-1201-5>
- Banfield, C.C., Pausch, J., Kuzyakov, Y., Dippold, M.A., 2018. Microbial processing of plant residues in the subsoil – The role of biopores. *Soil Biol. Biochem.* 125, 309–318. <https://doi.org/10.1016/j.soilbio.2018.08.004>
- Barel, J.M., Kuyper, T.W., Paul, J., de Boer, W., Cornelissen, J.H.C., De Deyn, G.B., 2019. Winter cover crop legacy effects on litter decomposition act through litter quality and microbial community changes. *J. Appl. Ecol.* 56, 132–143. <https://doi.org/10.1111/1365-2664.13261>
- Berendse, F., 1981. Competition between plant populations with different rooting depths II. Pot experiments. *Oecologia* 48, 334–341. <https://doi.org/10.1007/BF00346491>
- Blagodatskaya, E., Khomyakov, N., Myachina, O., Bogomolova, I., Blagodatsky, S., Kuzyakov, Y., 2014. Microbial interactions affect sources of priming induced by cellulose. *Soil Biol. Biochem.* 74, 39–49. <https://doi.org/10.1016/j.soilbio.2014.02.017>
- Blagodatskaya, E., Kuzyakov, Y., 2008. Mechanisms of real and apparent priming effects and their dependence on soil microbial biomass and community structure: critical review. *Biol. Fertil. Soils* 45, 115–131. <https://doi.org/10.1007/s00374-008-0334-y>
- Blanco-Canqui, H., Jasa, P.J., 2019. Do Grass and Legume Cover Crops Improve Soil Properties in the Long Term? *Soil Sci. Soc. Am. J.* 83, 1181–1187. <https://doi.org/10.2136/sssaj2019.02.0055>
- Bradford, M.A., Berg, B., Maynard, D.S., Wieder, W.R., Wood, S.A., 2016. FUTURE DIRECTIONS: Understanding the dominant controls on litter decomposition. *J. Ecol.* 104, 229–238.
- Bromand, S., Whalen, J.K., Janzen, H.H., Schjoerring, J.K., Ellert, B.H., 2001. A pulse-labelling method to generate <sup>13</sup>C-enriched plant materials 5.
- Brookes, P.C., Landman, A., Pruden, G., Jenkinson, D.S., 1985. Chloroform fumigation and the release of soil nitrogen: A rapid direct extraction method to measure microbial biomass nitrogen in soil. *Soil Biol. Biochem.* 17, 837–842. [https://doi.org/10.1016/0038-0717\(85\)90144-0](https://doi.org/10.1016/0038-0717(85)90144-0)
- Brookes, P.C., Powlson, D.S., Jenkinson, D.S., 1982. Measurement of microbial biomass phosphorus in soil. *Soil Biol. Biochem.* 14, 319–329. [https://doi.org/10.1016/0038-0717\(82\)90001-3](https://doi.org/10.1016/0038-0717(82)90001-3)
- Chaves, B., Redin, M., Giacomini, S.J., Schmatz, R., Léonard, J., Ferchaud, F., Recous, S., 2021. The combination of residue quality, residue placement and soil mineral N content drives C and N dynamics by modifying N availability to microbial decomposers. *Soil Biol. Biochem.* 163, 108434. <https://doi.org/10.1016/j.soilbio.2021.108434>
- Chen, G., Weil, R.R., 2011. Root growth and yield of maize as affected by soil compaction and cover crops. *Soil Tillage Res.* 117, 17–27. <https://doi.org/10.1016/j.still.2011.08.001>
- Chen, G., Weil, R.R., 2010. Penetration of cover crop roots through compacted soils. *Plant Soil* 331, 31–43. <https://doi.org/10.1007/s11104-009-0223-7>
- Cleveland, C.C., Liptzin, D., 2007. C:N:P stoichiometry in soil: is there a “Redfield ratio” for the microbial biomass? *Biogeochemistry* 85, 235–252. <https://doi.org/10.1007/s10533-007-9132-0>
- Cotrufo, M.F., Wallenstein, M.D., Boot, C.M., Deneff, K., Paul, E., 2013. The Microbial Efficiency-Matrix Stabilization (MEMS) framework integrates plant litter decomposition with soil organic matter stabilization: do labile plant inputs form stable soil organic matter? *Glob. Change Biol.* 19, 988–995. <https://doi.org/10.1111/gcb.12113>
- Couëdel, A., Alletto, L., Tribouillois, H., Justes, É., 2018. Cover crop crucifer-legume mixtures provide effective nitrate catch crop and nitrogen green manure ecosystem services. *Agric. Ecosyst. Environ.* 254, 50–59. <https://doi.org/10.1016/j.agee.2017.11.017>
- da Silva, J.P., Teixeira, R. da S., da Silva, I.R., Soares, E.M.B., Lima, A.M.N., 2022. Decomposition and nutrient release from legume and non-legume residues in a tropical soil. *Eur. J. Soil Sci.* 73, e13151. <https://doi.org/10.1111/ejss.13151>
- De Notaris, C., Olesen, J.E., Sørensen, P., Rasmussen, J., 2020. Input and mineralization of carbon and nitrogen in soil from legume-based cover crops. *Nutr. Cycl. Agroecosystems* 116, 1–18. <https://doi.org/10.1007/s10705-019->

- Faucon, M.-P., Houben, D., Lambers, H., 2017. Plant Functional Traits: Soil and Ecosystem Services. *Trends Plant Sci.* 22, 385–394. <https://doi.org/10.1016/j.tplants.2017.01.005>
- Feng, J., He, K., Zhang, Q., Han, M., Zhu, B., 2022. Changes in plant inputs alter soil carbon and microbial communities in forest ecosystems. *Glob. Change Biol.* 28, 3426–3440. <https://doi.org/10.1111/gcb.16107>
- Feng, X., Hao, Y., Latifmanesh, H., Lal, R., Cao, T., Guo, J., Deng, A., Song, Z., Zhang, W., 2018. Effects of Subsoiling Tillage on Soil Properties, Maize Root Distribution, and Grain Yield on Mollisols of Northeastern China. *Agron. J.* 110, 1607–1615. <https://doi.org/10.2134/agronj2018.01.0027>
- Feng, X., Wang, S., 2023. Plant influences on soil microbial carbon pump efficiency. *Glob. Change Biol.* 29, 3854–3856. <https://doi.org/10.1111/gcb.16728>
- Finney, D.M., Kaye, J.P., 2017. Functional diversity in cover crop polycultures increases multifunctionality of an agricultural system. *J. Appl. Ecol.* 54, 509–517. <https://doi.org/10.1111/1365-2664.12765>
- Freund, L., Mariotte, P., Santonja, M., Buttler, A., Jeangros, B., 2021. Species identity, rather than species mixtures, drives cover crop effects on nutrient partitioning in unfertilized agricultural soil. *Plant Soil* 460, 149–162. <https://doi.org/10.1007/s11104-020-04782-z>
- Garba, I.I., Bell, L.W., Chapman, S.C., deVoil, P., Kamara, A.Y., Williams, A., 2023. Modelling the impacts of diverse cover crops on soil water and nitrogen and cash crop yields in a sub-tropical dryland. *Field Crops Res.* 301, 109019. <https://doi.org/10.1016/j.fcr.2023.109019>
- Geisseler, D., Horwath, W.R., Joergensen, R.G., Ludwig, B., 2010. Pathways of nitrogen utilization by soil microorganisms – A review. *Soil Biol. Biochem.* 42, 2058–2067. <https://doi.org/10.1016/j.soilbio.2010.08.021>
- Gentsch, N., Heuermann, D., Boy, J., Schierding, S., von Wirén, N., Schweneker, D., Feuerstein, U., Kümmerer, R., Bauer, B., Guggenberger, G., 2022. Soil nitrogen and water management by winter-killed catch crops. *SOIL* 8, 269–281. <https://doi.org/10.5194/soil-8-269-2022>
- Gfeller, A., Herrera, J.M., Tschuy, F., Wirth, J., 2018. Explanations for *Amaranthus retroflexus* growth suppression by cover crops. *Crop Prot.* 104, 11–20. <https://doi.org/10.1016/j.cropro.2017.10.006>
- Gill, R.A., Burke, I.C., 2002. Influence of soil depth on the decomposition of *Bouteloua gracilis* roots in the shortgrass steppe. *Plant Soil* 241, 233–242. <https://doi.org/10.1023/A:1016146805542>
- Hagedorn, F., Bundt, M., 2002. The age of preferential flow paths. *Geoderma* 108, 119–132. [https://doi.org/10.1016/S0016-7061\(02\)00129-5](https://doi.org/10.1016/S0016-7061(02)00129-5)
- Halde, C., Entz, M.H., 2016. Plant species and mulch application rate affected decomposition of cover crop mulches used in organic rotational no-till systems. *Can. J. Plant Sci.* 96, 59–71. <https://doi.org/10.1139/cjps-2015-0095>
- Hamza, M.A., Anderson, W.K., 2005. Soil compaction in cropping systems: A review of the nature, causes and possible solutions. *Soil Tillage Res.* 82, 121–145. <https://doi.org/10.1016/j.still.2004.08.009>
- Han, E., Czaban, W., Dresbøll, D.B., Thorup-Kristensen, K., 2022. Exploitation of neighbouring subsoil for nutrient acquisition under annual-perennial strip intercropping systems. *Agric. Ecosyst. Environ.* 338, 108106. <https://doi.org/10.1016/j.agee.2022.108106>
- Heinrich, S., Dippold, M.A., Werner, C., Wiesenberg, G.L.B., Kuzyakov, Y., Glaser, B., 2015. Allocation of freshly assimilated carbon into primary and secondary metabolites after in situ <sup>13</sup>C pulse labelling of Norway spruce (*Picea abies*). *Tree Physiol.* tpv083. <https://doi.org/10.1093/treephys/tpv083>
- Heuermann, D., Gentsch, N., Guggenberger, G., Reinhold-Hurek, B., Schweneker, D., Feuerstein, U., Heuermann, M.C., Groß, J., Kümmerer, R., Bauer, B., von Wirén, N., 2022. Catch crop mixtures have higher potential for nutrient carry-over than pure stands under changing environments. *Eur. J. Agron.* 136, 126504. <https://doi.org/10.1016/j.eja.2022.126504>
- Hirsh, S.M., Duiker, S.W., Graybill, J., Nichols, K., Weil, R.R., 2021. Scavenging and recycling deep soil nitrogen using cover crops on mid-Atlantic, USA farms. *Agric. Ecosyst. Environ.* 309, 107274. <https://doi.org/10.1016/j.agee.2020.107274>
- Hoang, D.T.T., Bauke, S.L., Kuzyakov, Y., Pausch, J., 2017. Rolling in the deep: Priming effects in earthworm biopores in topsoil and subsoil. *Soil Biol. Biochem.* 114, 59–71. <https://doi.org/10.1016/j.soilbio.2017.06.021>
- Hoang, D.T.T., Pausch, J., Razavi, B.S., Kuzyakova, I., Banfield, C.C., Kuzyakov, Y., 2016. Hotspots of microbial activity induced by earthworm burrows, old root channels, and their combination in subsoil. *Biol. Fertil. Soils* 52, 1105–1119. <https://doi.org/10.1007/s00374-016-1148-y>
- Holtham, D.A.L., Matthews, G.P., Scholefield, D.S., 2007. Measurement and simulation of void structure and hydraulic changes caused by root-induced soil structuring under white clover compared to ryegrass. *Geoderma* 142, 142–151. <https://doi.org/10.1016/j.geoderma.2007.08.018>
- Jensen, E.S., 1996. Grain yield, symbiotic N<sub>2</sub> fixation and interspecific competition for inorganic N in pea-barley intercrops. *Plant Soil* 182, 25–38. <https://doi.org/10.1007/BF00010992>
- Jian, J., Du, X., Reiter, M.S., Stewart, R.D., 2020. A meta-analysis of global cropland soil carbon changes due to cover cropping. *Soil Biol. Biochem.* 143, 107735. <https://doi.org/10.1016/j.soilbio.2020.107735>
- Jilling, A., Keiluweit, M., Contosta, A.R., Frey, S., Schimel, J., Schnecker, J., Smith, R.G., Tiemann, L., Grandy, A.S., 2018. Minerals in the rhizosphere: overlooked mediators of soil nitrogen availability to plants and microbes. *Biogeochemistry* 139, 103–122. <https://doi.org/10.1007/s10533-018-0459-5>
- Johnson, J.M.-F., Barbour, N.W., Weyers, S.L., 2007. Chemical Composition of Crop Biomass Impacts Its Decomposition. *Soil Sci. Soc. Am. J.* 71, 155–162. <https://doi.org/10.2136/sssaj2005.0419>
- Kautz, T., Amelung, W., Ewert, F., Gaiser, T., Horn, R., Jahn, R., Javaux, M., Kemna, A., Kuzyakov, Y., Munch, J.-C., Pätzold, S., Peth, S., Scherer, H.W., Schloter, M., Schneider, H., Vanderborght, J., Vetterlein, D., Walter, A., Wiesenberg, G.L.B., Köpke, U., 2013. Nutrient acquisition from arable subsoils in temperate climates: A review.

- Soil Biol. Biochem. 57, 1003–1022. <https://doi.org/10.1016/j.soilbio.2012.09.014>
- Kaye, J.P., Quemada, M., 2017. Using cover crops to mitigate and adapt to climate change. A review. *Agron. Sustain. Dev.* 37, 4. <https://doi.org/10.1007/s13593-016-0410-x>
- Kell, D.B., 2011. Breeding crop plants with deep roots: their role in sustainable carbon, nutrient and water sequestration. *Ann. Bot.* 108, 407–418. <https://doi.org/10.1093/aob/mcr175>
- Kirkby, C.A., Kirkegaard, J.A., Richardson, A.E., Wade, L.J., Blanchard, C., Batten, G., 2011. Stable soil organic matter: A comparison of C:N:P:S ratios in Australian and other world soils. *Geoderma* 163, 197–208. <https://doi.org/10.1016/j.geoderma.2011.04.010>
- Kirkby, C.A., Richardson, A.E., Wade, L.J., Passioura, J.B., Batten, G.D., Blanchard, C., Kirkegaard, J.A., 2014. Nutrient availability limits carbon sequestration in arable soils. *Soil Biol. Biochem.* 68, 402–409. <https://doi.org/10.1016/j.soilbio.2013.09.032>
- Kühling, I., Mikuszies, P., Helfrich, M., Flessa, H., Schlathöller, M., Sieling, K., Kage, H., 2023. Effects of winter cover crops from different functional groups on soil-plant nitrogen dynamics and silage maize yield. *Eur. J. Agron.* 148, 126878. <https://doi.org/10.1016/j.eja.2023.126878>
- Kuzyakov, Y., Blagodatskaya, E., 2015. Microbial hotspots and hot moments in soil: Concept & review. *Soil Biol. Biochem.* 83, 184–199. <https://doi.org/10.1016/j.soilbio.2015.01.025>
- Kuzyakov, Y., Domanski, G., 2000. Carbon input by plants into the soil. *Review. J. Plant Nutr. Soil Sci.* 163, 421–431. [https://doi.org/10.1002/1522-2624\(200008\)163:4<421::AID-JPLN421>3.0.CO;2-R](https://doi.org/10.1002/1522-2624(200008)163:4<421::AID-JPLN421>3.0.CO;2-R)
- Lavergne, S., Vanasse, A., Thivierge, M.-N., Halde, C., 2021. Using fall-seeded cover crop mixtures to enhance agroecosystem services: A review. *Agrosystems Geosci. Environ.* 4, e20161. <https://doi.org/10.1002/agg2.20161>
- Li, L., Tilman, D., Lambers, H., Zhang, F.-S., 2014. Plant diversity and overyielding: insights from belowground facilitation of intercropping in agriculture. *New Phytol.* 203, 63–69. <https://doi.org/10.1111/nph.12778>
- Li, L., Wilson, C.B., He, H., Zhang, X., Zhou, F., Schaeffer, S.M., 2019. Physical, biochemical, and microbial controls on amino sugar accumulation in soils under long-term cover cropping and no-tillage farming. *Soil Biol. Biochem.* 135, 369–378. <https://doi.org/10.1016/j.soilbio.2019.05.017>
- Liang, C., Schimel, J.P., Jastrow, J.D., 2017. The importance of anabolism in microbial control over soil carbon storage. *Nat. Microbiol.* 2, 1–6. <https://doi.org/10.1038/nmicrobiol.2017.105>
- Liu, S., He, F., Kuzyakov, Y., Xiao, H., Hoang, D.T.T., Pu, S., Razavi, B.S., 2022. Nutrients in the rhizosphere: A meta-analysis of content, availability, and influencing factors. *Sci. Total Environ.* 826, 153908. <https://doi.org/10.1016/j.scitotenv.2022.153908>
- Ma, Y., Yue, K., Heděnc, P., Li, C., Li, Y., Wu, Q., 2023. Global patterns of rhizosphere effects on soil carbon and nitrogen biogeochemical processes. *CATENA* 220, 106661. <https://doi.org/10.1016/j.catena.2022.106661>
- Mayer, J., Buegger, F., Jensen, E.S., Schloter, M., Heß, J., 2003. Estimating N rhizodeposition of grain legumes using a <sup>15</sup>N in situ stem labelling method. *Soil Biol. Biochem.* 35, 21–28. [https://doi.org/10.1016/S0038-0717\(02\)00212-2](https://doi.org/10.1016/S0038-0717(02)00212-2)
- McClelland, S.C., Paustian, K., Schipanski, M.E., 2021. Management of cover crops in temperate climates influences soil organic carbon stocks: a meta-analysis. *Ecol. Appl.* 31, e02278. <https://doi.org/10.1002/eap.2278>
- Merkel, A., 2022. Climate LTA Achterwehr und Uelzen [WWW Document]. *Clim. based ECMWF Data (Copernicus Clim. Chang. Serv. 1991–2021)*.
- Michaelis, L., Menten, M.L., 1913. Die kinetik der invertinwirkung. *Biochem Z* 49, 352.
- Moore, E. b., Wiedenhoef, M. h., Kaspar, T. c., Cambardella, C. a., 2014. Rye Cover Crop Effects on Soil Quality in No-Till Corn Silage–Soybean Cropping Systems. *Soil Sci. Soc. Am. J.* 78, 968–976. <https://doi.org/10.2136/sssaj2013.09.0401>
- Muhammad, I., Wang, J., Sainju, U.M., Zhang, S., Zhao, F., Khan, A., 2021. Cover cropping enhances soil microbial biomass and affects microbial community structure: A meta-analysis. *Geoderma* 381, 114696. <https://doi.org/10.1016/j.geoderma.2020.114696>
- Murungu, F.S., Chiduzza, C., Muchaonyerwa, P., Mnkeni, P.N.S., 2011. Decomposition, nitrogen and phosphorus mineralization from winter-grown cover crop residues and suitability for a smallholder farming system in South Africa. *Nutr. Cycl. Agroecosystems* 89, 115–123. <https://doi.org/10.1007/s10705-010-9381-5>
- Nannipieri, P., Giagnoni, L., Renella, G., Puglisi, E., Ceccanti, B., Masciandaro, G., Fornasier, F., Moscatelli, M.C., Marinari, S., 2012. Soil enzymology: classical and molecular approaches. *Biol. Fertil. Soils* 48, 743–762. <https://doi.org/10.1007/s00374-012-0723-0>
- Nevins, C.J., Lacey, C., Armstrong, S., 2020. The synchrony of cover crop decomposition, enzyme activity, and nitrogen availability in a corn agroecosystem in the Midwest United States. *Soil Tillage Res.* 197, 104518. <https://doi.org/10.1016/j.still.2019.104518>
- Nevins, C.J., Nakatsu, C., Armstrong, S., 2018. Characterization of microbial community response to cover crop residue decomposition. *Soil Biol. Biochem.* 127, 39–49. <https://doi.org/10.1016/j.soilbio.2018.09.015>
- Ning, T., Liu, Z., Hu, H., Li, G., Kuzyakov, Y., 2022. Physical, chemical and biological subsoiling for sustainable agriculture. *Soil Tillage Res.* 223, 105490. <https://doi.org/10.1016/j.still.2022.105490>
- O’Dea, J.K., Miller, P.R., Jones, C.A., 2013. Greening summer fallow with legume green manures: On-farm assessment in north-central Montana. *J. Soil Water Conserv.* 68, 270–282. <https://doi.org/10.2489/jswc.68.4.270>
- Oram, N.J., Ravenek, J.M., Barry, K.E., Weigelt, A., Chen, H., Gessler, A., Gockele, A., de Kroon, H., van der Paauw, J.W., Scherer-Lorenzen, M., Smit-Tiekstra, A., van Ruijven, J., Mommer, L., 2018. Below-ground complementarity effects in a grassland biodiversity experiment are related to deep-rooting species. *J. Ecol.* 106, 265–277. <https://doi.org/10.1111/1365-2745.12877>

- Parton, W., Silver, W.L., Burke, I.C., Grassens, L., Harmon, M.E., Currie, W.S., King, J.Y., Adair, E.C., Brandt, L.A., Hart, S.C., Fasth, B., 2007. Global-Scale Similarities in Nitrogen Release Patterns During Long-Term Decomposition. *Science* 315, 361–364. <https://doi.org/10.1126/science.1134853>
- Paul, E.A., 2016. The nature and dynamics of soil organic matter: Plant inputs, microbial transformations, and organic matter stabilization. *Soil Biol. Biochem.* 98, 109–126. <https://doi.org/10.1016/j.soilbio.2016.04.001>
- Pausch, J., Kramer, S., Scharroba, A., Scheunemann, N., Butenschoen, O., Kandeler, E., Marhan, S., Riederer, M., Scheu, S., Kuzyakov, Y., Ruess, L., 2016. Small but active – pool size does not matter for carbon incorporation in below-ground food webs. *Funct. Ecol.* 30, 479–489. <https://doi.org/10.1111/1365-2435.12512>
- Peixoto, L., Elsgaard, L., Rasmussen, J., Kuzyakov, Y., Banfield, C.C., Dippold, M.A., Olesen, J.E., 2020. Decreased rhizodeposition, but increased microbial carbon stabilization with soil depth down to 3.6 m. *Soil Biol. Biochem.* 150, 108008. <https://doi.org/10.1016/j.soilbio.2020.108008>
- Peixoto, L., Olesen, J.E., Elsgaard, L., Enggrob, K.L., Banfield, C.C., Dippold, M.A., Nicolaisen, M.H., Bak, F., Zang, H., Dresbøll, D.B., Thorup-Kristensen, K., Rasmussen, J., 2022. Deep-rooted perennial crops differ in capacity to stabilize C inputs in deep soil layers. *Sci. Rep.* 12, 5952. <https://doi.org/10.1038/s41598-022-09737-1>
- Poeplau, C., Aronsson, H., Myrbeck, Å., Kätterer, T., 2015. Effect of perennial ryegrass cover crop on soil organic carbon stocks in southern Sweden. *Geoderma Reg.* 4, 126–133. <https://doi.org/10.1016/j.geodrs.2015.01.004>
- Ramírez-García, J., Carrillo, J.M., Ruiz, M., Alonso-Ayuso, M., Quemada, M., 2015. Multicriteria decision analysis applied to cover crop species and cultivars selection. *Field Crops Res.* 175, 106–115. <https://doi.org/10.1016/j.fcr.2015.02.008>
- Ramirez-Garcia, J., Gabriel, J.L., Alonso-Ayuso, M., Quemada, M., 2015. Quantitative characterization of five cover crop species. *J. Agric. Sci.* 153, 1174–1185. <https://doi.org/10.1017/S0021859614000811>
- Ramirez-Garcia, Javier, Martens, H.J., Quemada, M., Thorup-Kristensen, K., 2015. Intercropping effect on root growth and nitrogen uptake at different nitrogen levels. *J. Plant Ecol.* 8, 380–389. <https://doi.org/10.1093/jpe/rtu024>
- Ranells, N.N., Wagger, M.G., 1997. Grass–Legume Bicultures as Winter Annual Cover Crops. *Agron. J.* 89, 659–665. <https://doi.org/10.2134/agronj1997.00021962008900040019x>
- Razavi, B.S., Blagodatskaya, E., Kuzyakov, Y., 2015. Nonlinear temperature sensitivity of enzyme kinetics explains canceling effect—a case study on loamy haplic Luvisol. *Front. Microbiol.* 6.
- Rosa, A.T., Creech, C.F., Elmore, R.W., Rudnick, D.R., Lindquist, J.L., Butts, L., de Faria, I.K.P., Werle, R., 2021. Contributions of individual cover crop species to rainfed maize production in semi-arid cropping systems. *Field Crops Res.* 271, 108245. <https://doi.org/10.1016/j.fcr.2021.108245>
- Rouge, A., Adeux, G., Busset, H., Hugard, R., Martin, J., Matejicek, A., Moreau, D., Guillemain, J.-P., Cordeau, S., 2023. Carry-over effects of cover crops on weeds and crop productivity in no-till systems. *Field Crops Res.* 295, 108899. <https://doi.org/10.1016/j.fcr.2023.108899>
- Saar, S., Semchenko, M., Barel, J.M., De Deyn, G.B., 2016. Legume presence reduces the decomposition rate of non-legume roots. *Soil Biol. Biochem.* 94, 88–93. <https://doi.org/10.1016/j.soilbio.2015.11.026>
- Sainju, U.M., Singh, B.P., Whitehead, W.F., Wang, S., 2006. Carbon Supply and Storage in Tilled and Nontilled Soils as Influenced by Cover Crops and Nitrogen Fertilization. *J. Environ. Qual.* 35, 1507–1517. <https://doi.org/10.2134/jeq2005.0189>
- Sanaullah, M., Chabbi, A., Leifeld, J., Bardoux, G., Billou, D., Rumpel, C., 2011. Decomposition and stabilization of root litter in top- and subsoil horizons: what is the difference? *Plant Soil* 338, 127–141. <https://doi.org/10.1007/s11104-010-0554-4>
- Schimel, J.P., Bennett, J., 2004. Nitrogen Mineralization: Challenges of a Changing Paradigm. *Ecology* 85, 591–602. <https://doi.org/10.1890/03-8002>
- Sedghi, N., Weil, R., 2022. Fall cover crop nitrogen uptake drives reductions in winter-spring leaching. *J. Environ. Qual.* 51, 337–351. <https://doi.org/10.1002/jeq2.20342>
- Smith, R.G., Atwood, L.W., Warren, N.D., 2014. Increased Productivity of a Cover Crop Mixture Is Not Associated with Enhanced Agroecosystem Services. *PLOS ONE* 9, e97351. <https://doi.org/10.1371/journal.pone.0097351>
- Snapp, S.S., Swinton, S.M., Labarta, R., Mutch, D., Black, J.R., Leep, R., Nyiraneza, J., O’Neil, K., 2005. Evaluating Cover Crops for Benefits, Costs and Performance within Cropping System Niches. *Agron. J.* 97, 322–332. <https://doi.org/10.2134/agronj2005.0322a>
- Sommer, J., Dippold, M., Kuzyakov, Y., 2017. Different responses of ash and beech on nitrate versus ammonium leaf labeling. *J. Plant Nutr. Soil Sci.* 180, 446–453. <https://doi.org/10.1002/jpln.201600385>
- St Aime, R., Bridges Jr., W.C., Narayanan, S., 2023. Fall–winter cover crops promote soil health and weed control in the southeastern clayey soils. *Agron. J.* 115, 242–260. <https://doi.org/10.1002/agj2.21246>
- Sterner, R.W., Elser, J.J., 2017. Ecological Stoichiometry: The Biology of Elements from Molecules to the Biosphere, in: *Ecological Stoichiometry*. Princeton University Press. <https://doi.org/10.1515/9781400885695>
- Tadiello, T., Potenza, E., Marino, P., Perego, A., Torre, D.D., Michelon, L., Bechini, L., 2022. Growth, weed control, and nitrogen uptake of winter-killed cover crops, and their effects on maize in conservation agriculture. *Agron. Sustain. Dev.* 42, 18. <https://doi.org/10.1007/s13593-021-00747-3>
- Thapa, R., Mirsky, S.B., Tully, K.L., 2018. Cover Crops Reduce Nitrate Leaching in Agroecosystems: A Global Meta-Analysis. *J. Environ. Qual.* 47, 1400–1411. <https://doi.org/10.2134/jeq2018.03.0107>
- Thorup-Kristensen, K., Halberg, N., Nicolaisen, M., Olesen, J.E., Crews, T.E., Hinsinger, P., Kirkegaard, J., Pierret, A., Dresbøll, D.B., 2020. Digging Deeper for Agricultural Resources, the Value of Deep Rooting. *Trends Plant Sci.* 25, 406–417. <https://doi.org/10.1016/j.tplants.2019.12.007>
- Tonitto, C., David, M.B., Drinkwater, L.E., 2006. Replacing bare fallows with cover crops in fertilizer-intensive cropping systems: A meta-analysis of crop yield and N dynamics. *Agric. Ecosyst. Environ.* 112, 58–72.

<https://doi.org/10.1016/j.agee.2005.07.003>

- Tribouillois, H., Cohan, J.-P., Justes, E., 2016. Cover crop mixtures including legume produce ecosystem services of nitrate capture and green manuring: assessment combining experimentation and modelling. *Plant Soil* 401, 347–364. <https://doi.org/10.1007/s11104-015-2734-8>
- Vance, E.D., Brookes, P.C., Jenkinson, D.S., 1987. An extraction method for measuring soil microbial biomass C. *Soil Biol. Biochem.* 19, 703–707. [https://doi.org/10.1016/0038-0717\(87\)90052-6](https://doi.org/10.1016/0038-0717(87)90052-6)
- Vann, R.A., Reberg-Horton, S. c., Castillo, M. s., McGee, R. j., Mirsky, S. b., 2019. Winter Pea, Crimson Clover, and Hairy Vetch Planted in Mixture with Small Grains in the Southeast United States. *Agron. J.* 111, 805–815. <https://doi.org/10.2134/agronj2018.03.0202>
- Wahlström, E.M., Kristensen, H.L., Thomsen, I.K., Labouriau, R., Pulido-Moncada, M., Nielsen, J.A., Munkholm, L.J., 2021. Subsoil compaction effect on spatio-temporal root growth, reuse of biopores and crop yield of spring barley. *Eur. J. Agron.* 123, 126225. <https://doi.org/10.1016/j.eja.2020.126225>
- Walker, T.S., Bais, H.P., Grotewold, E., Vivanco, J.M., 2003. Root Exudation and Rhizosphere Biology. *Plant Physiol.* 132, 44–51. <https://doi.org/10.1104/pp.102.019661>
- Wang, S., Zhang, X., Zhou, J., Xu, Z., Ma, Q., Chu, J., Zang, H., Yang, Y., Peixoto, L., Zeng, Z., Razavi, B.S., 2023. Transition of spatio-temporal distribution of soil enzyme activity after straw incorporation: From rhizosphere to detritusphere. *Appl. Soil Ecol.* 186, 104814. <https://doi.org/10.1016/j.apsoil.2023.104814>
- Werner, C., Meredith, L.K., Ladd, S.N., Ingrisch, J., Kübert, A., Van Haren, J., Bahn, M., Bailey, K., Bamberger, I., Beyer, M., Blomdahl, D., Byron, J., Daber, E., Deleeuw, J., Dippold, M.A., Fudyma, J., Gil-Loaiza, J., Honeker, L.K., Hu, J., Huang, J., Klüpfel, T., Krechmer, J., Kreuzwieser, J., Kühnhammer, K., Lehmann, M.M., Meeran, K., Misztal, P.K., Ng, W.-R., Pfannerstill, E., Pugliese, G., Purser, G., Roscioli, J., Shi, L., Tfaily, M., Williams, J., 2021. Ecosystem fluxes during drought and recovery in an experimental forest. *Science* 374, 1514–1518. <https://doi.org/10.1126/science.abj6789>
- Wu, J., Joergensen, R.G., Pommerening, B., Chaussod, R., Brookes, P.C., 1990. Measurement of soil microbial biomass C by fumigation-extraction—an automated procedure. *Soil Biol. Biochem.* 22, 1167–1169. [https://doi.org/10.1016/0038-0717\(90\)90046-3](https://doi.org/10.1016/0038-0717(90)90046-3)
- Zhang, Z., Kaye, J.P., Bradley, B.A., Amsili, J.P., Suseela, V., 2022. Cover crop functional types differentially alter the content and composition of soil organic carbon in particulate and mineral-associated fractions. *Glob. Change Biol.* 28, 5831–5848. <https://doi.org/10.1111/gcb.16296>
- Zhou, G., Xu, S., Ciais, P., Manzoni, S., Fang, J., Yu, G., Tang, X., Zhou, P., Wang, W., Yan, J., Wang, G., Ma, K., Li, S., Du, S., Han, S., Ma, Y., Zhang, D., Liu, J., Liu, S., Chu, G., Zhang, Q., Li, Y., Huang, W., Ren, H., Lu, X., Chen, X., 2019. Climate and litter C/N ratio constrain soil organic carbon accumulation. *Natl. Sci. Rev.* 6, 746–757. <https://doi.org/10.1093/nsr/nwz045>
- Zhou, J., Shao, G., Kumar, A., Shi, L., Kuzyakov, Y., Pausch, J., 2022. Carbon fluxes within tree-crop-grass agroforestry system: <sup>13</sup>C field labeling and tracing. *Biol. Fertil. Soils* 58, 733–743. <https://doi.org/10.1007/s00374-022-01659-4>

## Supplementary

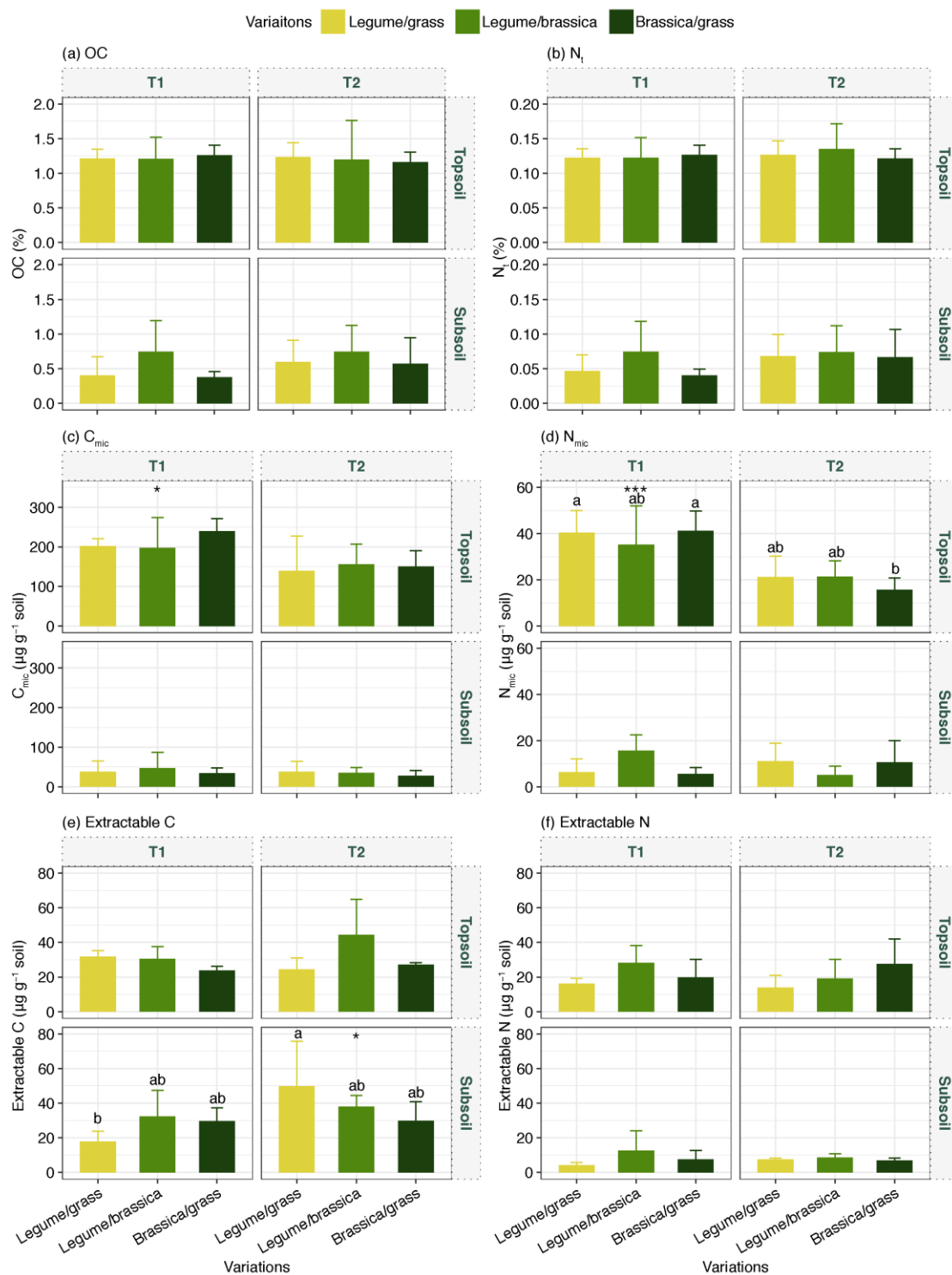


**Figure S1-1** Contents of soil organic C and N in (a, b) soil, in (c, d) microbial biomass, and in (e, f) extractable pool in the rhizosphere of cover crops in the topsoil and the subsoil at two time points. The effects of cover crop mixtures and time points and their interaction were tested using two-way ANOVA (add supplementary table of the statistical result). Lowercase letters indicate significant differences between cover crop mixture variations at all time points, within a soil layer ( $p < 0.05$ , with interaction effects of cover crop mixture variations and time points). Asterisks represent significant differences between the main factor of time points within a soil layer (\* represents  $p < 0.05$ ; \*\* represents  $p < 0.01$ ; \*\*\* represents  $p < 0.001$ ). Asterisks were noted under the time point with a significantly higher result than the other.

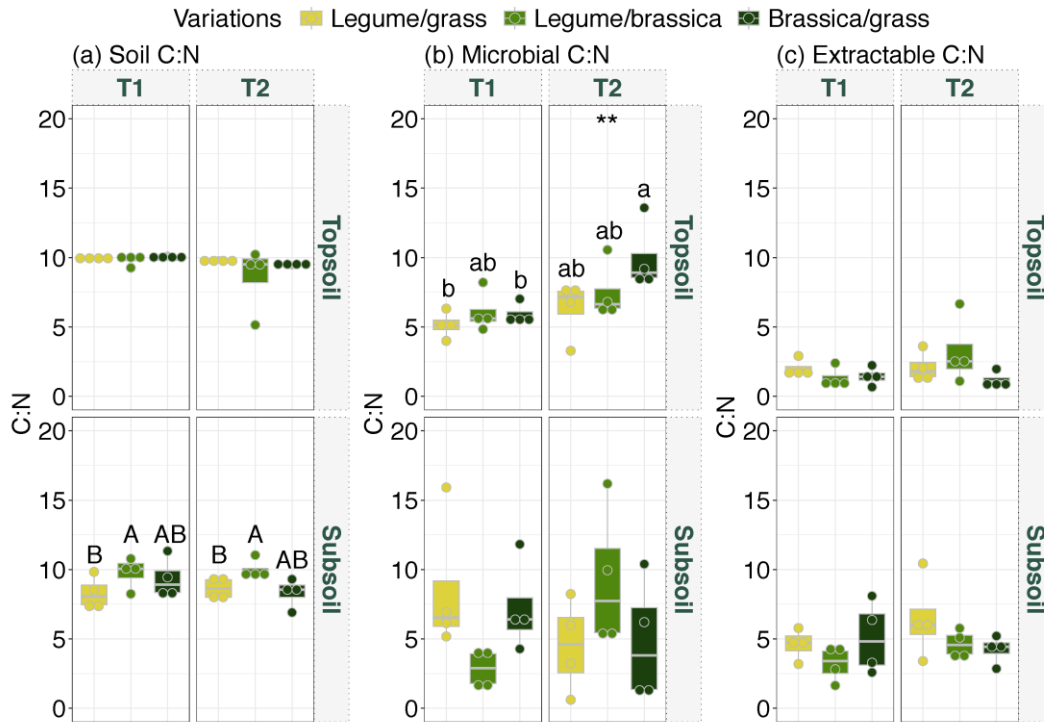


**Figure S1-2** C:N ratios in (a) soil, (b) microbial biomass, and (c) extractable pool in the rhizosphere of cover crops in the topsoil and the subsoil at two time points. Lowercase letters indicate significant differences between cover crop mixture variations at all time points, within a soil layer ( $p < 0.05$ , with interaction effects of cover crop mixture variations and time points). Capital letters indicate significant differences between the main factor of cover crop mixture variations within a soil layer ( $p < 0.05$ , without interaction effects of time points). Asterisks represent significant differences between the main factor of time points within a soil layer (\*\* represents  $p < 0.01$ ). Asterisks were noted under the time point with a significantly higher result than the other.

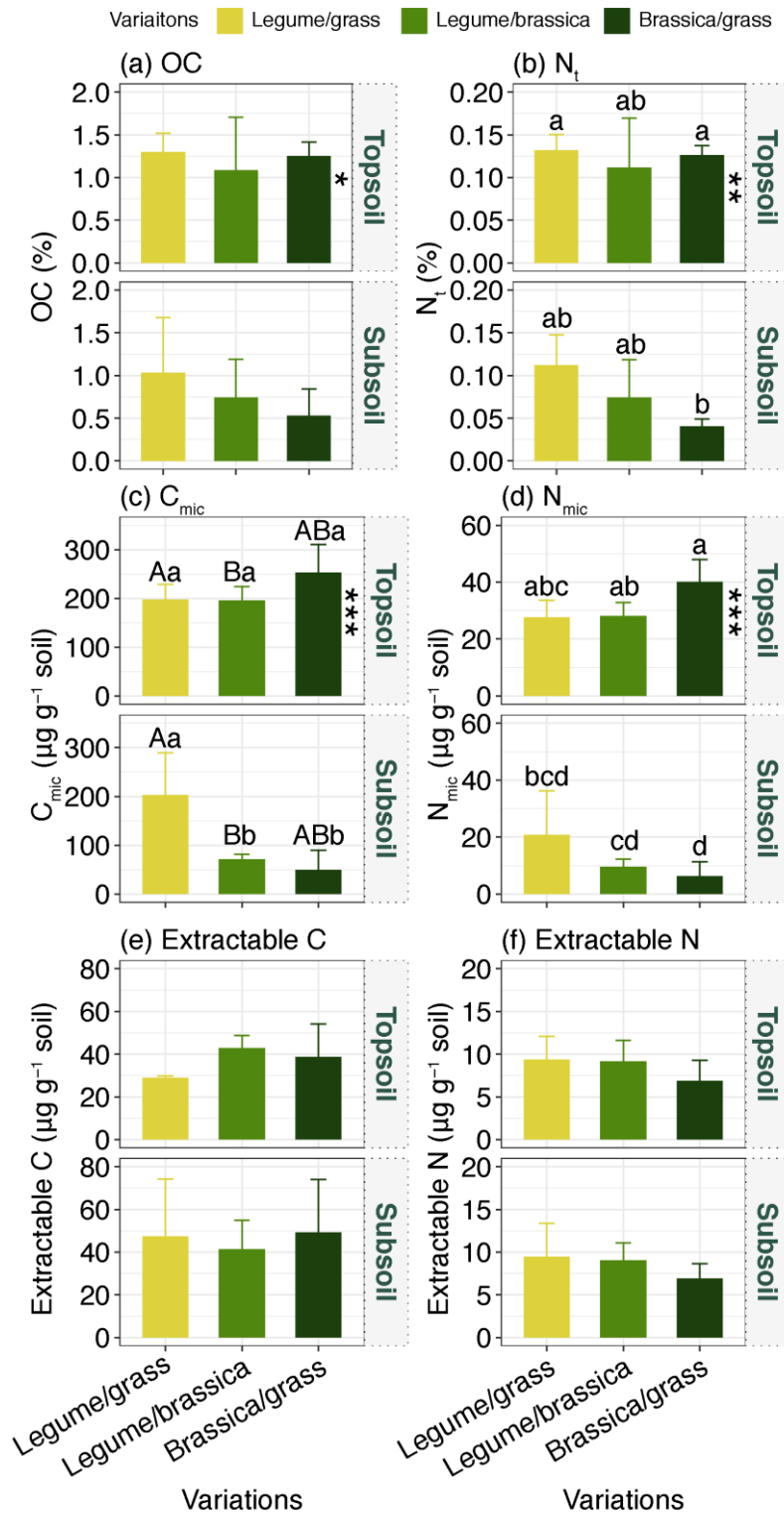


**Figure S1-3** Contents of soil organic C and N in (a, b) soil, in (c, d) microbial biomass, and in (e, f) extractable pool in the rhizosphere of maize in cover crop root channels in the topsoil and the subsoil at T2 (maize growth stage BBCH 33). The effects of cover crop mixtures and soil layers and their interaction were tested using two-way ANOVA (add supplementary table of the statistical result). Lowercase letters indicate significant differences between cover crop mixtures in both soil layers ( $p < 0.05$ , with interaction effects of cover crop mixtures and soil layers). Capital letters indicate significant differences between the main factor of cover crop mixtures ( $p < 0.05$ , without interaction effects of soil layers). Asterisks represent significant differences between the main factor of soil layers (\* represents  $p < 0.05$ ; \*\* represents  $p < 0.01$ ; \*\*\*\* represents  $p < 0.001$ ). Asterisks were noted in the soil layer with a significantly higher result than the other.

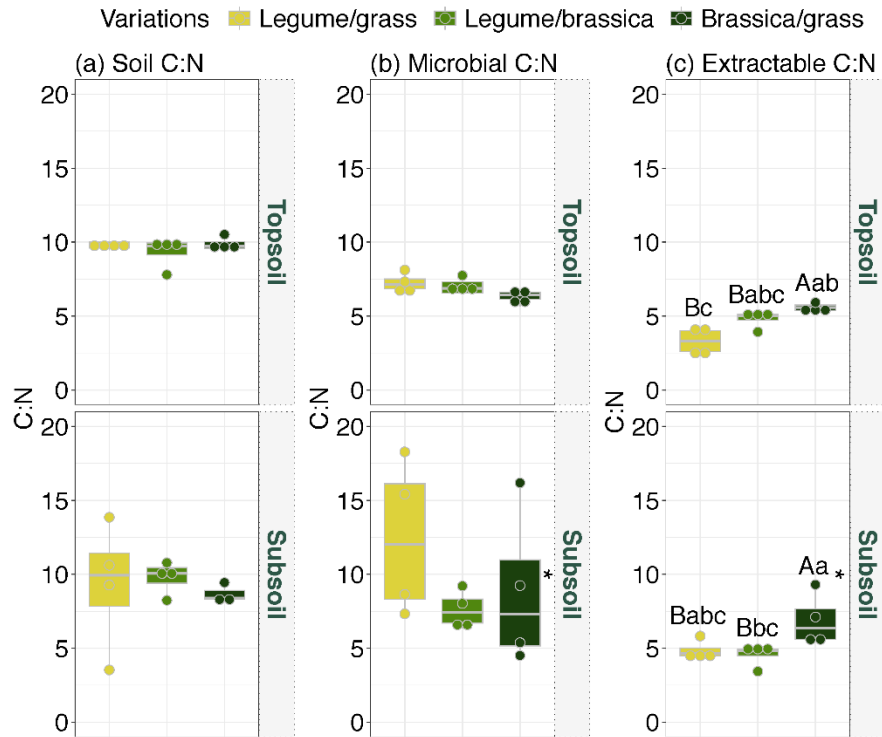


**Figure S1-4** C:N ratios in (a) soil, (b) microbial biomass, and (c) extractable pool in maize rhizosphere in cover crop root channels in the topsoil and the subsoil at T2 (maize growth stage BBCH 33). The effects of cover crop mixtures and soil layers and their interaction were tested using two-way ANOVA (add supplementary table of the statistical result). Lowercase letters indicate significant differences between cover crop mixtures in both soil layers ( $p < 0.05$ , with interaction effects of cover crop mixtures and soil layers). Capital letters indicate significant differences between the main factor of cover crop mixtures ( $p < 0.05$ , without interaction effects of soil layers). Asterisks represent significant differences between the main factor of soil layers (\* represents  $p < 0.05$ ). Asterisks were noted in the soil layer with a significantly higher result than the other.

## 2.2 Study 2. Site-specific Legacy Effect of Cover Crop Mixtures on C-cycling Enzyme Activities in the Subsequently Growing Maize (*Zea mays* L.) Rhizosphere under Drought

Yijie Shi<sup>1</sup>, Iris Zimmermann<sup>1</sup>, Debjyoti Ghosh<sup>2</sup>, Shang Wang<sup>3</sup>, Bahar S. Razavi<sup>3</sup>, Michaela A. Dippold<sup>4,5</sup>, Sandra Spielvogel<sup>1</sup>

**Status: In preparation**

<sup>1</sup> *Institute of Plant Nutrition and Soil Science, Christian-Albrechts-University Kiel, Germany*

<sup>2</sup> *Molecular Systems Biology, Helmholtz Centre for Environmental Research GmbH, Leipzig, Germany*

<sup>3</sup> *Department of Soil and Plant Microbiome, Institute of Phytopathology, Christian-Albrecht University of Kiel, Germany*

<sup>4</sup> *Geo-Biosphere Interactions, Department of Geosciences, University of Tuebingen, Germany*

<sup>5</sup> *Biogeochemistry of Agroecosystems, University of Goettingen, Germany*

---

### Abstract

Deep-rooting cover crops increase C input in agricultural soils, and thus have the potential to help cash crops to cope with climate change, e. g., drought, by providing soil organic carbon (SOC) in the deep soil to support rhizosphere activity. However, few studies have investigated the C mineralization in the rhizosphere of cash crops growing after deep-rooting cover crops. To fill this knowledge gap, we designed a field experiment to compare the effects of two cover crop mixtures with deep- and shallow-rooting species (clover/grass; brassica/grass) on C-cycling enzyme activities in following maize (*Zea mays* L.) rhizosphere at three experimental sites with different soil texture (sandy sand, sandy loam, and silty loam) in Germany. A drought stress treatment was established during maize cultivation to determine the effects of cover crops on enzyme activities in the subsoil rhizosphere of the cash crop under drought. We determined the hotspots area of maize rhizosphere by zymography and measured C-cycling enzyme activities in maize rhizosphere by fluorometric microplate assays. The results showed that, under drought, cover crop mixtures positively affected C-cycling enzyme activities in maize rhizosphere in sandy loamy soil, and negatively affected C-cycling enzyme activities in maize rhizosphere in sandy soil and silty loamy soil. The effect sizes of cover crops on enzyme activities in maize rhizosphere were negatively correlated with microbial functional diversity under drought. We conclude that the effect of cover crops on the increase of subsoil enzyme activities in the rhizosphere of maize exposed to drought stress is highly site-specific.

**Keywords:** winter cover crops; deep-rooting species; subsoil C mobilization; drought stress;  $\beta$ -glucosidase activity; cellobiohydrolase activity; xylanase activity.

## 1. Introduction

Cover crop mixtures increase belowground carbon (C) amount, accelerate C cycling due to fresh C input, and change the associated belowground microbial communities and activities, and abiotic properties in farming systems (Finney and Kaye, 2017; Smith et al., 2014; St Aime et al., 2023; Stavi et al., 2012; Tamburini et al., 2020; Topps, 2021). Increasing plant diversity in agricultural ecosystem can also reduce C loss, improve soil water retention and ensure plant primary productivity under climate change, e.g., under drought stress (Eisenhauer et al., 2013; St Aime et al., 2023, 2020). However, knowledge gaps remain in terms of if and how cover crop mixtures help the following cash crops to cope with drought, and how microbial activity in cash crop rhizosphere in the subsoil is affected by cover crop residues under drought.

Deep-rooting cover crops have been broadly discussed due to their potential to enhance subsoil C storage and access nutrients and water from the subsoil with their deep-reaching roots (Hoekstra et al., 2015; Peixoto et al., 2022; Pierret et al., 2016; Rasmussen et al., 2020). Considering the slow C decomposition rate in subsoil (Button et al., 2022; Hobley et al., 2017; Salomé et al., 2010), the input of fresh C by the cover crop roots can be a vast energy source for microorganisms living in the following cash crop rhizosphere. Subsoil microorganisms have also been shown to benefit from cover crop carbon inputs, as they assimilated a large proportion of cover crop-derived C into their biomass, and their activity and diversity also increased (Fontaine et al., 2007; Liang et al., 2018; Peixoto et al., 2020). Moreover, cover crop mixtures that combine deep- and shallow-rooting species have been proven to be more efficient in utilizing resources in deep soil depths (Berendse, 1981; Han et al., 2022; Oram et al., 2018). However, this positive effect may also origin from the combination of different functional classes, e.g., legumes and nonlegumes, in the mixtures, and not only from combining shallow and deep-rooting species (Hoekstra et al., 2015).

Recent studies in diverse agricultural systems have demonstrated a link between plant biodiversity and functional traits, e.g., increasing rhizodeposition, and improving litter quality (Cortez et al., 2007; Finney and Kaye, 2017; Li et al., 2014; Redin et al., 2014; Tribouillois et al., 2015). For example, a higher plant diversity in cover cropping would increase the chemical diversity of rhizodeposits, including carbohydrates, organic and amino acids, phenolics, fatty acids, sterols, enzymes, vitamins, hormones, and nucleosides (Dignac et al., 2017; Jones et al., 2009; Steinauer et al., 2016). Functional classes of cover crops with high root exudation rates or large C inputs (e.g., grasses) have distinct functional traits that would favor a beneficial microbial community (Faucon et al., 2017; Pausch and Kuzyakov, 2018), thus, affect microbial C mobilization process.

The different biochemical, physiological, and morphological traits of cover crop species lead to various organic C (OC) compositions as different substrates for the microbes living in the next cash crops' rhizosphere. This carry-over effect is critical in shaping soil biodiversity and agroecosystem functions (Crotty et al., 2016; Faucon et al., 2017; Lange et al., 2015; Tiemann et al., 2015). Cover crop roots may trigger microbial activity in the subsoil by releasing a large proportion of glucose, cellulose, and organic acids (Fontaine et al., 2007; Heitkötter et al., 2017; Karhu et al., 2016). Cover crop diversity and the chemical composition of their residues may affect soil microbial activity and diversity on different levels. For example, legume species have been proven to strongly accelerate soil enzyme activity compared to nonlegume species (Lupwayi et al., 2021; Lupwayi and Soon, 2016). Cover crop mixtures increase microbial functional diversity more than monocultures during the decomposition of residues (Drost et al., 2020).

The reduced soil moisture under drought conditions affects the plant-soil interactions by reducing plant root activity, soil microbial activity, and plant primary productivity (Ciais et al., 2005; Fu et al., 2020; Ge et al., 2022; Jones et al., 2022; Qu et al., 2023; Wang et al., 2021; Zhang et al., 2023). Organic matter input helps the soil to retain moisture under drought, and improves the diversity and activity of soil microbes (Bastida et al., 2008; Hueso et al., 2012). Facing water deficiency, soil microbes tend to adjust their substrate use strategies to retain cellular motility (Schimel, 2018). The functional response of soil microbes to drought is altered by substrate quality (Malik et al., 2020). Selection of cover crop

mixtures based on the chemical quality of cover crop litter could affect microbial community related to resource acquisition and will affect drought tolerance of soil microorganisms, which may in turn retain the following cash crop root activity.

Enzymes, excreted by both plants and microbes, are the main mediators of organic matter decomposition (Nannipieri et al., 2018; Sinsabaugh et al., 2008). Even a small shift in the activity of one or two enzymes can significantly alter the decomposition rates of organic matter (Caldwell, 2005; Sinsabaugh et al., 2002). The higher chemical diversity of litter residues of cover crop mixtures compared with monocultures leads to a higher diversity of the extracellular enzymes and increases the probability of priming effects occurring (Fontaine et al., 2003; Wu et al., 1993). Soil enzyme activity also has been widely used for assessing soil quality changes by agricultural management (García-Ruiz et al., 2008; Ghosh et al., 2020; Xu et al., 2020). It is of great value to evaluate soil enzyme activity in the cash crop rhizosphere after cover cropping to be able to select the best group of cover crops to help the subsoil microorganisms, as well as the cash crop, to overcome drought stress.

In this study, field experiments with winter cover crop mixtures and a control variation were conducted on three experimental sites with different soil types. All plots were subsequently planted with maize (*Zea mays* L.), and rain shelters were used to simulate summer drought during the maize growing season. We determined the activities of cellulose, cellobiose, and Xylooligosaccharide hydrolysis enzymes as affected by the interaction between cover crop residues and living maize roots in the subsoil. We assessed the effects of cover crop mixtures on enzyme activity in the following maize crop rhizosphere in the subsoil under drought and under normal rainfall conditions. We hypothesize that: (1) cover crop mixtures promote microbial hydrolyzation of OC in maize rhizosphere in the subsoil, with higher C-cycling enzyme activities in legume/grass due to the low C:N ratio of legume residues compared to brassica; (2) the legacy effects of cover crop mixtures on OC hydrolyzation in maize rhizosphere under drought are site-specific and highly related to soil water content and texture; (3) cover crop mixtures show larger effects on enzyme activities in the following maize rhizosphere under drought than under rainfall condition, as microorganisms require more energy resources to maintain microbial activity to overcome water deficiency.

## 2. Materials and methods

### 2.1 Experimental sites and design

The experiment was conducted in three sites in Germany, differing in soil types. Two experimental farms of Kiel University (1) Hohenschulen (HS, 54°18'46.5"N 9°59'55.0"E), with a Luvisol soil (IUSS Working Group WRB, 2022). The average (1991–2020) annual precipitation at this site is 769 mm and the mean temperature is 9.4 °C. (2) Karkendamm (KD, 53°55'38.8"N 9°55'51.0"E), with a gleyic Podzol soil. The 30-year average annual temperature is 8.6 °C and mean annual precipitation is 865 mm. One experimental farm of Goettingen University (3) Reinshof (RH, 51°29'08.5"N 9°53'34.9"E), with a Phaeozem soil. The long-term average annual precipitation at this site is 645 mm and the mean temperature is 8.7 °C. Soil properties in the subsoil of the three experimental sites shows in Table 2-1.

**Table 2-1** Soil properties in the subsoil of three experimental sites. Soil water content was measured at rainfall side and simulated drought side at sampling time. (OC: organic carbon; N<sub>t</sub>: total nitrogen)

Sites	Soil texture	pH (0.01M CaCl <sub>2</sub> )	OC content (%)	N <sub>t</sub> content (%)	Soil water content (%)	
					Rainfall	Drought
HS	Sandy loam	6.5	0.67	0.07	13.37	11.33
KD	Sandy sand	5.2	0.65	0.04	7.86	3.09
RH	Silty loam	7.2	0.56	0.05	29.41	27.84

Two cover crop mixtures (legume/grass; brassica/grass) and a control (black fallow in winter) were set up at the three sites in autumn 2022. The legumes were *Trifolium pratense* L. (red clover, deep-rooting) and *Trifolium repens* L. (white clover shallow-rooting); grasses were *Festuca arundinaceae*

(tall fescue, deep-rooting) and *Lolium perenne* (German ryegrass, shallow-rooting); and the brassica group contained *Raphanus sativus* L. var. *oleiformis* (oil radish, deep-rooting) and *Brassica napus* L. (winter forage rape, shallow-rooting). Each variation had 4 plots with a size of 6 × 12 m as replicates. Plot replicates were randomly distributed in a block design at each site. The cover crops were grown until May 2023. After cover crop termination with an herbicide and shallow (15 cm) tillage of the topsoil, maize was sown. One month after sowing maize, subplots with rainfall reduction were created by covering the spaces between the maize rows with inclined greenhouse foil lanes to exclude  $\geq 50\%$  of rainfall in every plot. Water content sensors (Teros 10, Meter Group, München, Germany) were installed in the control plots (in 30–60 cm depth, with two replicates per depth under rainout shelter and rainfall side) at each experimental site. At maize germination, plastic root windows (30 x 55 cm) were vertically inserted into the soil for conducting zymography at each drought side and rainfall side. Each root window was placed 2 m from the plot borders to avoid boundary effects.

## 2.2 Soil sampling

Soil sampling was conducted at maize growth stage BBCH 50 in July 2023. Soil profiles (60 cm deep, 1 m distance from the plot borders) were dug out in all plots at three sites. Soil samples from maize rhizosphere in the subsoil layer (30–60 cm) were collected from the profile walls by carefully scraping out the immediate vicinity of the roots with a micro spatula. The soil samples were stored at 4 °C for transport to the lab. Subsamples for enzyme activity measurement were immediately separated into sterile centrifuge tubes, and short-term stored at 4 °C in the fridge for subsequent analysis.

## 2.3 Soil *in-situ* zymography

Zymography was performed at maize growth stage of BBCH 50 as an *in situ* non-invasive technique to study the spatial patterns of C-cycling enzyme activity in maize rhizosphere as affected by cover crop mixtures as pre-cropping strategies. We followed the protocol of Razavi et al. (2016). Membranes saturated with 4-methylumbelliferone (MUF) substrates were used for visualization of enzyme activities. 4-Methylumbelliferyl- $\beta$ -D-glucoside (abcr GmbH, Karlsruhe, Germany) was used as substrate to detect  $\beta$ -glucosidase activity. Polyamide membrane filters (Tao Yuan, China) with a diameter of 20 cm and a pore size of 0.45 mm were cut into 10 × 10 cm pieces and saturated with the 4-Methylumbelliferyl- $\beta$ -D-glucoside. In the field, the root windows were opened just before conducting zymography, and the membranes saturated with substrate were attached to the soil to where maize roots were. In each plot, two pieces of membrane was put in 45 cm depth, respectively. After incubation for one hour, the membranes were carefully lifted off the soil surface and soil particles on the membranes were gently removed by brush. One hour of incubation time was selected based on preliminary experiments.

The calibration was based on zymography of 2 × 2 cm membranes soaked in a solution of MUF with concentrations of 0.1, 0.2, 0.3, 0.4, 0.5, 0.6, 0.7, 0.8, 0.9, 1.0 mM. The amount of MUF on an area basis was calculated from the solution volume taken up by the membrane and its size. The membranes used for calibration were photographed (EOS 6D, Canon, Tokyo, Japan) under UV light (365 nm wavelength) and analyzed in the same way as membranes applied in the field (Razavi et al., 2016).

## 2.4 Image processing

The fluorescent images were processed in MATLAB R2023a (The MathWorks, Inc., USA), according to Razavi et al. (2016). All images were first transformed to 16-bit grayscale images as matrices and corrected for light variations and camera noise. The scaled black flat field identical in all images was considered as a background (reference object) during the whole image processing, and this gray value was used as the referencing point. Thereafter we calculated an average background gray value through the zymograms of calibration lines at MUF concentration of zero, and subtracted this value from all the zymograms (Liu et al., 2017). The gray value of each zymography pixel was converted to enzyme activity using the calibration regression line obtained from a series of MUF concentrations. Hotspots

were considered to be areas in which the gray values of five adjacent pixels (each equals  $0.1 \times 0.1$  mm) all exceeded the average gray value of the whole image (i.e.,  $> 0.7$ ) (Hoang et al., 2016).

## 2.5 Enzyme kinetics

The kinetics of three enzymes that target organic C compounds were assayed using fluorogenically labelled substrates (Razavi et al., 2015). One gram of fresh soil was added to 50 mL sterile water in autoclaved jars and shaken on a horizontal shaker with 180 rpm for 30 minutes. Three types of 4-methylumbelliferone (MUF)-based fluorogenic substrates were used to assess the activity of enzymes: 4-methylumbelliferyl- $\beta$ -D-glucosidase for  $\beta$ -glucosidase (BG) activity, 4-methylumbelliferyl- $\beta$ -N-acetyl-D-glucosaminide for cellobiohydrolase (CE) activity, and 4-methylumbelliferyl- $\beta$ -D-xylopyranoside for xylanase (BX) activity. Substrates and chemicals were purchased from abcr GmbH (Karlsruhe, Germany). The enzyme activities were determined at a range of substrate concentrations (0, 5, 10, 15, 20, 25, 50, 100  $\mu\text{mol g}^{-1}$  soil). The saturation concentrations of the fluorogenic substrates were determined in preliminary experiments. Fluorescence (caused by the release of MUF from the substrate) was immediately measured with a micro-plate reader CLARIOstar Plus (BMG LABTECH, Ortenberg, Germany).

## 2.6 Calculations

Enzyme activities were determined by fitting non-linear saturation curves of the Michaelis-Menten equation 1 in GraphPad Version 8 (Prism, Boston, USA):

$$V = \frac{V_{max} [S]}{(K_m + [S])} \quad (1)$$

Where V is the reaction velocity ( $\text{nmol g}^{-1} \text{h}^{-1}$ ),  $V_{max}$  is the maximal rate of enzyme activity at saturated substrate concentration,  $K_m$  is the substrate concentration at half of the  $V_{max}$  and S is the substrate concentration (Michaelis and Menten, 1913; Nannipieri et al., 2012).

The geometric mean of the assayed enzyme activities (GMea) was calculated by equation 2 (Hinojosa et al., 2004; Paz-Ferreiro et al., 2012):

$$GMea \text{ (nm MUF g}^{-1} \text{soil h}^{-1}) = \sqrt[3]{BG \times CE \times BX} \quad (2)$$

Where BG, CE, and BX represent soil  $\beta$ -glucosidase activity, cellobiohydrolase activity and xylosidase activity, respectively.

Soil functional diversity was calculated as Shannon's diversity index following equation 3 (Ghosh et al., 2020; Lagomarsino et al., 2011; Raiesi and Beheshti, 2014):

$$\text{Shannon's diversity index} = - \sum_{i=1}^3 P_i \times \ln(P_i) \quad (3)$$

Where,  $P_i$  is the ratio of each of the three enzymes activity to the sum of all enzyme activities.

To compare the effect of cover crop mixtures on maize rhizosphere C cycling mechanisms under drought and under normal rainfall condition, the C-cycling enzyme activities were converted into effect size following equation 4 (Wang et al., 2023):

$$\text{Effect size (\%)} = \frac{EA_{cc} - EA_{control}}{EA_{control}} \times 100 \quad (4)$$

Where  $EA_{cc}$  and  $EA_{control}$  represent the enzyme activity in maize rhizosphere in cover crop mixtures and in control, respectively.

## 2.7 Statistical analysis

Statistical analyses were performed in R studio (Version 2023.06.1+524). All data were tested for normal distribution (Shapiro-Wilk test) and homogeneity of variance (Bartlett's test). Outliers were tested by Nalimov's test and removed ( $\leq 1$  within one variation). Two-way ANOVA was performed to test the main effects of cover crop mixtures and drought/rainfall conditions on hotspots area,

geometric mean of enzyme activity, Shannon's diversity index and effect size of cover crop mixtures on enzyme activities. After getting significance of main effects and interactions ( $p < 0.05$ ), the means were compared with Tukey's HSD test. Correlations analysis between Shannon's diversity index, GMea, hotspots area,  $\beta$ -glucosidase activity, and soil water content in control plots were done respectively by Spearman correlation coefficient ( $p < 0.05$ ) to test whether the enzyme indicators in soils are highly correlated with the initial soil moisture. Correlations analysis between Shannon's diversity index with geometric mean of enzyme activity and effect size on enzyme activities in cover crop mixtures were tested by Spearman correlation coefficient ( $p < 0.05$ ).

### **3. Results**

#### **3.1 Hotspots area in maize rhizosphere**

The hotspots area from small to large at HS was: brassica/grass < legume/grass < control (Figure 2-1 a). The hotspot area was 4-fold higher in control than in brassica/grass mixtures at HS, disregarding drought and rainfall conditions.

Zymograms showed less abundant roots and lower  $\beta$ -glucosidase activities at KD site than at HS (Figure 2-1 b). Compared with control, using cover crop mixtures did not change  $\beta$ -glucosidase activities and hotspots area at KD. The effect of using cover crops on  $\beta$ -glucosidase activities and hotspots in maize rhizosphere were similar under rainfall and drought conditions.

Zymograms showed higher  $\beta$ -glucosidase activity and larger hotspots area from RH than HS and KD (Fig. 1c). The median of hotspots area of  $\beta$ -glucosidase under drought was higher in legume/grass and brassica/grass than in control, while the median of hotspots area was highest under rainfall in control.

#### **3.2 Effect size of cover crop mixtures on C-cycling enzyme activities**

Using cover crop mixtures showed positive effects on  $\beta$ -glucosidase, cellobiohydrolase, and xylanase activity in maize rhizosphere at HS under drought, and the effect sizes of cover crops were significantly higher under drought than under rainfall condition (Figure 2-2 a-c). Within drought condition, the positive effect size on  $\beta$ -glucosidase activity was 1-fold higher of brassica/grass than legume/grass mixture. The effect size on cellobiohydrolase activity was 1-fold larger under drought than under rainfall conditions, and the effects from brassica/grass and legume/grass were similar. The effect size of cover crops was lower on xylanase activity than on  $\beta$ -glucosidase, cellobiohydrolase.

Use of cover crops negatively affected  $\beta$ -glucosidase and cellobiohydrolase activities in maize rhizosphere under rainfall and drought conditions at KD (Figure 2-2 d-e). Legume/grass affected xylanase activity positively under drought but negatively under rainfall (Figure 2-2 f). Brassica/grass negatively affected xylanase activity under both rainfall and drought conditions.

Contrary to HS, using cover crop mixtures showed higher effect sizes on  $\beta$ -glucosidase, cellobiohydrolase, and xylanase activity in maize rhizosphere under rainfall than drought at RH, and the effect sizes of cover crops under drought were all negative (Figure 2-2 g-i). Noticeably, legume/grass showed positive effect size on cellobiohydrolase and xylanase activity. Brassica/grass had positive effect size on cellobiohydrolase activity but negative effect sizes on  $\beta$ -glucosidase and xylanase activities.

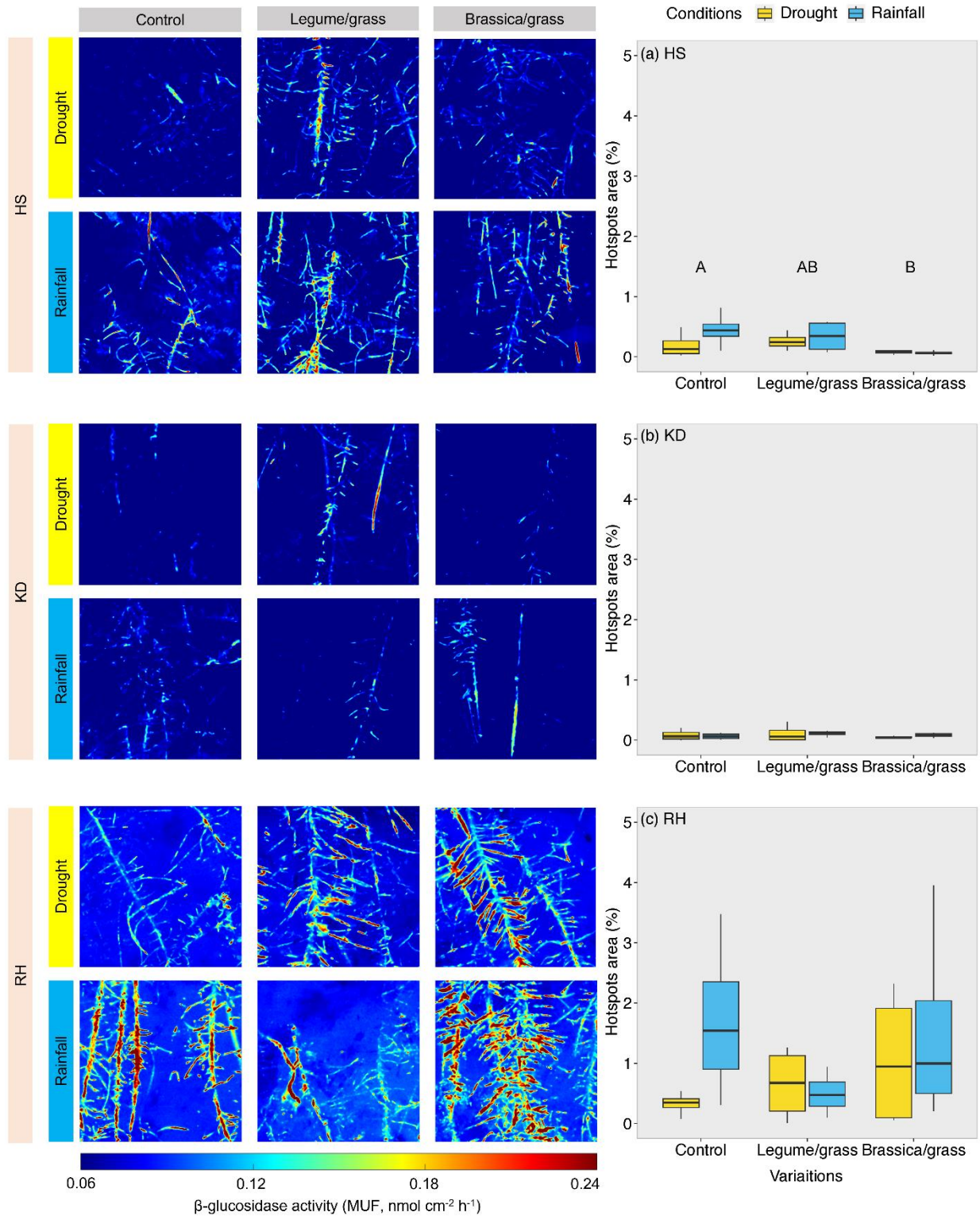


**Figure 2-1** Zymograms of  $\beta$ -glucosidase activity and hotspots distribution of maize rhizosphere in the subsoil (30-60 cm) under drought and rainfall condition at three sites. Maize was growing after cover crop mixtures or control. The color bar on the bottom side represents the activity of  $\beta$ -glucosidase. Hotspots area (%) of  $\beta$ -glucosidase activity determined from Zymograms from maize rhizosphere in control and cover crop variations at three sites: (a) HS, (b) KD, and (c) RH. Capital letters represent significant difference between three variations ( $n=4$ ,  $p<0.05$ ).

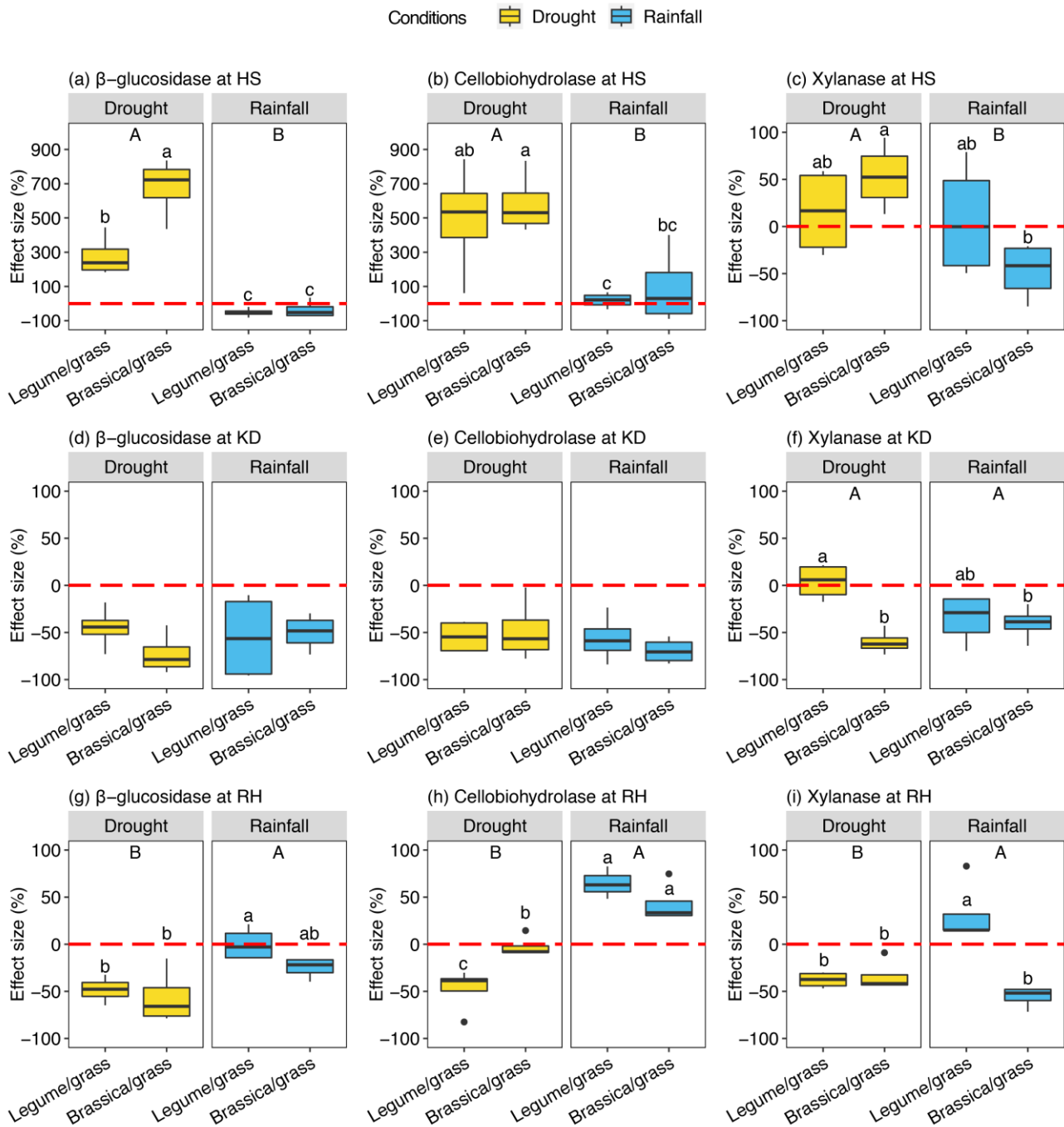


**Figure 2-2** Effects of using cover crop mixtures on C-cycling enzyme activities in maize rhizosphere under drought and rainfall conditions. (a)  $\beta$ -glucosidase activity at HS; (b) cellobiohydrolase activity at HS; (c) xylanase activity at HS; (d)  $\beta$ -glucosidase activity at KD; (e) cellobiohydrolase activity at KD; (f) xylanase activity at KD; (g)  $\beta$ -glucosidase activity at RH; (h) cellobiohydrolase activity at RH; (i) xylanase activity at RH. The red dashed line in the figure is the threshold at which the effect size is zero. Capital letters represent significant difference between drought and rainfall conditions. Lowercase letters represent significant difference between variations under drought and under rainfall conditions ( $n=4$ ,  $p<0.05$ ).

### 3.3 Geometric mean of enzyme activity and Shannon's diversity index

The GMea in maize rhizosphere was significantly higher under drought than rainfall at HS (Figure 2-3 a). Under drought condition, the GMea was 3-fold higher in brassica/grass than control. Using cover crops did not change the GMea under rainfall condition at HS. KD had a similar range of GMea as HS, but using cover crop variations did not significantly affect GMea compared with the control at KD

(Figure 2-3 b). GMea was lowest at RH among the three sites, and there was no difference between variations and conditions (Figure 2-3 c).

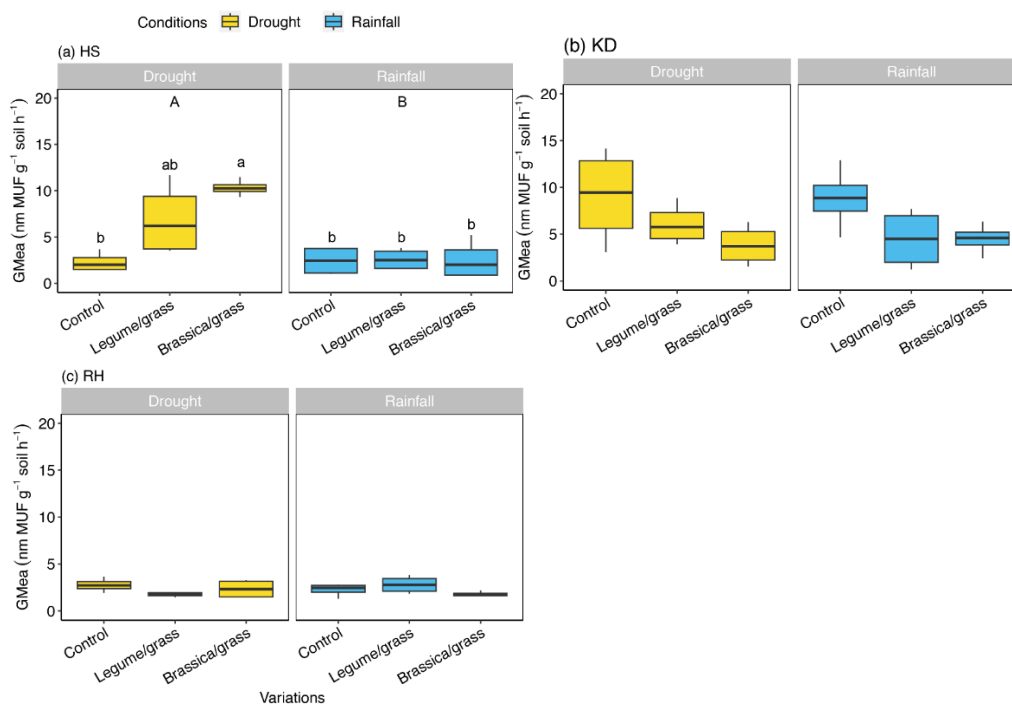


**Figure 2-3** Geometric mean enzyme activity (GMea) in the rhizosphere of maize in control and after cover cropping at three sites. Capital letters represent significant differences between drought and rainfall conditions. Lowercase letters represent significant difference between variations under drought and under rainfall conditions ( $n=4$ ,  $p<0.05$ ).

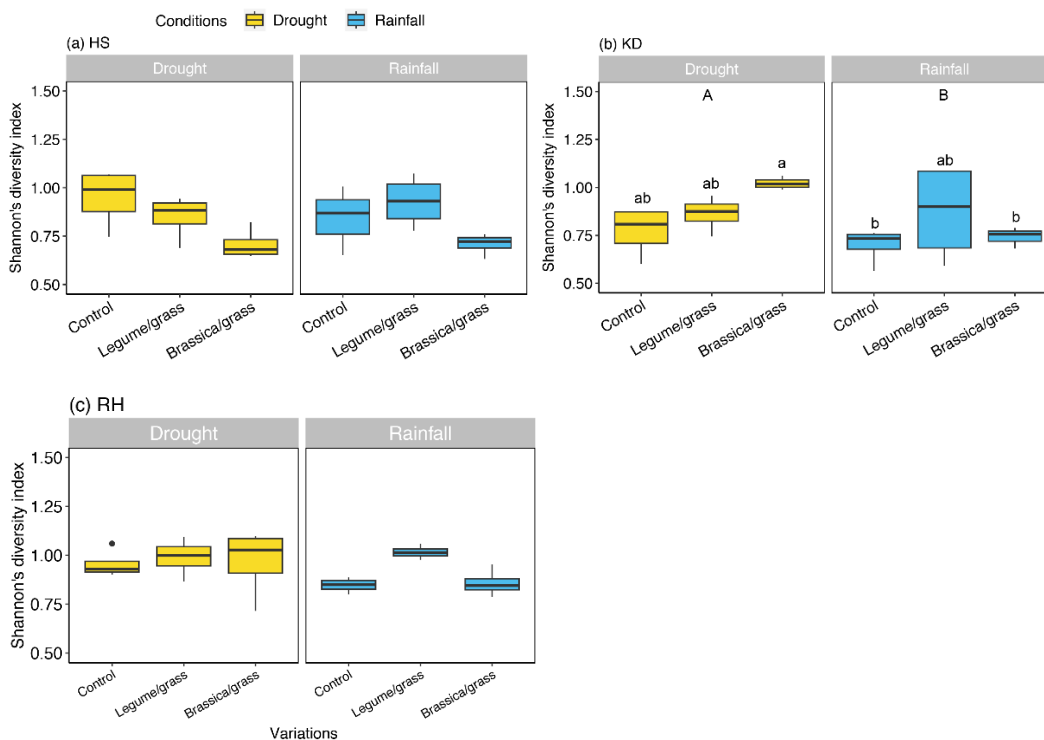


**Figure 2-4** Shannon's diversity index based on enzyme activities at (a) HS, (b) KD and (c) RH. Capital letters represent significant differences between drought and rainfall conditions. Lowercase letters represent significant difference between variations under drought and under rainfall conditions ( $n=4$ ,  $p<0.05$ ).

Shannon's diversity index in maize rhizosphere was 0.46–1.07 at HS, and was not affected by cover crop mixtures and conditions (Figure 2-4 a). Shannon's diversity index was 0.50–1.09 at KD, and it was significantly higher under drought than under rainfall condition (Figure 2-4 b). At RH, Shannon's diversity index was 0.72–1.10 (Figure 2-5 c), without impact from variations and conditions.

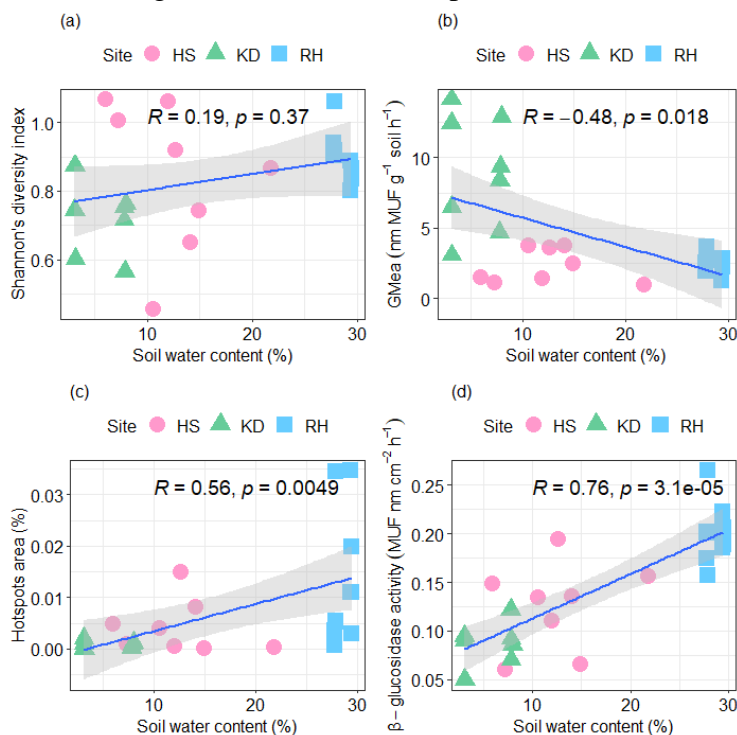


**Figure 2-5** Linear relationship of soil water content (%) with (a) Shannon's diversity index with (b) geometric mean of enzyme activity, (c) hotspots area (d)  $\beta$ -glucosidase activity in the rhizosphere of maize in control plots (Spearman correlation coefficient,  $p < 0.05$ ).

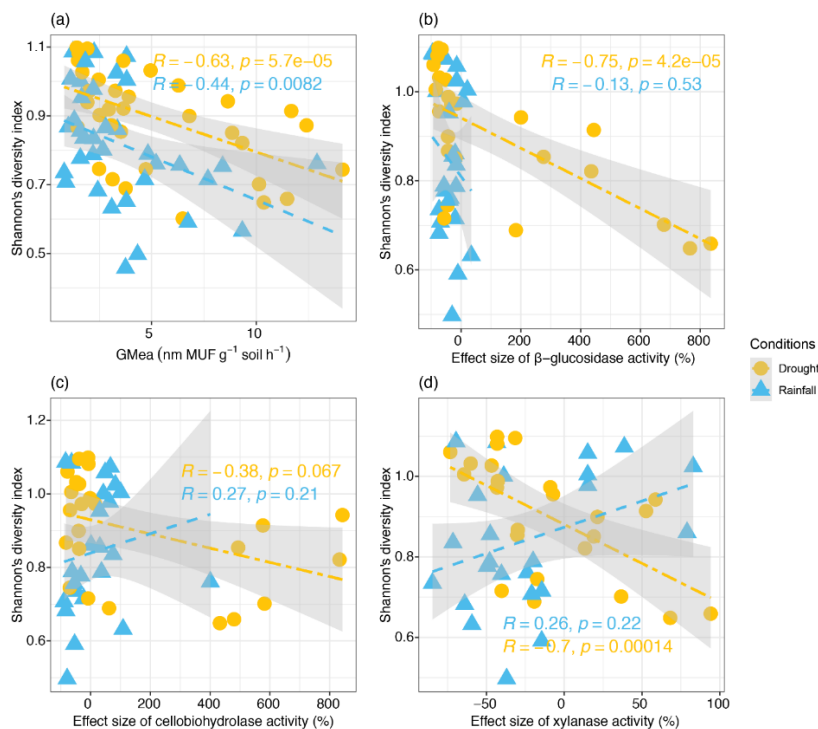


**Figure 2-6** Linear relationship of Shannon's diversity index with (a) geometric mean of enzyme activity and effect size of cover crop mixtures on (b)  $\beta$ -glucosidase activity, (c) cellobiohydrolase activity and (d) xylosidase activity (Spearman correlation coefficient,  $p < 0.05$ ).

### 3.4 Effects of cover crops on enzyme activities under drought and rainfall conditions

The Shannon's diversity index in initial soils was independent of soil water content (Figure 2-5 a). GMea in maize rhizosphere was negatively correlated with soil water content in the control at the three sites (Figure 2-5 b). The hotspots area and  $\beta$ -glucosidase activity were positively correlated with soil water content in the control (Figure 2-5 c-d), proving that the initial enzyme activities of the three soils were closely related to their respective soil water contents.

Cove crop mixtures not only changed Shannon's diversity index but also affected the enzyme activities, and the patterns of the effects from cover crops differed between drought and rainfall conditions (Figure 2-6). Shannon's diversity index was negatively correlated with GMea in cover crop mixtures under both drought and rainfall conditions (Figure 2-7 a). The effect size of cover crop mixtures on  $\beta$ -glucosidase activity only showed a negative correlation with Shannon's diversity index under drought condition (Figure 2-7 b). There were significantly positive correlations between Shannon's diversity index and effect size of cellobiohydrolase and xylanase activities under drought condition (Figure 2-7 c, d), suggesting that a decrease of microbial functional diversity in maize rhizosphere by cover crop mixtures may increase the effect on enzyme activities under drought.

## 4. Discussion

Cover crop roots and their residues can enhance the activity of enzymes in the soil (Chavarría et al., 2016; Niewiadomska et al., 2020; Piotrowska-Długosz and Wilczewski, 2020; Thapa et al., 2021). Using cover crops did not affect enzyme activities in maize rhizosphere at maize growth stage BBCH 50 at HS under rainfall condition, possibly because cover crop root residues have completed early decomposition with a suitable soil water content when the samples were taken in July 2023. Cover crops as pre-cropping had great positive effect sizes on  $\beta$ -glucosidase, cellobiohydrolase, and xylanase activities in maize rhizosphere under drought at HS, indicating intensive cellulose and hemicellulose degradation in maize rhizosphere at BBCH 50 (Sinsabaugh and Follstad Shah, 2011). High cellulolytic activities usually occur during early stages of plant litter decomposition (Moorhead and Sinsabaugh, 2006), the decomposition of cover crop residues in the subsoil at HS may be slowed down under drought compared with rainfall condition. Considering only drought condition, the decomposition of brassica/grass residues was in an earlier stage than that of legume/grass. Since there is not much difference in cellulose content in the two mixtures (Garba et al., 2022; Pittman et al., 2020), the extended cellulose decomposition in brassica/grass mixture is probably caused by the large C/N ratio (Clark et al., 1997; Kuo et al., 1996; Kuo and Sainju, 1998; Wagger, 1989). Cover crops increased GMea in maize rhizosphere and tended to reduce its microbial functional diversity under drought, indicating that the microbial community at HS maintained its dominant species and was mainly dedicated to decomposing plant-derived OC. Our first finding partially confirms the hypothesis that cover crop mixtures promote microbial hydrolyzation of OC in maize rhizosphere in the subsoil, but grass mixed with brassica increases C-cycling enzyme activities in maize rhizosphere more than legumes due to slower decomposition of the residues.

Despite cover crop residues can provide more cellulose than control as a substrate for cellobiohydrolase, both legume/grass and brassica/grass mixtures showed negative effects on  $\beta$ -glucosidase and cellobiohydrolase activities in maize rhizosphere disregarding rainfall and drought conditions at KD site, suggesting low microbial activity in the rhizosphere of maize after cover crops. Additionally, the use of brassica/grass increased microbial functional diversity in the maize rhizosphere under drought. Previous studies have reported a significant increase of microbial functional diversity by legumes in a wheat system (Nivelle et al., 2016) and by rye in a vegetable system (Nair and Ngouajio, 2012). Our result suggests that the effect of cover crops on microbial functional diversity in maize rhizosphere is site-specific, likely related to the composition of microbial community in the initial soil, and the effect is stronger under drought than under rainfall at KD. This is in line with the study of Siebielec et al. (2020) which revealed that microbial community is more

sensitive to drought in sandy soils, and the input of additional OC is of great importance to protect microbial activity in sandy soils.

At RH, we observed neither changes in GMea nor changes in microbial functional diversity, but the use of cover crops negatively affected C-cycling enzymes in maize rhizosphere under drought, indicating that cover crops were unable to alleviate drought-induced decrease in enzyme activity. Under rainfall condition, cover crop mixtures, especially legume/grass, had a significantly positive effect on C-cycling enzymes, possibly due to the high N demand of microorganisms, because of sufficient available carbon mobilized by  $\beta$ -glucosidase enzyme secreted by maize roots (Esen, 1993). The distribution of hotspots in our results better represented the extracellular  $\beta$ -glucosidase activity of maize because highly active areas are only distributed on the root surface and the rhizosphere extension of maize roots is typically very narrow (Ma et al., 2018). The larger hotspots area concentrated on the maize root surfaces at RH, especially under rainfall conditions, suggests that maize roots at this site contributed much to decomposing easily available carbon.

Studies have reported that using cover crops can significantly increase the total amount of microorganisms, promote microbial activity, and increase the abundance of bacterial community during the growth of cover crops and even a long time after cover cropping (Balota et al., 2014; Feng et al., 2021; Finney et al., 2017), our results suggest that the functional diversity of the microbial community in the following maize rhizosphere may not be influenced by cover crop mixtures, probably because the dominate microbial phylae in maize rhizosphere has already adjusted to the soil with the different cover crop as organic substrate.

Cover crop mixtures had site-specific effects on C mobilization functions of soil microbial communities in maize rhizosphere. This is in agreement with Rutan et al. (2023) who suggested that using cover crops may have differing impacts to bacterial diversity, evenness, and richness in maize rhizosphere on different sites. However, Gregorutti and Caviglia (2019) have demonstrated that white sweet clover and wheat did not affect the activity and abundance of cellulolytic microorganisms. The different results as ours may come from (1) the cover crops being monocultures, greater biomass production of cover crop mixtures than monocultures may cause a larger legacy effect on enzyme activities in soils (Couëdel et al., 2018; Drost et al., 2020; Gentsch et al., 2020); (2) difference in soil types, Muhammad et al. (2021) demonstrated that the effect of cover crops on microbial C/N ratio in the soil was higher in medium-textured soils compared to coarser or fine-textured soils. This is in line with our findings that HS site, with sandy loam texture, showed the greatest effect size of cover crop mixtures on C-cycling enzyme activities; (3) and lack of influence of living cash crop roots. Enzyme activity from newly colonized maize roots was shown to be site-specific and highly correlated with soil water conditions, which would affect microbial C mobilizing functions. In addition,  $\beta$ -glucosidase and cellobiohydrolase exudation are proven to be more related to abiotic factors (e.g., pH, nutrient availability, and clay minerals) than xylanase (Burns and Dick, 2002; Tischer et al., 2014), that explained the greater site-specific effects of cover crops on cellulolytic enzyme activities than xylanase.

The effects of cover crops on corn rhizosphere enzyme activities show distinct patterns under drought conditions and rainfall conditions, possibly due to changes in plant root activity, microbial activity, community composition, and soil water-soluble properties under drought (Gao et al., 2021; Preece et al., 2019; Wu et al., 2011). In cover crop treatments, high GMea tended to have low microbial functional diversity disregarding drought and rainfall conditions, indicating that cover crops selected specific microbial species with rapid C mobilizing functions. However, under rainfall conditions, the Shannon diversity index was not related to the effect size of enzyme activity, indicating that microbial functional decomposition under rainfall conditions did not fully rely on microbial enzymes to obtain resources, plant and soil fauna-derived C-cycling enzymes may also be huge driving forces of C acquisition. Under drought, plant root deposition was affected, microorganisms had to rely on their own C mobilizing functions to survive. Drought stress mainly causes a reduction in the diversity of the bacterial community (Gao et al., 2021). Consequently, the fungal community, the main producer

of extracellular hydrolytic enzymes (Schneider et al., 2012), became the dominant species due to its high resistance to drought. This explained the decrease of functional diversity accompanied by positive effects on C-cycling enzymes under drought conditions. 3.4 times increase in fungal biomass after cover crop mixtures compared with fallow has been reported by (Gentsch et al., 2020), supporting our explanation that cover crop mixtures can enhance microbial community carbon mobilization by strengthening the fungal community.

## **5. Conclusion**

We evaluated the effect of using deep- and shallow-rooting cover crop mixtures on C-cycling enzyme activities and functional diversity of soil microorganisms in the following maize rhizosphere in the subsoil under drought and rainfall conditions. The effect of cover crops on subsoil enzyme activity in the rhizosphere of maize under drought stress is highly site-specific, depending on the soil texture and the corresponding water retention capacity. Cover crop mixtures promoted enzyme activities in maize rhizosphere only in sandy loamy soil under drought at HS. Grass mixed with brassica increases C-cycling enzyme activities in maize rhizosphere more than legumes due to slow decomposition of the residues. Cover crop mixtures did not positively affect C-cycling enzyme activities in maize rhizosphere under drought at KD with sandy soil and RH with silty soil. Considering the balance between subsoil enzyme activity and economic input of using cover crop mixtures, combining deep- and shallow-rooting mixtures to support cash crops to overcome drought stress may be the best choice in medium-textured soils. This discovery holds significant implications for sustainable farming practices, as subsoil resources have been proposed to have huge potential for cash crops to overcome drought stress. Specially designed cover crop mixtures based on different soil properties could be applied as tools for the targeted subsoil management of microbial communities to deliver specific functions as legacy effects and enhance overall ecosystem service to following cash crops.

## **Acknowledgment**

This work is part of the Rhizo4Bio Project Network (Plant roots and soil ecosystems, significance of the rhizosphere for the bio-economy) RootWayS (Deep-rooting cover crop mixtures: Creating highways to subsoil water and nutrient resources). The authors received the funding from German Federal Ministry of Education and Research (BMBF), project number 031B0911A.

## References

- Balota, E.L., Calegari, A., Nakatani, A.S., Coyne, M.S., 2014. Benefits of winter cover crops and no-tillage for microbial parameters in a Brazilian Oxisol: A long-term study. *Agric. Ecosyst. Environ.* 197, 31–40. <https://doi.org/10.1016/j.agee.2014.07.010>
- Bastida, F., Kandeler, E., Moreno, J.L., Ros, M., García, C., Hernández, T., 2008. Application of fresh and composted organic wastes modifies structure, size and activity of soil microbial community under semiarid climate. *Appl. Soil Ecol.* 40, 318–329. <https://doi.org/10.1016/j.apsoil.2008.05.007>
- Berendse, F., 1981. Competition between plant populations with different rooting depths II. Pot experiments. *Oecologia* 48, 334–341. <https://doi.org/10.1007/BF00346491>
- Burns, R.G., Dick, R.P., 2002. *Enzymes in the Environment: Activity, Ecology, and Applications*. CRC Press.
- Button, E.S., Pett-Ridge, J., Murphy, D.V., Kuzyakov, Y., Chadwick, D.R., Jones, D.L., 2022. Deep-C storage: Biological, chemical and physical strategies to enhance carbon stocks in agricultural subsoils. *Soil Biol. Biochem.* 170, 108697. <https://doi.org/10.1016/j.soilbio.2022.108697>
- Caldwell, B.A., 2005. Enzyme activities as a component of soil biodiversity: A review. *Pedobiologia* 49, 637–644. <https://doi.org/10.1016/j.pedobi.2005.06.003>
- Chavarría, D.N., Verdenelli, R.A., Serri, D.L., Restovich, S.B., Andriulo, A.E., Meriles, J.M., Vargas-Gil, S., 2016. Effect of cover crops on microbial community structure and related enzyme activities and macronutrient availability. *Eur. J. Soil Biol.* 76, 74–82. <https://doi.org/10.1016/j.ejsobi.2016.07.002>
- Ciais, P., Reichstein, M., Viovy, N., Granier, A., Ogée, J., Allard, V., Aubinet, M., Buchmann, N., Bernhofer, C., Carrara, A., Chevallier, F., De Noblet, N., Friend, A.D., Friedlingstein, P., Grünwald, T., Heinesch, B., Keronen, P., Knohl, A., Krinner, G., Loustau, D., Manca, G., Matteucci, G., Miglietta, F., Ourcival, J.M., Papale, D., Pilegaard, K., Rambal, S., Seufert, G., Soussana, J.F., Sanz, M.J., Schulze, E.D., Vesala, T., Valentini, R., 2005. Europe-wide reduction in primary productivity caused by the heat and drought in 2003. *Nature* 437, 529–533. <https://doi.org/10.1038/nature03972>
- Clark, A.J., Decker, A.M., Meisinger, J.J., McIntosh, M.S., 1997. Kill Date of Vetch, Rye, and a Vetch–Rye Mixture: I. Cover Crop and Corn Nitrogen. *Agron. J.* 89, 427–434. <https://doi.org/10.2134/agronj1997.00021962008900030010x>
- Cortez, J., Garnier, E., Pérez-Harguindeguy, N., Debussche, M., Gillon, D., 2007. Plant traits, litter quality and decomposition in a Mediterranean old-field succession. *Plant Soil* 296, 19–34. <https://doi.org/10.1007/s11104-007-9285-6>
- Couëdel, A., Alletto, L., Tribouillois, H., Justes, É., 2018. Cover crop crucifer-legume mixtures provide effective nitrate catch crop and nitrogen green manure ecosystem services. *Agric. Ecosyst. Environ.* 254, 50–59. <https://doi.org/10.1016/j.agee.2017.11.017>
- Crotty, F.V., Fychan, R., Sanderson, R., Rhymes, J.R., Bourdin, F., Scullion, J., Marley, C.L., 2016. Understanding the legacy effect of previous forage crop and tillage management on soil biology, after conversion to an arable crop rotation. *Soil Biol. Biochem.* 103, 241–252. <https://doi.org/10.1016/j.soilbio.2016.08.018>
- Dignac, M.-F., Derrien, D., Barré, P., Barot, S., Cécillon, L., Chenu, C., Chevallier, T., Freschet, G.T., Garnier, P., Guenet, B., Hedde, M., Klumpp, K., Lashermes, G., Maron, P.-A., Nunan, N., Roumet, C., Basile-Doelsch, I., 2017. Increasing soil carbon storage: mechanisms, effects of agricultural practices and proxies. A review. *Agron. Sustain. Dev.* 37, 14. <https://doi.org/10.1007/s13593-017-0421-2>
- Drost, S.M., Rutgers, M., Wouterse, M., de Boer, W., Bodelier, P.L.E., 2020. Decomposition of mixtures of cover crop residues increases microbial functional diversity. *Geoderma* 361, 114060. <https://doi.org/10.1016/j.geoderma.2019.114060>
- Eisenhauer, N., Dobies, T., Cesarz, S., Hobbie, S.E., Meyer, R.J., Worm, K., Reich, P.B., 2013. Plant diversity effects on soil food webs are stronger than those of elevated CO<sub>2</sub> and N deposition in a long-term grassland experiment. *Proc. Natl. Acad. Sci.* 110, 6889–6894. <https://doi.org/10.1073/pnas.1217382110>
- Esen, A., 1993.  $\beta$ -Glucosidases, in: *SS-Glucosidases*, ACS Symposium Series. American Chemical Society, pp. 1–14. <https://doi.org/10.1021/bk-1993-0533.ch001>
- Faucon, M.-P., Houben, D., Lambers, H., 2017. Plant Functional Traits: Soil and Ecosystem Services. *Trends Plant Sci.* 22, 385–394. <https://doi.org/10.1016/j.tplants.2017.01.005>
- Feng, H., Sekaran, U., Wang, T., Kumar, S., 2021. On-farm assessment of cover cropping effects on soil C and N pools, enzyme activities, and microbial community structure. *J. Agric. Sci.* 159, 216–226. <https://doi.org/10.1017/S002185962100040X>
- Finney, D.M., Buyer, J.S., Kaye, J.P., 2017. Living cover crops have immediate impacts on soil microbial community structure and function. *J. Soil Water Conserv.* 72, 361–373. <https://doi.org/10.2489/jswc.72.4.361>
- Finney, D.M., Kaye, J.P., 2017. Functional diversity in cover crop polycultures increases multifunctionality of an agricultural system. *J. Appl. Ecol.* 54, 509–517. <https://doi.org/10.1111/1365-2664.12765>
- Fontaine, S., Barot, S., Barré, P., Bdioui, N., Mary, B., Rumpel, C., 2007. Stability of organic carbon in deep soil layers controlled by fresh carbon supply. *Nature* 450, 277–280. <https://doi.org/10.1038/nature06275>

- Fontaine, S., Mariotti, A., Abbadie, L., 2003. The priming effect of organic matter: a question of microbial competition? *Soil Biol. Biochem.* 35, 837–843. [https://doi.org/10.1016/S0038-0717\(03\)00123-8](https://doi.org/10.1016/S0038-0717(03)00123-8)
- Fu, Z., Ciais, P., Bastos, A., Stoy, P.C., Yang, H., Green, J.K., Wang, B., Yu, K., Huang, Y., Knohl, A., Šigut, L., Gharun, M., Cuntz, M., Arriga, N., Roland, M., Peichl, M., Migliavacca, M., Cremonese, E., Varlagin, A., Brümmner, C., Gourlez de la Motte, L., Fares, S., Buchmann, N., El-Madany, T.S., Pitacco, A., Vendrame, N., Li, Z., Vincke, C., Magliulo, E., Koebsch, F., 2020. Sensitivity of gross primary productivity to climatic drivers during the summer drought of 2018 in Europe. *Philos. Trans. R. Soc. B Biol. Sci.* 375, 20190747. <https://doi.org/10.1098/rstb.2019.0747>
- Gao, W., Reed, S.C., Munson, S.M., Rui, Y., Fan, W., Zheng, Z., Li, L., Che, R., Xue, K., Du, J., Cui, X., Wang, Y., Hao, Y., 2021. Responses of soil extracellular enzyme activities and bacterial community composition to seasonal stages of drought in a semiarid grassland. *Geoderma* 401, 115327. <https://doi.org/10.1016/j.geoderma.2021.115327>
- Garba, I.I., Fay, D., Apriani, R., Yusof, D.Y.P., Chu, D., Williams, A., 2022. Fallow replacement cover crops impact soil water and nitrogen dynamics in a semi-arid sub-tropical environment. *Agric. Ecosyst. Environ.* 338, 108052. <https://doi.org/10.1016/j.agee.2022.108052>
- García-Ruiz, R., Ochoa, V., Hinojosa, M.B., Carreira, J.A., 2008. Suitability of enzyme activities for the monitoring of soil quality improvement in organic agricultural systems. *Soil Biol. Biochem.*, Special Section: Enzymes in the Environment 40, 2137–2145. <https://doi.org/10.1016/j.soilbio.2008.03.023>
- Ge, X., Wang, C., Wang, L., Zhou, B., Cao, Y., Xiao, W., Li, M.-H., 2022. Drought changes litter quantity and quality, and soil microbial activities to affect soil nutrients in moso bamboo forest. *Sci. Total Environ.* 838, 156351. <https://doi.org/10.1016/j.scitotenv.2022.156351>
- Gentsch, N., Boy, J., Batalla, J.D.K., Heuermann, D., von Wirén, N., Schweneker, D., Feuerstein, U., Groß, J., Bauer, B., Reinhold-Hurek, B., Hurek, T., Céspedes, F.C., Guggenberger, G., 2020. Catch crop diversity increases rhizosphere carbon input and soil microbial biomass. *Biol. Fertil. Soils* 56, 943–957. <https://doi.org/10.1007/s00374-020-01475-8>
- Ghosh, A., Singh, A.B., Kumar, R.V., Manna, M.C., Bhattacharyya, R., Rahman, M.M., Sharma, P., Rajput, P.S., Misra, S., 2020. Soil enzymes and microbial elemental stoichiometry as bio-indicators of soil quality in diverse cropping systems and nutrient management practices of Indian Vertisols. *Appl. Soil Ecol.* 145, 103304. <https://doi.org/10.1016/j.apsoil.2019.06.007>
- Gregorutti, V.C., Caviglia, O.P., 2019. Impact of crop aerial and root biomass inputs on soil nitrifiers and cellulolytic microorganisms. *Soil Tillage Res.* 191, 85–97. <https://doi.org/10.1016/j.still.2019.03.018>
- Han, E., Czaban, W., Dresbøll, D.B., Thorup-Kristensen, K., 2022. Exploitation of neighbouring subsoil for nutrient acquisition under annual-perennial strip intercropping systems. *Agric. Ecosyst. Environ.* 338, 108106. <https://doi.org/10.1016/j.agee.2022.108106>
- Heitkötter, J., Heinze, S., Marschner, B., 2017. Relevance of substrate quality and nutrients for microbial C-turnover in top- and subsoil of a Dystric Cambisol. *Geoderma* 302, 89–99. <https://doi.org/10.1016/j.geoderma.2017.04.029>
- Hinojosa, M.B., García-Ruiz, R., Viñeola, B., Carreira, J.A., 2004. Microbiological rates and enzyme activities as indicators of functionality in soils affected by the Aznalcóllar toxic spill. *Soil Biol. Biochem.*, Enzymes in the Environment: Activity, Ecology and Applications 36, 1637–1644. <https://doi.org/10.1016/j.soilbio.2004.07.006>
- Hoang, D.T.T., Razavi, B.S., Kuznyakov, Y., Blagodatskaya, E., 2016. Earthworm burrows: Kinetics and spatial distribution of enzymes of C-, N- and P- cycles. *Soil Biol. Biochem.* 99, 94–103. <https://doi.org/10.1016/j.soilbio.2016.04.021>
- Hobley, E., Baldock, J., Hua, Q., Wilson, B., 2017. Land-use contrasts reveal instability of subsoil organic carbon. *Glob. Change Biol.* 23, 955–965. <https://doi.org/10.1111/gcb.13379>
- Hoekstra, N.J., Suter, M., Finn, J.A., Husse, S., Lüscher, A., 2015. Do belowground vertical niche differences between deep- and shallow-rooted species enhance resource uptake and drought resistance in grassland mixtures? *Plant Soil* 394, 21–34. <https://doi.org/10.1007/s11104-014-2352-x>
- Hueso, S., García, C., Hernández, T., 2012. Severe drought conditions modify the microbial community structure, size and activity in amended and unamended soils. *Soil Biol. Biochem.* 50, 167–173. <https://doi.org/10.1016/j.soilbio.2012.03.026>
- IUSS Working Group WRB, 2022. WRB: World Reference Base for Soil Resources. International soil classification system for naming soils and creating legends for soil maps., 4th ed. ed. International Union of Soil Sciences (IUSS), Vienna, Austria.
- Jones, D.L., Nguyen, C., Finlay, R.D., 2009. Carbon flow in the rhizosphere: carbon trading at the soil–root interface. *Plant Soil* 321, 5–33. <https://doi.org/10.1007/s11104-009-9925-0>
- Jones, J.M., Boehm, E.L., Kahmark, K., Lau, J., Evans, S., 2022. Microbial community response to drought depends on crop. *Elem. Sci. Anthr.* 10, 00110. <https://doi.org/10.1525/elementa.2021.00110>
- Karhu, K., Hiltavuori, E., Fritze, H., Biasi, C., Nykänen, H., Liski, J., Vanhala, P., Heinonsalo, J., Pumpanen, J., 2016. Priming effect increases with depth in a boreal forest soil. *Soil Biol. Biochem.* 99, 104–107. <https://doi.org/10.1016/j.soilbio.2016.05.001>

- Kuo, S., Sainju, U.M., 1998. Nitrogen mineralization and availability of mixed leguminous and non-leguminous cover crop residues in soil. *Biol. Fertil. Soils* 26, 346–353. <https://doi.org/10.1007/s003740050387>
- Kuo, S., Sainju, U.M., Jellum, E., 1996. Winter cover cropping influence on nitrogen mineralization, presidedress soil nitrate test, and corn yields. *Biol. Fertil. Soils* 22, 310–317. <https://doi.org/10.1007/BF00334575>
- Lagomarsino, A., Benedetti, A., Marinari, S., Pompili, L., Moscatelli, M.C., Roggero, P.P., Lai, R., Ledda, L., Grego, S., 2011. Soil organic C variability and microbial functions in a Mediterranean agro-forest ecosystem. *Biol. Fertil. Soils* 47, 283–291. <https://doi.org/10.1007/s00374-010-0530-4>
- Lange, M., Eisenhauer, N., Sierra, C.A., Bessler, H., Engels, C., Griffiths, R.I., Mellado-Vázquez, P.G., Malik, A.A., Roy, J., Scheu, S., Steinbeiss, S., Thomson, B.C., Trumbore, S.E., Gleixner, G., 2015. Plant diversity increases soil microbial activity and soil carbon storage. *Nat. Commun.* 6, 6707. <https://doi.org/10.1038/ncomms7707>
- Li, L., Tilman, D., Lambers, H., Zhang, F.-S., 2014. Plant diversity and overyielding: insights from belowground facilitation of intercropping in agriculture. *New Phytol.* 203, 63–69. <https://doi.org/10.1111/nph.12778>
- Liang, Z., Elsgaard, L., Nicolaisen, M.H., Lyhne-Kjærbye, A., Olesen, J.E., 2018. Carbon mineralization and microbial activity in agricultural topsoil and subsoil as regulated by root nitrogen and recalcitrant carbon concentrations. *Plant Soil* 433, 65–82. <https://doi.org/10.1007/s11104-018-3826-z>
- Liu, S., Razavi, B.S., Su, X., Maharjan, M., Zarebanadkouki, M., Blagodatskaya, E., Kuzyakov, Y., 2017. Spatio-temporal patterns of enzyme activities after manure application reflect mechanisms of niche differentiation between plants and microorganisms. *Soil Biol. Biochem.* 112, 100–109. <https://doi.org/10.1016/j.soilbio.2017.05.006>
- Lupwayi, N.Z., Schwinghamer, T.D., Tidemann, B.D., Kubota, H., Turkington, T.K., Khakbazan, M., St. Luce, M., 2021. Causal relationships from legume crops to soil microbial properties relative to canola. *Agron. J.* 113, 172–186. <https://doi.org/10.1002/agj2.20493>
- Lupwayi, N.Z., Soon, Y.K., 2016. Soil microbial properties during decomposition of pulse crop and legume green manure residues in three consecutive subsequent crops. *Can. J. Soil Sci.* 96, 413–426. <https://doi.org/10.1139/cjss-2016-0039>
- Ma, X., Zarebanadkouki, M., Kuzyakov, Y., Blagodatskaya, E., Pausch, J., Razavi, B.S., 2018. Spatial patterns of enzyme activities in the rhizosphere: Effects of root hairs and root radius. *Soil Biol. Biochem.* 118, 69–78. <https://doi.org/10.1016/j.soilbio.2017.12.009>
- Malik, A.A., Swenson, T., Weihe, C., Morrison, E.W., Martiny, J.B.H., Brodie, E.L., Northen, T.R., Allison, S.D., 2020. Drought and plant litter chemistry alter microbial gene expression and metabolite production. *ISME J.* 14, 2236–2247. <https://doi.org/10.1038/s41396-020-0683-6>
- Michaelis, L., Menten, M.L., 1913. Die kinetik der invertinwirkung. *Biochem Z* 49, 352.
- Moorhead, D.L., Sinsabaugh, R.L., 2006. A Theoretical Model of Litter Decay and Microbial Interaction. *Ecol. Monogr.* 76, 151–174.
- Muhammad, I., Wang, J., Khan, A., Ahmad, S., Yang, L., Ali, I., Zeeshan, M., Ullah, S., Fahad, S., Ali, S., Zhou, X.B., 2021. Impact of the mixture versus solo residue management and climatic conditions on soil microbial biomass carbon to nitrogen ratio: a systematic review. *Environ. Sci. Pollut. Res.* 28, 64241–64252. <https://doi.org/10.1007/s11356-021-15579-7>
- Nair, A., Ngouajio, M., 2012. Soil microbial biomass, functional microbial diversity, and nematode community structure as affected by cover crops and compost in an organic vegetable production system. *Appl. Soil Ecol.* 58, 45–55. <https://doi.org/10.1016/j.apsoil.2012.03.008>
- Nannipieri, P., Giagnoni, L., Renella, G., Puglisi, E., Ceccanti, B., Masciandaro, G., Fornasier, F., Moscatelli, M.C., Marinari, S., 2012. Soil enzymology: classical and molecular approaches. *Biol. Fertil. Soils* 48, 743–762. <https://doi.org/10.1007/s00374-012-0723-0>
- Nannipieri, P., Trasar-Cepeda, C., Dick, R.P., 2018. Soil enzyme activity: a brief history and biochemistry as a basis for appropriate interpretations and meta-analysis. *Biol. Fertil. Soils* 54, 11–19. <https://doi.org/10.1007/s00374-017-1245-6>
- Niewiadomska, A., Majchrzak, L., Borowiak, K., Wolna-Maruwka, A., Waraczewska, Z., Budka, A., Gaj, R., 2020. The Influence of Tillage and Cover Cropping on Soil Microbial Parameters and Spring Wheat Physiology. *Agronomy* 10, 200. <https://doi.org/10.3390/agronomy10020200>
- Nivelle, E., Verzeaux, J., Habbib, H., Kuzyakov, Y., Decocq, G., Roger, D., Lacoux, J., Duclercq, J., Spicher, F., Nava-Saucedo, J.-E., Catterou, M., Dubois, F., Tetu, T., 2016. Functional response of soil microbial communities to tillage, cover crops and nitrogen fertilization. *Appl. Soil Ecol.* 108, 147–155. <https://doi.org/10.1016/j.apsoil.2016.08.004>
- Oram, N.J., Ravenek, J.M., Barry, K.E., Weigelt, A., Chen, H., Gessler, A., Gockele, A., de Kroon, H., van der Paauw, J.W., Scherer-Lorenzen, M., Smit-Tiekstra, A., van Ruijven, J., Mommer, L., 2018. Below-ground complementarity effects in a grassland biodiversity experiment are related to deep-rooting species. *J. Ecol.* 106, 265–277. <https://doi.org/10.1111/1365-2745.12877>
- Pausch, J., Kuzyakov, Y., 2018. Carbon input by roots into the soil: Quantification of rhizodeposition from root to ecosystem scale. *Glob. Change Biol.* 24, 1–12. <https://doi.org/10.1111/gcb.13850>

- Paz-Ferreiro, J., Gascó, G., Gutiérrez, B., Méndez, A., 2012. Soil biochemical activities and the geometric mean of enzyme activities after application of sewage sludge and sewage sludge biochar to soil. *Biol. Fertil. Soils* 48, 511–517. <https://doi.org/10.1007/s00374-011-0644-3>
- Peixoto, L., Elsgaard, L., Rasmussen, J., Kuzyakov, Y., Banfield, C.C., Dippold, M.A., Olesen, J.E., 2020. Decreased rhizodeposition, but increased microbial carbon stabilization with soil depth down to 3.6 m. *Soil Biol. Biochem.* 150, 108008. <https://doi.org/10.1016/j.soilbio.2020.108008>
- Peixoto, L., Olesen, J.E., Elsgaard, L., Enggrob, K.L., Banfield, C.C., Dippold, M.A., Nicolaisen, M.H., Bak, F., Zang, H., Dresbøll, D.B., Thorup-Kristensen, K., Rasmussen, J., 2022. Deep-rooted perennial crops differ in capacity to stabilize C inputs in deep soil layers. *Sci. Rep.* 12, 5952. <https://doi.org/10.1038/s41598-022-09737-1>
- Pierret, A., Maeght, J.-L., Clément, C., Montoroi, J.-P., Hartmann, C., Gonkhamdee, S., 2016. Understanding deep roots and their functions in ecosystems: an advocacy for more unconventional research. *Ann. Bot.* 118, 621–635. <https://doi.org/10.1093/aob/mcw130>
- Piotrowska-Długosz, A., Wilczewski, E., 2020. Influence of field pea (*Pisum sativum* L.) as catch crop cultivated for green manure on soil phosphorus and P-cycling enzyme activity. *Arch. Agron. Soil Sci.* 66, 1570–1582. <https://doi.org/10.1080/03650340.2020.1715950>
- Pittman, K.B., Barney, J.N., Flessner, M.L., 2020. Cover crop residue components and their effect on summer annual weed suppression in corn and soybean. *Weed Sci.* 68, 301–310. <https://doi.org/10.1017/wsc.2020.16>
- Preece, C., Verbruggen, E., Liu, L., Weedon, J.T., Peñuelas, J., 2019. Effects of past and current drought on the composition and diversity of soil microbial communities. *Soil Biol. Biochem.* 131, 28–39. <https://doi.org/10.1016/j.soilbio.2018.12.022>
- Qu, Q., Wang, Z., Gan, Q., Liu, R., Xu, H., 2023. Impact of drought on soil microbial biomass and extracellular enzyme activity. *Front. Plant Sci.* 14.
- Raiesi, F., Beheshti, A., 2014. Soil specific enzyme activity shows more clearly soil responses to paddy rice cultivation than absolute enzyme activity in primary forests of northwest Iran. *Appl. Soil Ecol.* 75, 63–70. <https://doi.org/10.1016/j.apsoil.2013.10.012>
- Rasmussen, C.R., Thorup-Kristensen, K., Dresbøll, D.B., 2020. Uptake of subsoil water below 2 m fails to alleviate drought response in deep-rooted Chicory (*Cichorium intybus* L.). *Plant Soil* 446, 275–290. <https://doi.org/10.1007/s11104-019-04349-7>
- Razavi, B.S., Blagodatskaya, E., Kuzyakov, Y., 2015. Nonlinear temperature sensitivity of enzyme kinetics explains canceling effect—a case study on loamy haplic Luvisol. *Front. Microbiol.* 6.
- Razavi, B.S., Zarebanadkouki, M., Blagodatskaya, E., Kuzyakov, Y., 2016. Rhizosphere shape of lentil and maize: Spatial distribution of enzyme activities. *Soil Biol. Biochem.* 96, 229–237. <https://doi.org/10.1016/j.soilbio.2016.02.020>
- Redin, M., Recous, S., Aita, C., Dietrich, G., Skolaude, A.C., Ludke, W.H., Schmatz, R., Giacomini, S.J., 2014. How the chemical composition and heterogeneity of crop residue mixtures decomposing at the soil surface affects C and N mineralization. *Soil Biol. Biochem.* 78, 65–75. <https://doi.org/10.1016/j.soilbio.2014.07.014>
- Rutan, J., Rosenzweig, N., Steinke, K., 2023. Impact of Cover Crops and Nitrogen Management on Soil Bacterial Alpha Diversity. *Commun. Soil Sci. Plant Anal.* 54, 2113–2125. <https://doi.org/10.1080/00103624.2023.2211605>
- Salomé, C., Nunan, N., Pouteau, V., Lerch, T.Z., Chenu, C., 2010. Carbon dynamics in topsoil and in subsoil may be controlled by different regulatory mechanisms. *Glob. Change Biol.* 16, 416–426. <https://doi.org/10.1111/j.1365-2486.2009.01884.x>
- Schimel, J.P., 2018. Life in Dry Soils: Effects of Drought on Soil Microbial Communities and Processes. *Annu. Rev. Ecol. Evol. Syst.* 49, 409–432. <https://doi.org/10.1146/annurev-ecolsys-110617-062614>
- Schneider, T., Keiblinger, K.M., Schmid, E., Sterflinger-Gleixner, K., Ellersdorfer, G., Roschitzki, B., Richter, A., Eberl, L., Zechmeister-Boltenstern, S., Riedel, K., 2012. Who is who in litter decomposition? Metaproteomics reveals major microbial players and their biogeochemical functions. *ISME J.* 6, 1749–1762. <https://doi.org/10.1038/ismej.2012.11>
- Siebielec, S., Siebielec, G., Klimkiewicz-Pawlas, A., Gałazka, A., Grządziel, J., Stuczyński, T., 2020. Impact of Water Stress on Microbial Community and Activity in Sandy and Loamy Soils. *Agronomy* 10, 1429. <https://doi.org/10.3390/agronomy10091429>
- Sinsabaugh, R.L., Carreiro, M.M., Repert, D.A., 2002. Allocation of extracellular enzymatic activity in relation to litter composition, N deposition, and mass loss. *Biogeochemistry* 60, 1–24. <https://doi.org/10.1023/A:1016541114786>
- Sinsabaugh, R.L., Follstad Shah, J.J., 2011. Ecoenzymatic stoichiometry of recalcitrant organic matter decomposition: the growth rate hypothesis in reverse. *Biogeochemistry* 102, 31–43. <https://doi.org/10.1007/s10533-010-9482-x>
- Sinsabaugh, R.L., Lauber, C.L., Weintraub, M.N., Ahmed, B., Allison, S.D., Crenshaw, C., Contosta, A.R., Cusack, D., Frey, S., Gallo, M.E., Gartner, T.B., Hobbie, S.E., Holland, K., Keeler, B.L., Powers, J.S., Stursova, M., Takacs-Vesbach, C., Waldrop, M.P., Wallenstein, M.D., Zak, D.R., Zeglin, L.H., 2008. Stoichiometry of soil enzyme activity at global scale. *Ecol. Lett.* 11, 1252–1264. <https://doi.org/10.1111/j.1461-0248.2008.01245.x>

- Smith, R.G., Atwood, L.W., Warren, N.D., 2014. Increased Productivity of a Cover Crop Mixture Is Not Associated with Enhanced Agroecosystem Services. *PLOS ONE* 9, e97351. <https://doi.org/10.1371/journal.pone.0097351>
- St Aime, R., Bridges Jr., W.C., Narayanan, S., 2023. Fall–winter cover crops promote soil health and weed control in the southeastern clayey soils. *Agron. J.* 115, 242–260. <https://doi.org/10.1002/agj2.21246>
- St Aime, R., Zehnder, G.W., Talley, C., Narayanan, S., 2020. Differences in Biomass Production and Water Use Efficiency among Seven Different Cover Crops in the Wet Winter Seasons of 2016/17 and 2018 in South Carolina. *Agronomy* 10, 463. <https://doi.org/10.3390/agronomy10040463>
- Stavi, I., Lal, R., Jones, S., Reeder, R.C., 2012. Implications of Cover Crops for Soil Quality and Geodiversity in a Humid-Temperate Region in the Midwestern Usa. *Land Degrad. Dev.* 23, 322–330. <https://doi.org/10.1002/ldr.2148>
- Steinauer, K., Chatzinotas, A., Eisenhauer, N., 2016. Root exudate cocktails: the link between plant diversity and soil microorganisms? *Ecol. Evol.* 6, 7387–7396. <https://doi.org/10.1002/ece3.2454>
- Tamburini, G., Bommarco, R., Wanger, T.C., Kremen, C., van der Heijden, M.G.A., Liebman, M., Hallin, S., 2020. Agricultural diversification promotes multiple ecosystem services without compromising yield. *Sci. Adv.* 6, eaba1715. <https://doi.org/10.1126/sciadv.aba1715>
- Thapa, V.R., Ghimire, R., Acosta-Martínez, V., Marsalis, M.A., Schipanski, M.E., 2021. Cover crop biomass and species composition affect soil microbial community structure and enzyme activities in semiarid cropping systems. *Appl. Soil Ecol.* 157, 103735. <https://doi.org/10.1016/j.apsoil.2020.103735>
- Tiemann, L.K., Grandy, A.S., Atkinson, E.E., Marin-Spiotta, E., McDaniel, M.D., 2015. Crop rotational diversity enhances belowground communities and functions in an agroecosystem. *Ecol. Lett.* 18, 761–771. <https://doi.org/10.1111/ele.12453>
- Tischer, A., Blagodatskaya, E., Hamer, U., 2014. Extracellular enzyme activities in a tropical mountain rainforest region of southern Ecuador affected by low soil P status and land-use change. *Appl. Soil Ecol.* 74, 1–11. <https://doi.org/10.1016/j.apsoil.2013.09.007>
- Topps, D., 2021. Impact of Cover Crop Monocultures and Mixtures on Organic Carbon Contents of Soil Aggregates 10.
- Tribouillois, H., Fort, F., Cruz, P., Charles, R., Flores, O., Garnier, E., Justes, E., 2015. A Functional Characterisation of a Wide Range of Cover Crop Species: Growth and Nitrogen Acquisition Rates, Leaf Traits and Ecological Strategies. *PLOS ONE* 10, e0122156. <https://doi.org/10.1371/journal.pone.0122156>
- Wagger, M.G., 1989. Time of Desiccation Effects on Plant Composition and Subsequent Nitrogen Release from Several Winter Annual Cover Crops. *Agron. J.* 81, 236–241. <https://doi.org/10.2134/agronj1989.00021962008100020020x>
- Wang, C., Sun, Y., Chen, H.Y.H., Yang, J., Ruan, H., 2021. Meta-analysis shows non-uniform responses of above- and belowground productivity to drought. *Sci. Total Environ.* 782, 146901. <https://doi.org/10.1016/j.scitotenv.2021.146901>
- Wang, S., Zhang, X., Zhou, J., Xu, Z., Ma, Q., Chu, J., Zang, H., Yang, Y., Peixoto, L., Zeng, Z., Razavi, B.S., 2023. Transition of spatio-temporal distribution of soil enzyme activity after straw incorporation: From rhizosphere to detritusphere. *Appl. Soil Ecol.* 186, 104814. <https://doi.org/10.1016/j.apsoil.2023.104814>
- Wu, J., Brookes, P.C., Jenkinson, D.S., 1993. Formation and destruction of microbial biomass during the decomposition of glucose and ryegrass in soil. *Soil Biol. Biochem.* 25, 1435–1441. [https://doi.org/10.1016/0038-0717\(93\)90058-J](https://doi.org/10.1016/0038-0717(93)90058-J)
- Wu, Z., Dijkstra, P., Koch, G.W., Peñuelas, J., Hungate, B.A., 2011. Responses of terrestrial ecosystems to temperature and precipitation change: a meta-analysis of experimental manipulation. *Glob. Change Biol.* 17, 927–942. <https://doi.org/10.1111/j.1365-2486.2010.02302.x>
- Xu, H., Qu, Q., Lu, B., Li, P., Xue, S., Liu, G., 2020. Response of soil specific enzyme activity to vegetation restoration in the Loess hilly region of China. *CATENA* 191, 104564. <https://doi.org/10.1016/j.catena.2020.104564>
- Zhang, X., Bilyera, N., Fan, L., Duddek, P., Ahmed, M.A., Carminati, A., Kaestner, A., Dippold, M.A., Spielvogel, S., Razavi, B.S., 2023. The spatial distribution of rhizosphere microbial activities under drought: water availability is more important than root-hair-controlled exudation. *New Phytol.* 237, 780–792. <https://doi.org/10.1111/nph.18409>

## 2.3 Study 3. Redundancy of Microbial P Mobilization in Beech Forest Soils with Contrasting P Stock: A Microbial Dilution Experiment

Yijie Shi<sup>1</sup>, Sasya Samhita<sup>2,3</sup>, Sebastian Loeppmann<sup>1</sup>, Iris Zimmermann<sup>1</sup>, Michaela A. Dippold<sup>2,4</sup>, Sandra Spielvogel<sup>1</sup>

**Status:** Submitted to *Applied Soil Ecology*

<sup>1</sup> Institute of Plant Nutrition and Soil Science, Christian-Albrechts-University Kiel, Germany

<sup>2</sup> Biogeochemistry of Agroecosystems, University of Goettingen, Germany

<sup>3</sup> Department of Plant Ecology and Ecosystem Research, University of Goettingen, Germany

<sup>4</sup> Geo-Biosphere Interactions, Department of Geosciences, University of Tuebingen, Germany

---

### Abstract

Soil microorganisms drive the phosphorus (P) cycle in forest soils. To assess key mechanisms of microbial P mobilization and uptake in forest soils, we produced <sup>33</sup>P labeled root- and leaf-litter of *Fagus Sylvatica*. P-poor and P-rich soils with different microbial diversities were established by re-inoculating gamma-irradiated soil with serially diluted soil suspensions from the original soil. The re-inoculated soil was incubated in microcosms with the <sup>33</sup>P labeled litter for four weeks. The kinetics of P cycling enzyme and the flux of <sup>33</sup>P into different soil pools were determined. Carbon (C), nitrogen (N), and phosphorus (P), in soil microbial biomass and in extractable pools (e.g., P<sub>resin</sub>) were measured and calculated as stoichiometry ratios. The results showed that acid phosphatase activity differed significantly among dilutions at P-rich site, indicating a disturbance of P mobilization by microbial diversity loss. The acid phosphatase activity at P-poor site was overall higher than P-rich site and it was unaffected by the microbial diversity reduction, indicating a high functional redundancy of P mobilization. Higher recovery of litter-derived <sup>33</sup>P in soil microbial biomass and in P<sub>resin</sub> were detected in all microbial dilution variants of the P-poor soil, suggesting a tight cycling of litter-derived P in microbial biomass and the soil solution. Our study confirms that the high functional redundancy of microbial P acquisition at P-poor forest site aims to keep all essential processes ongoing even under loss of biodiversity. In contrast, at P-rich sites, individual processes such as litter-P mobilization are less redundant than in P-poor soils.

**Keywords:** P mineralization, P cycling, serial microbial dilution, litter addition, <sup>33</sup>P wick labeling

## 1. Introduction

European beech (*Fagus sylvatica* L.) is the most common broad-leaf tree species in Central Europe, occupying nearly 12 million hectares of forest area (Schraml and Rennenberg, 2002; Geßler et al., 2007; Netzer et al., 2017), but the future growth trend declines from  $-20\%$  to more than  $-50\%$  by 2090 (Martinez del Castillo et al., 2022). According to the Second National Forest Soil Inventory in Germany (NFSI II), 60 % of all *Fagus sylvatica* L. trees showed insufficient P nutrition (Niederberger et al., 2019). Considering the highlighted decline of foliar phosphorus (P) concentration of beech forests in recent decades (Jonard et al., 2015; Talkner et al., 2015; Lang et al., 2017), a better understanding of P cycling strategies is of great importance for improving sustainable forest strategies. Different from farmland ecosystems, where P deficiency can be compensated by fertilization (Valkama et al., 2009; Weeks and Hettiarachchi, 2019), forest soils mainly rely on weathering of P-bearing minerals (Buendía et al., 2010), atmospheric deposition (Ben-Ami et al., 2010; Das and Lawrence, 2013), and mineralization of litter-P (Estiarte and Peñuelas, 2015; Sohrt et al., 2018; Peng et al., 2023) and microbial necromass-P (Schmitt et al., 2022), to cope with P deficiency. Soil microorganisms not only decompose organic P via the production of extracellular enzymes but also, they are able to take it up directly (Wasner et al., 2023) and immobilize the organic P in their biomass (Richardson, 2001; Oberson and Joner, 2005). The absence of litter decreases the available P and the microbial functions of nutrient mobilization in beech forest soil (Maillard et al., 2019). The importance of leaf litter-derived P as an essential energy and nutrient source for the soil microbial community has been well discussed (Richardson and Simpson, 2011), and the amount of leaf litter has been determined approximately 48% of annual litter inputs, and the decomposition rate of leaf litter is 1.5- and 2.8-fold faster than fine stems and fine roots in forests (Freschet et al., 2013). However, seeing as a whole litter composition, information based on the effect of combined leaf and root litter on forest P cycling is still missing.

The concept of ecological stoichiometry reflects a powerful indicator to explore the functioning of terrestrial ecosystems (Sterner and Elser, 2017) and soil microorganisms can be linked to various ecosystem functions and services that follow the concept of ecological stoichiometry (Sinsabaugh and Follstad Shah, 2012; Loepmann et al., 2016; Bai et al., 2021) enabling the identification of key ecological processes for carbon (C) and nutrient cycles of ecosystems. The regulation of microbial P mobilization under various soil nutritional levels is governed by microbial C: nitrogen (N):P stoichiometry (Mooshammer et al., 2012). Microorganisms cope with the imbalance of stoichiometry between their biomass and the added organic substrate by (i) adjusting microbial community composition; (ii) releasing extracellular enzymes to mobilize additional nutrients; and (iii) regulating their element use efficiencies by e.g., increasing the cellular respiration (Manzoni et al., 2008; Mooshammer et al., 2014; Spohn and Widdig, 2017). An imbalanced element input to soil lead to non-homeostatic properties and C: N: P variation of soil microorganisms (Bai et al., 2021). This leads to a microbial diversity loss which has been demonstrated especially for forest soils in recent decades (Kennedy and Smith, 1995; Holden and Treseder, 2013; Singh and Gupta, 2018; Preece et al., 2019). There are studies indicating that the microbial resistance and resilience to changing environmental conditions have positive relations with microbial diversity (Griffiths et al., 2004; Girvan et al., 2005; Philippot et al., 2013), while others showed that highly redundant functional processes such as respiration and C mineralization (Wertz et al., 2006; Baumann et al., 2013). A recent study has revealed that microbial biomass storage synthesis is a key mechanism for resistance and resilience of microbial communities facing environmental change (Mason-Jones et al., 2023), and the re-use of soil microbial biomass has been determined as the main P acquisition strategy in P deficient beech forests (Lang et al., 2017). Given the importance of the microorganisms as an initial driver and intermediate pool of soil P cycling, researching how microbial diversity loss affects microbial P mobilization and uptake remains an urgent issue.

The dilution/extinction approach has been used a number of times for manipulating original microbial diversity in a certain ecosystem (Garland and Lehman, 1999; Franklin et al., 2001; Griffiths et al.,

2001). The experimental simulation of microbial diversity reduction by serially diluting soil microbial suspensions from the respective soils has been proven efficient to induce a remarkable decrease of microbial diversity with ongoing dilution (Wertz et al., 2006; Tardy et al., 2014; Yan et al., 2015). To assess the key mechanisms of microbial P mobilization in forest soils of contrasting P stock (P-poor vs. P-rich soil), we produced  $^{33}\text{P}$  labeled leaf- and root-litter via radioisotope wick labeling, and conducted six serial microbial dilutions of soils suspensions at P-rich site (Skeletal Cambisol) and P-poor site (Hyperdystric Folic Cambisol). By re-inoculating the soil with its diluted native microbial community and covering with labeled leaf- and root-litter, we investigated the allocation of P during the microbial decomposition of root and leaf litter. We hypothesized that: (1) acid phosphatase activity is higher in P-poor than in P-rich soil because microbes under the pressure of P deficiency tend to invest in the further production of phosphatases in order to mine additional P; (2) MBP as an intermediate P reservoir is higher in P-rich soil since sufficient P is available and any resource limitation is lacking (3) Microbial P mobilization is a function of low redundancy, which slows P mineralization as a result of microbial diversity loss, and such a functional loss is accompanied by non-homeostatic microbial C:N:P ratios.

## 2. Material and Methods

### 2.1. Site description

Soil samples were taken from the Ah horizons of two European beech (*Fagus sylvatica* L.) forest sites with contrasting levels of total soil P. The Bad Brückenau (BBR) site with P-rich soil (Table 3-1, P stock is  $904 \text{ g m}^{-2}$  in BBR) is located in Northern Bavaria, Germany ( $50^{\circ}21'7.26'' \text{ N}$ ,  $9^{\circ}55'44.53'' \text{ E}$ ). The mean annual temperature is  $5.8 \text{ }^{\circ}\text{C}$  and the mean annual precipitation is 1031 mm. The soil at BBR is classified as Dystric skeletal Cambisol and has developed from Basalt (Lang et al., 2017). The Lüss (LUE) site with P-poor soil (Table 1, P stock is  $164 \text{ g m}^{-2}$  in LUE) is located in Lower Saxony, Germany ( $52^{\circ}50'21.77'' \text{ N}$ ,  $10^{\circ}16'2.37'' \text{ E}$ ). The mean annual temperature is  $8.0 \text{ }^{\circ}\text{C}$  and the mean annual precipitation is 779 mm. The soil is classified as Hyperdystric Folic Cambisol and has developed on sandy till (WRB 2015; Lang et al., 2017).

**Table 3-1** Soil properties of the study sites.

	Bad Brückenau (BBR)	Lüss (LUE)
Humus Layer <sup>1</sup>	Mull-like moder	Mor-like moder
pH (H <sub>2</sub> O) of A horizon <sup>1</sup>	3.8	3.5
Texture (topsoil) (WRB 2015) <sup>1</sup>	Silty clay loam	Loamy sand
P stock ( $\text{mg g}^{-1}$ ) <sup>2</sup>	1.02	0.08
N stock ( $\text{mg g}^{-1}$ ) <sup>2</sup>	7.8	1.5
C stock ( $\text{mg g}^{-1}$ ) <sup>2</sup>	117	34
Clay in A horizon (%) <sup>3</sup>	37	6
Fe oxalate in A horizon ( $\text{mg g}^{-1}$ ) <sup>3</sup>	29.3	0.9
Al oxalate in A horizon ( $\text{mg g}^{-1}$ ) <sup>3</sup>	8.4	0.3

<sup>1</sup>(Lang et al., 2017); <sup>2</sup>(Brödlin et al., 2019b); <sup>3</sup>(Brödlin et al., 2019a)

### 2.2 Sampling of plants and soil

European beech seedlings (*Fagus sylvatica* L.) were collected at the beginning of March 2019. We collected seedlings of beech trees from randomly chosen positions at both sampling sites. Soil samples were taken from the Ah horizon of the respective site at six randomly chosen positions. The soil samples were pooled, homogenized and cooled at  $4 \text{ }^{\circ}\text{C}$  during transport.

#### 2.2.1 Pre-incubation of soil and inoculation of microbial suspension

Soil samples were sieved ( $< 2 \text{ mm}$ ), divided into 800 g portions and gamma irradiated for sterilization. Fifty grams of sieved and air-dried, gamma-irradiated soil was preincubated in autoclaved microcosms

for four weeks under laminar flow conditions. Gravimetric water content of the soil samples was determined by weighing and the water contents were monitored gravimetrically throughout the entire experiment (Brödlin et al., 2019). To ensure soil aeration, microcosms were uncovered during preincubation leading to a partial loss of soil water content.

The resident microbial community stock solution ( $10^0$ ) was prepared by adding 1 g fresh soil to 10 ml demineralized water (Gowsalya et al. 2014). Subsequently, six levels of dilution ( $10^{-1}$ ,  $10^{-2}$ ,  $10^{-3}$ ,  $10^{-4}$ ,  $10^{-5}$ ,  $10^{-6}$ ) were prepared from the stock solution. From each dilution level, 1 ml of soil suspension was added to the respective microcosm, containing the sterile soil (Griffiths et al. 2004), before the preincubation started.

### 2.2.2 $^{33}\text{P}$ labeling of beech seedlings and litter collection

The beech trees that were collected from BBR and LUE were grown in climate chambers under artificial light ( $11 \text{ h d}^{-1}$ ; 400W; KIND LED, USA) at  $20 \text{ }^\circ\text{C}$  for four weeks, until the buds opened, and the leaves emerged. Each plant was fed with  $^{33}\text{P}$  as 1 ml  $\text{H}_3\text{PO}_4$  solution to the beech stem using the wick labeling method (Russell and Fillery, 1996; Mayer et al., 2003). We drilled a small hole into the stem, inserted the cotton string and sealed the hole with plasticine to avoid harm to the plant. After 96 hours the radiolabeled solution was taken up. To avoid solute residue in the tube, 1 ml tap-water was added and the complete uptake of this volume of water was awaited before harvest. After 7 days of labeling, we separately harvested and freeze-dried (Beta1-8, LSC plus, Martin Christ GmbH, Osterode, Germany) the roots and leaves from all trees. Before adding to microcosms, we homogenously mixed the freeze-dried roots and leaves with a dry mass ratio of 2:1. All root and leaf litter were cut into  $1 \text{ cm}^2$  pieces for easier decomposition. To quantify the total P content and the  $^{33}\text{P}$  activity of the mixed litter debris, 1 g of the litter mixture was ball milled and pressure digested with 65%  $\text{HNO}_3$  at  $160^\circ\text{C}$  for 12 h (Heinrichs et al. 1986). Thereafter, the  $^{33}\text{P}$  activity of the leaves and roots was measured by ICP-OES (ICAP 7400 ICP-OES Duo, Thermo Fisher Scientific, Dreieich, Germany) and via scintillation counter (Hidex 300SL, Turku, Finland). The  $^{33}\text{P}$  activity of each plant biomass unit was determined as follows (equation 1):

$$^{33}\text{P activity (Bq (g biomass)}^{-1}) = \frac{\text{Total } ^{33}\text{P (Bq)}}{\text{Plant biomass (g)}} \quad (1)$$

### 2.2.3 Incubation of microbial inoculated soil with $^{33}\text{P}$ labeled litter

To trace litter-derived P mobilization, 1.44 g of homogeneously mixed litter debris, representing half of the annual litter fall and containing 2265 kBq of  $^{33}\text{P}$ , was put on the soil surface in each microcosm and incubated for four weeks at room temperature. The microcosms were aerated by opening the lids every two days. The water content was adjusted gravimetrically every week to compensate the water loss by evaporation. After four weeks of incubation, the microcosms were harvested, and the litter debris was removed from the microcosms to maintain the homogenous isotopic activity in the soil. The soil samples in the microcosms were collected and stored at  $+4 \text{ }^\circ\text{C}$  until analysis ( $< 7$  days). Five grams of moist soil were dried at  $105 \text{ }^\circ\text{C}$  for 24 h to measure the gravimetric soil water content.

## 2.3 Microbial biomass phosphorus (MBP), extractable phosphorus ( $\text{P}_{\text{resin}}$ ) and microbial uptake of litter-derived $^{33}\text{P}$

MBP was determined by the fumigation extraction method using anion exchange resin membranes (Kouno et al., 1995). Two grams of soil were horizontally shaken in 30 ml autoclaved water along with a resin membrane ( $6 \text{ cm} \times 2 \text{ cm}$ , #55164, BDH company) for 20 hours. Three subsamples were prepared from each sample, namely, (1) a fumigated subsample with 1 ml of 1-hexanol ( $\text{P}_{\text{fum}}$ ), (2) a non-fumigated subsample with sterile water ( $\text{P}_{\text{resin}}$ ), (3) a non-fumigated subsample containing a P spike of 1 ml solution ( $35 \text{ mg}$  and  $6 \text{ mg P kg}^{-1}$  for BBR and LUE samples, respectively) ( $\text{P}_{\text{spike}}$ ). According to (Bünemann et al., 2004; Bünemann et al., 2016) we did not account for the conversion factor for cell lyses. To determine total P concentration, the eluates were dissolved in ammonium molybdate reagent and the reducing agent ascorbic acid, and thereafter heated in a water bath ( $90 \text{ }^\circ\text{C}$ )

for five minutes. P concentrations were determined photometrically (820 nm, Tecan i-control, infinite 200, Switzerland) (Bünemann et al., 2016). <sup>33</sup>P activity in all three subsamples was determined by mixing eluent and scintillation cocktail in a ratio of 3:4 and measuring them at a scintillation counter (Hidex 300SL, Turku, Finland) (Wang et al., 2022).

#### 2.4 Microbial biomass (MBC) and microbial biomass nitrogen (MBN)

MBC and MBN were determined using the chloroform fumigation extraction method (Brookes et al., 1982; Vance et al., 1987). Briefly, 7.5 g of moist soil was fumigated for 24 h using chloroform. To measure the extractable C and N pool, the fumigated and the same amount of unfumigated soil was extracted with 30 ml of 0.05 M K<sub>2</sub>SO<sub>4</sub> in an overhead shaker for 1 h with 40 rpm (Bruulsema and Duxbury, 1996). After 10 min of centrifugation at 2500 g, the supernatant of the soil suspension was filtered through Rotilabo-rondfilters (type 15A, Carl Roth GmbH & Co.KG). The fumigated and unfumigated extracts were analysed using a TOC/TN Element analyzer (Analytik Jena, multi-N/C 21005, Jena, Germany). The conversion factor of 0.45 and 0.54 was used to correct the content of MBC and MBN for extraction efficiency, respectively (Jenkinson and Ladd, 1981).

#### 2.5 Enzyme kinetics assay

We used 4-methylumbelliferone-phosphate (MUF-P) to determine the kinetics of soil extracellular acid phosphatases. Half a gram of moist soil was weighed into sterilized 100 ml glass bottles with polypropylene lids, and 50 ml of autoclaved water was added. The soil solutions were shaken at 200 rpm for 30 minutes at 22 °C on a horizontal shaker. Thereafter, the soil solutions were sonicated (UW2200, Bandelin) at 40 J s<sup>-1</sup> pulsed energy output for two minutes. Fifty µl of soil suspension were pipetted into 96-well microplates (polystyrol black, Grainer bio-one, Germany). Then 50 µl of 0.1 M MES buffer (C<sub>6</sub>H<sub>13</sub>NO<sub>4</sub>SNa<sub>0.5</sub>, pH = 6.1) was added into each well (Marx et al., 2005; Loeppmann et al., 2016). The same pH of the buffer was chosen for better site comparability as done by (Loeppmann et al., 2020) and (Fetzer et al., 2021). Standard working solutions in each well were mixed with 100 µl MUF-P substrate solutions with seven concentrations of 5 µM, 20 µM, 50 µM, 100 µM, 200 µM, 300 µM, 400 µM. The microplates were incubated for three hours at 22 °C. Fluorescence (excitation: 355 nm; emission: 460 nm) was measured after 30, 60, 120, and 180 minutes of incubation using a Victor 1420-050 Multi label Counter (Perkin Elmer, UK). Enzyme kinetics was determined via Michaelis–Menten equation (equation 2):

$$V = \frac{V_{max} [S]}{(K_m + [S])} \quad (2)$$

Where  $V$  is the reaction velocity (nmol g<sup>-1</sup> h<sup>-1</sup>),  $V_{max}$  is the maximal rate of enzyme activity at saturated substrate concentration,  $K_m$  is the substrate concentration at half of the  $V_{max}$  and  $S$  is the substrate concentration (Michaelis and Menten, 1913; Nannipieri et al., 2012).

#### 2.6 Oxalate-extractable P (P<sub>oxal</sub>) and dithionite-citrate-extractable P (P<sub>dith</sub>)

The content of P bound to pedogenic Fe- and Al-oxides / -hydroxides was determined according to the dithionate citrate method according to Prietzel et al. (2016). The extraction with dithionite-citrate-bicarbonate solution was prepared using the method of Mehra and Jackson (2013), and Holmgren (1967). The extraction with acidic ammonium oxalate following the method by Schwertmann (1964) was used to quantify the P contents precipitated with Fe-bound in poorly crystalline pedogenic minerals and Al-bound in Al(OH)<sub>3</sub>, interlayer Al hydroxy polymers, imogolite, and allophane (Prietzel et al., 2016; Werner et al., 2017). The amounts of extracted P in both extractions were finally measured by ICP-OES (ICAP 7400 ICP-OES Duo, Thermo Fisher Scientific, Dreieich, Germany).

## 2.7 Calculations

The measured P concentrations were converted to contents by dividing through the extracted amount of soil. The soil MBP content was calculated as follows (equation 3):

$$MBP (mg kg^{-1}) = \frac{P_{fum}(mg kg^{-1}) - P_{resin}(mg kg^{-1})}{P_{rec}} \quad (3)$$

Where  $P_{fum}$  and  $P_{resin}$  are P contents of fumigated and non-fumigated subsamples, and  $P_{rec}$  (equation 4) is the recovered fraction of  $P_{spike}$ .

$$P_{rec}(\%) = \frac{P_{spike} - P_{resin}}{P_{spike}} \quad (4)$$

Where  $P_{spike}$  is the concentration of P measured in the P-spike subsample 3 and  $P_{spike}$  is the amount of P added with the 1 ml spike solution.

The  $^{33}P$  activity in soil microbial biomass (SMB) was calculated according equation 5:

$$^{33}P_{SMB} (Bq g^{-1}) = \frac{(^{33}P_{fum}(Bq g^{-1}) - ^{33}P_{resin}(Bq g^{-1}))}{P_{rec}} \quad (5)$$

Where  $^{33}P_{SMB}$  is the activity of  $^{33}P$  in the microbial biomass,  $^{33}P_{fum}$  and  $^{33}P_{resin}$  are the  $^{33}P$  activity of fumigated and non-fumigated subsamples.

The  $^{33}P_{total-SMB}$  was the total activity of  $^{33}P$  in the soil microbial biomass per microcosm, and it was calculated as (equation 6):

$$^{33}P_{total-SMB} (Bq) = ^{33}P_{SMB} (Bq g^{-1}) \times \text{soil dry mass (g)} \quad (6)$$

Where soil dry mass is the dry weight of soil per microcosm.

The recovery of litter-derived  $^{33}P$  in a given P pool was calculated according to equation 7:

$$^{33}P_{recovered} (\%) = \frac{^{33}P_{total} (Bq)}{^{33}P_{applied litter} (Bq)} \times 1000\% \quad (7)$$

Where the  $^{33}P_{recovered}$  was the recovery of litter-derived  $^{33}P$  in a certain P pool, e.g. total soil P pool,  $P_{resin}$ , and microbial P.  $^{33}P_{total}$  was the total  $^{33}P$  in the given P pool.  $^{33}P_{applied litter}$  was the total  $^{33}P$  of applied litter.

The specific  $^{33}P$  activity of a given P pool was calculated as follows:

$$\text{Specific } ^{33}P \text{ activity (Bq } \mu g^{-1} P) = \frac{^{33}P (Bq g^{-1})}{P (mg kg^{-1})} \quad (8)$$

Where the  $^{33}P$  is the activity of  $^{33}P$  in the given P pool, and  $P$  is the P concentration in the given P pool.

The microbial P immobilization was calculated as follows:

$$P_{immobilization} (mg P kg^{-1} \text{ soil}) = \frac{\text{specific } ^{33}P_{SMB} \text{ activity (Bq } \mu g^{-1} P)}{\text{specific } ^{33}P_{resin} \text{ activity (Bq } \mu g^{-1} P)} \times MBP(mg kg^{-1}) \quad (9)$$

## 2.8 Statistical analysis

All the statistical analyses and figures were performed and made in GraphPad Version 8 (Prism, USA). Kinetic parameters were fitted to the model equation (Michaelis–Menten equation) and the statistical analyses. All data were tested for normal distribution (Shapiro-Wilk test) and homogeneity of variance (Bartlett's test). Two-way ANOVA was performed to analyze the significant differences of the main factors of 'site', 'microbial dilution' and their interactions, followed by Tukey's HSD test as post-hoc test ( $p < 0.05$ ).

### 3. Results

#### 3.1 Soil acid phosphatase activity

On average,  $V_{\max}$  of acid phosphatase in P-poor soil was 105% higher compared to  $V_{\max}$  in P-rich soil indicating a stronger need to acquire P. Two-way ANOVA determined that the variable “site” had a statistically significant effect on  $V_{\max}$  of acid phosphatase (Figure 3-1 a). The  $V_{\max}$  of acid phosphatases gradually increased by 252% from  $10^{-1}$  to  $10^{-4}$  dilution and with further dilution decreased by 75–92% from the level of  $10^{-4}$  to  $10^{-5}$  and  $10^{-6}$  dilution in P-rich soil.

The catalytic efficiency ( $V_{\max}/K_m$ ) was significantly higher in P-poor soil inoculated with diluted microbial community than P-rich soil (Figure 3-1 b). The variable ‘dilution’ had a significant effect on the catalytic efficiency of acid phosphatase (Figure 3-1 b), with a decrease of catalytic efficiency by the increase of dilution of microbial communities at both sites. The catalytic efficiency gradually decreased 94% in P-rich soil, but increased 70% in P-poor soil, by the decrease of microbial diversity.

#### 3.2 Oxalate- and dithionite-/citrate-extractable P

A significant effect of the variable “site” on  $P_{\text{dith}}$  confirmed the expectations on P-rich soil and P-poor soil (Figure 3-2 a). Likewise, the content of  $P_{\text{oxal}}$  confirmed the contrasting amounts of different P forms, fluctuating from 496 to 452 mg kg<sup>-1</sup> and from 39 to 48 mg kg<sup>-1</sup> in P-rich soil and P-poor soil, respectively (Figure 3-2 b).  $P_{\text{dith}}$  and  $P_{\text{oxal}}$  accounted to 10- to 11-fold higher mean value in P-rich soil than in P-poor soil, respectively, a factor that agrees with the ratio in P stocks of these two sites (Table 3-1).

#### 3.3 Specific <sup>33</sup>P activity and recovery of litter-derived <sup>33</sup>P in different soil P pools

After 4 weeks of incubation, the specific <sup>33</sup>P activity of total soil P pool was insignificantly changed by the increased dilution levels within P-rich and P-poor soil (Figure 3-3 a, Table 3-2). Both P-poor and P-rich soil, demonstrated a detectable recovered <sup>33</sup>P from the litter into the total soil P pool (Figure 3-3 b). The recovery of litter-derived <sup>33</sup>P in total P pool of P-rich soil was significantly lower than that of P-poor soil (Figure 3-3b, Table 3-2)

The specific <sup>33</sup>P activity of SMB was higher in higher level of microbial dilutions (Table 3-2). The specific <sup>33</sup>P activity of SMB was 4-fold higher in P-poor soil inoculated by  $10^{-6}$  microbial dilution than  $10^{-2}$  and  $10^{-4}$  microbial dilution (Figure 3-3 c). The recovery of litter-derived <sup>33</sup>P in SMB was overall 5-fold higher in P-poor soil than in P-rich soil (Figure 3-3 d, Table 3-2). The specific <sup>33</sup>P activity of  $P_{\text{resin}}$  showed insignificant different among dilutions and sites (Figure 3-3 e, Table 3-2). The recovery of <sup>33</sup>P in  $P_{\text{resin}}$  was 1-fold greater in P-poor soil than in P-rich soil (Figure 3-3 f, Table 3-2). The interaction of site and dilution lead to a significant difference among dilutions in P-poor soil, where the soil inoculated with  $10^{-6}$  microbial dilution showed significantly lower recovery of <sup>33</sup>P in  $P_{\text{resin}}$  than  $10^{-1}$  to  $10^{-3}$  dilutions.

The microbial P immobilization during the incubation time was 6-fold higher in P-poor soil than in P-rich soil (Figure 3-4). Within each site, the microbial P immobilization was insignificant between soils inoculated with different dilutions, indicating an unaltered function of P immobilization.

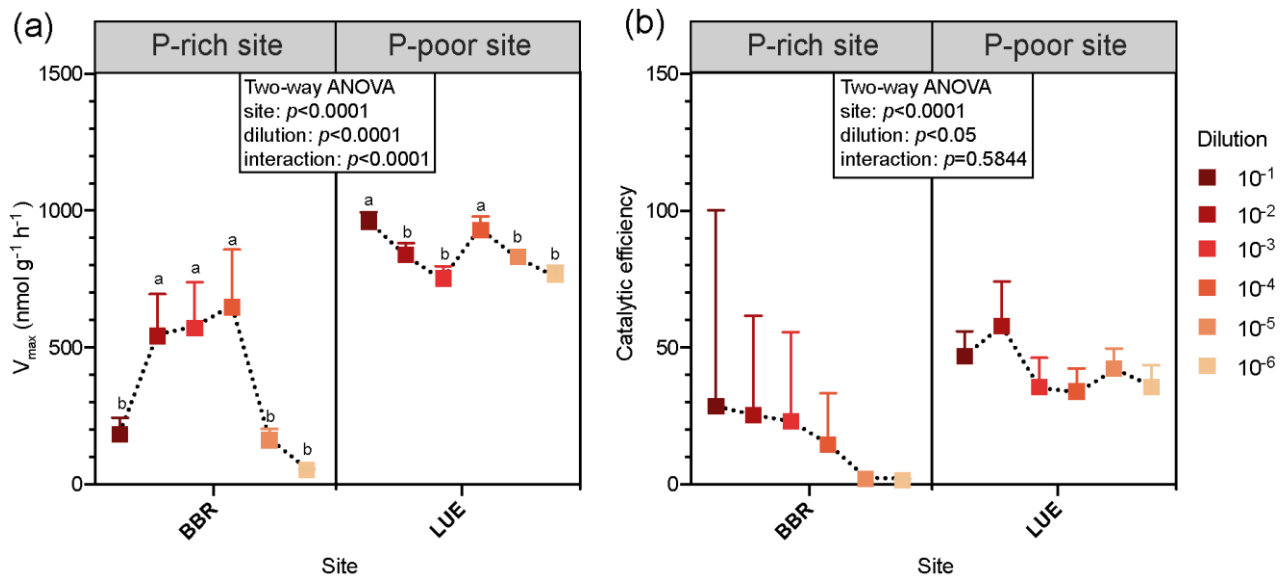


**Figure 3-1** (a) Potential extracellular activity ( $V_{max}$ ) and (b) catalytic efficiency of acid phosphatase across dilutions of microbial inoculum after mixed litter addition in P-rich (BBR) and P-poor (LUE) soil. Error bars show standard deviation ( $n = 4$ ). Lower-case letters indicate significant differences among all dilutions within one site ( $p < 0.05$ ).

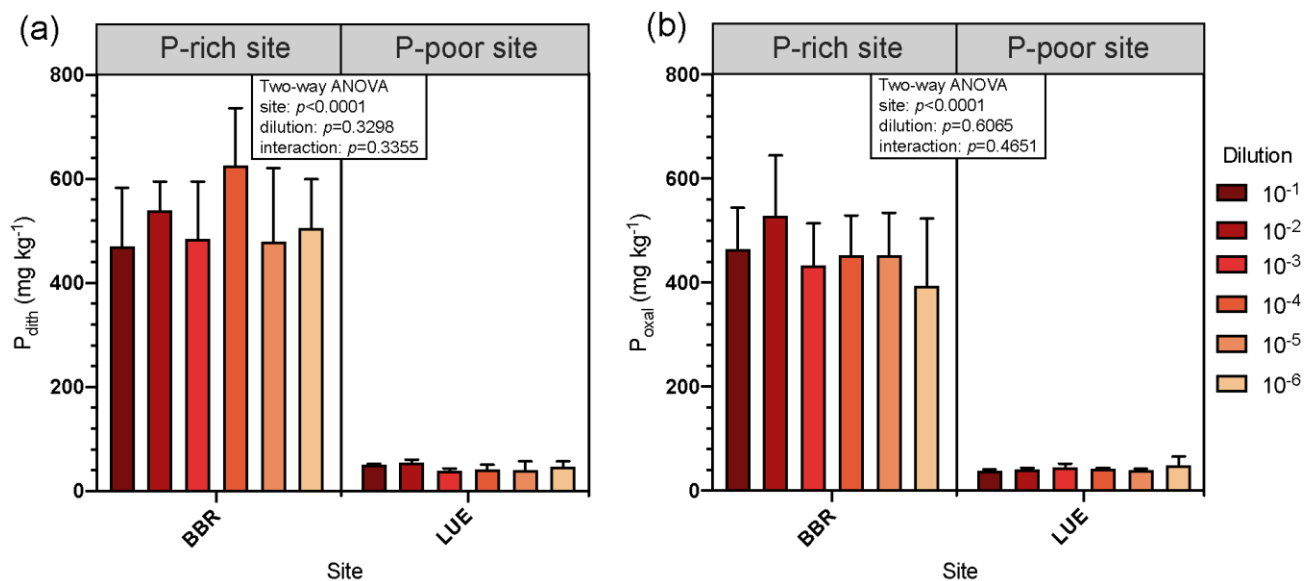


**Figure 3-2** Content of (a) dithionite-citrate extractable P and (b) oxalate-extractable P in P-rich (BBR) and P-poor (LUE) soils. Error bars represent standard deviation. Lower-case letters indicate significant differences among all dilutions within one site ( $n=4$ ,  $p < 0.05$ ).

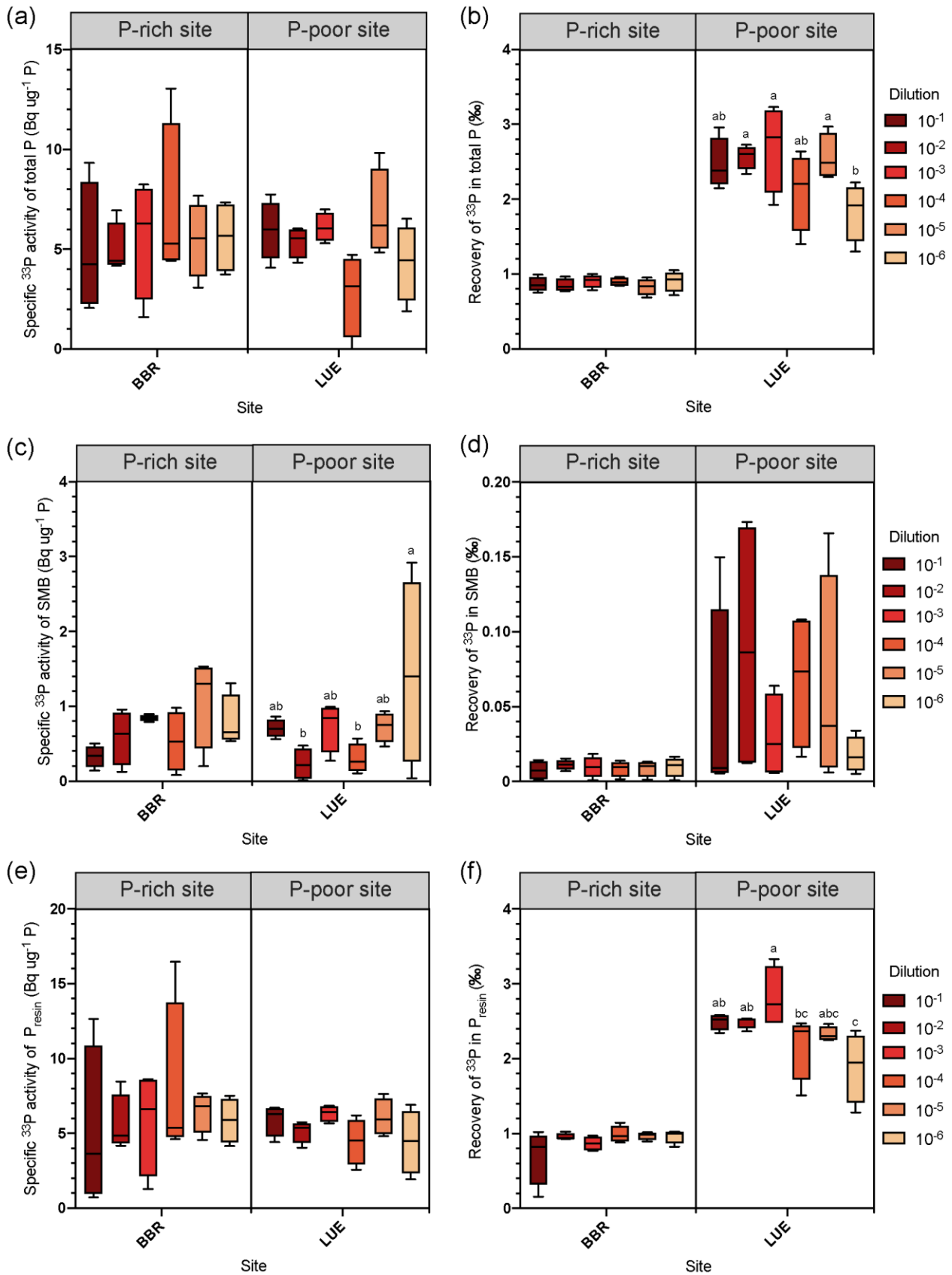


**Figure 3-3** (a) Specific  $^{33}\text{P}$  activity of total soil P pool, (b) Recovery of applied litter-derived  $^{33}\text{P}$  in total soil P pool, (c) specific  $^{33}\text{P}$  activity of SMB, (d) Recovery of applied litter-derived  $^{33}\text{P}$  in SMB, (e) specific  $^{33}\text{P}$  activity of  $P_{\text{resin}}$ , and (f) Recovery of applied litter-derived  $^{33}\text{P}$  in  $P_{\text{resin}}$ . Whiskers represent the minimal and maximal values. Lower-case letters indicate significant differences among dilutions within each site. ( $n = 4$ ,  $p < 0.05$ ).

**Table 3-2** Analysis of variance for the recovery of  $^{33}\text{P}$  and specific  $^{33}\text{P}$  activity in soil P pools.

Compartments of litter-derived $^{33}\text{P}$ recovery and specific activity	Site	Dilution	Site x Dilution
Recovery of $^{33}\text{P}$ total soil P pool	<b>&lt; 0.0001 ****</b>	ns	<b>&lt; 0.05 *</b>
Specific $^{33}\text{P}$ activity of total soil P pool	ns	ns	ns
Recovery of $^{33}\text{P}$ in $\text{P}_{\text{resin}}$	<b>&lt; 0.0001 ****</b>	ns	<b>&lt; 0.01 **</b>
Specific $^{33}\text{P}$ activity of $\text{P}_{\text{resin}}$	ns	ns	ns
The recovery of $^{33}\text{P}$ in SMB	<b>&lt; 0.01 **</b>	ns	ns
Specific $^{33}\text{P}$ activity of SMB	ns	<b>&lt; 0.05 *</b>	ns

The bold numbers indicate significant differences based on two-way ANOVA. (Significant codes: '\*\*\*\*'  $p < 0.0001$ , '\*\*\*'  $p < 0.001$ , '\*\*'  $p < 0.01$ , '\*'  $p < 0.05$ )

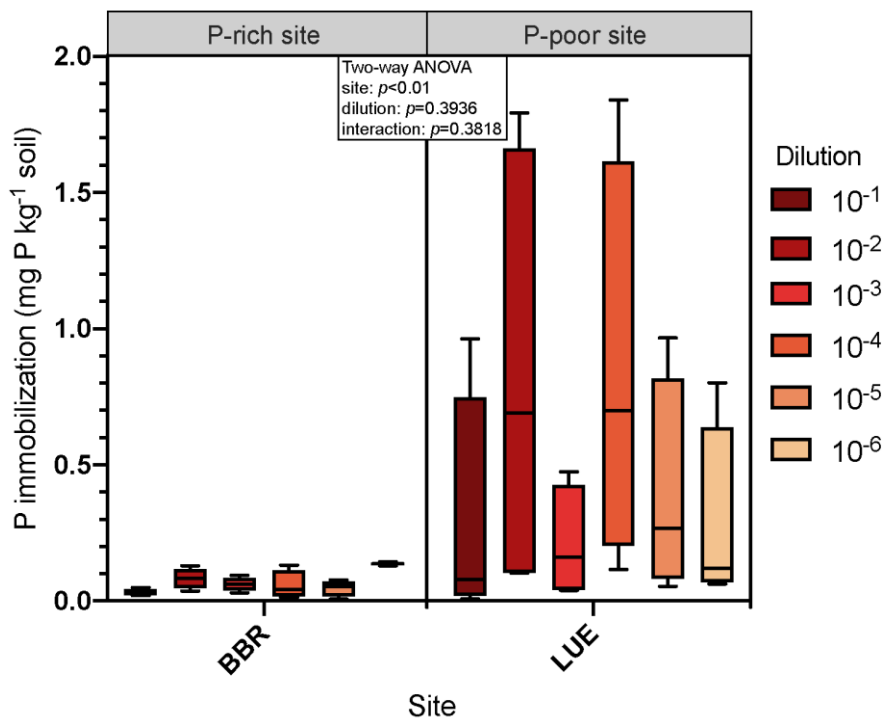


**Figure 3-4** P immobilization of P-rich and P-poor soil. Bars represent the minimal and maximal values. Whiskers represent the minimal and maximal values. ( $n = 4$ ).

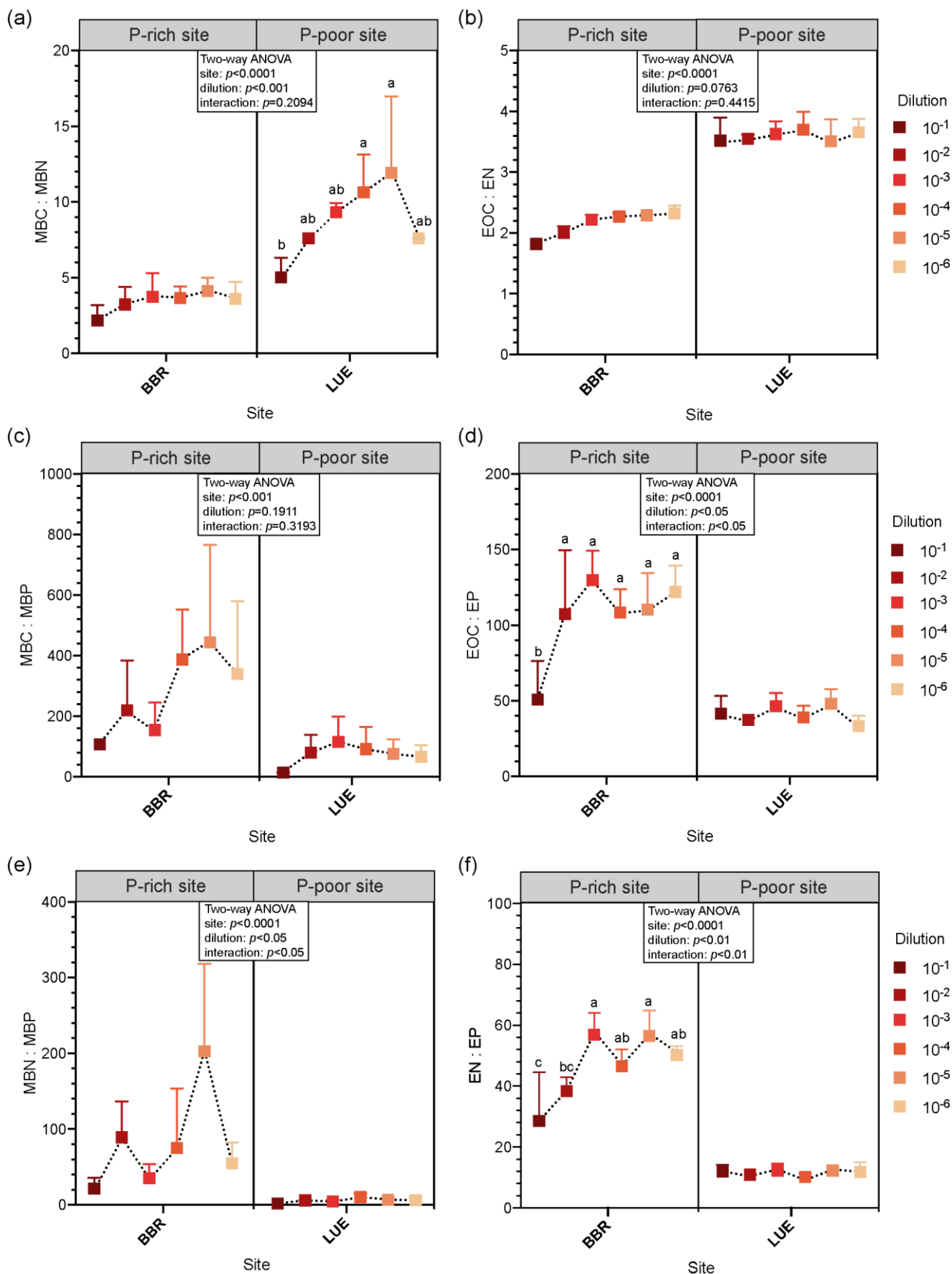


**Figure 3-5** The C : N : P ratios of microbial biomass (MBC, MBN, and MBP) and the correspondent extractable C, N, and P pools (EOC, EN, and EP) in P-rich (BBR) and P-poor (LUE) soil. Error bars show standard deviations. Lower-case letters indicate significant differences among dilutions within each site ( $n=4$ ,  $p < 0.05$ ).

### 3.4 C: N: P ratios of microbial biomass and of salt-extractable pools

The mean MBC: MBN ratio in the P-poor soil was higher than in the P-rich soil (Figure 3-5 a). In contrast, in P-rich soil, both MBC: MBP and MBN: MBP ratios were higher than in P-poor soil (Figure 3-5 c, e). Overall, the C: N: P ratios of the salt-extractable pools differ between the two sites at a significance level of  $p < 0.0001$  (Figure 3-5 b, d, f). The extractable pools of P-rich soil showed higher C: P and N: P ratios compared to P-poor soil, indicating improved substrate availability of the latter.

## 4. Discussion

### 4.1. Acid phosphatase kinetics and microbial P mobilization

Higher activity of acid phosphatase in P-poor soil than in P-rich soil demonstrated the strong microbial P mobilization which is in line with the high activity of this enzyme in the forests with low P stock (Lang et al., 2017; Müller et al., 2020). Similarly, the higher catalytic efficiency is consistent with the conclusion of high organic P mineralization under P-limited condition (Peng et al., 2023). The overall higher acid phosphatase activity among all P-poor soil with decreased microbial diversity confirmed the potential of efficient P cycling with a high functional redundancy exhibited for P-poor soil. One explanation might be that as long as C and N are not the limiting elements microorganisms are able to produce acid phosphatases immediately at similar activities as in P-rich soil (Loeppmann et al., 2020). Another explanation could be a higher inhibition of acid phosphatase in P-rich compared to P-poor soil because of higher aluminum oxides concentration in the mineral topsoil (Lang et al., 2017). The quantity and quality of soil organic P influence enzyme- and substrate-dependent catalysis of these compounds such as phosphatases and proteases (Quiquampoix and Mousain, 2005; Noll et al., 2019). The constant acid phosphatase activity across dilutions demonstrated an overall functional redundancy of microbial P mobilization in P-poor soil. However, in P-rich soil, the activity of acid phosphatase tended to increase first, thereafter, it declined at a given degree of microbial diversity loss, i.e.,  $10^{-5}$  and  $10^{-6}$  dilutions of the microbial inoculum. At low microbial diversity, the catalytic efficiency of acid phosphatase to the substrate strongly decreased in P-rich soil. Subsequently, the P-acquiring microbes prove a comparatively lower functional redundancy of P mobilization in P-rich compared to P-poor soil. A recent study has confirmed a steady phosphomonoesterase activity with the shift of fungal community composition in beech forest soil with contrasting P stocks, and came up with a functional redundancy in fungal-derived P cycling enzymes (Müller et al., 2020). We proved that the microbial community in P-poor soil to be more stable in producing P cycling enzymes, as the  $V_{max}$  and catalytic efficiency were stabilized during the reconstitution of reduced community diversity in P-poor soil.

Philippot et al. (2013) demonstrated that a dilution of five orders of magnitude resulted in a 75% decrease in estimated richness and the addition of wheat residues significantly increased the differences in potential denitrification between diversity levels, suggesting that the resource level may influence the shape of the microbial diversity–functioning relationship. Here, the microbial community could compensate the microbial diversity–functioning relationship in P-poor soil solely. The existence of microbial groups (named compartmentalization) that have a higher probability of interacting with each other than with other groups, significantly increases both resistance and resilience against any perturbation because such compartments act to buffer the propagation of extinctions (May, 1972; Stouffer and Bascompte, 2011). Therefore, a highly connected and nested architecture promotes community stability in mutualistic networks, whereas stability is increased in compartmented and weakly connected architectures in trophic networks (Thébault and Fontaine, 2010; Griffiths and Philippot, 2013). Overall, our results are in line with that of (Griffiths et al., 2008) demonstrating that soil biological stability is governed by the physico-chemical structure of the soil through its effect on microbial community composition and microbial physiology.

## 4.2 Microbial P immobilization

The recovery of litter-derived  $^{33}\text{P}$  in SMB regardless of the dilution degree of the microbial inoculum indicates that the immobilization of litter-derived  $^{33}\text{P}$  was not affected by microbial diversity in P-poor soil. The 2-fold higher MBP in P-poor soil (Figure S3-1 e) is in accordance with the high microbial P immobilization (i.e the tighter cycle of P among MBP and soil solution) in P-poor soil as demonstrated by Bünemann et al. (2016), and Pistocchi et al. (2018). Notably, the higher recovery of litter- $^{33}\text{P}$  in SMB demonstrates a higher proportion of litter P contribution to the microbial P pool in the P-poor soil. And the similar specific  $^{33}\text{P}$  activity of both P-rich and P-poor soil suggests that the microbes also took comparable amount of soil organic and/or inorganic P into their biomass. It implies the fast acquisition of P by microorganisms under P deficiency comes from litter and soil organic pools.

The largely varied P immobilization of microorganisms with the decrease of microbial diversity in P-poor soil indicates that litter  $^{33}\text{P}$  immobilization is not a linear loss along with microbial diversity loss. This can be explained by the experimental time frame for the progress on litter decomposition by the microbial community. There is plenty of time for a new establishment of a microbial community in the detritosphere and/or the interlayer between the litter and the soil that is more efficient in growth and life strategy in order to mine more P even with a lower initial microbial biomass caused by dilution.

## 4.3 Biological controls of soil inorganic P processes

The constant  $P_{\text{dith}}$  and  $P_{\text{oxal}}$  in P-rich soil and P-poor soil indicate that the biological release of P through desorption and dissolution was unaffected by microbial diversity loss. Although the portion of dissolved P readily available to plants and microorganisms is usually less than 0.1% of total P (Zhu et al., 2011), the microbial function of solubilization of Fe/Al oxyhydroxides is easily altered by microbial diversity loss and leads to an imbalance of P acquisition (Sims and Pierzynski, 2005; Marschner et al., 2011). While they may still have a contrasting pattern (site-effect) of inorganic P desorption and dissolution: P-poor soil tends to desorb more inorganic P into its salt-extractable P pool than P-rich soil, although P-rich soil has way more  $P_{\text{dith}}$  and  $P_{\text{oxal}}$ . This explanation can be supported by the higher recovery of litter  $^{33}\text{P}$  in  $P_{\text{resin}}$  in P-poor soil but the similar specific  $^{33}\text{P}$  activity of  $P_{\text{resin}}$  as P-rich soil, which implies that P-poor soil intensively acquired P not only from litter but also from another pool, e.g., soil organic P and/or desorb and dissolve adsorbed P. The gross inorganic P sorption was positively related to soil total P content (Wanek et al., 2019), and P-rich soil has higher content of clay minerals (Table 1) which increase the formation of P fixing (Violante and Pigna, 2002). Although P supply from the mineral phase is the main source of available P in P-rich soils but not in P-poor soil (Prietz et al., 2016), but the startup of biological desorption and dissolution can be fast in P-poor soil, as P-poor soil has much higher P solubilization parental materials and higher abundance of P-solubilizing bacteria (Pastore et al., 2022). Therefore, the biologically driven inorganic P release from P-poor soils seems to have great potential and possibly due to its functionally redundancy of the microbial community.

## 4.4 Effect on microbial C: N: P ratios

The small variation in microbial C: N: P ratios along the gradient of decreasing microbial diversity showed a clear functional redundancy of microorganisms at P-poor site, aiming to maintain stable microbial element ratios, especially MBC: MBP and MBN: MBP (Figure 3-5 c, e). This reflects a fast recovery and re-growth of the microbial guilds already adapted to a balanced mining of nutrients across all dilutions. The greatly varied MBC: MBP and MBN: MBP in P-rich soil suggest an altered function of microbial P uptake. Microbial C: N: P ratios were consistent with the respective element ratios in the soil extractable pool, indicating that irrespective of the total soil nutrient pools the microbial element demand triggers the nutrient concentration in soil solution via microbial community specific mobilization mechanisms the element stoichiometry in the soil solution (Chen et al., 2016). Microbial resilience is connected to specific population traits, such as the ability to grow rapidly and to exhibit physiological plasticity (Allison and Martiny, 2008). Such features allow microbial communities to

recover from environmental perturbation (Schimel et al., 2007; Shade et al., 2012). Numerous factors influence soil stability (resistance and resilience) organic matter, such as aggregation, the quantity and quality of carbon inputs and, to a lesser extent, clay content and soil pH (Griffiths and Philippot, 2013). The litter stoichiometry directly affects the nutrient stoichiometry of the soil which determines the resource availability of the microorganisms. For example, litter C: N and C: P ratios have been shown negatively related to cellulase, peroxidase and phenoloxidase activities three and six months after incubation (Leitner et al., 2012).

The high EOC content in both P-rich and P-poor soil stimulates not only microbial activity as readily available energy source, but also shifts the stoichiometric balance between C, N, and P (Sinsabaugh and Moorhead, 1994; Cheng and Kuzyakov, 2005; Stock et al., 2019). This induces compensating effects such as an upregulation of enzyme synthesis and a degradation of nutrient-rich compounds to maintain stoichiometric homeostasis when labile C is available (Cheng and Kuzyakov, 2005; Phillips et al., 2011; Sinsabaugh and Follstad Shah, 2012; Stock et al., 2019).

## **Conclusions**

Our study expanded the understanding of the mobilization and recycling of litter-derived P in beech forest soils with contrasting P stock. As a P-deficient soil that highly relies on litter P recycling to fast compensate for available P, its communities in P-poor soil maintained high acid phosphatase release with the microbial diversity loss. P-rich soil that does not highly rely on fast litter P recycling driven by microorganisms does not show the functional redundancy of microbial P mobilization. P-poor soil tends to greatly immobilize litter-derived P into microbial biomass even under the pressure of microbial diversity loss. Microbial P mobilization shows a high functional redundancy, without decelerating P mineralization and microbial P uptake as a result of microbial diversity loss and only at sites with high mineral P stocks and availabilities, where this function is much less essential, microbial dilution results in a loss in P mineralization functions. However, we confirm that P-deficient ecosystems strongly rely on soil microbial P recycling and are often resistant to microbial diversity loss due to its functional redundancy.

## **Acknowledgment**

The authors thank the participating German Forest Service Authorities for supporting our research. This project was conducted in the framework of the priority programme 1685 “Ecosystem Nutrition: Forest Strategies for limited Phosphorus Resources” funded by the German Research Foundation (DFG) (project DI 2136/6) in cooperation with the Swiss National Foundation (SNF) (project SS 200021E-171173).

## Reference

- Allison, Steven D., and Jennifer B. H. Martiny. 2008. Resistance, resilience, and redundancy in microbial communities. *Proceedings of the National Academy of Sciences of the United States of America* 105. Washington: Natl Acad Sciences: 11512–11519. <https://doi.org/10.1073/pnas.0801925105>.
- Bai, Xuejuan, Michaela A. Dippold, Shaoshan An, Baorong Wang, Haixin Zhang, and Sebastian Loeppmann. 2021. Extracellular enzyme activity and stoichiometry: The effect of soil microbial element limitation during leaf litter decomposition. *Ecological Indicators* 121: 107200. <https://doi.org/10.1016/j.ecolind.2020.107200>.
- Baumann, Karen, Marie-France Dignac, Cornelia Rumpel, Gérard Bardoux, Amadou Sarr, Markus Steffens, and Pierre-Alain Maron. 2013. Soil microbial diversity affects soil organic matter decomposition in a silty grassland soil. *Biogeochemistry* 114: 201–212. <https://doi.org/10.1007/s10533-012-9800-6>.
- Ben-Ami, Y., I. Koren, Y. Rudich, P. Artaxo, S. T. Martin, and M. O. Andreae. 2010. Transport of North African dust from the Bodélé depression to the Amazon Basin: a case study. *Atmospheric Chemistry and Physics* 10: 7533–7544. <https://doi.org/10.5194/acp-10-7533-2010>.
- Brödlin, Dominik, Klaus Kaiser, Arnim Kessler, and Frank Hagedorn. 2019. Drying and rewetting foster phosphorus depletion of forest soils. *Soil Biology and Biochemistry* 128: 22–34. <https://doi.org/10.1016/j.soilbio.2018.10.001>.
- Brookes, P. C., D. S. Powlson, and D. S. Jenkinson. 1982. Measurement of microbial biomass phosphorus in soil. *Soil Biology and Biochemistry* 14: 319–329. [https://doi.org/10.1016/0038-0717\(82\)90001-3](https://doi.org/10.1016/0038-0717(82)90001-3).
- Bruulsema, T. W., and J. M. Duxbury. 1996. Simultaneous Measurement of Soil Microbial Nitrogen, Carbon, and Carbon Isotope Ratio. *Soil Science Society of America Journal* 60: 1787–1791. <https://doi.org/10.2136/sssaj1996.03615995006000060025x>.
- Buendía, C., A. Kleidon, and A. Porporato. 2010. The role of tectonic uplift, climate, and vegetation in the long-term terrestrial phosphorous cycle. *Biogeosciences* 7: 2025–2038. <https://doi.org/10.5194/bg-7-2025-2010>.
- Bünemann, E. K., F. Steinebrunner, P. C. Smithson, E. Frossard, and A. Oberson. 2004. Phosphorus Dynamics in a Highly Weathered Soil as Revealed by Isotopic Labeling Techniques. *Soil Science Society of America Journal* 68: 1645–1655. <https://doi.org/10.2136/sssaj2004.1645>.
- Bünemann, E.K., S. Augstburger, and E. Frossard. 2016. Dominance of either physicochemical or biological phosphorus cycling processes in temperate forest soils of contrasting phosphate availability. *Soil Biology and Biochemistry* 101: 85–95. <https://doi.org/10.1016/j.soilbio.2016.07.005>.
- Chen, Yong-Liang, Lei-Yi Chen, Yun-Feng Peng, Jin-Zhi Ding, Fei Li, Gui-Biao Yang, Dan Kou, et al. 2016. Linking microbial C:N:P stoichiometry to microbial community and abiotic factors along a 3500-km grassland transect on the Tibetan Plateau. *Global Ecology and Biogeography* 25: 1416–1427. <https://doi.org/10.1111/geb.12500>.
- Cheng, Weixin, and Yakov Kuzyakov. 2005. Root Effects on Soil Organic Matter Decomposition. In *Roots and Soil Management: Interactions between Roots and the Soil*, 119–143. John Wiley & Sons, Ltd. <https://doi.org/10.2134/agronmonogr48.c7>.
- Das, R., and D. Lawrence. 2013. Contributions of long-distance dust transport to atmospheric P inputs in the Yucatan Peninsula[J]. *Global Biogeochemical Cycles*. *Global Biogeochemical Cycles* 27: 167–175. <https://doi.org/10.1029/2012GB004420>.
- Estiarte, Marc, and Josep Peñuelas. 2015. Alteration of the phenology of leaf senescence and fall in winter deciduous species by climate change: effects on nutrient proficiency. *Global Change Biology* 21: 1005–1017. <https://doi.org/10.1111/gcb.12804>.
- Fetzer, Jasmin, Sebastian Loeppmann, Emmanuel Frossard, Aamir Manzoor, Dominik Brödlin, Klaus Kaiser, and Frank Hagedorn. 2021. Leaching of Phosphomonoesterase Activities in Beech Forest Soils: Consequences for Phosphorus Forms and Mobility. *Frontiers in Forests and Global Change* 4: 684069. <https://doi.org/10.3389/ffgc.2021.684069>.
- Franklin, Rima B., Jay L. Garland, Carl H. Bolster, and Aaron L. Mills. 2001. Impact of Dilution on Microbial Community Structure and Functional Potential: Comparison of Numerical Simulations and Batch Culture Experiments. *Applied and Environmental Microbiology* 67: 702–712. <https://doi.org/10.1128/AEM.67.2.702-712.2001>.
- Freschet, Grégoire T., William K. Cornwell, David A. Wardle, Tatyana G. Elumeeva, Wendan Liu, Benjamin G. Jackson, Vladimir G. Onipchenko, Nadejda A. Soudzilovskaia, Jianping Tao, and Johannes H.C. Cornelissen. 2013. Linking litter decomposition of above- and below-ground organs to plant–soil feedbacks worldwide. *Journal of Ecology* 101: 943–952. <https://doi.org/10.1111/1365-2745.12092>.
- Garland, Jay L., and R. Michael Lehman. 1999. Dilution/extinction of community phenotypic characters to estimate relative structural diversity in mixed communities. *FEMS Microbiology Ecology* 30: 333–343. <https://doi.org/10.1111/j.1574-6941.1999.tb00661.x>.
- Geßler, Arthur, Claudia Keitel, Jürgen Kreuzwieser, Rainer Matyssek, Wolfgang Seiler, and Heinz Rennenberg. 2007. Potential risks for European beech (*Fagus sylvatica* L.) in a changing climate. *Trees* 21: 1–11. <https://doi.org/10.1007/s00468-006-0107-x>.

- Girvan, M. S., C. D. Campbell, K. Killham, J. I. Prosser, and L. A. Glover. 2005. Bacterial diversity promotes community stability and functional resilience after perturbation. *Environmental Microbiology* 7: 301–313. <https://doi.org/10.1111/j.1462-2920.2005.00695.x>.
- Gowsalya, A., V. Ponnusami, and K. R. Sugumaran. 2014. Isolation of bacteria from soil sample for exo-polysaccharide production. *International Journal of ChemTech Research* 6. Sphinx Knowledge House: 2925–2928.
- Griffiths, B. S., P. D. Hallett, H. L. Kuan, A. S. Gregory, C. W. Watts, and A. P. Whitmore. 2008. Functional resilience of soil microbial communities depends on both soil structure and microbial community composition. *Biology and Fertility of Soils* 44. Springer: 745–754.
- Griffiths, B. S., H. L. Kuan, K. Ritz, L. A. Glover, A. E. McCaig, and C. Fenwick. 2004. The relationship between microbial community structure and functional stability, tested experimentally in an upland pasture soil. *Microbial ecology* 47. Springer: 104–113.
- Griffiths, Bryan S., and Laurent Philippot. 2013. Insights into the resistance and resilience of the soil microbial community. *FEMS Microbiology Reviews* 37: 112–129. <https://doi.org/10.1111/j.1574-6976.2012.00343.x>.
- Griffiths, B.S, K Ritz, R Wheatley, H.L Kuan, B Boag, S Christensen, F Ekelund, S.J Sørensen, S Muller, and J Bloem. 2001. An examination of the biodiversity–ecosystem function relationship in arable soil microbial communities. *Soil Biology and Biochemistry* 33: 1713–1722. [https://doi.org/10.1016/S0038-0717\(01\)00094-3](https://doi.org/10.1016/S0038-0717(01)00094-3).
- Griffiths, Robert I, Mike Manefield, Nick Ostle, Niall McNamara, Anthony G O'Donnell, Mark J Bailey, and Andrew S Whiteley. 2004. <sup>13</sup>C<sub>2</sub> pulse labelling of plants in tandem with stable isotope probing: methodological considerations for examining microbial function in the rhizosphere. *Journal of Microbiological Methods* 58: 119–129. <https://doi.org/10.1016/j.mimet.2004.03.011>.
- Heinrichs, H., H.-J. Brumsack, N. Loftfield, and N. König. 1986. Verbessertes Druckaufschlußsystem für biologische und anorganische Materialien. *Zeitschrift für Pflanzenernährung und Bodenkunde* 149: 350–353. <https://doi.org/10.1002/jpln.19861490313>.
- Holden, Sandra, and Kathleen Treseder. 2013. A meta-analysis of soil microbial biomass responses to forest disturbances. *Frontiers in Microbiology* 4.
- Holmgren, George GS. 1967. A rapid citrate-dithionite extractable iron procedure. *Soil Science Society of America Journal* 31. Wiley Online Library: 210–211.
- Jenkinson, David S., and J. N. Ladd. 1981. Microbial biomass in soil: measurement and turnover. *Soil biochemistry* 5. Marcel Dekker, New York: 415–471.
- Jonard, Mathieu, Alfred Fürst, Arne Verstraeten, Anne Thimonier, Volkmar Timmermann, Nenad Potočić, Peter Waldner, et al. 2015. Tree mineral nutrition is deteriorating in Europe. *Global Change Biology* 21: 418–430. <https://doi.org/10.1111/gcb.12657>.
- Kennedy, A. C., and K. L. Smith. 1995. Soil microbial diversity and the sustainability of agricultural soils. *Plant and Soil* 170: 75–86. <https://doi.org/10.1007/BF02183056>.
- Kouno, Kenji, Yasuhiro Tuchiya, and Tadao Ando. 1995. Measurement of soil microbial biomass phosphorus by an anion exchange membrane method. *Soil Biology and Biochemistry* 27: 1353–1357. [https://doi.org/10.1016/0038-0717\(95\)00057-L](https://doi.org/10.1016/0038-0717(95)00057-L).
- Lang, F., J. Krüger, W. Amelung, S. Willbold, E. Frossard, E. K. Bünemann, J. Bauhus, et al. 2017. Soil phosphorus supply controls P nutrition strategies of beech forest ecosystems in Central Europe. *Biogeochemistry* 136: 5–29. <https://doi.org/10.1007/s10533-017-0375-0>.
- Leitner, Sonja, Wolfgang Wanek, Birgit Wild, Ieda Haemmerle, Lukas Kohl, Katharina M. Keiblinger, Sophie Zechmeister-Boltenstern, and Andreas Richter. 2012. Influence of litter chemistry and stoichiometry on glucan depolymerization during decomposition of beech (*Fagus sylvatica* L.) litter. *Soil Biology and Biochemistry* 50: 174–187. <https://doi.org/10.1016/j.soilbio.2012.03.012>.
- Loeppmann, Sebastian, Evgenia Blagodatskaya, Johanna Pausch, and Yakov Kuzyakov. 2016. Enzyme properties down the soil profile - A matter of substrate quality in rhizosphere and detritusphere. *Soil Biology and Biochemistry* 103: 274–283. <https://doi.org/10.1016/j.soilbio.2016.08.023>.
- Loeppmann, Sebastian, Andreas Breidenbach, Sandra Spielvogel, Michaela A. Dippold, and Evgenia Blagodatskaya. 2020. Organic Nutrients Induced Coupled C- and P-Cycling Enzyme Activities During Microbial Growth in Forest Soils. *Frontiers in Forests and Global Change* 3: 100. <https://doi.org/10.3389/ffgc.2020.00100>.
- Loeppmann, Sebastian, Mikhail Semenov, Evgenia Blagodatskaya, and Yakov Kuzyakov. 2016. Substrate quality affects microbial- and enzyme activities in rooted soil. *Journal of Plant Nutrition and Soil Science* 179: 39–47. <https://doi.org/10.1002/jpln.201400518>.
- Maillard, François, Valentin Leduc, Cyrille Bach, Arnaud Reichard, Laure Fauchery, Laurent Saint-André, Bernhard Zeller, and Marc Buée. 2019. Soil microbial functions are affected by organic matter removal in temperate deciduous forest. *Soil Biology and Biochemistry* 133: 28–36. <https://doi.org/10.1016/j.soilbio.2019.02.015>.
- Manzoni, Stefano, Robert B. Jackson, John A. Trofymow, and Amilcare Porporato. 2008. The Global Stoichiometry of Litter Nitrogen Mineralization. *Science* 321. American Association for the Advancement of Science: 684–686. <https://doi.org/10.1126/science.1159792>.

- Marschner, Petra, David Crowley, and Zed Rengel. 2011. Rhizosphere interactions between microorganisms and plants govern iron and phosphorus acquisition along the root axis – model and research methods. *Soil Biology and Biochemistry* 43: 883–894. <https://doi.org/10.1016/j.soilbio.2011.01.005>.
- Martinez del Castillo, Edurne, Christian S. Zang, Allan Buras, Andrew Hacket-Pain, Jan Esper, Roberto Serrano-Notivoli, Claudia Hartl, et al. 2022. Climate-change-driven growth decline of European beech forests. *Communications Biology* 5: 163. <https://doi.org/10.1038/s42003-022-03107-3>.
- Marx, M. -C., E. Kandeler, M. Wood, N. Wermbter, and S. C. Jarvis. 2005. Exploring the enzymatic landscape: distribution and kinetics of hydrolytic enzymes in soil particle-size fractions. *Soil Biology and Biochemistry* 37: 35–48. <https://doi.org/10.1016/j.soilbio.2004.05.024>.
- Mason-Jones, Kyle, Andreas Breidenbach, Jens Dyckmans, Callum C. Banfield, and Michaela A. Dippold. 2023. Intracellular carbon storage by microorganisms is an overlooked pathway of biomass growth. *Nature Communications* 14: 2240. <https://doi.org/10.1038/s41467-023-37713-4>.
- May, Rm. 1972. Will a Large Complex System Be Stable. *Nature* 238. London: Macmillan Magazines Ltd: 413-. <https://doi.org/10.1038/238413a0>.
- Mayer, Jochen, Franz Buegger, Erik Steen Jensen, Michael Schloter, and Jürgen Heß. 2003. Estimating N rhizodeposition of grain legumes using a 15N in situ stem labelling method. *Soil Biology and Biochemistry* 35: 21–28. [https://doi.org/10.1016/S0038-0717\(02\)00212-2](https://doi.org/10.1016/S0038-0717(02)00212-2).
- Mehra, O. P., and M. L. Jackson. 2013. Iron oxide removal from soils and clays by a dithionite–citrate system buffered with sodium bicarbonate. In *Clays and clay minerals*, 317–327. Elsevier.
- Michaelis, Leonor, and Maud L. Menten. 1913. Die kinetik der invertinwirkung. *Biochem. z* 49. Berlin: 352.
- Mooshammer, Maria, Wolfgang Wanek, Jörg Schnecker, Birgit Wild, Sonja Leitner, Florian Hofhansl, Andreas Blöchl, et al. 2012. Stoichiometric controls of nitrogen and phosphorus cycling in decomposing beech leaf litter. *Ecology* 93: 770–782. <https://doi.org/10.1890/11-0721.1>.
- Mooshammer, Maria, Wolfgang Wanek, Sophie Zechmeister-Boltenstern, and Andreas Richter. 2014. Stoichiometric imbalances between terrestrial decomposer communities and their resources: mechanisms and implications of microbial adaptations to their resources. *Frontiers in Microbiology* 5.
- Müller, Karolin, Nadine Kubsch, Sven Marhan, Paula Mayer-Gruner, Pascal Nassal, Dominik Schneider, Rolf Daniel, Hans-Peter Piepho, Andrea Polle, and Ellen Kandeler. 2020. Saprotrophic and Ectomycorrhizal Fungi Contribute Differentially to Organic P Mobilization in Beech-Dominated Forest Ecosystems. *Frontiers in Forests and Global Change* 3: 47. <https://doi.org/10.3389/ffgc.2020.00047>.
- Nannipieri, P., L. Giagnoni, G. Renella, E. Puglisi, B. Ceccanti, G. Masciandaro, F. Fornasier, M. C. Moscatelli, and S. Marinari. 2012. Soil enzymology: classical and molecular approaches. *Biology and Fertility of Soils* 48: 743–762. <https://doi.org/10.1007/s00374-012-0723-0>.
- Netzer, Florian, Cora Schmid, Cornelia Herschbach, and Heinz Rennenberg. 2017. Phosphorus-nutrition of European beech (*Fagus sylvatica* L.) during annual growth depends on tree age and P-availability in the soil. *Environmental and Experimental Botany* 137: 194–207. <https://doi.org/10.1016/j.envexpbot.2017.02.009>.
- Niederberger, Jörg, Martin Kohler, and Jürgen Bauhus. 2019. Distribution of phosphorus fractions with different plant availability in German forest soils and their relationship with common soil properties and foliar P contents. *SOIL* 5: 189–204. <https://doi.org/10.5194/soil-5-189-2019>.
- Noll, Lisa, Shasha Zhang, Qing Zheng, Yuntao Hu, and Wolfgang Wanek. 2019. Wide-spread limitation of soil organic nitrogen transformations by substrate availability and not by extracellular enzyme content. *Soil Biology and Biochemistry* 133: 37–49. <https://doi.org/10.1016/j.soilbio.2019.02.016>.
- Oberson, A., and E. J. Joner. 2005. Microbial turnover of phosphorus in soil. In ‘Organic phosphorus in the environment’. (Eds BL Turner, E Frossard, DS Baldwin) pp. 133–164. CABI Publishing: Wallingford, UK.
- Pastore, Giovanni, Alfons R. Weig, Eduardo Vazquez, and Marie Spohn. 2022. Weathering of calcareous bedrocks is strongly affected by the activity of soil microorganisms. *Geoderma* 405: 115408. <https://doi.org/10.1016/j.geoderma.2021.115408>.
- Peng, Ziyang, Yuntao Wu, Lulu Guo, Lu Yang, Bin Wang, Xin Wang, Weixing Liu, Yanjun Su, Jin Wu, and Lingli Liu. 2023. Foliar nutrient resorption stoichiometry and microbial phosphatase catalytic efficiency together alleviate the relative phosphorus limitation in forest ecosystems. *New Phytologist* 238: 1033–1044. <https://doi.org/10.1111/nph.18797>.
- Philippot, Laurent, Aymé Spor, Catherine Hénault, David Bru, Florian Bizouard, Christopher M Jones, Amadou Sarr, and Pierre-Alain Maron. 2013. Loss in microbial diversity affects nitrogen cycling in soil. *The ISME Journal* 7: 1609–1619. <https://doi.org/10.1038/ismej.2013.34>.
- Phillips, Richard P., Adrien C. Finzi, and Emily S. Bernhardt. 2011. Enhanced root exudation induces microbial feedbacks to N cycling in a pine forest under long-term CO<sub>2</sub> fumigation. *Ecology Letters* 14: 187–194. <https://doi.org/10.1111/j.1461-0248.2010.01570.x>.
- Pistocchi, Chiara, Éva Mészáros, Federica Tamburini, Emmanuel Frossard, and Else Katrin Bünemann. 2018. Biological processes dominate phosphorus dynamics under low phosphorus availability in organic horizons of temperate forest soils. *Soil Biology and Biochemistry* 126: 64–75. <https://doi.org/10.1016/j.soilbio.2018.08.013>.

- Preece, Catherine, Erik Verbruggen, Lei Liu, James T. Weedon, and Josep Peñuelas. 2019. Effects of past and current drought on the composition and diversity of soil microbial communities. *Soil Biology and Biochemistry* 131: 28–39. <https://doi.org/10.1016/j.soilbio.2018.12.022>.
- Prietzl, Jörg, Wantana Klysubun, and Florian Werner. 2016. Speciation of phosphorus in temperate zone forest soils as assessed by combined wet-chemical fractionation and XANES spectroscopy. *Journal of Plant Nutrition and Soil Science* 179: 168–185. <https://doi.org/10.1002/jpln.201500472>.
- Quiquampoix, H., and D. Mousain. 2005. Enzymatic hydrolysis of organic phosphorus. *Organic phosphorus in the environment*. CABI Books: 89–112. <https://doi.org/10.1079/9780851998220.0089>.
- Richardson, Alan E. 2001. Prospects for using soil microorganisms to improve the acquisition of phosphorus by plants. *Functional Plant Biology* 28. CSIRO PUBLISHING: 897–906. <https://doi.org/10.1071/pp01093>.
- Richardson, Alan E., and Richard J. Simpson. 2011. Soil Microorganisms Mediating Phosphorus Availability Update on Microbial Phosphorus. *Plant Physiology* 156: 989–996. <https://doi.org/10.1104/pp.111.175448>.
- Russell, C. A., and I. R. P. Fillery. 1996. In situ <sup>15</sup>N labelling of lupin below-ground biomass. *Australian Journal of Agricultural Research* 47. CSIRO PUBLISHING: 1035–1046. <https://doi.org/10.1071/ar9961035>.
- Schimel, Joshua, Teri C. Balsler, and Matthew Wallenstein. 2007. Microbial Stress-Response Physiology and Its Implications for Ecosystem Function. *Ecology* 88: 1386–1394. <https://doi.org/10.1890/06-0219>.
- Schmitt, Marius, Klaus A. Jarosch, Robert Hertel, Sandra Spielvogel, Michaela A. Dippold, and Sebastian Loeppmann. 2022. Manufacturing triple-isotopically labeled microbial necromass to track C, N and P cycles in terrestrial ecosystems. *Applied Soil Ecology* 171: 104322. <https://doi.org/10.1016/j.apsoil.2021.104322>.
- Schraml, Carmen, and H. Rennenberg. 2002. Ökotypen der Rotbuche (*Fagus sylvatica* L.) zeigen unterschiedliche Reaktionen auf Trockenstress. *Forstwissenschaftliches Centralblatt vereinigt mit Tharandter forstliches Jahrbuch* 121: 59–72. <https://doi.org/10.1046/j.1439-0337.2002.00059.x>.
- Schwertmann, von U. 1964. The differentiation of iron oxide in soils by a photochemical extraction with acid ammonium oxalate. *Zeitschrift für Pflanzenernährung und Bodenkunde* 105: 194–201.
- Shade, Ashley, Jordan S. Read, Nicholas D. Youngblut, Noah Fierer, Rob Knight, Timothy K. Kratz, Noah R. Lottig, et al. 2012. Lake microbial communities are resilient after a whole-ecosystem disturbance. *The ISME Journal* 6. Nature Publishing Group: 2153–2167. <https://doi.org/10.1038/ismej.2012.56>.
- Sims, J.T., and J.M Pierzynski. 2005. Chemistry of Phosphorus in Soils. In: Tabatabai, M.A., Sparks, D.L. (Eds.). In *SSSA Book Series Soil Science Society of America*, 151–192. Madison.
- Singh, Jay Shankar, and Vijai Kumar Gupta. 2018. Soil microbial biomass: A key soil driver in management of ecosystem functioning. *Science of The Total Environment* 634: 497–500. <https://doi.org/10.1016/j.scitotenv.2018.03.373>.
- Sinsabaugh, R. L., and D. L. Moorhead. 1994. Resource allocation to extracellular enzyme production: A model for nitrogen and phosphorus control of litter decomposition. *Soil Biology and Biochemistry* 26: 1305–1311. [https://doi.org/10.1016/0038-0717\(94\)90211-9](https://doi.org/10.1016/0038-0717(94)90211-9).
- Sinsabaugh, Robert L., and Jennifer J. Follstad Shah. 2012. Ecoenzymatic Stoichiometry and Ecological Theory. *Annual Review of Ecology, Evolution, and Systematics* 43: 313–343. <https://doi.org/10.1146/annurev-ecolsys-071112-124414>.
- Sohrt, Jakob, Cornelia Herschbach, and Markus Weiler. 2018. Foliar P- but not N resorption efficiency depends on the P-concentration and the N:P ratio in trees of temperate forests. *Trees* 32: 1443–1455. <https://doi.org/10.1007/s00468-018-1725-9>.
- Spohn, Marie, and Meike Widdig. 2017. Turnover of carbon and phosphorus in the microbial biomass depending on phosphorus availability. *Soil Biology and Biochemistry* 113: 53–59. <https://doi.org/10.1016/j.soilbio.2017.05.017>.
- Sturner, Robert W., and James J. Elser. 2003. Ecological Stoichiometry: The Biology of Elements from Molecules to the Biosphere. In *Ecological Stoichiometry*. Princeton University Press. <https://doi.org/10.1515/9781400885695>.
- Stock, Svenja C., Moritz Köster, Michaela A. Dippold, Francisco Nájera, Francisco Matus, Carolina Merino, Jens Boy, Sandra Spielvogel, Anna Gorbushina, and Yakov Kuzyakov. 2019. Environmental drivers and stoichiometric constraints on enzyme activities in soils from rhizosphere to continental scale. *Geoderma* 337: 973–982. <https://doi.org/10.1016/j.geoderma.2018.10.030>.
- Stouffer, Daniel B., and Jordi Bascompte. 2011. Compartmentalization increases food-web persistence. *Proceedings of the National Academy of Sciences of the United States of America* 108. Washington: Natl Acad Sciences: 3648–3652. <https://doi.org/10.1073/pnas.1014353108>.
- Talkner, Ulrike, Karl Josef Meiwes, Nenad Potočić, Ivan Seletković, Nathalie Cools, Bruno De Vos, and Pasi Rautio. 2015. Phosphorus nutrition of beech (*Fagus sylvatica* L.) is decreasing in Europe. *Annals of Forest Science* 72. BioMed Central: 919–928. <https://doi.org/10.1007/s13595-015-0459-8>.
- Tardy, Vincent, Olivier Mathieu, Jean Lévêque, Sébastien Terrat, Abad Chabbi, Philippe Lemanceau, Lionel Ranjard, and Pierre-Alain Maron. 2014. Stability of soil microbial structure and activity depends on microbial diversity: Linking microbial diversity and stability. *Environmental Microbiology Reports* 6: 173–183. <https://doi.org/10.1111/1758-2229.12126>.

- Thébault, Elisa, and Colin Fontaine. 2010. Stability of Ecological Communities and the Architecture of Mutualistic and Trophic Networks. *Science* 329. American Association for the Advancement of Science: 853–856. <https://doi.org/10.1126/science.1188321>.
- Valkama, Elena, Risto Uusitalo, Kari Ylivainio, Perttu Virkajärvi, and Eila Turtola. 2009. Phosphorus fertilization: A meta-analysis of 80 years of research in Finland. *Agriculture, Ecosystems & Environment* 130: 75–85. <https://doi.org/10.1016/j.agee.2008.12.004>.
- Vance, E. D., P. C. Brookes, and D. S. Jenkinson. 1987. An extraction method for measuring soil microbial biomass C. *Soil Biology and Biochemistry* 19: 703–707. [https://doi.org/10.1016/0038-0717\(87\)90052-6](https://doi.org/10.1016/0038-0717(87)90052-6).
- Violante, Antonio, and Massimo Pigna. 2002. Competitive Sorption of Arsenate and Phosphate on Different Clay Minerals and Soils. *Soil Science Society of America Journal* 66: 1788–1796. <https://doi.org/10.2136/sssaj2002.1788>.
- Wanek, Wolfgang, David Zezula, Daniel Wasner, Maria Mooshammer, and Judith Prommer. 2019. A novel isotope pool dilution approach to quantify gross rates of key abiotic and biological processes in the soil phosphorus cycle. Preprint. *Biogeochemistry: Soils*. <https://doi.org/10.5194/bg-2018-519>.
- Wang, Chaoqun, Lukas Thielemann, Michaela A. Dippold, Georg Guggenberger, Yakov Kuzyakov, Callum C. Banfield, Tida Ge, et al. 2022. Microbial iron reduction compensates for phosphorus limitation in paddy soils. *Science of The Total Environment* 837: 155810. <https://doi.org/10.1016/j.scitotenv.2022.155810>.
- Wasner, Daniel, Judith Prommer, David Zezula, Maria Mooshammer, Yuntao Hu, and Wolfgang Wanek. 2023. Tracing <sup>33</sup>P-labelled organic phosphorus compounds in two soils: New insights into decomposition dynamics and direct use by microbes. *Frontiers in Soil Science* 3: 1097965. <https://doi.org/10.3389/fsoil.2023.1097965>.
- Weeks, Joseph J., and Ganga M. Hettiarachchi. 2019. A Review of the Latest in Phosphorus Fertilizer Technology: Possibilities and Pragmatism. *Journal of Environmental Quality* 48: 1300–1313. <https://doi.org/10.2134/jeq2019.02.0067>.
- Werner, Florian, Tilman René de la Haye, Sandra Spielvogel, and Jörg Prietzel. 2017. Small-scale spatial distribution of phosphorus fractions in soils from silicate parent material with different degree of podzolization. *Geoderma* 302: 52–65. <https://doi.org/10.1016/j.geoderma.2017.04.026>.
- Wertz, Sophie, Valérie Degrange, James I. Prosser, Franck Poly, Claire Commeaux, Thomas Freitag, Nadine Guillaumaud, and Xavier Le Roux. 2006. Maintenance of soil functioning following erosion of microbial diversity. *Environmental Microbiology* 8: 2162–2169. <https://doi.org/10.1111/j.1462-2920.2006.01098.x>.
- WRB. 2015. World reference base for soil resources 2014, update 2015. International soil classification system for naming soils and creating legends for soil maps. World soil resources reports. FAO. Rome.
- Yan, Yan, Eiko E. Kuramae, Peter G. L. Klinkhamer, and Johannes A. van Veen. 2015. Revisiting the Dilution Procedure Used To Manipulate Microbial Biodiversity in Terrestrial Systems. Edited by F. E Löffler. *Applied and Environmental Microbiology* 81: 4246–4252. <https://doi.org/10.1128/AEM.00958-15>.
- Zhu, Fengling, Lingyun Qu, Xuguang Hong, and Xiuqin Sun. 2011. Isolation and Characterization of a Phosphate-Solubilizing Halophilic Bacterium *Kushneria* sp. YCWA18 from Daqiao Saltern on the Coast of Yellow Sea of China. *Evidence-Based Complementary and Alternative Medicine* 2011: 1–6. <https://doi.org/10.1155/2011/615032>.

## Supplementary

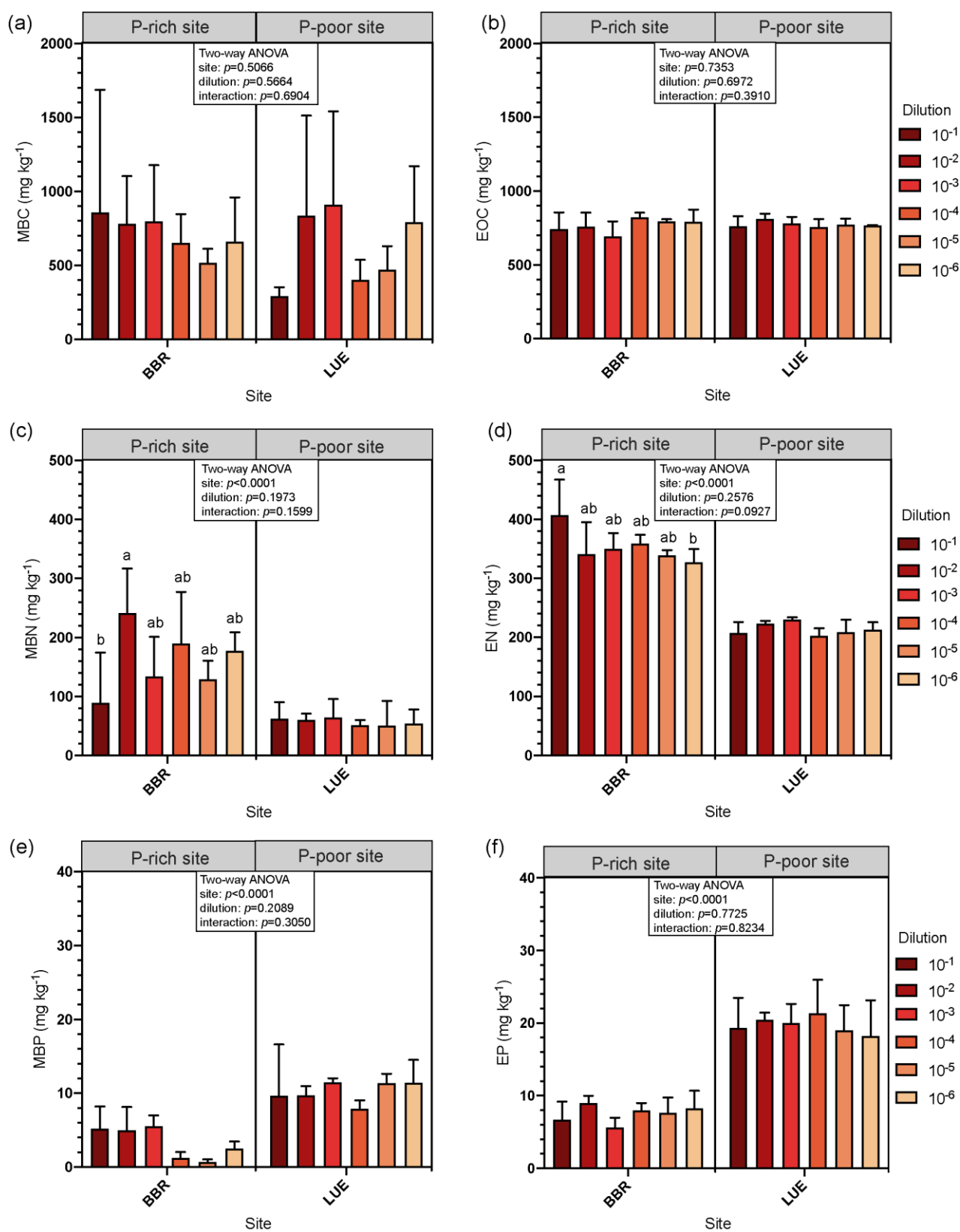


**Figure S3-1** Microbial biomass C, N, and P and the correspondent extractable C, N, and P pools (EOC, EN, and EP) in P-rich (BBR) and P-poor (LUE) soil. Error bars represent the standard deviations. Lower-case letters indicate significant differences among dilutions within each site ( $n=4$ ,  $p < 0.05$ ).

## 2.4 Study 4. Peroxidase Activity of Fresh Apple Root: A Novel Approach of Resorufin-based Micro-zymography

Yijie Shi<sup>1</sup>, Sebastian Loepmann<sup>1</sup>, Jiem Krüger<sup>2</sup>, Jens Boy<sup>2</sup>, Georg Guggenberger<sup>2</sup>, Sandra Spielvogel<sup>1</sup>, Evgenia Blagodatskaya<sup>3</sup>

**Status: In preparation**

<sup>1</sup> *Institute of Plant Nutrition and Soil Science, Christian-Albrechts-University Kiel, Germany*

<sup>2</sup> *Institute of Soil Science, Leibniz University Hannover, Germany*

<sup>3</sup> *Department of Soil Ecology, Helmholtz Centre for Environmental Research – UFZ, Halle, Germany*

---

### Abstract

The oxidative enzymes responsible for complex redox reactions in the rhizosphere are noted for their rapid activity and specific distribution. To investigate these oxidative reactions spatially and temporally, a high-resolution visualization approach is essential. We examined a micro-zymography method combining a fluorometric assay of Amplex Red with the presence of H<sub>2</sub>O<sub>2</sub> to detect the activity and distribution of peroxidase in apple (*Malus domestica*) seedlings' rhizosphere grown in rhizotrons. Fresh root tissues of the apple seedlings were categorized into root tips, roots with dense vs. sparse root hair, based on root morphology and image analysis. We found strong linear correlation between the concentration of resorufin (0-0.01 mmol) and the average fluorescence intensity of the micro-zymograph, which provides an accurate reference for the spatial quantification of the peroxidation rate at the rhizoplane and rhizosphere soil. Our results demonstrate two times higher activity for roots with dense than roots with sparse root hair. Furthermore, the hotspot area of peroxidase activity was 11 times higher in roots with dense than with sparse root hair. Additionally, the mean peroxidase activity at calyptra (root cap) was twice as high as in apical meristem (zone of cell division). The findings from our resorufin-based micro-zymography assay were consistent with the observed distribution of peroxidase in different root zones. This approach enables the visualization of peroxidase activity without using any membrane or gel at the rhizoplane and the rhizosphere soil in time and space.

**Keywords:** Amplex Red, peroxidase activity, apple root, microscope, micro-zymography, enzyme visualization

## 1. Introduction

Enzymes are crucial biocatalysts that facilitate many biologically significant transformations within plant-soil systems, thereby regulating various physiological processes. The decomposition of complex organic compounds begins with oxidation processes catalyzed by multiple oxidoreductases, such as phenol oxidases and peroxidases (Burns et al., 2013; Sinsabaugh, 2010). Current methods for studying oxidative enzymes are limited by their highly variable spatial distribution. For instance, peroxidase activity can vary significantly between the L and H horizons (just 1 cm apart) of oak (*Quercus petraea*) forest soils (Sinsabaugh, 2010). Additionally, the rapid turnover rates of these enzymes pose challenges for the determination approaches; phenol oxidase, for example, can perform 20 times faster than the hydrolytic enzyme  $\beta$ -glucosidase (Allison, 2006). Therefore, to accurately study oxidative enzymes, it is essential to refine methodologies for real-time spatial-temporal visualization, taking into account root type and morphology in complex plant-soil systems.

The term "peroxidase" encompasses a group of specific enzymes, such as NADH peroxidase (Enzyme Commission number (EC) 1.11.1.1), glutathione peroxidase (EC 1.11.1.9), and iodide peroxidase (EC 1.11.1.8), as well as a broader group of nonspecific enzymes referred to simply as peroxidases. Peroxidase activity has been identified in both plants and microorganisms (Hamid and Khalil-ur-Rehman, 2009). In plants, these enzymes are involved in the lignification process (Wakamatsu and Takahama, 1993) and play a role in defense mechanisms against physical damage or infection (Biles and Martyn, 1993). In soils, microbial peroxidase activity is influenced by various factors, including the concentration of soluble phenolic compounds, the lignin content of plant litter, soil pH, and nitrogen availability (Sinsabaugh, 2010; Sinsabaugh et al., 2002). At the plant-soil system scale, peroxidase activity varies with plant species and is affected by the combined effects of microbial community composition and soil properties (References are missing).

Current methods to determine enzyme activity in plant-soil systems are either colorimetric, using p-nitrophenol (pNP)-linked substrates (Burns et al., 2013; German et al., 2011), or fluorometric, using fluorescent dye-conjugated substrates e.g., 4-methylumbelliferone (MUF) and 7-amino-4-methyl coumarin (AMC), the latter are used for a wide range of soil hydrolases (Loeppmann et al., 2016; Marx et al., 2001; Nannipieri et al., 2012). Although kinetic parameters ( $V_{max}$  and  $K_m$ ) of peroxidases have been successfully estimated using 3,3',5,5'-tetramethylbenzidine (TMB) as a substrate (Triebwasser-Freese et al., 2015). However, this method is limited by a narrow pH range and a specific redox potential of the substrate (Bach et al., 2013). Zymography is the most common method for visualizing the spatio-temporal distribution of enzyme activities (Bilyera and Kuzyakov, 2024; Tegmeier et al., 2021). Thus, the determination of peroxidase and phenol oxidase activities using the aforementioned methods is complicated by the free-radical, non-specific nature of the oxidation reaction under variable redox conditions, as well as complex interactions between enzymes, substrates, and the soil matrix (Bach et al., 2013; German et al., 2011; Sinsabaugh, 2010).

Recent medical studies have reported using an Amplex Red (10-acetyl-10H-Phenoxazine-3,7-diol; ADHP)-based fluorometric assay (Tian et al., 2021) for the estimation of peroxidase activity and H<sub>2</sub>O<sub>2</sub> concentration in human and animal cells and tissues (Mishin et al., 2010; Zhao et al., 2012). Similarly, plant scientists have used Amplex Red to quantify hydrogen peroxide in plant tissues (Chakraborty et al., 2016). Recently, the application of Amplex Red to soil has enabled the i) determination of peroxidase kinetic parameters via the Michaelis-Menten equation (Khosrozadeh et al., 2022a), and the ii) visualization of the spatial distribution of peroxidase and phenol oxidase activity using soil oxidoreductase zymography (Khosrozadeh et al., 2022b). Additionally, Ghaderi et al. (2022) developed a new technology to visualize the spatial distribution of hydrolases on the root surface using a microscope. The authors revealed the heterogeneous distribution of acid phosphatase at scales between 50 to 500  $\mu$ m. Although this imaging method used membranes for the activity determination which may alter substrate diffusion processes, it demonstrated the potential of microscopy as an imaging tool for extracellular enzyme activity at the microscale. We stepped forward enabling the

visualization of peroxidase activity without using any membrane or gel at the rhizoplane and the rhizosphere soil in time and space.

Here we tested to i) pinpoint the peroxidation process in localized areas of tiny root segments and to ii) capture its transient reactions via micro-zymography in combination with fluorescence microscopy. Our objective was to evaluate whether peroxidase activity can be visualized onto rhizoplane and the rhizosphere in-situ without the use of any membrane or gel at the microscale. In more detail we were interested whether micro-zymography by using Amplex Red as a substrate exhibit contrasting peroxidase activity at specific root compartments such as the calyptra (root cap) versus apical meristem (zone of cell division) as well as roots with sparse root hair versus roots with dense root hair.

## **2. Materials and Methods**

### **2.1 Root sample preparation**

The soil samples were taken from sites in Germany named Heidgraben and Ruthe; these soils are classified as Luvisol, with 93% sand, 3% silt, and 3% clay and with 9% sand, 77% silt, and 11% clay, respectively. The respective soils were filled in rhizotrons with the size of 21×12×3 cm and planted with three apple seeds (*Malus domestica*) and thinned to one plant per rhizotron after germination of the seeds. The soil bulk density accounted approximately 1.1 g cm<sup>-3</sup> and the water content was adjusted to 60% of water holding capacity in the rhizotrons and was kept constant throughout tree growth by calculating their daily weight loss. All rhizotrons were placed in climate chambers at 20 in day- and 18°C nighttime, 12 h artificial light (LEDs) per day was supplied to the plants, and position of rhizotrons were regularly changed within the chamber during tree growth to ensure equal conditions. We sampled root segments and rhizosphere soil at two time points (after 4 and 6 weeks) during tree growth, and selected roots at different growth stages. 1 cm long of root segments were randomly selected as replicates from each rhizotron, respectively.

### **2.2 Preparation of substrate solution, calibration standards, and images acquisition**

An Amplex Red (Invitrogen, Paisley, UK) stock solution was prepared according to the manual of Thermo Fisher Scientific Inc. (Waltham, USA). Amplex® Red is a non-fluorescent and colorless compound that upon enzymatic oxidation is transformed into fluorescent resorufin. For calibration, A 1 mM resorufin (7-hydroxy-3H-phenoxazin-3-one sodium salt, C<sub>12</sub>H<sub>6</sub>NNaO<sub>3</sub>) stock solution was prepared by dissolving resorufin in 50 mM Trizma buffer (50 mM, pH 7.4) (Khosrozadeh et al., 2022). Thereafter, a concentration series from 0.001 to 0.01 mM of resorufin working solution was made by diluting the stock solution with Trizma buffer. For the stock solution of Amplex Red, 2.5 mg of Amplex Red power were weighed, and 100 µl DMSO and 100 µl autoclaved water were added. For the working solution, 100 µl of the stock solution was diluted in 2.5 ml Trizma buffer (50 mM, pH 7.4) in a Eppendorf vial and 10 µl of 0.3% H<sub>2</sub>O<sub>2</sub> was added. The working solution was bubbled with inert gas (N<sub>2</sub>) in the dark for 5 min to prevent oxidation. To protect the resorufin solution from degradation by light, all solutions of Amplex Red were prepared in a dark room and all previously autoclaved flasks were wrapped in aluminum foil.

In a darkroom the settings of the microscope (Zeiss Axio Imager M1, Oberkochen, Germany) were pre-tested to set image and video acquisition for fluorescence signal detection for the calibration solutions at constant distance in relation to the imaged micro-zymographs. The pre-defined optimal microscope settings remained unchanged for all images. Based on the properties of resorufin, the standard solutions were excited ~671 nm and detected between 585–640 nm emission wavelength with an exposure time of 1000 ms for each field of view with an objective magnification of 5x. For the establishment of a calibration line, we pipetted 5 µl of each concentration of calibration solution directly on a sterile glass slide and imaged it immediately via fluorescence microscopy.

Each segment of apple-root tissue was put on a sterile glass slide without cover glass. Root samples were additionally imaged under bright field (BF) condition for image registration. To document the rapid oxidation process, we used the function of video recording which started shortly before adding

5 µl Amplex Red working solution onto the root tissue to capture the complete reaction including the auto-fluorescence signals. Each video lasted at least 5 min, depending on the real-time reaction rate observed under the eyepiece. The resulting image file reflects a sequence of images taken every second.

### 2.3 Images Acquisition

The files were edited in Zeiss Zen 3.0 (2019), with appropriate time intervals and regions of interest selected, exported as image sequences in 8-bit.tiff format, and further analyzed in FIJI (FIJI is just ImageJ, Version: 2.14.0/1.54f) and MATLAB R2023a (The MathWorks, Inc., USA). Image analysis of the exported (8-bit) calibration images (tiff format) revealed good regression between gray values and resorufin concentrations ( $R^2 = 0.99$ ) which corresponded well to the calibration of Khosrozadeh et al., (2022b) (Figure 4-1 a).

To correct for the autofluorescence signal emitted from root and rhizosphere soil particles, the gray value of auto-fluorescent image of the respective channel (image before the application of Amplex Red) was subtracted from the resulting image sequence after application of the Amplex Red. In addition, the mean gray value of micro-zymographs was determined each second and subsequently and linearly regressed with time, to calibrate the accumulation of resorufin rate. To avoid the disturbance of pipetting the starting time of 10s after application was set for the calculation below. Micro-zymographs were color-coded using MATLAB and aligned with the respective BF image.

To test the effect of dense vs. sparse root hair on peroxidase activity, we separated roots with contrasting density of root hair using the method of Vincent et al. (2017). We selected the area of interest using the polygon selection tool. The area of interest should include a complete area of root hair zone. The root hair zone (from the root border to the longest root hair) were chosen and the gray value was determined for each segment of root tissue. The lower the mean gray value of cropped root zone, the higher the root hair density. Thereafter, the obtained gray value was tested against an empirically derived threshold gray value of 200 to distinguish dense from sparse root hair by one-way ANOVA. The peroxidase activity of each root sample was calculated as below:

$$V_{i+10} = \frac{a \times (G_{i+10} - G_{10})}{t_{i+10} - t_{10}} \quad (1)$$

Where  $V_{i+10}$  is the activity of peroxidase from  $t_{10}$  to  $t_{i+10}$ ,  $a$  is the slope of calibration equation,  $G_{i+10}$  is the mean gray value in the micro-zymograph at  $t_{i+10}$ ,  $G_{10}$  is the mean gray value of the fluorescence signal in the micro-zymograph at  $t_{10}$  (10 s after application of Amplex Red).

The root segments with rhizosphere soil were selected for analyzing the difference of gray value from organic soil particles, quartz, and rhizoplane. The dark soil particles were identified as organic soil particles. The gray value was analyzed for organic soil particles, minerals (e.g., quartz), and the rhizoplane at every minute after adding Amplex Red.

The peroxidase activity along the root tip from the calyptra (root cap) to the apical meristem (zone of cell division) was also determined. We have drawn a straight line from the top of the calyptra to the apical meristem was marked using the line tool in ImageJ to test the gray value change along the root tips. The mean peroxidase activity of the calyptra to the apical meristem was calculated according to the equation (1). The micro-zymographs reflected the spatial distribution of peroxidase activity along the root tips after 1 and 5 min after adding Amplex Red.

### 2.4 Statistical analysis

The presumptions of the calibration data were continuous and with homogeneity of variance, and T-test was used to check if the slope in a linear regression was significantly different from zero before using the regression equation for further calculation. The data for the samples was first checked for normality (Shapiro–Wilk,  $p > 0.05$ ). The Welch's t test was applied to differentiate the normally distributed values of root hair density and peroxidase activity of roots with dense and sparse root hair. Further, Kruskal-Wallis test was used to test the not normally distributed values, followed by

Bonferroni Post Hoc Test. The Mann-Whitney test was used to examine the significant differences in peroxidases activity at calyptra and on apical meristem. All statistical analyses were carried out in GraphPad Prism 8.4.0 (2020).

### 3. Results

#### 3.1 Intensity-based analysis of peroxidases via fluorescence microscopy

For low signal images (gray value < 5) we found a weak regression between fluorescence intensity expressed a gray value with time across all analyzed root segments of both the soils, Heidgraben and Ruthe (Figure 4-1 b). In contrast, micro-zymographs with a higher fluorescence intensity (gray value > 5) showed strong linear regression with reaction time across all the roots analyzed (Figure 4-1 c). The fluorescence intensity and distribution in the micro-zymograph increased over observation time (1–500s) (Figure 4-2). The image in the first frame (1s) of Figure 2 showed a hampered fluorescent signal, with very low autofluorescence of the root tissue. After adding substrate, the area of interest was fully covered by a fluorescent signal within 1–2 s. However, no clear peak established the first 10 s of the reaction which may be attributed to the disturbance by pipetting or the lagged establishment of the peroxidase reaction. Subsequently, strong fluorescent signal appeared in localized areas of the root segments and increased with time. Comparing the intensity of fluorescence at 500 s (Figure 4-2 d) with autofluorescence image (Figure 4-2 c), almost all the signal derived from the peroxidase reaction itself.

#### 3.2 Spatiotemporal distribution of peroxidase activity in rhizosphere soil at the microscale

The fluorescence signal increased onto the rhizoplane and the soil particles after the addition of the substrate. Noticeably, the highest fluorescence intensity appeared at the boundary of the root surface and the soil particles which might be due to reflection and/or autofluorescence (Loeppmann et al., 2023). Fluorescence lifetime imaging reflects an excellent technique to overcome such a bias in fluorescence intensity signaling. Here, after one minute the signal at the rhizoplane increased by 57% up to 7 minutes after application whereas the fluorescence signal at soil particles' surfaces increased by 178%. The organic components of the rhizosphere soil, however showed a much lower fluorescence signal (reduction of 70%) than the quartz (Figure 4-4). The fluorescence partially appeared on the organic particles close to the root surface (Figure 4-4 a). The gray value of the quartz and root area increased by 89% and 85% compared to the organic soil particles 1 min after applying Amplex Red (Figure 4-4 c). Across time mineral components and root did not show significant differences of peroxidase activity (Figure 4-4).

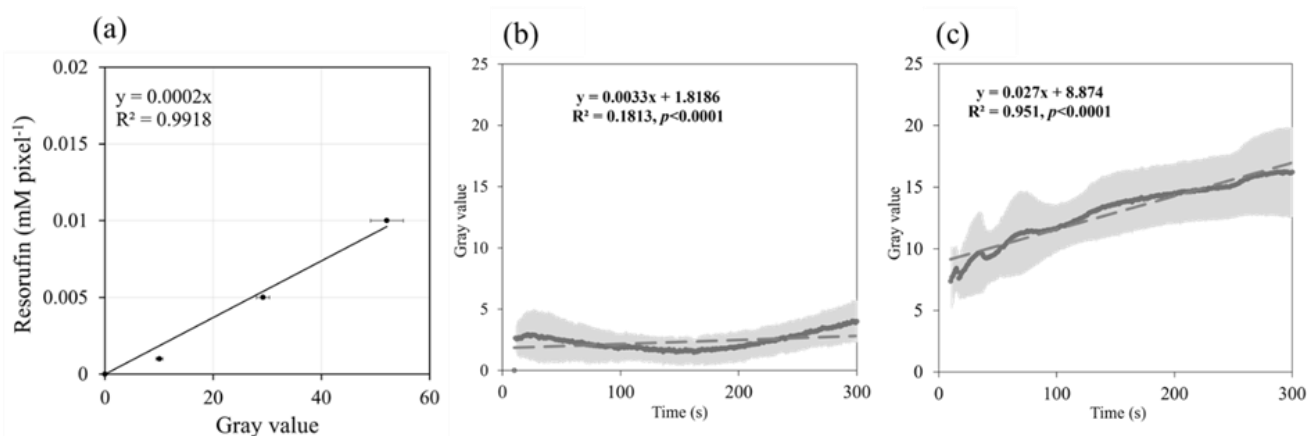


**Figure 4-1** Calibration of micro-zymography images based on (a) resorufin concentration ( $\text{mM pixel}^{-1}$ ) and the mean gray value across each image. Error bars represent standard deviation. Regressions between gray values and time after adding Amplex Red onto root tissue with (b) low activity and (c) high activity. Gray area represents standard deviation, and yellow dashed lines represent regression lines ( $n = 4$ ,  $p < 0.001$ )

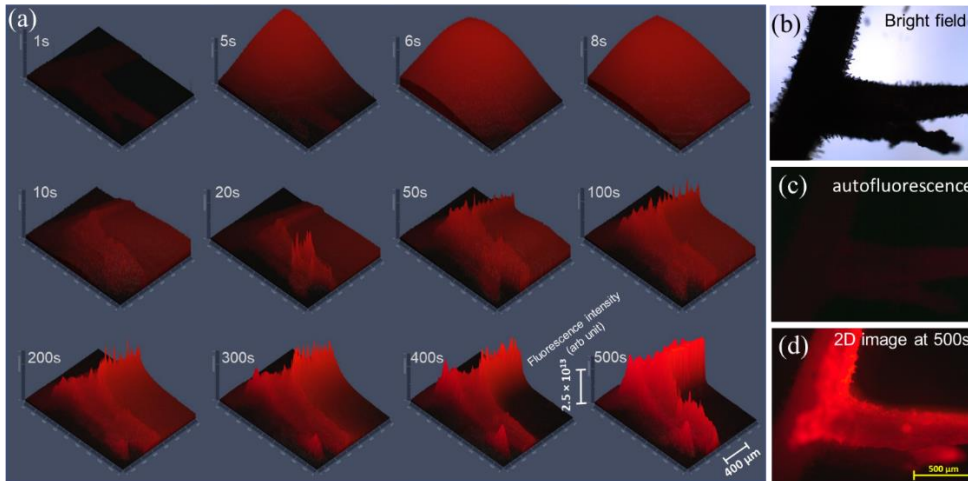


**Figure 4-2** (a) An example of 2.5D surface topography of fluorescent intensity at the root surface after adding Amplex Red; (b) root tissue imaged in bright field; (c) autofluorescence of root tissue in C1 red channel wavelength; (d) the fluorescence on the root tissue 500s after adding Amplex Red.

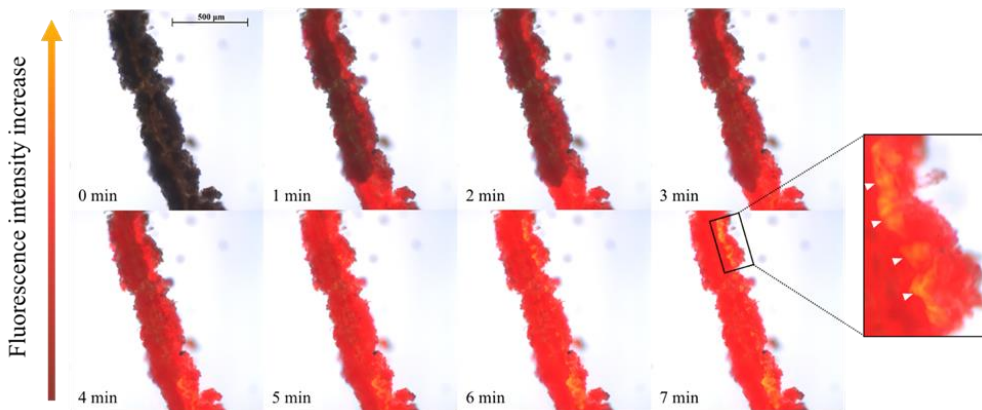


**Figure 4-3** Overlay of bright field image and fluorescent images of root tissue with soil particles at every minute after application of Amplex Red. 0 min: before application of Amplex Red (autofluorescence). The zoom-in image shows the high fluorescence intensity from the boundary within the root and soil particles. White triangles mark the points with high fluorescence and are distributed linearly.

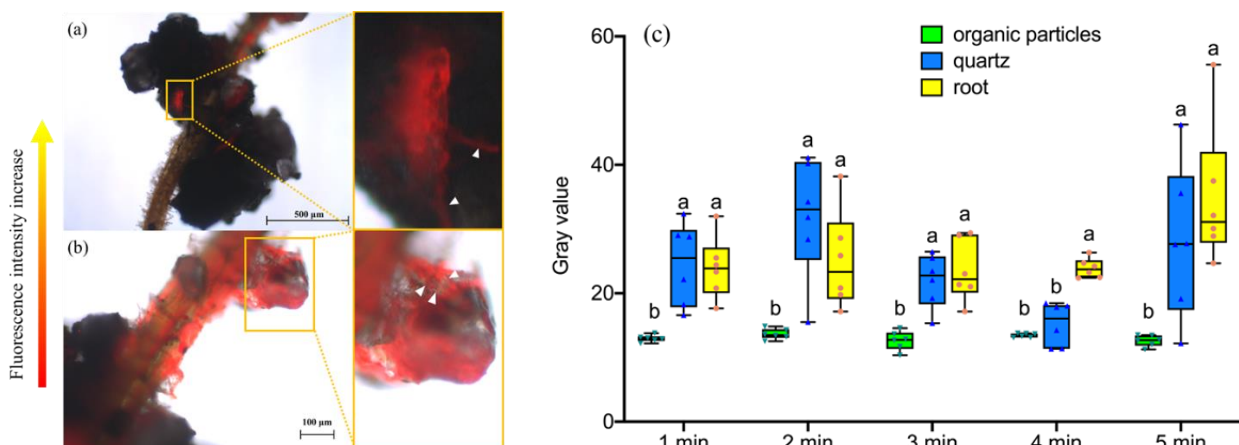


**Figure 4-4** Overlay of bright field image and fluorescent image of root with (a) organic soil particles and (b) quartz 5 minutes after adding Amplex Red. (c) The mean gray value of organic soil particles, quartz, and root. Lowercase letters represent significant differences between organic particles, quartz, and roots within the same reaction time ( $n = 6$ ,  $p < 0.01$ ). White triangles mark the points with high fluorescence potentially from fine roots associated with soil particles or reflection from quartz.

### 3.3 Effect of root hair density on the spatio-temporal distribution of peroxidase activity at the microscale

The mean activity of peroxidases was about 2-fold higher for the calyptra than for the apical meristem between 1 and 5 minutes (e.g., Figure 4-5). A statistical analysis ( $n=4$ ) on root tips for the peroxidase activity of the calyptra and the apical meristem demonstrated a significant difference in peroxidase activity 5 minutes after application of Amplex Red (Figure 4-5). Peroxidase activity with time shifted slower between 5 and 9 minutes suggesting a stabilization enzymatic reaction.

Since we have been interested whether micro-zymography by using Amplex Red as a substrate exhibit contrasting peroxidase activity along the root tip, we determined the peroxidase activity of baldy roots (sparse root hair) versus roots with dense root hair (Figure 4-6) via image separation. The peroxidase activity was 2-fold higher in roots with dense than with sparse root hair (Figure 4-6).

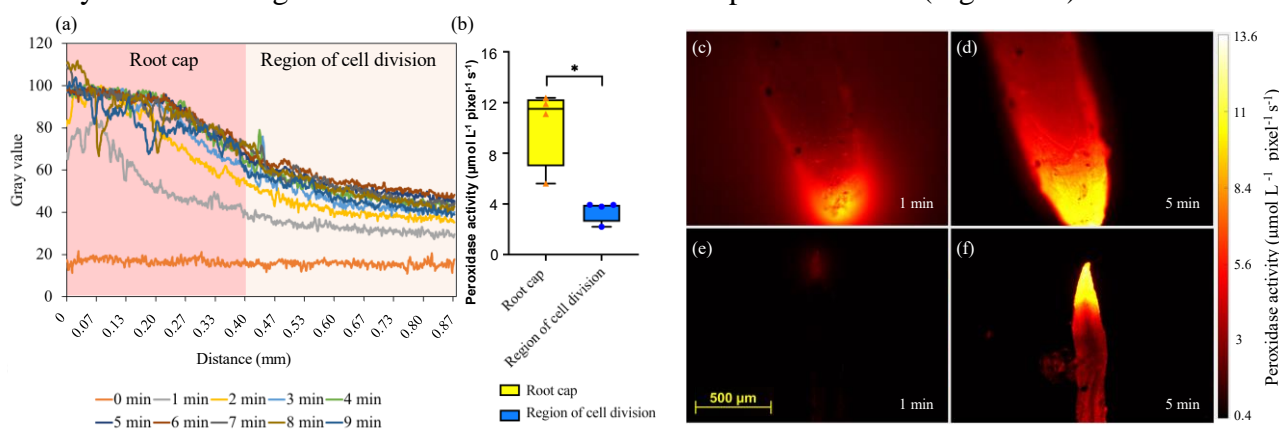


**Figure 4- 5** Spatial and temporal distribution of peroxidase activity at the root tips. (a) Variation of gray value over time from the root cap to the region of cell division. (0 represents the start of the root cap.) (b) Peroxidase activity of the root cap and the region of cell division ( $n = 4$ ,  $p < 0.05$ ). Spatial distribution of peroxidase activity of (c, e) two root tips after 1 minute of reaction and (d, f) two root tips after 5 minutes of reaction time.

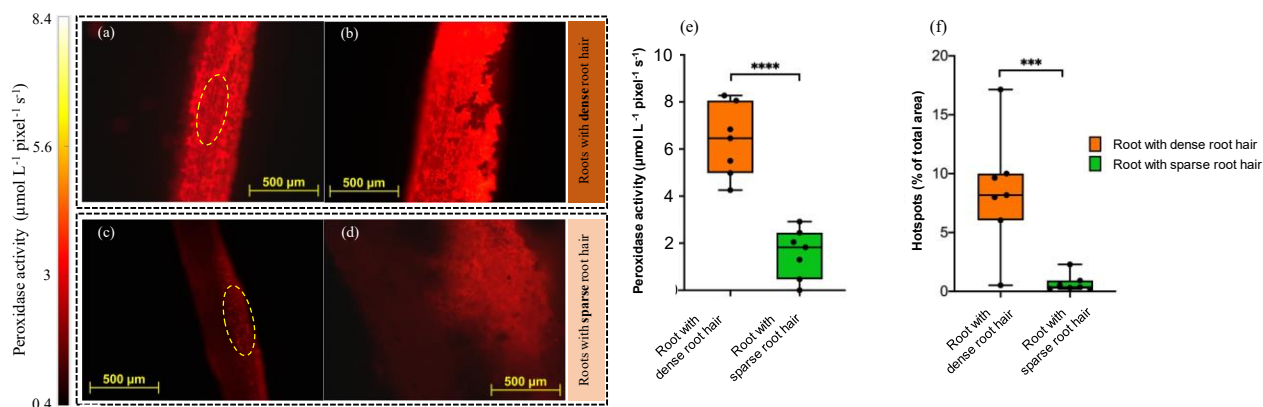


**Figure 4- 6** Spatial distribution of peroxidase activity on roots with dense root hair (a-b, two pieces of root tissues with dense root hair), and roots with sparse root hair (c-d, two pieces of root tissues with sparse root hair) at the same reaction time of 5 minutes after application of Amplex Red. (Ellipses on the images mark the points of high peroxidase activity from the root hair, which can be easily seen in the area.) (e) The peroxidase activity of the root with dense root hair and the root with sparse root hair. (f) Hotspot area on the root with dense root hair and the root with sparse root hair ( $n = 7$ , \*\*\* represents  $p < 0.001$  and \*\*\*\* represents  $p < 0.0001$ ).

### 3.4 Spatio-temporal variation of peroxidase activity along root tips

The gray value of the root tips over the distance from the calyptra to the apical meristem (0.4 to 0.9 mm distance) showed a stable low intensity fluorescent signal before applying Amplex Red (Figure 4-5 a), implying low autofluorescence of the root tip. After adding substrate, the calyptra showed

increased peroxidase activity up to 0.20 ( $\mu\text{mol L}^{-1} \text{ pixel}^{-1} \text{ s}^{-1}$ ) within the first minute of reaction. Afterwards the mean peroxidase activity was 0.13 ( $\mu\text{mol L}^{-1} \text{ pixel}^{-1} \text{ s}^{-1}$ ) within 2 minutes. Between 2 and 9 minutes, the gray values of the root tips varied within a small range and remained stable across experimental duration. Slightly lower intensity was detected for the apical meristem within the first minute after the application of the substrate. Thereafter the peroxidase activity varied between 40–60 for the apical meristem across experimental duration. The mean activity of peroxidase was 2-fold higher at the calyptra than at the apical meristem between 1 and 5 minutes.

## **4 Discussion**

### **4.1 Advances in micro-zymography using fluorescence microscopy**

The linear calibration of resorufin enabled the usage of using Amplex Red as substrate to quantify peroxidase activity at the microscale using fluorescence microscope to expand the spatio-temporal resolution on oxidases. In contrast to MUF-based micro-zymography (Ghaderi et al., 2022) and basic soil zymography (Spohn et al., 2016), and spatio-temporal soil zymography (Tegtmeier et al., 2021), we did not incubate the resorufin before imaging by means without the use of membrane or gel which may alter diffusion processes within the reaction volume. The restriction resulting from a fixed reaction time is the lack of information on the instantaneous response of enzyme activity, which may be acceptable for hydrolases but not for fast reacting oxidases. The advantage of temporally highly resolved micro-zymographs: it allows deeper insights into the spatial distribution of e.g., peroxidases at the microscale.

Filter-, membrane-, or gel-, based (micro-) zymography techniques may not be sensitive enough in order to detect autofluorescence intensity signals inferring the wavelength interval for detection. For example, Khosrozadeh et al. (2022b), who used Amplex Red via traditional soil zymography, could not detect any autofluorescence. The detection of autofluorescence is not always something bad it may give additional information without any interference at a different wavelength interval for detection. As we detected a low fluorescent signal already before application of Amplex Red at the rhizoplane we were able to correct for it. Therefore, even autofluorescent substances in the plant cells can be detected via fluorescence microscopy (Kurihara et al., 2015; Müller et al., 2013) and should be considered when working at the microscale. For example, some proteins, e.g., anthocyanins and azulenes in the vacuole, show red fluorescence in the range of 600–630 nm of emission wavelength (Roshchina, 2012). Moreover, the degree of autofluorescence of plant tissue under a microscope depends largely on the imaging parameters (e.g., excitation wavelength, and emission filters) (DeVree et al., 2021).

Khosrozadeh et al. (2022b) used the soil zymography method and found that the highest peroxidase activity occurred within 15 minutes after the application of Amplex Red. Here, we confirmed that a stable and intensive reaction of peroxidase activity at the rhizoplane occurred already earlier – within 5–10 minutes. In addition, in line with Zhao et al. (2012) we detected an increase in fluorescence intensity over time.

### **4.2 How to overcome the problems of autofluorescence in micro-zymography of rhizosphere soil**

The detected mineral soil particles (e.g., quartz) that were attached as so-called rhizosphere soil to the root surface showed high peroxidase activity, however no signal was observed from organic matter that was attached to the root. This suggested that in this special case the autofluorescence of the organic material was very low at our detection wave length interval. Although the existence of peroxidases in soils has been proven (Bach et al., 2013; Sinsabaugh et al., 2002) and quantified by resorufin-based Michaelis–Menten kinetics (Khosrozadeh et al., 2022a), peroxidase production of soil microorganisms on a single soil particle is much lower than in fresh plant tissue (Gramss et al., 1999). The major contribution of root-released oxidoreductases to oxidative degradation processes in soils has been confirmed by Gramss et al. (1999). Thus, the fluorescence of the soil mineral particles on the images may come from three sources: 1) excess of resorufin produced by peroxidase activity of roots diffuses

into the free space between root surface and soil particles; 2) fine roots covered by soil particles produced resorufin after applying Amplex Red; 3) fluorescence from the reflection of quartz (Lee et al., 2022). Filter-, membrane-, or gel-, based (micro-) zymography techniques may not be sensitive enough in order to detect autofluorescence intensity signals inferring the wavelength interval for detection. Mineral particles like quartz may diminish our results caused by autofluorescence and/or reflection. To overcome this problem, we will combine micro-zymography with fluorescence lifetime imaging (Loeppmann et al., 2023).

### **4.3 Peroxidase activity of root tissues**

The mineral soil particles (quartz) that were attached to the root showed high peroxidase activity via high fluorescence signals, but no signal was observed in the dark organic soil particles that were attached to the root. Although the existence of peroxidases in soils has been proved (Bach et al., 2013; Sinsabaugh et al., 2002) and quantified by resorufin-based Michaelis–Menten kinetics (Khosrozadeh et al., 2022a), peroxidase production of soil microorganisms on a single soil particle is much lower than in fresh plant tissue. The major contribution of root-released oxidoreductases to oxidative degradation processes in soils has been confirmed by Gramss et al. (1999). Thus, the fluorescence of the soil particles on the images may come from three sources: 1) excess of resorufin produced by peroxidation of roots flows into the space within soil particles; 2) soil particles wrapped by resorufin as the products of peroxidation after applying Amplex Red; 3) fluorescence from the reflection of quartz. Therefore, it is advisable to exclude the interference of soil particles when applying this micro-zymography approach for the determination of resorufin-based peroxidase activity of root.

### **4.4 Peroxidase activity of root tissues**

Peroxidases have been suggested to play an active role in cell wall lignification in many plant species (Laitinen et al., 2017; Shigeto and Tsutsumi, 2016). Root hair is a typical zone of fast cell wall expansion, as the root hair is initiated by the formation of a cell wall bulge at the basal end of the cell. The subsequent rapid elongation of the root hair is accompanied by a fast cell wall expansion as well. This explains the higher peroxidase activity of roots with dense vs roots with sparse root hair. The visibly higher peroxidase activity at the area covered with root hair compared to rhizoplane (Figure 4-6 a, c) further confirmed this assumption. In addition, the fluorescence signal covered the entire epidermis while its presence around the cell wall was clearly intense which is related to the cross-linking of cell wall compounds by radicals produced in the peroxidative cycle, including the formation of lignin and suberin within the cell wall (Dufil et al., 2020). For example, the “peroxidase 64” was detected in the endodermis during root growth and it was localized to the Casparian strip (Lee et al., 2013). Overall, precise localization of oxidases in specific cell wall domains may be a key determinant of spatial patterns of lignin deposition (Yi Chou et al., 2018). Therefore, the determination of hotspots at the current scale is necessary.

Another relevant root compartment is the root tip, which has a variety of different growth characteristics within a small area. The highest activity of peroxidases has been derived from the calyptra which was in line with Hall and Sexton (1972), who found that peroxidase activity is predominately localized at the root cap, while the low peroxidase activity has been detected at the region of cell division. This is due to the combination of a thin cell wall and a large nucleus. Similar investigation of low peroxidase activity at the apical meristem was also confirmed by Dunand et al. (2007). Thus, the resorufin-based micro-zymography method is able to differentiate the spatio-temporal variation of peroxidase activities along the root tips.

Peroxidases are also known as mediators of oxidative cross-linking during plant defense reactions. Plant cells can quickly produce apoplastic peroxidases that are regulated by stressful conditions (Farvardin et al., 2020). The peroxidase activity of the apple root tissues in this study may be higher than the normal intact roots, because cutting the root into small pieces may have caused an oxidative burst generated by the defense mechanism under wounding condition (Bolwell and Wojtaszek, 1997).

A promising future improvement we are working on is an imaging peroxidase activity of an intact root based on the present method.

## **5 Conclusion**

Compared with the membrane-based zymography using Amplex Red as substrate, we improved temporal and spatial resolution by capturing the micro-zymographs of peroxidase activity within each second at the microscale. The linear calibration of resorufin enabled to quantify peroxidase activity using fluorescence microscope to expand the spatio-temporal resolution of oxidases. Overall, this study holds great promise for the spatio-temporal visualization of the peroxidase activity of fresh root tissue and rhizosphere soil. In contrast to MUF-based micro-zymography, basic soil zymography, and spatio-temporal soil zymography, we did not incubate the resorufin before imaging by means without the use of membrane or gel which may alter diffusion processes within the reaction volume. Mineral particles like quartz may diminish our results caused by autofluorescence and/or reflection. To overcome this problem, we will combine micro-zymography with fluorescence lifetime imaging.

## **Acknowledgement**

We sincerely thank the help of Negar Ghaderi for her assistance in lab work at UFZ Halle. We deeply appreciate the financial support of the German Federal Ministry of Education and Research (BMBF) to “ORDIAmur” project, to provide us with the root samples. We would also like to sincerely thank the German Federal Ministry of Education and Research (BMBF) for funding the project “RootWayS” (number 031B0911A) to provide Yijie Shi the opportunity to do her PhD.

## References

- Allison, S.D., 2006. Soil minerals and humic acids alter enzyme stability: implications for ecosystem processes. *Biogeochemistry* 81, 361–373. <https://doi.org/10.1007/s10533-006-9046-2>
- Bach, C.E., Warnock, D.D., Van Horn, D.J., Weintraub, M.N., Sinsabaugh, R.L., Allison, S.D., German, D.P., 2013. Measuring phenol oxidase and peroxidase activities with pyrogallol, l-DOPA, and ABTS: Effect of assay conditions and soil type. *Soil Biology and Biochemistry* 67, 183–191. <https://doi.org/10.1016/j.soilbio.2013.08.022>
- Biles, C.L., Martyn, R.D., 1993. Peroxidase, polyphenoloxidase, and shikimate dehydrogenase isozymes in relation to tissue type, maturity and pathogen induction of watermelon seedlings. *Plant Physiology and Biochemistry* 31, 499–506.
- Bilyera, N., Kuz'yakov, Y., 2024. Soil zymography: A decade of rapid development in microbial hotspot imaging. *Soil Biology and Biochemistry* 189, 109264. <https://doi.org/10.1016/j.soilbio.2023.109264>
- Bolwell, G.P., Wojtaszek, P., 1997. Mechanisms for the generation of reactive oxygen species in plant defence – a broad perspective. *Physiological and Molecular Plant Pathology* 51, 347–366. <https://doi.org/10.1006/pmpp.1997.0129>
- Burns, R.G., DeForest, J.L., Marxsen, J., Sinsabaugh, R.L., Stromberger, M.E., Wallenstein, M.D., Weintraub, M.N., Zoppini, A., 2013. Soil enzymes in a changing environment: Current knowledge and future directions. *Soil Biology and Biochemistry* 58, 216–234. <https://doi.org/10.1016/j.soilbio.2012.11.009>
- Chakraborty, S., Hill, A.L., Shirsekar, G., Afzal, A.J., Wang, G.-L., Mackey, D., Bonello, P., 2016. Quantification of hydrogen peroxide in plant tissues using Amplex Red. *Methods* 109, 105–113. <https://doi.org/10.1016/j.ymeth.2016.07.016>
- DeVree, B.T., Steiner, L.M., Głazowska, S., Ruhnnow, F., Herburger, K., Persson, S., Mravec, J., 2021. Current and future advances in fluorescence-based visualization of plant cell wall components and cell wall biosynthetic machineries. *Biotechnol Biofuels* 14, 78. <https://doi.org/10.1186/s13068-021-01922-0>
- Dufil, G., Parker, D., Gerasimov, J.Y., Nguyen, T.-Q., Berggren, M., Stavrinidou, E., 2020. Enzyme-assisted in vivo polymerisation of conjugated oligomer-based conductors. *J. Mater. Chem. B* 8, 4221–4227. <https://doi.org/10.1039/D0TB00212G>
- Dunand, C., Crèvecoeur, M., Penel, C., 2007. Distribution of superoxide and hydrogen peroxide in Arabidopsis root and their influence on root development: possible interaction with peroxidases. *New Phytologist* 174, 332–341. <https://doi.org/10.1111/j.1469-8137.2007.01995.x>
- Farvardin, A., González-Hernández, A.I., Llorens, E., García-Agustín, P., Scalschi, L., Vicedo, B., 2020. The Apoplast: A Key Player in Plant Survival. *Antioxidants* 9, 604. <https://doi.org/10.3390/antiox9070604>
- German, D.P., Weintraub, M.N., Grandy, A.S., Lauber, C.L., Rinkes, Z.L., Allison, S.D., 2011. Optimization of hydrolytic and oxidative enzyme methods for ecosystem studies. *Soil Biology and Biochemistry* 43, 1387–1397. <https://doi.org/10.1016/j.soilbio.2011.03.017>
- Ghaderi, N., Schmidt, H., Schlüter, S., Banfield, C., Blagodatskaya, E., 2022. Development of micro-zymography: Visualization of enzymatic activity at the microscopic scale for aggregates collected from the rhizosphere. *Plant Soil*. <https://doi.org/10.1007/s11104-022-05573-4>
- Giles, C.D., Dupuy, L., Boitt, G., Brown, L.K., Condrón, L.M., Darch, T., Blackwell, M.S.A., Menezes-Blackburn, D., Shand, C.A., Stutter, M.I., Lumsdon, D.G., Wendler, R., Cooper, P., Wearing, C., Zhang, H., Haygarth, P.M., George, T.S., 2018. Root development impacts on the distribution of phosphatase activity: Improvements in quantification using soil zymography. *Soil Biology and Biochemistry* 116, 158–166. <https://doi.org/10.1016/j.soilbio.2017.08.011>
- Gramss, G., Voigt, K.-D., Kirsche, B., 1999. Oxidoreductase enzymes liberated by plant roots and their effects on soil humic material. *Chemosphere* 38, 1481–1494. [https://doi.org/10.1016/S0045-6535\(98\)00369-5](https://doi.org/10.1016/S0045-6535(98)00369-5)
- Hall, J.L., Sexton, R., 1972. Cytochemical localization of peroxidase activity in root cells. *Planta* 108, 103–120. <https://doi.org/10.1007/BF00386073>
- Hamid, M., Khalil-ur-Rehman, 2009. Potential applications of peroxidases. *Food Chemistry* 115, 1177–1186. <https://doi.org/10.1016/j.foodchem.2009.02.035>
- Khosrozadeh, S., Dorodnikov, M., Reitz, T., Blagodatskaya, E., 2022a. An Improved Amplex Red-based Fluorometric Assay of Phenol Oxidases and Peroxidases Activity: A Case Study on Haplic Chernozem. *European J Soil Science*. <https://doi.org/10.1111/ejss.13225>
- Khosrozadeh, S., Guber, A., Kravchenko, A., Ghaderi, N., Blagodatskaya, E., 2022b. Soil oxidoreductase zymography: Visualizing spatial distributions of peroxidase and phenol oxidase activities at the root-soil interface. *Soil Biology and Biochemistry* 167, 108610. <https://doi.org/10.1016/j.soilbio.2022.108610>
- Kurihara, D., Mizuta, Y., Sato, Y., Higashiyama, T., 2015. ClearSee: a rapid optical clearing reagent for whole-plant fluorescence imaging. *Development* dev.127613. <https://doi.org/10.1242/dev.127613>
- Laitinen, T., Morreel, K., Delhomme, N., Gauthier, A., Schiffthaler, B., Nickolov, K., Brader, G., Lim, K.-J., Teeri, T.H., Street, N.R., Boerjan, W., Kärkönen, A., 2017. A Key Role for Apoplastic H<sub>2</sub>O<sub>2</sub> in Norway Spruce Phenolic

- Metabolism. *Plant Physiol.* 174, 1449–1475. <https://doi.org/10.1104/pp.17.00085>
- Lee, J., Hestrin, R., Nuccio, E.E., Morrison, K.D., Ramon, C.E., Samo, T.J., Pett-Ridge, J., Ly, S.S., Laurence, T.A., Weber, P.K., 2022. Label-Free Multiphoton Imaging of Microbes in Root, Mineral, and Soil Matrices with Time-Gated Coherent Raman and Fluorescence Lifetime Imaging. *Environ. Sci. Technol.* 56, 1994–2008. <https://doi.org/10.1021/acs.est.1c05818>
- Lee, Y., Rubio, M.C., Alassimone, J., Geldner, N., 2013. A Mechanism for Localized Lignin Deposition in the Endodermis. *Cell* 153, 402–412. <https://doi.org/10.1016/j.cell.2013.02.045>
- Loeppmann, S., Blagodatskaya, E., Pausch, J., Kuzyakov, Y., 2016. Enzyme properties down the soil profile - A matter of substrate quality in rhizosphere and detritosphere. *Soil Biology and Biochemistry* 103, 274–283. <https://doi.org/10.1016/j.soilbio.2016.08.023>
- Marx, M.-C., Wood, M., Jarvis, S.C., 2001. A fluorimetric assay for the study of enzyme diversity in soils. *Soil Biology and Biochemistry* 33, 1633–1640.
- Mishin, V., Gray, J.P., Heck, D.E., Laskin, D.L., Laskin, J.D., 2010. Application of the Amplex red/horseradish peroxidase assay to measure hydrogen peroxide generation by recombinant microsomal enzymes. *Free Radical Biology and Medicine* 48, 1485–1491. <https://doi.org/10.1016/j.freeradbiomed.2010.02.030>
- Müller, S.M., Galliardt, H., Schneider, J., Barisas, B.G., Seidel, T., 2013. Quantification of Förster resonance energy transfer by monitoring sensitized emission in living plant cells. *Front. Plant Sci.* 4. <https://doi.org/10.3389/fpls.2013.00413>
- Nannipieri, P., Giagnoni, L., Renella, G., Puglisi, E., Ceccanti, B., Masciandaro, G., Fornasier, F., Moscatelli, M.C., Marinari, S., 2012. Soil enzymology: classical and molecular approaches. *Biol Fertil Soils* 48, 743–762. <https://doi.org/10.1007/s00374-012-0723-0>
- Roshchina, V.V., 2012. Vital Autofluorescence: Application to the Study of Plant Living Cells. *International Journal of Spectroscopy* 2012, 1–14. <https://doi.org/10.1155/2012/124672>
- Shigeto, J., Tsutsumi, Y., 2016. Diverse functions and reactions of class III peroxidases. *New Phytol* 209, 1395–1402. <https://doi.org/10.1111/nph.13738>
- Sinsabaugh, R.L., 2010. Phenol oxidase, peroxidase and organic matter dynamics of soil. *Soil Biology and Biochemistry* 42, 391–404. <https://doi.org/10.1016/j.soilbio.2009.10.014>
- Sinsabaugh, R.L., Carreiro, M.M., Repert, D.A., 2002. Allocation of extracellular enzymatic activity in relation to litter composition, N deposition, and mass loss. *Biogeochemistry* 60, 1–24. <https://doi.org/10.1023/A:1016541114786>
- Tegtmeier, J., Dippold, M.A., Kuzyakov, Y., Spielvogel, S., Loeppmann, S., 2021. Root-o-Mat: A novel tool for 2D image processing of root-soil interactions and its application in soil zymography. *Soil Biology and Biochemistry* 157, 108236. <https://doi.org/10.1016/j.soilbio.2021.108236>
- Tian, L., Feng, H., Dai, Z., Zhang, R., 2021. Resorufin-based responsive probes for fluorescence and colorimetric analysis. *J. Mater. Chem. B* 9, 53–79. <https://doi.org/10.1039/D0TB01628D>
- Triebwasser-Freese, D.J., Tharayil, N., Preston, C.M., Gerard, P.G., 2015. Catalytic kinetics and activation energy of soil peroxidases across ecosystems of differing lignin chemistries. *Biogeochemistry* 124, 113–129. <https://doi.org/10.1007/s10533-015-0086-3>
- Vincent, C., Rowland, D., Na, C., Schaffer, B., 2017. A high-throughput method to quantify root hair area in digital images taken in situ. *Plant Soil* 412, 61–80. <https://doi.org/10.1007/s11104-016-3016-9>
- Wakamatsu, K., Takahama, U., 1993. Changes in peroxidase activity and in peroxidase isozymes in carrot callus. *Physiol Plant* 88, 167–171. <https://doi.org/10.1111/j.1399-3054.1993.tb01774.x>
- Yi Chou, E., Schuetz, M., Hoffmann, N., Watanabe, Y., Sibout, R., Samuels, A.L., 2018. Distribution, mobility, and anchoring of lignin-related oxidative enzymes in Arabidopsis secondary cell walls. *Journal of Experimental Botany* 69, 1849–1859. <https://doi.org/10.1093/jxb/ery067>
- Zhao, B., Summers, F.A., Mason, R.P., 2012. Photooxidation of Amplex red to resorufin: Implications of exposing the Amplex red assay to light. *Free Radical Biology and Medicine* 53, 1080–1087. <https://doi.org/10.1016/j.freeradbiomed.2012.06.034>

## 2.5 Study 5. Using Fluorescence Lifetime Imaging to Disentangle Microbes from the Heterogeneous Soil Matrix

Sebastian Loepmann<sup>1</sup>, Jan Tegtmeier<sup>1</sup>, **Yijie Shi**<sup>1</sup>, Alberto Andrino de la Fuente<sup>2</sup>, Jens Boy<sup>2</sup>, Georg Guggenberger<sup>2</sup>, Andreas Fulterer<sup>3</sup>, Martin Fritsch<sup>3</sup>, Sandra Spielvogel<sup>1</sup>

**Status: Published in *Biology and Fertility of Soils***

<sup>1</sup> Institute of Plant Nutrition and Soil Science, Christian-Albrechts-University Kiel, Hermann-Rodewald-Str. 2, 24118 Kiel, Germany

<sup>2</sup> Institute of Soil Science, Leibniz University Hannover, Hannover, Germany

<sup>3</sup> Leica Microsystems GmbH, Wetzlar, Germany



Loepmann, S., Tegtmeier, J., Shi, Y., De la Fuente, A. A., Boy, J., Guggenberger, G., ... & Spielvogel, S. (2023). Using fluorescence lifetime imaging to disentangle microbes from the heterogeneous soil matrix. *Biology and Fertility of Soils*, 59(2), 249-260. <https://doi.org/10.1007/s00374-023-01704-w>

### Abstract

Soil microbial communities are involved in most biogeochemical processes creating hotspots for nutrient cycling. The spatial visualization of such soil hotspots via microscopic techniques is still challenging caused by the intrinsic fluorescence and opacity of the soil. One way to differentiate microbial cells from the heterogeneous soil matrix is a fluorescence lifetime-based technique (FLIM) with subsequent phasor plot separation; it separates and visualizes the distinctly different photon arrival times of all photons per pixel. FLIM delivers additional independent information behind intensity-based image processing and image analysis which is often hampered by, e.g., autofluorescence, resolution issues, and photobleaching artifacts caused by the prevailing minerals and organic substances. We determined characteristic fluorescence lifetime profiles of BacLight™ Green for *Rhodotorula mucilaginosa* and *Bacillus subtilis* in phosphate-buffered saline (PBS) solution and water as well as in natural, autoclaved, glucose-activated, and soil mineral particles by FLIM measurements via confocal laser scanning fluorescence microscopy. *Rhodotorula mucilaginosa* and *Bacillus subtilis* from pure cultures measured in water and PBS accounted for 1.20 ( $\pm$  0.2) ns and 1.3 ( $\pm$  0.1) ns respectively. The lifetime profile within the cells was rather homogeneous for both microbial species tested. This suggests stable photon arrival times for microbial strains with minor effects of matrix components as tested in PBS and water. We identified a clear difference in fluorescence lifetime profiles between microorganisms (around 1 ns) and the surrounding soil matrix (0.2 to 0.7 ns, > 3.6 ns) via phasor plot separation. The results presented raise the feasibility to extend the applicability of FLIM to other soils and their accompanying microbiota.

**Keywords:** Photon arrival times, Confocal laser scanning microscopy, Soil staining, Microbial separation, Phasor plot, FLIM

## 1. Introduction

Soil biochemical processes are carried out by microbes and are affected by composition and activity of soil microbial communities which may depend on the microbial habitat (Eickhorst and Tippkötter 2008; Neu and Lawrence 2015; Loeppmann et al. 2018; Wang et al. 2020). Spatial visualization of soil microbes and microbial habitats is important for comprehensive understanding of soil biochemical cycling processes. Nowadays, direct microscopy techniques, e.g., confocal laser scanning fluorescence microscopy (CLSM), are valuable tools to determine the spatial distribution of soil microorganisms in their microhabitats (Eickhorst and Tippkötter 2008; Li et al. 2004; Tippkötter et al. 1986). CLSM observations have been reported for protists, fungi, inoculated bacteria, and rhizosphere microorganisms (Jaafar et al. 2014; Li et al. 2004; Lo Piccolo et al. 2010). Without soil, the small size of bacteria (e.g., Gram-negative cell  $\sim 1 \times 3 \mu\text{m}$ ) can be even visualized in a three-dimensional reconstruction of a single cell from confocal images as the optical resolution of a confocal image recorded with a single-photon excitation is at best 200 nm in lateral direction (Lipson et al. 2010; Zhang et al. 2021). However, one disadvantage of intensity-based imaging on soil microbes and microbial habitats via CLSM application is that the primary fluorescence of soil particles, intrinsic fluorescent proteins, and even autofluorescence present in bacteria such as aromatic amino acids (tryptophan, tyrosine, and phenylalanine) as well as several siderophores and cytochromes (Alimova et al. 2003) cannot be eliminated. Therefore, many kinds of tag staining techniques (e.g., fluorescence in situ hybridization FISH) are widely used and combined with CLSM (Tippkötter et al. 1986; Fernández-Suárez and Ting 2008; Pett-Ridge and Firestone 2018; Bokota et al. 2021). Although various imaging techniques have been applied to capture and visualize information about microbial distribution pattern (Moter and Göbel 2000; Musat et al. 2016; Oburger and Schmidt 2016; Sharma et al. 2020; Waters 2009), the technical limitations in applying fluorescence microscopy for soil ecological studies are still present. The application of digital image processing and analysis techniques to visualize soil microorganisms are complicated by autofluorescence, resolution problems, and photobleaching artifacts caused by the predominant minerals and organic matter (Li et al. 2004; Watt et al. 2006). For example, granitic rock contains a lot of microcracks and microporous minerals, while the porosity of sedimentary rocks arises mainly from nanoscale pores (Hellmuth et al. 2021), causing a more contrasting signal.

Many of the fluorescence intensity-based studies have been re-visited using fluorescence lifetime measurements, demonstrating that molecular fluorescence lifetime imaging could provide both complementary and additional unique information about the status of a target biomarker in cells (Balke et al. 2018; Digman et al. 2008; Hayek et al. 2007; Lee et al. 2021). This information helps to distinguish between different fluorophores and the intrinsic fluorescence of the samples. This concept of fluorescence lifetime imaging microscopy (FLIM) is an optical analog of magnetic resonance imaging, where the proton relaxation times at each location can be measured, and the numerical value of the relaxation time is used to create contrast in the calculated image. FLIM contrasts by using similar principles: the local environment determines the fluorescence lifetime, which is then used to calculate an image that is independent of probe concentration, signal intensity, photobleaching, and depth of probe. Despite the biologically relevant information provided by fluorescence lifetime, the widespread use of FLIM in imaging is still limited due to its slow image acquisition and processing speed, difficult implementation, and high instrument costs (Mannam et al. 2021).

To disentangle microorganisms from the heterogeneous soil matrix at the microscale, we performed fluorescence lifetime related CLSM along with a physical readout of lifetime-based information of the soil matrix. Although the confocal spatial resolution compared with other super-resolution imaging methods like structured illumination microscopy (SIM) (Gustafsson 2005), photoactivated localization microscopy (PALM) (Betzig et al. 2006), and stochastic optical reconstruction microscopy (STORM) (Rust et al. 2006) is lower, CLSM is a pure-optical measurement that can be applied with a variety of dyes in parallel, while being free from complex post-imaging calculation, similar to stimulated

emission depletion nanoscopy (STED).

On the one hand, we expected shorter fluorescence lifetimes in a region reflecting the mineral particles and longer lifetimes due to the presence of microorganisms as deduced from the study of Hellmuth et al. (2021), who measured minerals via FLIM-STED. On the other hand, we expected comparatively longer lifetimes for microorganisms as indicated by our results on fluorescence lifetime profiles of microorganisms grown in pure cultures. The FLIM technique provides image contrast to be based on the local decay times (Figure 5-1). The longer lifetime could be due to the presence of a chemical species, binding of the probe to a macromolecule or other environmental factors while their intensities could

be equally due to dye exclusion or other mechanisms. Therefore, the intensity image (Figure 5-1 b) will not reveal the different environments in regions 1 and 2. However, the FLIM technique allows image contrast to be based on the local decay times, which can be presented on a gray or color scale (Figure 5-1 c); or as a 3D surface in which the height represents the local lifetime contours (Figure 5-1 d).

The phasor approach presented simplifies the analysis of FLIM images providing a graphical global view of the processes affecting the fluorescence decay occurring at each pixel (Digman et al. 2008; Ma et al. 2016; Wang et al. 2021). The major advantages of phasor plot analysis to process frequency-domain FLIM data compared with conventional time-domain FLIM data analysis techniques are that the phasor plot analysis is instantaneous without complex fitting procedures and its visual representation of the fluorescence decay addresses even untrained user (Chen et al. 2013). The polar plot as a two-dimensional histogram (phasor plot) presents the values of the sine–cosine transforms, where each pixel of the image represents a dot in the phasor plot. The phasor plot is also used in a reciprocal mode in which each (occupied) point of the phasor plot can be mapped to a pixel of the image (Digman et al. 2008). Since every molecular species has a specific phasor, we can identify molecules by their position in the phasor plot (Alvarez et al. 2019).

In this study, we examine the differentiation of microorganisms from the heterogeneous soil matrix via FLIM and subsequent phasor plots separation technique. The gained additional information of the fluorescence lifetime profiles might be unique to the microbial biomass or at least to the microbial species used in dependence to the utilized fluorophore. We hypothesized that FLIM in combination with the phasor approach allows to disentangle the fluorescence lifetime of soil microorganisms from the organo-mineral phase, because the fluorescence lifetime is similar between cells in controls and within the soil environment in presence of the same dye. The reason for this study was to overcome the disturbing signals of autofluorescence and unwanted intrinsic fluorescence when trying to visualize microorganisms in soils. In a laboratory experiment, we established different soil environments reflecting natural forest soil, mineral substrate-induced (glucose-activated) soil (high nutrient availability and microbial biomass), autoclaved soil (high nutrient availability from lysed cells, low/no microbial biomass), and size-classed mineral particles spiked with stained *Rhodotorula mucilaginosa* or *Bacillus subtilis* (no interference of organics). We have chosen these treatments to exhibit (i) differences in lifetime profiles after microbial and/or soil staining, (ii) inconsistencies in the fluorescence lifetime profiles of the soil components as, e.g., the direct staining of soil with activated microbial biomass with *Rhodotorula mucilaginosa* or *Bacillus subtilis* might differ from neutral soil environment, and (iii) the lifetime profiles of cultured *Rhodotorula mucilaginosa* or *Bacillus subtilis* vs. stained soils and size-classed mineral particles.

## 2. Materials and Methods

### 2.1 Soil sampling, experimental design, and preparation of soil treatments

We sampled the Ah-horizon from two forest sites planted with *Fagus sylvatica* in soils of silicate parent material in Germany (Lüss, LUE and Bad Brückenau, BBR) (Fetzer et al. 2021; Lang et al. 2017). One hundred grams of fresh soil was sieved to < 2 mm and processed as follows to prepare four treatments of soil samples for each site. (i) Natural and field moist soil was weighed to 25 g and stored in plastic boxes; (ii) another 25 g was three-fold autoclaved (lysis of microbial cells); and (iii) another 25 g of natural soil, 10 mg·g<sup>-1</sup> glucose, 1.9 mg·g<sup>-1</sup> (NH<sub>4</sub>)<sub>2</sub>SO<sub>4</sub>, 2.25 mg·g<sup>-1</sup> K<sub>2</sub>HPO<sub>4</sub>, and 3.8 mg·g<sup>-1</sup> MgSO<sub>4</sub>·7H<sub>2</sub>O were added to stimulate microbial activity and growth in soil during 36 h of incubation at 25 °C (Loeppmann et al. 2016, 2018); and (iv) to the last quarter of soil was subjected to destruct the organic matter by hydrogen peroxide (H<sub>2</sub>O<sub>2</sub>). Thereafter, the H<sub>2</sub>O<sub>2</sub> treated soil was wet sieved < 200 µm and < 63 µm with distilled water and oven-dried at 105 °C to obtain dry 200 – 63 and < 63 µm sized soil mineral particles.

## 2.2 Staining of soil and microorganisms

We cultured bacteria in standard nutrient broth (Roth, Germany) comprising peptone 15 g l<sup>-1</sup>, yeast extract 3 g l<sup>-1</sup>, sodium chloride 6 g l<sup>-1</sup>, dextrose 1 g l<sup>-1</sup> at pH 7.5, and the yeast on agar (yeast extract 4 g l<sup>-1</sup>, malt extract 10 g l<sup>-1</sup>, dextrose 4 g l<sup>-1</sup>, agar 20 g l<sup>-1</sup>, pH 7.2). The microorganisms comprised a Gram-positive bacterium, i.e., *Bacillus subtilis* (DSM10), which was purchased from the German Collection of Microorganisms and Cell Cultures (DSMZ). Additionally, the yeast, *Rhodotorula mucilaginosa* (DSM70404) (Supplementary Fig. 1), inoculated on agar, which we received from Dr. M. Gube, Georg-August-University Göttingen. Cell cultivation and growth monitoring followed the techniques reported by Schmitt et al. (2022), as we aimed to avoid substrate limitation for consistent microbial growth and vital cells for sampling.

For staining soil and microorganisms (yeast and bacteria), we used BacLight™ Green (ThermoFischer, Germany). This dye is a non-nucleic acid labeling reagents for detecting and monitoring microbes via exhibiting bright green (absorption/emission ~ 480/516 nm). The preparation of the reagent and the staining processes followed the manufacturer's protocol without optional washing and fixing steps. To maintain cell viability and exclude the influence of solutes on the image, we prepared the bacteria not only in PBS buffer (1:10) as the manufacturer's guidelines but also in pure water (1:10). Staining was performed on (i) natural soil, (ii) autoclaved soil, (iii) glucose-activated soil + *Bacillus subtilis* or *Rhodotorula mucilaginosa*, (iv) controls, i.e., *Bacillus subtilis* or *Rhodotorula mucilaginosa* (in PBS buffer/water), and (v) stained *Bacillus subtilis* or *Rhodotorula mucilaginosa* + particle size fractions (200 – 63 and < 63 µm) from the respective soil. Direct staining of the treatment i, ii, and iii was performed in 2 ml Eppendorf tubes by mixing 20 mg soil, 1 ml PBS, and 1 µl working solution of BacLight™ Green without washing and centrifuging the samples. For the glucoseactivated soil, we added unstained *Bacillus subtilis* or *Rhodotorula mucilaginosa* to determine any differences of fluorescence lifetime profiles in presence of a microbial biomass-rich soil. The mineral particle-sized fractions (200 – 63 and < 63 µm) were spiked with stained *Bacillus subtilis* or *Rhodotorula mucilaginosa* as mentioned above for pure cultures. Each sample was pipetted 5 µl from the culture Eppendorf tube into a µ-slide (Ibidi GmbH, Germany). In parallel, we have tested the effect of washing procedure by using 20 mg of soil stained as mentioned above and subsequently transferred to SPIN filters and centrifuged for 5 min at 9000 rpm finally, repeated washing after the addition of 1 ml PBS. The washing did not improve the optical performance.

In addition, we measured the autofluorescence of the four treatments of each site by using a ZEISS LSM 900 Airyscan (Zeiss, Jena, Germany) for fast scanning of the samples (Fig. 2). Settings for image acquisition are as follows: z-stack, plan-apochromat 40 × /1.4 Oil DIC (UV) VIS-IR M27 objective, transmitted light excitation: 561 and 488 nm detection: 500 – 700 nm, Airyscan, Scan zoom 4, image size (scaled) 38.91 × 38.91 µm, 914 × 914 pixels.

Cultured and stained bacteria and yeast were imaged via CLSM and STED using STELLARIS 8 confocal scanner unit (LEICA Microsystems, Wetzlar, Germany) to assemble a high-resolution image of the cells' sizes and morphology (Supplementary Fig. 1). All samples were mounted with one drop

of Prolong Gold Antifade Mountant (ThermoFischer Scientific, Germany) for subsequent CLSM and STED without the necessity of any fixation of samples or resin embedding. Optical performance requires an environment with a homogeneous index of refraction to enable a high penetration depth and to minimize aberrations. Hence, the mounting medium should have a refractive index (here 1.46) that matches the immersion medium of the objective lens. Moreover, autofluorescence derived from the mounting medium should be negligible upon application of the laser. All samples were measured 24 h after preparation, meanwhile stored in the dark.

### **2.3 Fluorescence lifetime-based microscopy (FLIM) and image processing**

Single photon counting detecting devices in combination with CLSM systems afford time-correlated, single-photon counting (TCSPC) which is the core principle behind fluorescence lifetime imaging microscopy (FLIM) using CLSM (Alvarez et al. 2021). For imaging, the samples were point-scanned with a DMi8 microscope stand equipped with a STELLARIS 8 confocal scanner unit (LEICA Microsystems, Wetzlar, Germany). The integration of FLIM into the recent STELLARIS confocal platform (LEICA, Wetzlar, Germany) provides access to full FLIM analysis for image acquisition (Alvarez et al. 2021). The time difference between the arrival times of an excitation pulse and a pulse resulting from a photon detected from fluorescence emission is recorded via TCSPC (Becker et al. 2004). These time-tagged data are collected for many cycles of a periodic excitation source to establish a frequency distribution of photons (Bückers et al. 2011; Santra et al. 2018). To analyze the recorded FLIM data, we used the single molecule detection FLIM analysis software of LASX 3.5.5 and LASX 4.4.0 (LEICA Microsystems, Wetzlar, Germany). CLSM setting for image acquisition:  $93 \times / 1.3$  glycerol lens, z-stack reflection, confocal, transmitted light  $43 \times 43 \times 8.6 \mu\text{m}$ ,  $576 \times 576 \times 29$  pixel; excitation: 482 nm detection: 467 – 482 nm (reflection). The counts of both detectors (Including HydS 1; detection range 461–477 nm) were used to fit the final lifetime curve (counts) of the fluorophore. The overall image and analysis processing steps are as follows: (i) CLSM scan was performed for identification of area of interest; (ii) overlay of registered images enabled the visualization of fluorescence lifetime via FLIM. This allows (i) better image quality by an improved discrimination between signal and background, and (ii) the elimination of photons from the background using physical principles. To post-process and analyze the highly heterogenous fluorescence lifetime distribution of the organic and mineral components of an organic-rich Ah horizon, we applied the phasor approach based on a Fourier transformation to combine a fit-free lifetime estimation and to extract the different lifetime components (Datta et al. 2020; Digman et al. 2008). The phasor method transforms the histogram of the time delays at each pixel in a phasor, i.e., a vector (Alvarez et al. 2021; Digman et al. 2008). For interpretation of the phasor plot, see Supplementary Fig. 2.

## **3. Results and discussion**

### **3.1 Fluorescence intensity-based imaging**

Already more than a decade ago, the visualization of calcite surface topography with bacteria has been achieved by overlaying a series of images taken in confocal reflection contrast mode with a series of fluorescent CLSM images (Schultz et al. 2011). Nowadays, we still hamper the same problems in image processing of soils namely the autofluorescence of soil components. For example, a forest soil, comprised of, e.g., quartz mineral, organo-mineral associated material, and a plant megaspore (Figure 5-2), showed strong autofluorescence, e.g., in the green channel which reflects the wavelength spectra of the dye we have been working with, therefore biases the outcome of the steady-state intensity imaging for proper post-processing. In the absence of organic matter, we visualized microbial cells within the mineral environment, e.g., the visualization of  $< 63 \mu\text{m}$  mineral particles inoculated with bacteria at different modes via CLSM (Figure 5-3) following Schultz et al. (2011). However, in the presence of organic matter, the autofluorescence in the images increased strongly in all soils. The autofluorescence of organo-mineral associated material exhibited a different wavelength spectrum

(orange) compared to the plant spore in the overlay image (Figure 5-2 d). Moreover, autofluorescent clusters of the plant spore are tightly packed lacking any alignment across or along the surface. In contrast, the quartz mineral below the plant spore, its autofluorescence was neither detectable in the red (Figure 5-2 b) nor in the green (Figure 5-2 c) channel.

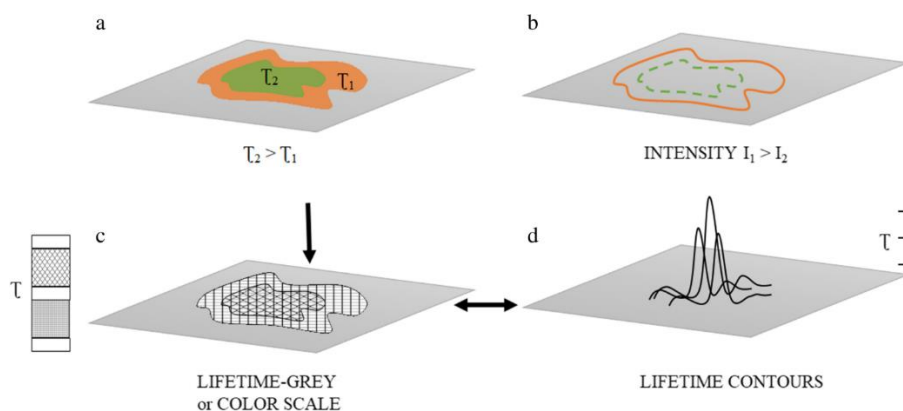


**Figure 5-1** Fluorescence lifetime adds information which is not available in steady-state imaging (modified after Lakowicz et al. 1992). The object is assumed to have two regions that display the same fluorescence intensity ( $I_1 = I_2$ ) but different decay times  $\tau_2 > \tau_1$  (a); object; b steady-state image; c grayscale or color lifetime image; and d lifetime surface. For further explanation, see the main text.

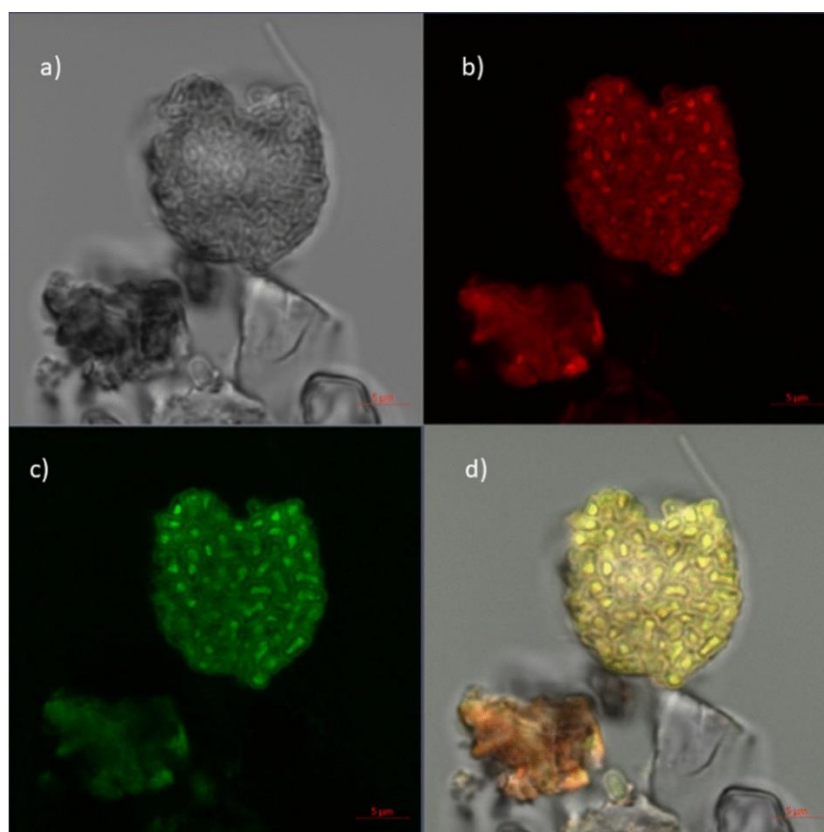


**Figure 5-2** CLSM image of soil collected from the Ah horizon at BBR site showed strong autofluorescence. Images were taken by using a ZEISS LSM 900 Airyscan, plan-apochromat 40 × /1.4 Oil DIC (UV) VIS-IR M27 objective, transmitted light excitation: 561 and 488 nm Detection: 500 – 700 nm, Airyscan, Scan zoom 4, image size (scaled) 38.91 × 38.91 μm, 914 × 914 pixels. **a** Brightfield image, **b** autofluorescence image spectral range red channel, **c** autofluorescence image spectral range green channel, and **d** overlay image: yellow color intrinsic autofluorescence of a plant spore, below the quartz mineral particle lower fluorescence intensity in the green and the channel, appear in orange color indicating organo-mineral association.

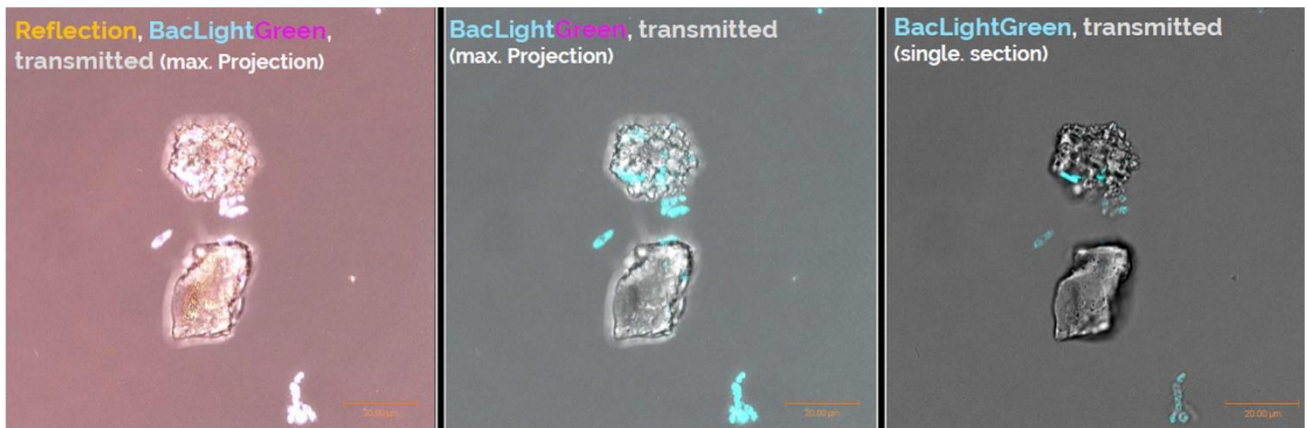


**Figure 5-3** Visualization by steady-state intensity imaging of treatment (iv) mineral particles (sized  $< 63 \mu\text{m}$ ) from LUE site spiked with BacLight™ Green stained *Rhodotorula mucilaginosa*. Image left shows the overlay (of transmission, fluorescence, and reflection channels), the intermediate image shows the overlay of fluorescence channel and transmitted, both in maximal projection and on the right, a single section overlay of the channel combinations. CLSM setting for image acquisition of DMi8 microscope stand equipped with a STELLARIS 8 confocal scanner unit (LEICA Microsystems, Wetzlar, Germany):  $93 \times / 1.3$  glycerol lens, z-stack reflection, confocal, transmitted light  $43 \times 43 \times 8.6 \mu\text{m}$ ,  $576 \times 576 \times 29$  pixel; excitation: 482 nm detection: 467 – 482 nm (reflection).

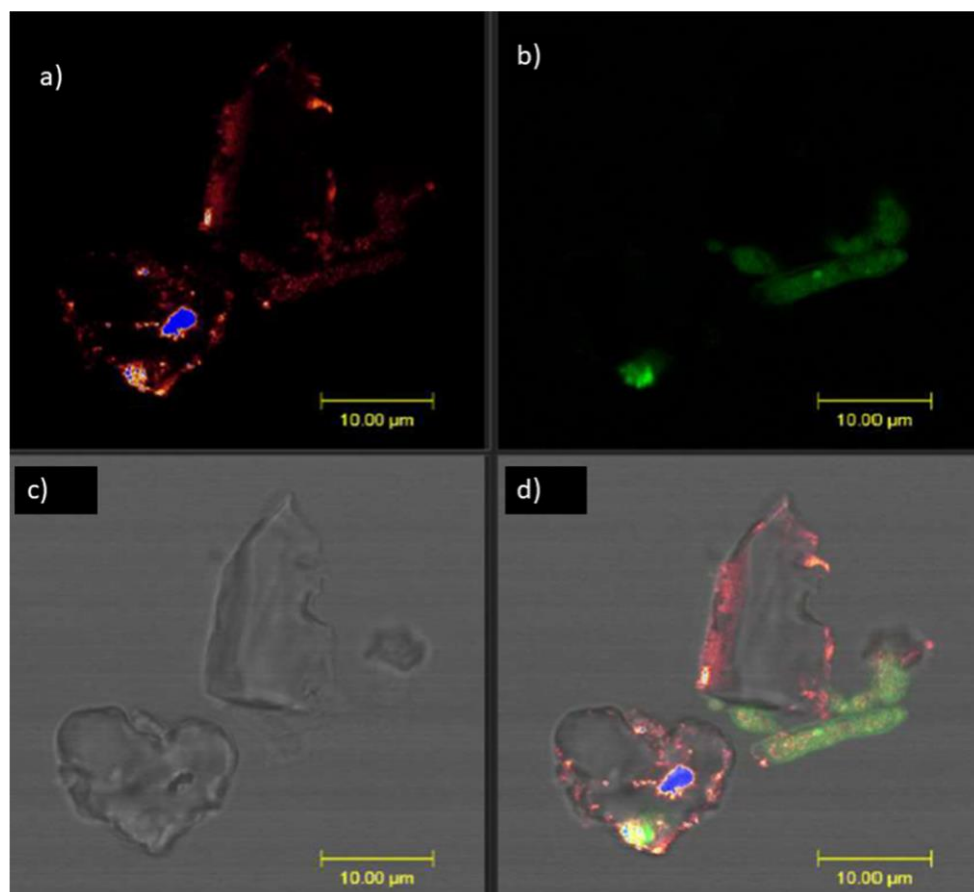


**Figure 5-4** Visualization by steady-state intensity of *Rhodotorula mucilaginosa*. **a** Reflection signal of the surfaces of soil mineral particles  $< 63 \mu\text{m}$  spiked with *Rhodotorula mucilaginosa*, **b** Confocal fluorescence signal of BacLight™ Green stained *Rhodotorula mucilaginosa*, and **c** transmitted light image; **d** an overlay of **a**, **b**, and **c**; blue area identified oversaturation of the signal. The reflection channel shows the surface with confocal z-resolution. CLSM setting for image acquisition of  $93 \times / 1.3$  glycerol lens, z-stack reflection, confocal, transmitted light  $43 \times 43 \times 8.6 \mu\text{m}$ ,  $576 \times 576 \times 29$  pixel; excitation: 482 nm, detection: 467 – 482 nm, reflection 500 – 620 nm BacLight™ Green.

By combining the channels for transmitted light and reflection, the confocal scan of the signal provided an enhanced distinctiveness between microorganisms and the mineral surfaces (Figure 5-3 and S5-4). The green signal from the stained *Rhodotorula mucilaginosa* easily differentiates with the reflection signal from the mineral surface, which gives a strong support for applying the confocal scan on direct visualization of the aggregate formation process in a certain time scale. For specific systems, Krause et al. (2019) hint at an aggregate formation process characterized by a rapid occlusion of mineral compounds, and, after the addition of microorganisms (*Pseudomonas protegens*, *Gordonia alkanivorans*) where the bacterial colonization of small microaggregates leads to an increase in aggregate size. For soil, it has been shown that substrate enhancement promotes soil microstructural stability compared to sterilized and untreated soil, whereby all soils reacted dynamically and irreversibly to the adjusted moisture conditions (Vu et al. 2022). Vu and colleagues (2022) showed significant positive correlations between microbial activity, wettability, and soil microstructural stability, indicating the presence of interparticulate microbial structures induced by soil moisture dynamics. This plays an important role for proper soil sample preparation to reproduce reliable imaging of soils. Beside the sample preparation, there are disadvantages in imaging for intensity-based images which may rely on the (i) variation in excitation source intensity, (ii) detector gain setting, (iii) optical loss in the optical path and/or sample, and (iv) variation in sample fluorophore concentration.

### 3.2 FLIM and phasor approach

To seclude several of the artifacts, we determined a characteristic phasor distribution or lifetime profile for the cultured *Bacillus subtilis* ( $1.3 \pm 0.1$  ns in PBS) (Figure 5-5 c) and for *Rhodotorula mucilaginosa* accounting  $1.2 (\pm 0.2)$  ns in PBS (Figure 5-6 a). FLIM in combination with phasor approach is sensitive to dynamic (or collisional) quenching that happens during the fluorescence decay process, when some excited-state fluorophores are de-excited upon contact with the quenchers and follow a nonradiative decay process whereas static quenching, as other unbound (hence still fluorescent) fluorophores retain their fluorescent properties (Chen et al. 2013). This leads to a faster decay of excited-state fluorophore population.

The phasor approach data (Figure 5-6 a, b) shows the modulation in phase and amplitude for the detected fluorescent signal allowing to differentiate lifetime properties of soil materials' phasor components and that of soil microorganisms at the microscale (Figure 5-6 b). This provides additional information to the intensity-based approaches, where steady-state fluorescence often hampers a clear differentiation, especially in soils with high carbon contents or specific minerals (Smith 2009). Overall, stable fluorescence lifetimes of the dye were measured for *Rhodotorula mucilaginosa* and *Bacillus subtilis* when comparing the controls (i) in PBS solution and (ii) in water (not shown). This indicates minor effects of matrix components as demonstrated by this fit-free (no iterative fit procedure) technique in which the fluorescence decay from each pixel is transformed into a point in two-dimensional phasor space providing a visual distribution of the molecular species in an image by clustering pixels with similar lifetimes (Becker et al. 2004; Datta et al. 2020). The phasor distributions correspond to similar lifetimes (decays) which can be chosen to locate the corresponding pixels in the image with similar lifetimes, even if they are spatially separated (Datta et al. 2020). By applying the phasor approach, a clear discrimination and separation of lifetime components from the background and the mineral soil particles was possible (Figure 5-5 b). Neglecting any assumption on the number of fluorescence species present in the biological sample, the phasor approach technique allows a straight-forward quantification of concentration and interaction of the involved fluorophore.

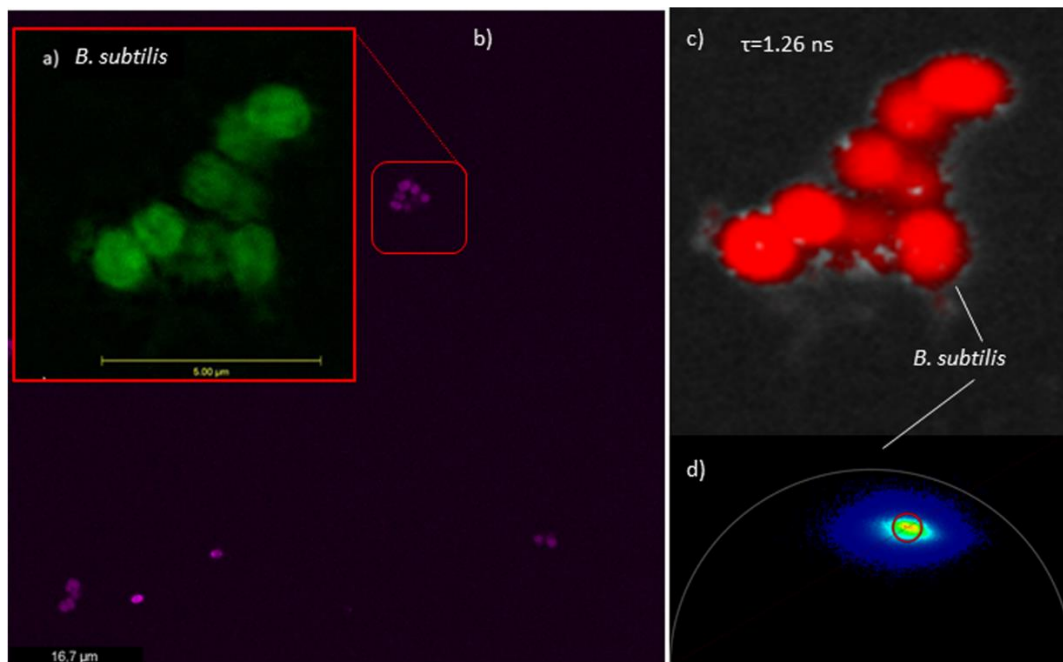


**Figure 5-5** Visualization of *B. subtilis*. **a** Steady-state intensity image of cultured *B. subtilis* imaged in PBS via CLSM. **b** Overview steady-state intensity image of *B. subtilis* imaged in PBS (CLSM image). **c** Fluorescence lifetime image of *B. subtilis*. **d** Fluorescence lifetime distribution of *B. subtilis* in the phasor plot. **d** Phasor plot of *B. subtilis* in PBS imaged via CLSM (red). CLSM setting for image acquisition DMi8 microscope stand equipped with a STELLARIS 8 confocal scanner unit (LEICA Microsystems, Wetzlar, Germany): 93 × / 1.3 glycerol lens, z-stack reflection, confocal, excitation: 482 nm detection: 467 – 482 nm (reflection).

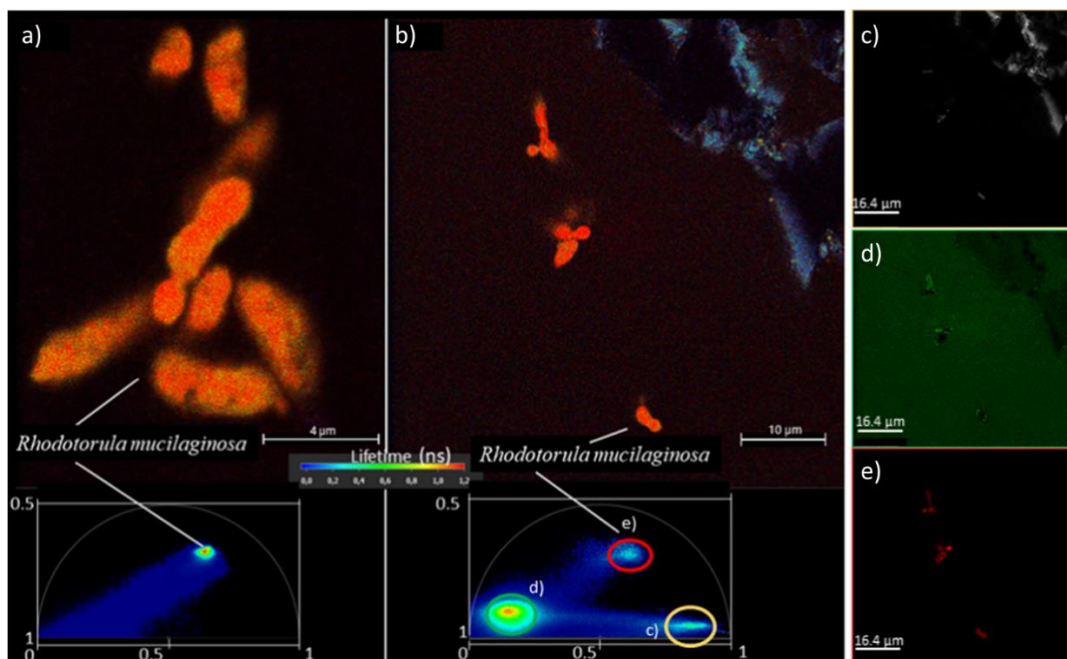


**Figure 5-6** **a** Phasor distribution of purely stained *Rhodotorula mucilaginosa* and **b** in combination with glucose-activated forest soil (BBR, Ah horizon). Shorter lifetime phasor distributions are indicated in blue reflecting the organo-mineral material. Comparing **a** with **b**, a comparable lifetime was found in PBS solution and in soil. The longer lifetime phasor distributions of the fluorophore are given in yellow–red color indicating the presence of microorganisms. The microorganisms with a fluorescence lifetime of 1 to 1.2 ns (visualized in orange-red) and with ~0.2 ns a much shorter lifetime for the mineral (visualized in blue). CLSM setting for image acquisition DMi8 microscope stand equipped with a STELLARIS 8 confocal scanner unit (LEICA Microsystems, Wetzlar, Germany): 93 × / 1.3 glycerol lens. **c–e** by phasor plot approach from **b**, we could separate three population with different fluorescence lifetime.

This method makes no assumptions on the number of fluorescence species present in the sample, permits fast processing speed, and allows to quantify the concentration and interactions of the involved fluorophores and intrinsic fluorescence signals (Ma et al. 2016). The location of bacteria around and within *Symbiodiniaceae* has been recently quantified along with their identity and spatial distribution via FLIM by Deore and colleagues (2022), since the broad spectrum hinders the use of FISH emission. The authors concluded for batch cultures that the fluorescence lifetime of the host and associated microbe cellular autofluorescence could be analyzed in terms of endogenous fluorophore composition (e.g., metabolic co-factors, aromatic amino acids) and serves as information for symbiotic versus parasitic host-microbe association. In this study, we did not measure the autofluorescence lifetime for the treatments since the dye would anyhow overrule the signal of the photon arrival time. Anionic fluorophores are excluded from the membrane interior in proportion to the membrane voltage and therefore have a lower risk for toxicity than their cationic counterparts (Dunkers et al. 2021). Anionic fluorophores are free to diffuse into the depolarized cells when bacteria are no longer viable and bind with cationic compounds and lipids. This consequently results in enhanced fluorescence intensity in viable cell compared cells alive.

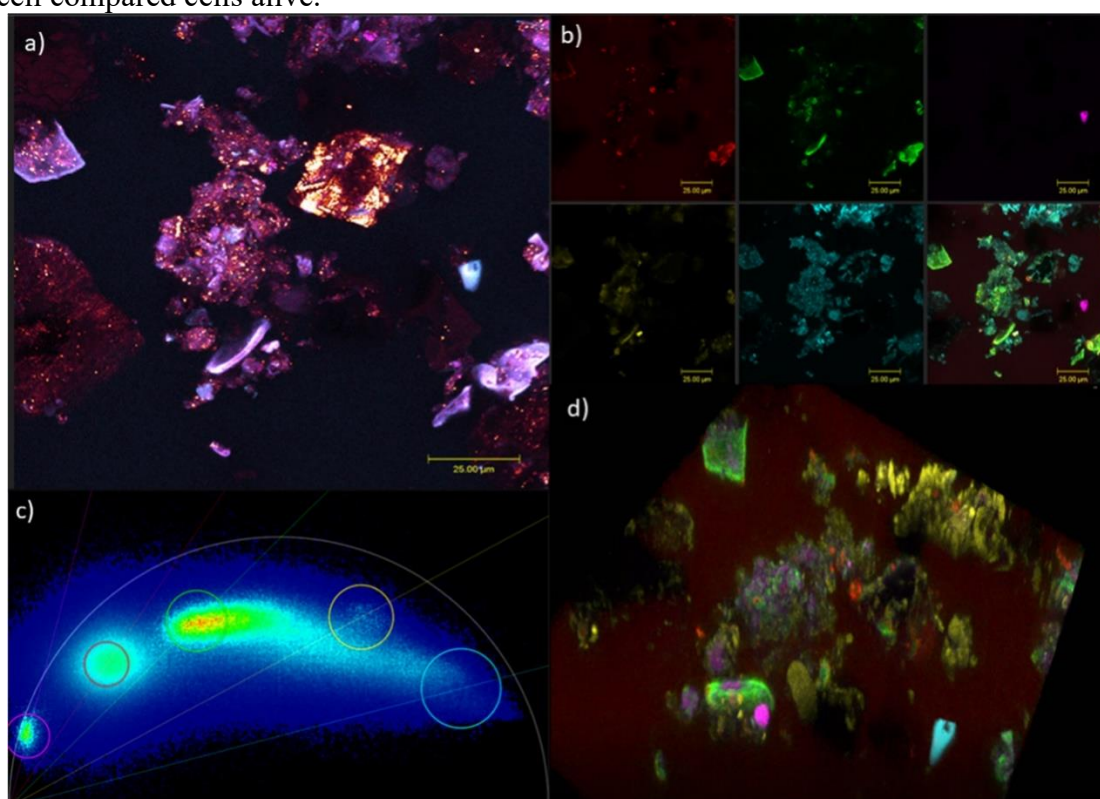


**Figure 5-7** *a* Zoomed view to the steady-state intensity image of natural soil (LUE); the overview image of the scene is shown in Supplementary Fig. 3. Both channels have been combined for FLIM analysis. *b* In the phasor plot, five different populations can be discriminated. All separated channels are shown in a maximum intensity projection of the stack in all five channels; additionally, all 5 channels represented in an overlay *c* 5 separated phasor population channels of the natural soil (LUE) directly stained with BacLight™ Green, based on specific phasor plot analysis. Average fluorescence lifetime after phasor plot separation in nanoseconds: mineral surface light-blue 0.18, different mineral surface (attached with microbes in red color in the upper middle part of the image) yellow 0.36, mineral material in green 0.67, microorganisms in red 0.99, possibly mineral coatings violet 3.61. *d* FLIM image of this sample is presented as a 3D movie in the Supplementary and as a screenshot in *d* (red color depicts the fluorescence lifetime of the microorganisms. FLIM image settings DMi8 microscope stand equipped with a STELLARIS 8 confocal scanner unit (LEICA Microsystems, Wetzlar, Germany): HC PL APO CS2 40 ×/1.25 GLYC; 146 × 146 × 15 μm; 512 × 512 × 43 voxel; voxel size: 287 × 287 × 360 nm, excitation: 470 nm, detection: reflection glow): 461–477 nm Green (cyan): 480–540 nm, red (magenta): 600–700 nm.

After amendment of stained microbes to mineral particles, irrespective the size of the fraction, the fluorescence lifetime profile was in line with that of the cultured microorganisms indicating low interference of silicate minerals from BBR and LUE site (Figure 5-3 LUE site). However, precise fluorophore lifetime mapping is crucial to measure the biological microenvironment. For example, low-light and fast measurements will maintain cell viability but may not produce images with high signal-to-noise ratio.

Indeed, even within the cell, the phasor plot showed a rather homogeneous pattern after phasor-based channel separation (Figure 5-5 c and 5-6 a). For most of the fluorescence lifetimes, a shorter lifetime profile was detected for mineral and organo-mineral material than for microorganisms (Figure 5-6 b and 5-7) except some mineral possibly mineral coatings with 3.6 ns of fluorescence lifetime (Figure 5-7). All replicates for the autoclaved soil failed for proper visualization after staining BacLight™ Green implying that the stained lysed cell fragments indicated from low unspecific to no fluorescence signal and microorganisms could not be detected via CLSM in this study. In addition, when the fluorescent dyes are conjugated to larger molecular structures such as lignin, organic acid, and protein randomly distributed on soil particles, the soil matrix may be constrained to produce fluorescence with specific properties (Coble et al. 2014). Therefore, the fluorescence signal from the stained soil matrix may include signals from soil organic matter, living cells, and membrane compromised cells. The intensity of the staining appears to depend on several factors, including gram character, outer membrane composition, and overall membrane integrity (Dunkers et al. 2021). Zhang and Fang (2004) used *Saccharomyces cerevisiae* (yeast strain) as a model and quantified the viabilities by CLSM deviated an average of 1.7% and those determined by flow cytometry by 1.4%.

A repeated measurement of several samples demonstrated a stable performance of the fluorescence lifetime even after 3 days (not shown). This indicates no significant microenvironmental effect on relative phasor distribution within measurements and infers a suitable differentiation from the soil matrix measured in this study. The phasor distribution or phasor lifetime of microorganisms was not prone to change in different types of the matrix and as in PBS solution or water in this experiment. However, it needs to be tested if the lifetime would differ in a completely different type of matrix. Organic materials and their autofluorescence biased intensity- based image processing of the soils (Figure 5-2) affecting the signal to noise ratio, whereas FLIM in combination with the phasor plot approach remains unaffected (Datta et al. 2020; Lakowicz et al. 1992). By contrast, during intensity-based image processing, the microscope optics convert each spot into a complex diffraction pattern (Airy disk). A pinhole spatially confines the airy disk to prevent out-of-focus light from reaching the detector. Closing the pinhole results in higher resolution, but fewer photons are captured in the process, which cannot be brought back even by deconvolution.

The fluorescence lifetime imaged via CLSM remained stable and similar to the lifetime of microbes in PBS solution and water in LUE soil (0.99 ns) for microorganisms visualized in the scene of natural soil (Figure 5-7) where we directly stained the soil with the dye. Therefore, measuring fluorescence lifetime provides a means of probing the local fluorophore environment (Figure 5-7) indicated in fluorescence lifetime-based phasor distribution for microorganisms ranging between 1 and 1.2 ns within the matrix of an Ah horizon of an organic-rich forest soil. Recently, Lee et al. (2021) showed multimodal multiphoton microscope images of *Serendipita bescii* fungal structures including lipid droplets stained with Nile Red (ThermoFischer Scientific, Germany) with similar range in photon arrival times as compared to the phasor-based lifetime distribution of the yeast stained with BacLight™ Green in our study.

### **3.3 Future direction of FLIM in soil science**

Since Lee et al. (2021) have imaged an artificial soil made of two components (kaolinite and organic matter), we step forward on the investigation of natural soil; its microenvironmental architecture could be separated from phasor distribution of microorganisms using multi-level threshold algorithms (Liao et al. 2001; Wang et al. 2010) and phasorbased separation (Digman et al. 2008). The presented imaging

technique implies importance on the visualization of soil microorganisms. However, yet, it cannot give insights into the functions. Moreover, there are several factors which may affect the FLIM signals such as cell age, metabolic activity, cell size, and localization as individual cell or in a biofilm. Current progress is on multiphoton FLIM enabling 3D optical sectioning and deeper imaging depth into soils' microenvironment. As the algorithms for FLIM analysis are under rapid development to (i) improve image segmentation, (ii) quantify multidimensional heterogeneity, and (iii) perform multiparametric analysis, we can expect that these computational tools are going to unravel spatial features of cellular abundance and physiology in soils. Overall, the technique might be valuable not only for the segmentation of soil components but also for soil containing enrichment cultures, stable isotope labeling incubation experiments, and microbial biofilm studies in soil and sediments. Further potential of applicability of the FLIM approach to visualize microbial cells stained by using other dyes, e.g., nucleic-acid fluorescent dyes or other labeling techniques providing unambiguous phylogenetic identification of microorganisms.

#### **4 Conclusion**

Steady-state fluorescence intensity is routinely employed as basic microscopic technique in ecological cell biology. However, intensity-based measurements are vulnerable to artifacts. Moreover, fluorophores with similar excitation and emission spectra may be impossible to disentangle using steady-state fluorescence intensity imaging. Here, we overcome these effects by using fluorescence lifetime imaging microscopy (FLIM) in combination with phasor approach technique to unravel the spatial microbial distribution in soil and mineral microsphere. We measured shorter fluorescence lifetimes in a region reflecting the organo-mineral environment and longer phasor lifetimes due to the presence of microorganisms. Overall, stable fluorescence lifetime-based phasor distributions of the dye were measured for both *Rhodotorula mucilaginosa* and *Bacillus subtilis* when comparing the two controls in PBS solution and in water suggesting minor effects of matrix components. Moreover, we identified a clear difference in fluorescence lifetime profiles between microorganisms (around 1 ns) and the surrounding soil matrix (0.2 to 0.7 ns, > 3.6 ns), via phasor plot separation. The lifetime profile within the cells was rather homogeneous for both microbial species tested. The results presented raise the feasibility to extend the applicability of this method to other soils and their accompanying microbiota. The subsequent determination and separation via phasor plots to visualize the component-specific lifetimes to establish training data for machine learning algorithms might pave the way for an automated detection and separation of microorganisms in soil via FLIM.

#### **Acknowledgements**

We thank Karl-Heinz Koertje (Leica Microsystems, Mannheim) for his technical assistance. We thank Dr. Evgenia Blagodatskaya (UFZ, Halle) and Prof. Dr. Andrea Polle (Forest Botany and Tree Physiology, Georg-August University, Göttingen) for hosting preliminary microscopic experiments. We thank the Central Microscopy Facility at the Department of Biology, Kiel University and Dr. Urksa Repnik (<https://www.biologie.uni-kiel.de/zm/>) for technical support in using Zeiss LSM 900.

#### **Funding**

This project was carried out in the framework of the priority program 1685 "Ecosystem Nutrition" funded by a SNF-DFG grant to Sandra Spielvogel (SS 20021E-171173).

#### **Declarations**

The authors declare no competing interests.

## References

- Alimova A, Katz A, Savage HE, Shah M, Minko G, Will DV, Rosen RB, McCormick SA, Alfano RR (2003) Native fluorescence and excitation spectroscopic changes in *Bacillus subtilis* and *Staphylococcus aureus* bacteria subjected to conditions of starvation. *Appl Opt* 42:4080. <https://doi.org/10.1364/ao.42.004080>
- Alvarez LAJ, Schwarz U, Friedrich L, Foelling J, Hecht F, Roberti MJ (2021) TauSTED : pushing STED beyond its limits with lifetime. *Nat Methods* 2021(1):1–3
- Alvarez LAJ, Widzowski B, Ossato G, Van Den Broek B, Jalink K, Kuschel L, Roberti MJ, Hecht F (2019) SP8 FALCON: a novel concept in fluorescence lifetime imaging enabling video-rate confocal FLIM. *Nat Methods* 20:2–4. <https://doi.org/10.1038/d42473-019-00261-x>
- Balke J, Volz P, Neumann F, Brodwolf R, Wolf A, Pischon H, Radbruch M, Mundhenk L, Gruber AD, Ma N, Alexiev U (2018) Visualizing oxidative cellular stress induced by nanoparticles in the subcytotoxic range using fluorescence lifetime imaging. *Small* 14:1–11. <https://doi.org/10.1002/sml.201800310>
- Becker W, Bergmann A, Hink MA, König K, Benndorf K, Biskup C (2004) Fluorescence lifetime imaging by time-correlated single-photon counting. *Microsc Res Tech* 63:58–66. <https://doi.org/10.1002/jemt.10421>
- Betzig E, Patterson GH, Sougrat R, Lindwasser OW, Olenych S, Bonifacino JS, Davidson MW, Lippincott-Schwartz J, Hess HF (2006) Imaging intracellular fluorescent proteins at nanometer resolution. *Science* 313(80):1642–1645. <https://doi.org/10.1126/science.1127344>
- Bokota G, Sroka J, Basu S, Das N, Trzaskoma P, Yushkevich Y, Grabowska A, Magalska A, Plewczynski D (2021) PartSeg: a tool for quantitative feature extraction from 3D microscopy images for dummies. *BMC Bioinformatics* 22:1–16. <https://doi.org/10.1186/s12859-021-03984-1>
- Bückers J, Wildanger D, Vicidomini G, Kastrop L, Hell SW (2011) Simultaneous multi-lifetime multi-color STED imaging for colocalization analyses. *Opt Express* 19:3130. <https://doi.org/10.1364/oe.19.003130>
- Chen LC, Lloyd III WR, Chang CW, Sud D, Mycek MA (2013) Fluorescence lifetime imaging microscopy for quantitative biological imaging. In: *Methods in cell biology*, vol 114. Academic Press, pp 457–488
- Coble PG, Lead J, Baker A, Reynolds DM, Spencer RG (eds) (2014) *Aquatic organic matter fluorescence*. Cambridge University Press
- Datta R, Heaster TM, Sharick JT, Gillette AA, Skala MC (2020) Fluorescence lifetime imaging microscopy: fundamentals and advances in instrumentation, analysis, and applications. *J Biomed Opt* 25:1. <https://doi.org/10.1117/1.jbo.25.7.071203>
- Deore P, Wanigasuriya I, Tsang Min Ching SJ, Brumley DR, Van Oppen MJH, Blackall LL, Hinde E (2022) Fluorescence lifetime imaging microscopy (FLIM): a non-traditional approach to study host-microbial symbioses. *Microbiol Aust* 43:22–27. <https://doi.org/10.1071/MA22008>
- Digman MA, Caiolfa VR, Zamai M, Gratton E (2008) The phasor approach to fluorescence lifetime imaging analysis. *Biophys J* 94:14–16. <https://doi.org/10.1529/biophysj.107.120154>
- Dunkers JP, Iyer H, Jones B, Camp Jr CH, Stranick, SJ, Lin NJ (2021) Toward absolute viability measurements for bacteria. *J Biophotonics* 14(12):e202100175
- Eickhorst T, Tippkötter R (2008) Detection of microorganisms in undisturbed soil by combining fluorescence in situ hybridization (FISH) and micropedological methods. *Soil Biol Biochem* 40:1284–1293. <https://doi.org/10.1016/j.soilbio.2007.06.019>
- Fernández-Suárez M, Ting AY (2008) Fluorescent probes for super-resolution imaging in living cells. *Nat Rev Mol Cell Biol* 9:929–943. <https://doi.org/10.1038/nrm2531>
- Fetzer J, Loeppmann S, Frossard E, Manzoor A, Brödlin D, Kaiser K, Hagedorn F (2021) Leaching of phosphomonoesterase activities in beech forest soils: consequences for phosphorus forms and mobility. *Front For Glob Chang* 4:1–15. <https://doi.org/10.3389/ffgc.2021.684069>
- Gustafsson MGL (2005) Nonlinear structured-illumination microscopy: wide-field fluorescence imaging with theoretically unlimited resolution. *Proc Natl Acad Sci U S A* 102:13081–13086. <https://doi.org/10.1073/pnas.0406877102>
- Hayek A, Grichine A, Huault T, Ricard C, Bolze F, Van Der Sanden B, Vial JC, Mély Y, Duperray A, Baldeck PL, Nicoud JF (2007) Cell-permeant cytoplasmic blue fluorophores optimized for in vivo two-photon microscopy with low-power excitation. *Microsc Res Tech* 70:880–885. <https://doi.org/10.1002/jemt.20493>
- Hellmuth KH, Sammaljärvi J, Siitari-Kauppi M, Robinet JC, Sardini P (2021) STED nanoscopy – a novel way to image the pore space of geological materials. *J Microsc*. <https://doi.org/10.1111/jmi.13016>
- Jaafar NM, Clode PL, Abbott LK (2014) Microscopy observations of habitable space in biochar for colonization by fungal hyphae from soil. *J Integr Agric* 13:483–490. [https://doi.org/10.1016/S2095-3119\(13\)60703-0](https://doi.org/10.1016/S2095-3119(13)60703-0)
- Krause L, Biesgen D, Treder A, Schweizer SA, Klumpp E, Knief C, Siebers N (2019) Initial microaggregate formation: association of microorganisms to montmorillonite-goethite aggregates under wetting and drying cycles. *Geoderma* 351:250–260. <https://doi.org/10.1016/j.geoderma.2019.05.001>
- Lakowicz JR, Szmacinski H, Nowaczyk K, Berndt KW, Johnson M (1992) Fluorescence lifetime imaging. *Anal Biochem* 202:316–330. [https://doi.org/10.1016/0003-2697\(92\)90112-K](https://doi.org/10.1016/0003-2697(92)90112-K)

- Lang F, Krüger J, Amelung W, Willbold S, Frossard E, Bünemann EK, Bauhus J, Nitschke R, Kandeler E, Marhan S, Schulz S, Bergkemper F, Schloter M, Luster J, Guggisberg F, Kaiser K, Mikutta R, Guggenberger G, Polle A, Pena R, Prietzel J, Rodionov A, Talkner U, Meessenburg H, von Wilpert K, Hölscher A, Dietrich HP, Chmara I (2017) Soil phosphorus supply controls P nutrition strategies of beech forest ecosystems in Central Europe. *Biogeochemistry* 136:5–29. <https://doi.org/10.1007/s10533-017-0375-0>
- Lee J, Hestrin R, Nuccio EE, Morrison KD, Ramon CE, Samo TJ, Pett-Ridge J, Ly SS, Laurence TA, Weber PK (2021) Label-free multiphoton imaging of microbes in root, mineral, and soil matrices with time-gated coherent Raman and fluorescence lifetime imaging. <https://doi.org/10.1021/acs.est.1c05818>
- Li Y, Dick WA, Tuovinen OH (2004) Fluorescence microscopy for visualization of soil microorganisms - a review. *Biol Fertil Soils* 39:301–311. <https://doi.org/10.1007/s00374-004-0722-x>
- Liao PS, Chen TS, Chung PC (2001) A fast algorithm for multilevel thresholding. *J Inf Sci Eng* 17:713–727. <https://doi.org/10.6688/JISE.2001.17.5.1>
- Lipson A, Lipson SG, Lipson H (2010) *Optical physics*. Cambridge University Press
- Lo Piccolo S, Ferraro V, Alfonzo A, Settanni L, Ercolini D, Burruano S, Moschetti G (2010) Presence of endophytic bacteria in *Vitis vinifera* leaves as detected by fluorescence in situ hybridization. *Ann Microbiol* 60:161–167. <https://doi.org/10.1007/s13213-010-0023-6>
- Loeppmann S, Semenov M, Blagodatskaya E, Kuzyakov Y (2016) Substrate quality affects microbial- and enzyme activities in rooted soil. *J Plant Nutr Soil Sci* 179:39–47. <https://doi.org/10.1002/jpln.201400518>
- Loeppmann S, Semenov M, Kuzyakov Y, Blagodatskaya E (2018) Shift from dormancy to microbial growth revealed by RNA:DNA ratio. *Ecol Indic* 85:603–612. <https://doi.org/10.1016/j.ecolind.2017.11.020>
- Ma N, Digman MA, Malacrida L, Gratton E (2016) Measurements of absolute concentrations of NADH in cells using the phasor FLIM method. *Biomed Opt Express* 7:2441. <https://doi.org/10.1364/boe.7.002441>
- Mannam V, Zhang Y, Yuan X, Hato T, Dagher PC, Nichols EL et al (2021) Convolutional neural network denoising in fluorescence lifetime imaging microscopy (FLIM). In: *Multiphoton microscopy in the biomedical sciences XXI*, vol 11648. SPIE, pp 101–108
- Moter A, Göbel UB (2000) Fluorescence in situ hybridization (FISH) for direct visualization of microorganisms. *J Microbiol Methods* 41:85–112. [https://doi.org/10.1016/S0167-7012\(00\)00152-4](https://doi.org/10.1016/S0167-7012(00)00152-4)
- Musat N, Musat F, Weber PK, Pett-Ridge J (2016) Tracking microbial interactions with NanoSIMS. *Curr Opin Biotechnol* 41:114–121. <https://doi.org/10.1016/j.copbio.2016.06.007>
- Neu TR, Lawrence JR (2015) Innovative techniques, sensors, and approaches for imaging biofilms at different scales. *Trends Microbiol* 23:233–242. <https://doi.org/10.1016/j.tim.2014.12.010>
- Oburger E, Schmidt H (2016) New methods to unravel rhizosphere processes. *Trends Plant Sci* 21:243–255. <https://doi.org/10.1016/j.tplants.2015.12.005>
- Pett-Ridge J, Firestone MK (2018) Using stable isotopes to explore root-microbe-mineral interactions in soil. *Rhizosphere* 3:244–253
- Rust MJ, Bates M, Zhuang X (2006) Sub-diffraction-limit imaging by stochastic optical reconstruction microscopy (STORM). *Nat Methods* 3:793–795. <https://doi.org/10.1038/nmeth929>
- Santra M, Jun YW, Reo YJ, Sarkar S, Choi W, Kwon JE, Park SY, Ahn KH (2018) Exploration of molecular shape-dependent luminescence behavior: fluorogenic organic nanoparticles based on bent shaped excited-state intramolecular proton-transfer dyes. *ACS Appl Bio Mater* 1:136–145. <https://doi.org/10.1021/acsabm.8b00040>
- Schmitt M, Jarosch KA, Hertel R, Spielvogel S, Dippold MA, Loeppmann S (2022) Manufacturing triple-isotopically labeled microbial necromass to track C, N and P cycles in terrestrial ecosystems. *Appl Soil Ecol* 171:104322. <https://doi.org/10.1016/j.apsoil.2021.104322>
- Schultz L, Pitts B, Mitchell AC, Cunningham AB, Gerlach R (2011) Imaging biologically induced mineralization in fully hydrated flow systems. *Micros Today* 19:12–15. <https://doi.org/10.1017/s1551929511000848>
- Sharma K, Palatinszky M, Nikolov G, Berry D, Shank EA (2020) Transparent soil microcosms for live-cell imaging and non-destructive stable isotope probing of soil microorganisms. *Elife* 9:1–28. <https://doi.org/10.7554/eLife.56275>
- Smith HD (2009) Designing an instrument based on native fluorescence to determine soil microbial content at a mars analog site. All graduate theses and dissertations. 614. <https://digitalcommons.usu.edu/etd/614>
- Tippkötter R, Ritz K, Darshbury JF (1986) The preparation of soil thin sections for biological studies. *J Soil Sci* 37:681–690. <https://doi.org/10.1111/j.1365-2389.1986.tb00396.x>
- Vu E, Schaumann GE, Buchmann C (2022) The contribution of microbial activity to soil–water interactions and soil microstructural stability of a silty loam soil under moisture dynamics. *Geoderma* 417:115822. <https://doi.org/10.1016/j.geoderma.2022.115822>
- Wang N, Li X, Chen X (2010) Fast three-dimensional Otsu thresholding with shuffled frog-leaping algorithm. *Pattern Recognit Lett* 31:1809–1815. <https://doi.org/10.1016/j.patrec.2010.06.002>
- Wang P, Hecht F, Ossato G, Tille S, Fraser SE, Junge JA (2021) Complex wavelet filter improves FLIM phasors for photon starved imaging experiments. *Biomed Opt Express* 12:3463. <https://doi.org/10.1364/boe.420953>

- Wang X, Wang C, Cotrufo MF, Sun L, Jiang P, Liu Z, Bai E (2020) Elevated temperature increases the accumulation of microbial necromass nitrogen in soil via increasing microbial turnover. *Glob Chang Biol* 26:5277–5289. <https://doi.org/10.1111/gcb.15206>
- Waters JC (2009) Accuracy and precision in quantitative fluorescence microscopy. *J Cell Biol* 185:1135–1148. <https://doi.org/10.1083/jcb.200903097>
- Watt M, Hugenholtz P, White R, Vinall K (2006) Numbers and locations of native bacteria on field-grown wheat roots quantified by fluorescence in situ hybridization (FISH). *Environ Microbiol* 8:871–884. <https://doi.org/10.1111/j.1462-2920.2005.00973.x>
- Zhang T, Fang HHP (2004) Quantification of *Saccharomyces cerevisiae* viability using BacLight. *Biotechnol Lett* 26:989–992. <https://doi.org/10.1023/B:BILE.0000030045.16713.19>
- Zhang Y, Guldner IH, Nichols EL, Benirschke D, Smith CJ, Zhang S, Howard SS (2021) Instant FLIM enables 4D in vivo lifetime imaging of intact and injured zebrafish and mouse brains. *Optica* 8:885. <https://doi.org/10.1364/optica.426870>